Thermomagnetic critical phenomena studies

Author:
Sydney, K. Ross

Publication Date:
1975

DOI:

License:

THERMOMAGNETIC CRITICAL PHENOMENA

STUDIES

by

K. Ross SYDNEY

Thesis submitted in accordance with the regulations for the

Degree of

DOCTOR OF PHILOSOPHY

Department of Physics,
Royal Military College, Duntroon.
Faculty of Military Studies,   July
University of New South Wales.   1975

CONTENTS

CONTENTS (Cont.)

CONTENTS (Cont.)

CONTENTS (Cont.)

CONTENTS (Cont.)

ACKNOWLEDGEMENTS

(iii)

Finally, I wish to thank my wife Lynne, and my children Tonia and Damien for the many sacrifices they have had to make during the course of this research.

ABSTRACT

An AC field temperature modulation technique has been developed for the study of phase transitions. It relies upon thermal modulation in an AC field and is ~ 1000 times more sensitive than previous DC techniques.

Using both AC and DC techniques in conjunction with conventional AC susceptibility studies, we have carried out a detailed study of polycrystalline gadolinium in the region of T_c in magnetic fields extending from $\sim 10^{-3}$ A/m to ~ 30 kA/m. Above T_c we have observed exchange enhanced susceptibility, and have used the AC modulation technique to measure γ. We obtain $\gamma = 1.37 \pm 0.05$ for $T_c = 292.8 \pm 0.2$K. This technique simultaneously determines T_c and γ and does not rely on an independent choice of T_c.

We have observed the nucleation of ferromagnetic domains at about 294K, and have researched the effects of domains on the susceptibility below this temperature. AC field frequencies from 0.2 Hz to 10 KHz have been used, and $\chi(T)$ in low fields ($\lesssim$ 8 A/m RMS) is field-independent. We believe this to be the first observation of initial field-independent behaviour in Gd; Gerstein and Olander (1971) used fields $\gtrsim$ 150 A/m which our results indicate are too large for such behaviour. For low fields, the AC suscept-ibility _decreases_ in the region of about 290 to 292K as the temperature is decreased, and temperature hysteresis is observed : the sample displays a higher susceptibility at these temperatures when being cooled than when being warmed.

Above about 8 A/m the susceptibility increases with field due to the more isotropic irreversible domain wall translation and rotation processes. The structure in $\chi(T)$ increases, and there is less temperature hysteresis.

The phase of χ relative to the AC field waveform agrees in form with the results of magnetic hysteresis measurements : the minor loop coercive force grows rapidly from about 294K to a maximum at about 291K near the trough in the low AC field $\chi(T)$ curves.

The satellite structure observed in the temperature dependence of the AC modulation signal in low AC fields does not correspond in the ferromagnetic region to the temperature derivative of the low AC field $\chi(T)$ curves. Furthermore, a phase lead is found in the region of 290K for the modulation signal in low AC fields; it is larger in warming experiments than in cooling experiments. These phenomena are explained in terms of relaxation effects observed in the low-field AC susceptibility with a characteristic time $\sim$ 2-6 secs. We have attributed this to effects associated with the contribution of the magnetic after-effect to the low-field domain wall processes.

A theory has been developed for the temperature modulation techniques. It encompasses a formulation of the susceptibility in terms of the intrinsic magnetization and a domain mobility factor $G(H,T)$. In the low-field region, $G(H,T)$ takes the form $g(T)H$; the effects described above are ascribed to $g(T)$ which consists of a frequency independent part and a part associated with the magnetic after-effect. This theory explains our experimental results.

A new manifestation of a magnetic after-effect has been observed in the AC susceptibility. A transient magnetic field superimposed on the AC field enhances the susceptibility at the AC field frequency.

Surveys of theories related to Gd, domains and critical phenomena are contained in Chapters 1, 2 and 3 respectively. Chapter 4 details our modulation theory. The experimental technique and the domain results are described in Chapters 5 and 6 respectively, while Chapter 7 deals with our critical exponent analysis. Chapter 8 concludes the thesis with ideas for future work.

CHAPTER ONE

INTRODUCTION

1.1   Ferromagnetism, Critical Phenomena and the Rare Earth Metals

Ferromagnetism is a large field of scientific and engineering interest extending from mathematical and microscopic studies of ferromagnetism in single-domain particles, through the examination of microscopic properties of domains, to the applied physical and engineering aspects of permanent magnets. When the ranges of temperature at which magnetic phase transitions occur are studied in detail, another very large field of research becomes relevant: the study of critical phenomena. In principle, magnetic phase transitions exhibit characteristics common to all other phase transitions. The applied mathematical work being carried out in this area is extensive; it does not allow for the existence of magnetic domains or finite applied magnetic fields, and so in many ways is at odds with the realities of experimental physics (Heller 1967). Nevertheless, as in many other fields the ultimate aim of both the theoretician and the experimentalist must be to obtain acceptable agreement between theory and practice so that a model and a set of theories can be devised which, if not within the bounds of conclusive proof, can at least be said to produce results in keeping with observed physical behaviour. The phase transition between the ferromagnetic and the paramagnetic state would be one of the most accessible vehicles for the study of critical phenomena if sufficiently low fields could be used to observe "true" critical behaviour and if the interference by domains could be properly overcome.

The study of the rare earths is another quickly developing area of research; a lot of work has been carried out over the past two decades, but on the whole little has been done in comparison, say, with the transition metals. It is only recently that ion exchange methods have been developed to overcome the chemical similarity of the lanthanides in order to prepare rare earth samples of desirable purity (Spedding et al 1952). Whereas the ferromagnetic properties of the transition metals are attributable to the 3d shell which is next to the valence 4s shell, most of the magnetic behaviour of the rare earths is due to their unfilled inner 4f shell which is separated from the valence shell by the filled 5s and 5p shells. With the exception of Gd they exhibit complicated spin structures not found in the transition metals; Gd, however, lying at the middle of the lanthanide series with a half-filled 4f shell, appears to have simple ferromagnetic behaviour. It thus enjoys a unique place vis a' vis the transition ferromagnetic metals on the one hand, and the rest of the rare earths on the other. Furthermore, because the Curie point, Tc, lies near room temperature, it lends itself to critical phenomena study without the necessity for elaborate cooling or heating procedures.

1.2   Aim

It was originally intended that this work should centre about the development of a new thermal modulation technique for magnetic critical studies. It was envisaged that this technique would be applied to other materials than Gd. The success of this technique was achieved early in the project; its accuracy was such that hitherto undiscovered phenomena associated with ferromagnetic domains in Gd were disclosed. It was necessary to fully investigate these effects by conventional means used in conjunction with the new technique, and as a result this

work has concentrated wholly on Gd, investigating its domain properties

near Tc, researching into the field, frequency and temperature

dependence of its susceptibility χ, and obtaining a value of the

susceptibility critical exponent γ above Tc (Sydney et al 1975 A and B).

1.3   Gadolinium

Gadolinium with an atomic number of 64 lies at the centre of a

group of elements called the rare earths extending from cerium (58) to

lutetium (71). Together with the chemically related lanthanum (57),

they form a separate sub-series of the periodic table called the

lanthanides, whose inner 4f shells of electrons are filling. All

contain three electrons in the outer 5d and 6s shells, and so are very

similar chemically, but the different extent to which the 4f shell is

filled as one proceeds across the series results in very different

magnetic properties with complicated spiral spin structures and

ordinary ferromagnetic, net antiferromagnetic and non-magnetic behaviour

occurring at different temperatures throughout the series.

In comparison with the rest of the series, the magnetic spin

structure of Gd is uncomplicated. Despite previous arguments to the

contrary (Belov et al 1961, 1962, 1965), Gd is now thought to be a

simple ferromagnet below the Curie point of about 293K. With the

maxima in the distributions of the 6s and 5d shells lying at about -6eV,

and the relatively localized maximum of the 4f shell occurring at about

-22eV, the 4f electrons are tightly bound to the atom with the three

outer electrons forming conduction electrons; this situation exists in

most of the rare earths (europium, ytterbium and one phase of cerium

are thought to be divalent) (Elliott 1972, Freeman 1972). The highly

localized moment due to the unpaired electrons in the 4f shell is

quite well given by the application of Hund's rules; Gd, with seven

4f electrons is, to a first approximation, a pure S-state ion (ie, its

orbital angular momentum L is zero). It has been upon the assumption

that most of the rare earths behave like a system of free trivalent

ions immersed in a sea of conduction electrons, rather like the

transition metals, that most theoretical work has been done. Recent

evidence collected by Koehler and his associates (1972) suggests,

however, that the free ion representation is inadequate for Gd: the

total magnetic moment must be ascribed in part to polarization of the

conduction electrons as well as the over-riding contribution from the

4f electrons.

1.4   Theory of Ferromagnetism in the Rare Earths

While bearing the above recent evidence in mind, it behoves us

to return to the free-ion approximation because through it much of the

interesting behaviour occurring in the rare earth metals has been

explained. One then is left with a single Hamiltonian for the 4f

localized moment system consisting of the three types of energy

contributions:

$$\mathcal{H} = \mathcal{H}_{ex} + \mathcal{H}_{cf} + \mathcal{H}_{ms} \tag{1}$$

these being the long-range oscillatory exchange interaction between

the ions via the conduction electrons, the energy of interaction between

the ion and its surrounding hcp lattice, and the magnetostriction

contribution to the energy, respectively. We now turn to explaining

these interactions; this will be done mainly in terms of the free-ion

model.

Magnetic Properties of Free Ions. In free ions, the magnetic

moment of the electrons gives an interaction energy with a magnetic

field $\underset{\sim}{H}$ of:

$$\sum \mu_B \, (\underset{\sim}{\ell_i} + 2\underset{\sim}{s_i}) \, . \, \underset{\sim}{H} = \mu_B \, (\underset{\sim}{L} + 2\underset{\sim}{S}).\underset{\sim}{H} \tag{2}$$

where $\underset{\sim}{\ell}_i$ and $\underset{\sim}{s}_i$ are the orbital and spin momenta of the ith electron, $\underset{\sim}{L}$ and $\underset{\sim}{S}$ are the total orbital and spin momenta of the system of electrons, and $\mu_B = \dfrac{e\hbar}{2m_e c}$ is the Bohr magneton. Spin-orbit coupling is relatively strong here, so that only the lowest J multiplet is normally occupied at room temperature. By Hund's rules, this is given by L − S if the shell is less than half-full, and L + S if it is greater than half full. For Gd, $\underset{\sim}{L}$ is zero. In the lowest J multiplet:

$$\mu_B (\underset{\sim}{L} + 2\underset{\sim}{S}) \cdot \underset{\sim}{H} = g_J \mu_B \underset{\sim}{H} \cdot \underset{\sim}{J} \tag{3}$$

where g_J is the Lande factor for electron spin:

$$g_J = 1 + [S(S+1) + J(J+1) - L(L+1)]/2J(J+1). \tag{4}$$

g_J is 2 for Gd. Whereas $\underset{\sim}{L}$ is always parallel to $\underset{\sim}{J}$, $\underset{\sim}{S}$ is antiparallel to $\underset{\sim}{J}$ in the first half of the rare earth series, and parallel in the second half. The paramagnetic susceptibility is given by the usual Curie law:

$$\chi = N g_J{}^2 \mu_B{}^2 J(J+1)/3kT \tag{5}$$

For Gd, $g_J{}^2 J(J+1) = 63$.

Exchange Interaction. We treat here the Ruderman-Kittel-Kasuya-Yosida theory, first proposed by Ruderman and Kittel to explain the effective long-range coupling between nuclear spins interacting via the Fermi hyperfine interaction (Ruderman and Kittel, 1954), and later extended by Kasuya (1956) and Yosida (1957) to treat local moment-conduction electron interactions. According to common usage, it will be referred to hereafter as the RKKY theory, and is summarized below.

The Hamiltonian of the exchange between localized and conduction electrons at sites $\underset{\sim}{R}_i$ and $\underset{\sim}{R}_j$ involves adding to the normal Bloch Hamiltonian a term describing the electron-electron interaction for a system of electrons; considering the electrons to be in states k and k' of k space, the exchange

integral $U(\underset{\sim}{q})$ where $\underset{\sim}{q} = \underset{\sim}{k} - \underset{\sim}{k}'$, is formed similarly to the 6s-4f and

5d-4f exchange integrals. Often it is convenient to use the Fourier

transform of this to obtain the exchange integral in direct space:

$$U(\underset{\sim}{r}) = \sum_{\underset{\sim}{q}} U(\underset{\sim}{q})e^{i\underset{\sim}{q}\cdot\underset{\sim}{r}} \tag{6}$$

Then the Hamiltonian for the exchange interaction may be written as:

$$\mathcal{H}_{ex_{ij}} = -\mathcal{J}(\underset{\sim}{R}_i - \underset{\sim}{R}_j)\underset{\sim}{S}_i \cdot \underset{\sim}{S}_j \tag{7}$$

where $\qquad \mathcal{J}(\underset{\sim}{R}_i - \underset{\sim}{R}_j) = \sum_{\underset{\sim}{q}} |U(\underset{\sim}{q})|^2 \chi(\underset{\sim}{q})e^{i\underset{\sim}{q}\cdot(\underset{\sim}{R}_i - \underset{\sim}{R}_j)} \;, \tag{8}$

$\chi(\underset{\sim}{q})$ being the non-local susceptibility tensor for the conduction

electrons. Because of the uncertainties arising from the various

approximations, the exchange integral is usually assumed to be isotropic

and a function of $|\underset{\sim}{k}-\underset{\sim}{k}'| = q$ only, and in the RKKY theory, $U(q)$ is taken

to be a constant U_o, leading to:

$$U(\underset{\sim}{r}-\underset{\sim}{R}) = U_o \,\delta(\underset{\sim}{r}-\underset{\sim}{R}) \tag{9}$$

The spin on the atom at i may be regarded as setting up a spin

polarization in the conduction electrons. Because the Fermi distribution

restricts the wave vector of the electrons which carry the polarization, this

tends to have an oscillatory component. The polarization couples to the

spins of other atoms to produce an effective long-range exchange.

The RKKY theory relies on a free-electron-like band structure

approximation for the conduction electrons, and non-overlapping of the

localized electrons on different sites. The second approximation is good

for Gd (Freeman 1972), but from the work of Dimmock et al (1964, 1965), it

is clear that the heavy rare earths differ markedly from the free-electron

model. The interaction is long-range, decreasing as R^{-3} for large R (R being

spatial distance), so that it is closely centred about the ion site. It

oscillates with a period $(2k_F)^{-1}$ where k_F is the radius of the conduction

electron Fermi surface which is taken to be spherical. (Note, however,

that the RKKY theory has been extended to include more general, non-spherical

Fermi surfaces) (Freeman 1972).

Cooper (1969) shows that the degree of spiral is determined by minimizing $\mathcal{J}(q)$ and therefore minimizing the energy (refer to Eq. 7). If the maximum of $\mathcal{J}(q)$ comes at $q = 0$, then the exchange favours a ferromagnetic alignment. While $\mathcal{J}(q)$ is a maximum at $q = 0$ in the free-electron model, a more realistic band structure for Gd can produce a maximum for $q \neq 0$. Yet, recent evidence from neutron diffraction and magnetization studies seems to show that Gd does not exhibit any spiral structure, but behaves like a normal ferromagnet below its Curie temperature (Graham 1963, Will et al 1964, Cable and Wollan 1968, Kuchin et al 1968). The first principle calculations of $\mathcal{J}(q)$ without the assumption of free-electron behaviour is involved, and one should refer to the review by Cooper (1969) for more detail; in general it appears that the transition to ferromagnetism is brought about by the differing contributions to the energy, of the three terms in Eq. 1.

Anisotropy Effects. The second contribution to Eq. 1 is the anisotropy energy of the unstrained lattice resulting from the interaction with the crystalline electric field of the distribution of the 4f electrons in a given ion. The array of charges around any ion produces an electric field at the 4f electrons which has a corresponding symmetry. In an S-state ion such as Gd, orbital angular momentum cannot give rise to magnetic anisotropy, which arises from spin-orbit coupling. The effect of the crystal-field terms on the energy levels is normally adequately calculated from first-order perturbation theory since the crystal field energy is small compared to the spin-orbit coupling. The crystal field interaction consists of a large axial and smaller planar anisotropy, and in general may be represented classically by:

$$\mathcal{E}_{cf} = \sum_i \{ K_2{}^O Y_2{}^O (\underset{\sim}{S}_i) + K_4{}^O Y_4{}^O (\underset{\sim}{S}_i) + K_6{}^O Y_6{}^O (\underset{\sim}{S}_i)$$

$$+ K_6{}^6 [Y_6{}^6 (\underset{\sim}{S}_i) + Y_6{}^{-6} (\underset{\sim}{S}_i)] \} \qquad (10)$$

where the $K_e{}^m$ are the anisotropy constants and the $Y_e{}^m (\underset{\sim}{S}_i)$ are operator equivalents of spherical harmonics (Cooper 1969, Koehler 1972), which are normalized to unity if the spin vector $\underset{\sim}{S}_i$ lies along the appropriate axis. The magnetic anisotropy energy in many of the rare earths is extremely large, and in contrast to the 3d transition metals is a significant perturbation on the exchange. $K_2{}^O$, $K_4{}^O$ and $K_6{}^O$, with their accompanying harmonics, describe the dominant uniaxial anisotropy, while the term $K_6{}^6$ refers to the six-fold basal plane component. In this convention, positive values of the $K_e{}^m$ favour moment alignment in the basal plane, while negative values favour alignment along the c axis. The minimum in the anisotropy potential energy expression (Eq. 10) determines the stable magnetization direction (ferromagnetic easy axis) except for the case of a conical ferromagnet where the angle is modified by the exchange energy.

In Gd, the anisotropy constants are an order of magnitude smaller than in other rare earths. To a good approximation, the ion is in a pure S-state where there is a completely spherical charge cloud, and all its multipole moments are zero. To this order, therefore, there is no crystal field effect. However, a small anisotropy of the spin magnetization will be produced by the crystal fields via the spin-orbit interactions. The effect of covalent bonding is also found to be important in determining the magnitude of these effects (Wybourne 1966).

It is found for Gd that the energy per unit volume necessary to magnetize a crystal in a direction making an angle θ with the c axis (0001), and an angle ϕ with the a (or b) axis (11$\bar{2}$0) in the basal plane can be simplified to (Mason 1954):

$$\mathcal{E}_{cf} = K_1 \sin^2\theta + K_2 \sin^4\theta + K_3 \sin^6\theta + K_4 \sin^6\theta \cos^6\phi \qquad (11)$$

where
$$-K_1 = \frac{3}{2} K_2^O + 5K_4^O + \frac{21}{2} K_6^O$$

$$K_2 = \frac{35}{8} K_4^O + \frac{189}{8} K_6^O$$

$$K_3 = \frac{-231}{16} K_6^O$$

and
$$K_4 = K_6^6$$

The results gained from various techniques (Corner et al 1962, Graham 1962, 1963 and 1967, Darby and Taylor 1965, Koehler et al 1970) point to the relatively large value of the basal plane anisotropy at low temperatures, and once again the interpretation is that a large part is played by the conduction electrons in the interactions. It becomes evident that the reason for the simple ferromagnetic behaviour of Gd below Tc may be largely associated with this contribution from the conduction electrons; it would appear that on the basis of the 4f electrons alone, Gd, having the lowest anisotropy and the lowest magnetoelastic energies of the rare earths, would be least likely to exhibit simple ferromagnetism. (Refer to the concluding remarks made in the preceding section dealing with the exchange interaction). (Freeman 1972).

Magnetostriction and Elastic Energy. The third contribution to Eq. 1, the magnetoelastic energy, arises from the modification of the static lattice model by the introduction of strain, either dynamic (arising from phonons), or static. The static strain contributions are of particular importance, giving rise to large magnetostrictive effects; they are also believed to be mainly responsible for the transitions between spiral structures and ferromagnetism (Cooper 1967).

Magnetostrictions are caused by the interdependence of magnetic and elastic energy, and occur to minimize the total free energy of the system. The strain-dependent energy density leading to the magnetostriction is:

$$\mathcal{H}_{ms} = \mathcal{H}_e + \mathcal{H}_{me} \qquad\qquad (12)$$

where $\mathcal{H}_e$ is the static component associated with homogeneous strains,

and $\mathcal{H}_{me}$ is the dynamic component coupling the spin system to the

strains. Callen and Callen (1963, 1965, 1968) expressed the magneto-

elastic Hamiltonian for a hexagonal lattice in terms of one and two-ion

magnetoelastic constants, and by minimizing Eq. 12 with respect to the

strain, obtained an expression for the magnetostriction, $\frac{\Delta\ell}{\ell}$, in terms

of six magnetostriction constants λ. In the single ion case, these

constants have a temperature dependence related to that of the magnetization.

Tsuya et al (1965) calculated the contribution to the one-ion

magneto-elastic coefficients arising from distortion of the crystal field

and strain rearrangement of the conduction electrons. The latter energy

contribution considers the redistribution of conduction electrons near

the 4f ion during lattice distortion while the former may be visualized

as a very oblate 4f charge cloud residing in a crystal field produced

by 3^+ ions on the hexagonal sites. The contribution from the

redistribution of the conduction electrons was found to be the larger

of the two sources (Rhyne 1972).

The lowering of the magnetic elastic energy in passing from the

helical to the ferromagnetic state is thought to be the basic driving

force behind the ferromagnetic transition (Cooper 1967, 1972). The

transition occurs because there is competition between the exchange

interaction for the undistorted hcp lattice favouring a spiral arrangement

on the one hand, and the magnetostriction on the hexagonal anistropy

effects favouring ferromagnetic alignment on the other. The spiral

arrangement serves to restrain each successive plane along the c axis

from developing the strain that would minimize the combined elastic and

magnetoelastic energies. Transition to a ferromagnet allows such

energetically favourable strains to develop. This cylindrically symmetric magnetostrictive energy equally favours ferromagnetism pointing in any direction in the hexagonal plane, and therefore does not enter into the experimentally measured hexagonal anisotropy energy.

Apart from Cooper's work (1967, 1969, 1972), another more detailed theory of the way in which magnetoelastic effects serve as the principal driving force stabilizing the ferromagnetic state is given by Evenson and Lui (1969). Their treatment gives a microscopic demonstration of the lattice clamping effects. They also show that when the magnetic ordering is periodic, there is a thin layer only a few lattice constants thick at the surface of the crystal where the lattice is distorted with the same periodicity.

Energy Band Theory for the Rare Earths. The Heisenberg model of ferromagnetism assumes that the electrons are localized at the atoms. This is clearly unrealistic for ferromagnetic rare earth materials because of the role of the conduction band electrons. Theories that consider mobile electrons or holes in unfilled bands have been developed; the earliest band calculations used a free electron model. The RKKY theory has already been treated; it assumes that the ionic spins do not greatly disturb the conduction electrons so that low order perturbation theory can be used. However, it has been seen that free electron theory is unable to account for many properties of the rare earths (the electronic contributions to the magnetic moment and the specific heat are examples). Furthermore, magnetic ordering in the rare earths has been seen to depend sensitively upon the geometry of the Fermi surface (Taylor and Darby 1972). Recently, however, Bloch-type wave functions have been used where the interaction between the electrons and the ion cores is considered. (Matthiess 1964). These band theories are based on a number of simplifying assumptions and approximations which reduce the many-body

problem involving the interaction between all the particles in the system to a one-electron model. The approximations are not completely justified, and may seriously affect some of the physical results obtained (Freeman 1972).

The first assumption is the Born-Oppenheimer approximation; it essentially reduces the problem to an electron-interacting system only; the second, the Hartree-Foch approximation, neglects the electron-electron correlations among electrons of opposite spins. The third assumption averages the exchange terms which arise in the Hartree-Foch equations. Using these approximations, the band methods then reduce to choosing a crystal potential and then solving the Schrödinger (or Dirac) equation using the assumed potential.

For energy band calculations on the rare earths, the augmented plane wave (APW) method has been used; here the crystal potential is spherically symmetric within a sphere about each atomic site with plane waves between sites outside the sphere ("muffin tin" potential). The coulombic and exchange contributions to the crystal potential are calculated separately and superimposed to construct the total potential. Next a set of basis functions called augmented plane waves are chosen. These are solutions of the spherically symmetric potential inside the sphere, and a plane wave $e^{i\underset{\sim}{k}\cdot\underset{\sim}{r}}$ in the constant regions. The solution inside the "muffin tin" is expanded in terms of products of radial wave functions and spherical harmonics; this facilitates the matching of solutions on the APW sphere, and eigenvalues and eigenfunctions are determined at selected $\underset{\sim}{k}$ values in the Brillouin zone.

Dimmock, Freeman and Watson (1964, 1965, 1966, 1968) have determined the energy band structure for hexagonal close-packed Gd, Tm, La and Lu using the non-relativistic APW method. The results for Gd

will be discussed in the following section. Relativistic effects have

been included by Loucks (1965), where energy eigenvalues are determined

as solutions of the single-particle Dirac equation with the same APW

potential. The major effect of the relativistic corrections is to

remove some of the degeneracies in the non-relativistic bands.

1.5   Physical Properties of Gadolinium.

Gadolinium has a density of 7.898×10^3 kgm/m^3 at room

temperature. It has a saturation magnetic moment of 3.37×10^{-4} wb-m/kgm

corresponding to a saturation magnetization of 2.45 wb/m^2 at OK, or 7.55

Bohr magnetons. Its crystal structure is hcp at room temperature. It

shows a sharp break in its thermal expansion at about 300K with a

negative coefficient from about 230K to about 300K(Banister et al 1954,

Barson et al 1957, Bozorth and Wakiyama 1962, 1963). Magnetothermal

measurements conducted by Bates and Pacey (1961) show a divergence of

the product of temperature and the isofield temperature derivative of

the magnetization near Tc.

Dimmock and Freeman (1964, 1972) have carried out calculations

on the band structure of Gd, and have written of the dominant role

played by the 5d bands which strongly hybridize with the 6s-p bands and give

rise to an unusually high density of flat bands near the Fermi energy.

The 4f levels appear to play no part in the formation of the conductions

bands.

Magnetization. Gadolinium has no orbital momentum contribution

to the total moment of its atomic system, and has magnetization curves

which are characteristic of an isotropic ferromagnet. Belov et al

(1961, 1962, 1965) observed that above 210K in weak fields the

magnetization falls rapidly and the coercive force rises. They also

found that the magnetization isotherms measured in the range 210 to 290K

exhibited marked kinks at critical fields, similar to the behaviour of

Dy which is known to have a helical antiferromagnetic structure at about 85K. They concluded, therefore, that Gd has a helical spin configuration in the range 210-290K below a critical field of less than 1200 A/m; this configuration is destroyed by fields greater than the critical field. However, neutron diffraction studies by Will et al (1964), Cable and Wollan (1968) and Kuchin et al (1969) seem to indicate that no such structure exists. Torque measurements by Corner et al (1962), Darby and Taylor (1965), Birss and Wallis (1965) and Graham (1962, 1963, 1967), and AC studies by Milstein and Robinson (1969) indicate that many of these results may be due to anisotropy effects and domain properties.

The paramagnetic Curie temperature θ_p is 317K (Rhyne 1972). Depending on the method used, the ferromagnetic Curie point, T_c, has been variously reported to lie between about 289K and 293.5K (Patrick 1954, Griffel et al 1954, Belov and Ped'ko 1962, Nigh et al 1963, Robinson et al 1964, Jelinek et al 1965). The temperature dependence of the b axis magnetization curve is reasonably well defined by the $S = \frac{7}{2}$ Brillouin function (Nigh et al 1963). The saturation magnetization is represented by a T^2 dependence from OK up to about 150K as expected on a spin-wave model (Kasuya 1966). The T = 0 value of saturation magnetic moment is theoretically predicted to be 3.13×10^{-4} wb-m/kgm if one assumes the only contribution comes from the 4f electrons with $S = \frac{7}{2}$. That the experimentally determined value is 3.37×10^{-4} wb-m/kgm is indicative of the important part played by the conduction electrons in contributing towards the magnetization. This value is also lower than the rest of the heavy rare earth metals due to the S-state character of the ion.

Short range ordering causes departure from Curie-Weiss behaviour of the paramagnetic susceptibility below about 370K

(Nigh et al 1963). The effective moment of the paramagnetic

susceptibility is 7.98 Bohr magnetons in good agreement with the

theoretical value of 7.94 Bohr magnetons. The investigation by

Arajs and Colven (1961) shows that the paramagnetic susceptibility

follows predictions based on the localized f-electron model of

interacting rare-earth ions.

Gerstein and Olander (1971) have carried out low-field

AC susceptibility studies near T_c with fields between about 160 and

2000 A/m. They observed temperature hysteresis in both the absorptive

and dispersive components, together with a trough in the $\chi(T)$ curve

just below Tc. They also found low-frequency effects which they

endeavoured, unsuccessfully, to attribute to domain wall dynamics.

A more detailed description of this work appears in Chapter 6.

The ferromagnetic and paramagnetic Curie points are isotropic

(Rhyne 1972). Patrick et al (1954) and Robinson et al (1964) have

shown that T_c decreases with pressure contrary to expectations from

the Bozorth interaction curve which plots the Curie temperature of

ferromagnetic elements against the ratio of the interatomic distance

to the diameter of the unfilled inner shell (Bozorth 1940). In view

of the quite different degree of localization of the main electronic

contributors to the magnetization in Gd and the transition metals,

it is not surprising that Gd does not conform to the same expectations.

Magnetic Anisotropy. Since Gd is an S-state ion, to first

order the single-ion contribution to the anisotropy vanishes. Torque

measurements of the axial anisotropy (Graham 1962, Corner et al 1962,

Darby and Taylor 1965, Birss and Wallis 1965) indicate a strong

variation in anisotropy energy with applied field, particularly near

T_c, resulting from increasing saturation (Russian literature refers

to this as the paraprocess effect). These measurements indicate that

the anisotropy in Gd is several times that of hcp Co. Corner et al

(1962) and Graham (1963) show the variation of anisotropy constants

with temperature. Graham makes the point that for any variation

of field there is no unique value of magnetic moment for any given

temperature, and so plots his anistropy constants against magnetic

moment for a range of temperatures. From these and the AC

susceptibility studies of Milstein and Robinson (1969) it is seen

that below T_c the c axis is the easy direction of magnetization

(Eq. 11). K_1 changes sign at 240K corresponding to a sudden change

in the moment orientation away from the c axis towards the basal

plane with the angle to the c axis being a maximum in the vicinity

of 180K. Neutron diffraction studies (Will et al 1964, Cable and

Wollan 1968) confirm the picture. It appears that just below 240K

the moments are prevented from aligning parallel to the basal plane

by a small energy maximum in that direction. Graham's torque

measurements (1962, 1963, 1967) indicate that the coefficient K_4 is

some 100 times smaller than the two-fold anisotropy at very low temper-

atures. Pressure greatly decreases the magnitude of K_1, and it can

even be made positive with very high pressures below 240K. On the

other hand, K_2 and K_3 are affected less, and have not been made to

change sign (Rhyne 1972).

Magnetostriction. The S-state character of the Gd ion also

rules out single-ion magneto-elastic contributions to the magnetization

energy. The magnetostriction is of the same order as for Co, but small

compared with the rest of the rare earth metals which display large

single-ion contributions. Mason (1954) and Bozorth and Wakiyama (1963)

have evaluated the four magnetostriction constants which Alstad and

Legvold (1964) have used to find the temperature dependence of the

magnetostriction. The latter authors found the behaviour does not

fit the single-ion theory, but seems more appropriate to a two-ion

model. Bozorth and Wakiyama (1963) showed that when comprehensive

stress is applied parallel to the a (or b) axis it increases the

molecular field. Callen and Callen (1965) used their six-constant

theory to account for the sign inversion of any particular

magnetostriction coefficient, and discussed the field dependence

of forced magnetostriction.

Specific Heat. Griffel et al (1954) have carried out a

study of the heat capacity of Gd in the range 15 to 355K. The

results show a broadened "lamba"-type anomaly at 291.8K. This

is lower than the T_c determined from magnetic methods. These

authors calculated the entropy, enthalpy and Gibbs function based

on a Debye temperature 152K. However, the determination of θ_D

is generally difficult because of the admixture of a large magnon

specific heat (spin wave scattering). Lounasmaa (1966) assumed

a linear increase in θ_D with atomic number across the rare earths,

with the end points being relatively unambiguously defined as

θ_D = 142K for La, and θ_D = 210K for Lu. On this basis, θ_D for Gd

would seem to be about 176K, agreeing well with the value obtained from

sound velocity measurements (Rhyne 1972).

Transport Properties. With the possible exception of numerous

studies of the superconducting behaviour of La and its alloys, there

has been significantly less work done on the transport properties of

the rare earths than on studies of their magnetic properties.

Electrical resistivity studies have been carried out on Gd by Nellis

and Legvold (1969). They observed an anamolous behaviour in the region

210-250K which corresponds to the region of rapid deviation of the

magnetic moment away from the hexagonal c axis. In other work by Nigh

et al (1963) it was shown that the a axis resistivity changes slope at

293.2K while the c axis resistivity exhibits a small maximum at about

292K (arising probably from short-range magnetic ordering effects)

(Taylor and Darby 1972), with a shallow minimum at 340K. No anomalous

behaviour in the region 210-250K appears in the c axis data, probably

because abnormally high scattering of electrons near and just below T_c

along the c axis obscures the effect of the change in the easy

direction. The hump at T_c could be due to a combined Fermi surface

plus fluctuation effect (Spedding 1972). In Gd the electrical

resistivity due to magnons (spin wave scattering) is the highest for

all the metals, and leads to the highest resistivity at room temperature,

the value being 140μΩ in the a axis direction. It appears that the

highest temperature slope for the saturation magnon resistivity

contribution along the a axis in Gd is approximately 1.2 times that

along the c axis, while the estimated ratio of the respective saturation

resistivities is about 1.1.

The thermal conductivity work of Nellis and Legvold (1969b)

shows a sharp rise at 20K and 30K for the c and a axis conductivities

respectively due to the enhanced contributions of phonons and magnons

at these temperatures. The ratio $K\rho/T$, (where K is thermal conductivity

and ρ is electrical resistivity) is too high to be accounted for by

electrons alone. Above 30K there is a marked decrease in thermal

conductivity due to the scattering by phonons and magnons. There is a

sharp minimum in the a axis data at T_c, but the corresponding minimum

in the c axis data is very broad. Above T_c the thermal conductivity

rises in what appears to be a monatonic fashion.

The Hall effect in Gd is higher than in other rare earths

by almost an order of magnitude. The c axis coefficient is positive

at low temperatures, decreasing almost monatonically with increasing

temperature, until it becomes negative at about 170K. The a axis

coefficient, on the other hand, is negative below 180K, and positive

at higher temperatures. The spin Hall coefficients are negative and very large along both axes (Wybourne 1965, Unsworth 1969).

Both the c and a axis Seebeck coefficients are negative over the temperature range from 10K to 300K. However, the c axis coefficient has a sharp peak at about 30K while the a axis coefficient behaves reasonably linearly (Lounasmaa and Sundström 1967). Legvold (1972) estimated the magnon contributions to the Seebeck coefficient and obtained the requisite near-zero value above T_c in the basal plane with a slight adjustment required to obtain this in the c direction. The magnon contribution is strongly peaked at 24K very close to the 24K thermal conductivity peak; this can be attributed to the split in the conduction band into the spin-up and spin-down bands due to the internal magnetic field.

CHAPTER 2

FERROMAGNETIC DOMAINS

2.1   The Free Energy of a Magnetic System

The discussion of Gd in the preceding chapter has shown that it behaves, in a microscopic way, like a "normal" ferromagnet: below T_c "it becomes spontaneously magnetized". That discussion, however, applies to a single domain particle; a multi-domained sample will not exhibit any net magnetization in the absence of an external field even below T_c. In the preceding chapter, the examination was a microscopic one, detailing how the various energy terms, principally the exchange, anisotropy and magnetostriction terms, give rise to the phenomenon of spontaneous magnetization within each domain of Gd below T_c. This chapter involves a more microscopic treatment where these and other terms give rise to magnetic domains wherein the ferromagnetic material spontaneously divides itself into volumes of saturated magnetic order so that its total energy can be minimized.

The Weiss theory of ferromagnetism (long-range order) is covered in Chapter 3 which deals with critical phenomena. The theoretical approach of that chapter must be applied, once again, only to a single domain particle. In a real crystal, the magnetic vectors of the various domains are isotropically aligned throughout the crystal, and the effect of the application of an external applied field is to align these vectors either by changes in domain shape or by actual rotation of the magnetization vectors.

Exchange Energy. At T_c the tendency of the magnetic carriers to become aligned is small compared to their thermal energy. The Weiss molecular field necessary to overcome the thermal fluctuations would be given by:

$$H_\omega \sim \frac{kT_c}{|\underset{\sim}{\mu}_s|} \simeq 10^9 \ A/m \qquad (13)$$

where k is Boltzmann's constant, and $\underset{\sim}{\mu}_s$ is the spin magnetic moment of an electron:

$$\underset{\sim}{\mu}_s = \frac{-g_J \ \mu_B}{\hbar} \ \underset{\sim}{s} \qquad (14)$$

($\hbar = \frac{h}{2\pi}$), h being Planck's constant. $\underset{\sim}{s}$ is the electron spin angular momentum. However, the field at any one point in a crystal due to the magnetic effect of an electron at a neighbouring point is only of the order:

$$H_e = \frac{|\underset{\sim}{\mu}_s|}{a^3} \simeq 10^5 \ A/m \qquad (15)$$

where a is the lattice parameter. In quantum mechanical terms, the parallel arrangement of spins is explained by the application of the Pauli exclusion principle to the specific atomic configuration. This may require that the spins be parallel or anti-parallel. In the ferromagnetic case the spins are parallel. In the Heisenberg model, we denote the extra term of interaction between neighbouring atoms by the exchange integral $\mathcal{J}$, which from molecular field theory is given by:

$$|\mathcal{J}| = \frac{3kT_c}{2ZS(S+1)} \qquad (16)$$

where Z is the number of nearest neighbours, and S is the spin quantum number. If we consider the exchange interactions occurring between nearest neighbours, and we neglect anisotropy effects, then the exchange energy is:

$$\mathcal{E}_{ex} = -2\mathcal{J}S^2 \sum_{i>j} \cos \phi_{ij} \qquad (17)$$

where ϕ_{ij} is the angle between the direction of the spin momentum vectors of atoms at sites i and j. For small ϕ_{ij}, we can replace $\cos_{ij}$ by $1 - \tfrac{1}{2}\phi_{ij}^2$, and the part of the exchange energy which varies with angle

between spins is given by:

$$\Delta \,\mathcal{E}_{ex} = \mathcal{J} \, S^2 \phi_{ij}{}^2 \tag{18}$$

Therefore, the exchange energy will be a minimum when the spins are parallel.

Magnetocrystalline Anisotropy Energy. The magnetic anisotropy contribution to the total free energy of a crystal will be a minimum when the various domain magnetizations lie along the easy direction of magnetization. The excess energy required to magnetize a crystal in a given direction over that required for the easy axis for a hcp lattice is given by Eq.11 of Chapter 1. Since the exchange interaction does not of itself lead to anisotropy, and the ordinary magnetic moment interaction between electrons leads to values too small to account for observed effects, the existence of anisotropy implies the interaction of the electronic orbits with the crystal lattice. This has been discussed more fully in Chapter 1.

Magnetostatic Energy. The action of an applied field $\underset{\sim}{H}_a$ on a domain magnetized to an intensity $\underset{\sim}{M}_s$ in a direction making an angle θ with $\underset{\sim}{H}_a$, is to exert on it a couple equal to $M_s H_a \, sin \, \theta$ per unit volume, tending to rotate the magnetization towards the field direction. The contribution to the free energy of the system is therefore:

$$\mathcal{E}_{mag} = -M_s H \, cos \, \theta \tag{19}$$

where $\underset{\sim}{H}$ is the field actually acting on the domain taking demagnetizing fields into account.

When no external field is applied, a magnetized body has a certain magnetostatic energy which may be calculated as the work required to assemble all the constituent dipoles, equal to:

$$\mathcal{E}_{mag} = -\tfrac{1}{2} \, M_s H_D \, cos \, \theta \tag{20}$$

The factor $\tfrac{1}{2}$ is introduced since without it each dipole would be accounted for once as a source of field, and again as a component of

magnetization. $H_{\sim D}$ is the demagnetizing field of the specimen; the demagnetizing field is generally far greater than that which would be required to overcome any magnetic crystalline effects, so that the uniformly magnetized or saturated state is unstable unless a high external field is applied. For an ellipsoid of revolution the demagnetizing field is given by:

$$H_{\sim D} = -N_{w}M_{\sim s} \qquad (21)$$

where N_w is the demagnetizing factor for the sample. Therefore:

$$\mathcal{E}_{mag} = \tfrac{1}{2} N_w M_s^{2} \cos\theta \qquad (22)$$

so that a minimum magnetostatic energy is attained for $\theta = \pi$ radians.

Magnetostriction. Because the exchange energy and the anistropy energy both depend on the interatomic spacing of the lattice, strain on a crystal will alter the direction of the intrinsic magnetization. In this way the preferred directions of domain magnetization may be affected not only by the magnetocrystalline anisotropy, but also by the presence of strained regions within the material. The effect of strain is to change the directions of the anisotropy energy minima with respect to the lattice. When the direction of easy magnetization is not parallel to the c axis, we may regard the magnetostriction constant as the fractional change in length that occurs when we change the direction of saturation from parallel to the c axis to any other direction. If the domain structure is such that the magnetization is always parallel or anti-parallel to a given direction defined by θ_0 and $\phi = 0$ (refer to Eq.11 of Chapter 1), λ in any direction (θ,ϕ) can be calculated by evaluating $\lambda(\theta, \phi) - \lambda(\theta_0,0)$ for the appropriate values of the direction cosines. If we assume that the domains in an unmagnetized crystal are oriented at random in a cone with semi-angle θ_0, we can use θ_0 and the anisotropy constants to calculate the magnetostriction in a direction when the material is saturated in this or any other direction.

<u>Domain Wall Energy.</u> Domains are a natural consequence of the minimization of the energy which consists of exchange, anisotropy, magnetostatic and magnetostrictive contributions. The exchange energy favours complete alignment of the spins, with anisotropy favouring the easy axis; due to the resulting large magnetostatic energy of the saturated state, the sample spontaneously subdivides into domains. Strains complete the picture by causing variations to the exchange and anisotropy contributions.

Given a crystal subdivided into domains where the magnetization is oriented parallel to one of the easy directions, we now have regions existing where the magnetization changes from one domain to the next. The change is not discontinuous because of the exchange energy required for that (Bloch 1932), and the regions of transition are called domain walls, or Bloch walls. A further contribution to the total free energy of an unsaturated crystal now arises because it is clear that domain boundaries may only form at the expense of a finite amount of energy.

While it is clear that the exchange energy does not allow a discontinuous change between domains, it is equally obvious that anisotropy will prevent the existence of an infinite Bloch wall. Within the wall, the tendency of the exchange interaction to make adjacent spins parallel is overcome, and each spin is misaligned slightly from its neighbours, the wall width being determined by the number of lattice distances traversed to produce an overall transition under the limitations imposed by anisotropy.

The simplest domain wall to consider mathematically is that separating two domains magnetized in opposite directions; this is known as the 180° Bloch wall. In the ideal case, it is assumed that the rotation of the magnetization across the wall is such that the magnetization always lies parallel to the plane of the wall. Assuming that

the domain configuration has made the magnetostatic energy zero,

the optimum width of the wall is that which makes the sum of the

exchange and anisotropy energies a minimum (Kittel and Galt 1956).

If we assume that there are a large number of atomic spacings in the

wall so that the angle between adjacent spins is small, the total wall

energy per unit area is:

$$W = \Delta \mathcal{E}_{ex} + \Delta \mathcal{E}_{cf} \tag{23}$$

$$= \mathcal{J} \frac{S^2 \pi^2}{N a^2} + K N a \tag{24}$$

where N is the number of lattice distances per wall width. The wall

energy is a minimum with respect to N when:

$$N = \left| \frac{\pi^2 A}{2 a^2 K} \right|^{\frac{1}{2}} \tag{25}$$

where $A = \frac{2 \mathcal{J} S^2}{a}$ is the exchange constant. The optimum width of the wall

is:

$$\delta = N a = \left| \frac{\pi^2 A}{2 K} \right|^{\frac{1}{2}} \tag{26}$$

and $$W = (2 \pi^2 A K)^{\frac{1}{2}} \tag{27}$$

An order of magnitude calculation for Gd in the region $T \simeq 290K$ has been

carried out using $A \simeq 4 \times 10^{-12} \ J/m$, $K = 2 \times 10^4 \ J/m^3$, and $a \simeq 4 \times 10^{-10} m$.

This leads to $N \simeq 45$ atoms, and $W \simeq 1.2 \times 10^{-3} \ J/m^2$, with both N and W

decreasing as M_s towards T_c.

2.2   Domains and Domain Walls

Domain Directions. If all the necessary physical properties

of the crystal and its surroundings are known, it should, in principle,

be possible to deduce the optimum domain configuration so that the

crystal is in a state of minimum free energy corresponding to a

particular value of the applied field, ie:

$$\mathcal{E} = \mathcal{E}_{ex} + \mathcal{E}_{cf} + \mathcal{E}_{mag} + \mathcal{E}_{ms} + \mathcal{E}_{W} \tag{28}$$

should be a minimum where $\mathcal{E}_W$ is the total wall energy:

$$\mathcal{E}_W = S_d W \tag{29}$$

S_d being the total domain wall area of the specimen. Given that the domain wall energy has been minimized by wall configurations, the domain directions will be largely determined by $\mathcal{E}_{cf}$, $\mathcal{E}_{mag}$ and $\mathcal{E}_{ms}$. Only when the material is sufficiently strain-free does $\mathcal{E}_{cf}$ decide the direction of the vectors. Also, only when $\mathcal{E}_{mag} \gg \mathcal{E}_{cf} + \mathcal{E}_{ms}$ can its direction be fixed uniquely (ie, domain wall rotation does not dominate in low fields). There must always exist a minimum internal stress:

$$S_T = \lambda E_{YM} \tag{30}$$

where E_{YM} is Young's modulus for the material, and it is therefore appropriate to divide ferromagnetic materials into two groups according to whether $\mathcal{E}_{cf} \gg \mathcal{E}_{ms}$ or not (Carey and Isaac 1966).

Domain Nucleation and De-nucleation. It appears that relatively little work has been carried out in the study of the nucleation of domains in a ferromagnetic material as it is cooled from the paramagnetic phase to the ferromagnetic phase. We have studied the nucleation of domains in Gd just above T_c, and details of the results appear in Chapter 6.

The nucleation and denucleation of domains in strong fields has received more attention. In zero applied field it has been shown that domains form spontaneously in order to minimize the total free energy of the sample. As the applied field is increased, however, the demagnetizing field will be overcome to the extent of allowing domains to denucleate. This state is approaching that of saturation. Brown (1945) calculated the lower limit of the critical field for saturation to be:

$$-H_{nf} \geqslant \frac{2K}{M_s} - N_w M_s \tag{31}$$

while the upper limit has been found to be:

$$-H_{nf} \leqslant \frac{2K}{M_s} - N_w M_s + 2\pi M_s f \left(\frac{R}{R_o}\right)^{-2} \tag{32}$$

(Brown 1957, Frei et al 1957), where R is the radius in a direction

perpendicular to z, of the ellipsoid of revolution studied; f is a

numerical factor equal to 1.38 for a sphere and 1.08 for an infinite

cylinder; and $R_0 = A^{\frac{1}{2}} M_s^{-1}$. For Gd just below T_c, the first term of

the right hand side of Eq.31 will largely determine H_{nf} due to the

finite anisotropy near T_c, and an order of magnitude calculation using

$M_s = 0.5 \ wb/m^2$ leads to $H_{nf} \simeq 4 \times 10^4 \ A/m$. This is the upper limit

for the existence of domains; it points to the relatively large

field required to prevent the nucleation of domains in Gd just below T_c.

Reverse domains can nucleate in an initially saturated

specimen. This should constitute a very considerable resistance to

the process of demagnetization in many specimens, but in fact it is only

rarely of importance. Brown (1945) has suggested that reverse domains would

not form in a uniquely magnetized specimen unless it were subjected to

very large reverse fields. Goodenough (1954) made a detailed study of

the possible centres at which reverse domains might nucleate in a

saturated polycrystalline sample, and concluded that centres most

likely to produce reverse domains are grain boundaries or the boundaries

between lamillar precipitates and the matrix. For grain boundaries, he

found the contribution to the coercive force from such a process to be:

$$H_c = \frac{\pi}{6M_s} (\rho*)_{av}^2 \tag{33}$$

where $(\rho*)_{av}$ is the average of the grain surface pole density;

for lamillar precipitates:

$$H_c = \frac{G \ V_p}{M_s} (\rho*)_{av}^2 \tag{34}$$

where G is a constant and V_p is the volume fraction of precipitate

present.

180° Bloch Wall. We return to a more accurate discussion of

the 180° Bloch wall as a prelude to a study of domain movement processes.

If we consider a square lattice with domain walls having magnetization

vectors parallel to the planes of the walls, and we minimize the
exchange and anisotropy energies with respect to θ (the angle between
the direction of the magnetization at any point in the wall and that
in one of the domains), we find that:

$$W = \sqrt{4AK} \tag{35}$$

and that the displacement perpendicular to the wall is given in terms
of θ by:

$$y = -\sqrt{\frac{A}{K}} \log \tan \theta \tag{36}$$

It can be seen that $|y| \to \infty$ for $\theta = 0$, $\frac{\pi}{2}$, so that the solution only
provides for a transition through 90°. This is because the chosen
co-ordinate axes are the directions of minimum anisotropy energy, and
90° is therefore the simplest transition from one easy direction to an
adjacent one. Both Néel (1944C) and Lifshitz (1944) have pointed out
that the solution for a 180° transition may be produced by considering
two such 90° transitions as occurring with an infinite distance between
them. However, the effects of magnetostriction are such as to make the
two 90° walls fuse into a single 180° wall because the domain that
would otherwise lie between the two would be in a state of strain.

Damped Domain Wall Motion. As a consequence of the angular
momentum associated with the atomic moments or spins, a domain wall
has an effective mass. Because the spins are confined to the plane of
the domain wall, the action of a field in pushing the wall along this
plane forces the spins to rotate; this force, moreover, induces
precession in each spin which results in a rotation of spins outside
the domain wall. This results in a component of magnetization perpen-
dicular to the wall which gives an additional energy contribution:

$$W_v = \tfrac{1}{2} M_W v_W^2 \tag{37}$$

where v_W is the wall velocity and M_W is the effective wall mass per
unit area:

$$M_W = \frac{\mu_0 W}{2\nu^2 A} \tag{38}$$

where ν is the gyromagnetic constant equal to $g_J e\, \mu_0/2m_e$. In linear co-ordinates, the equation of motion for damped wall motion is usually expressed as:

$$M_W \frac{d^2 y}{dt^2} + \frac{\beta dy}{dt} + ry = 2M_s H \tag{39}$$

where β is the damping coefficient and ry is the restoring force. The $2M_s H$ is the pressure acting for a 180° wall, and should be replaced by $\sqrt{2}\, M_s H$ for a 90° wall. In polar co-ordinates, the equations of motion can be evaluated from Gilbert's (1955) equation equating the torque due to the field to the rate of change of angular momentum:

$$\frac{d\underset{\sim}{M}}{dt} = \gamma_{mc}\, \underset{\sim}{M} \times \underset{\sim}{H} - \frac{r}{M}\, \underset{\sim}{M} \times \frac{d\underset{\sim}{M}}{dt} \tag{40}$$

where

$$\gamma_{mc} = \frac{g_J\, e}{2m_e c} \tag{41}$$

The spins are considered to be aligned at θ to the z axis in the plane of the wall and at ψ to the axis perpendicular to the wall in the plane perpendicular to the wall (Dillon 1963). Then:

$$\frac{d\underset{\sim}{M}}{dt} = \gamma_{mc} \left(\frac{\partial \mathscr{E}}{\partial \psi}\right) - \frac{r}{M}\, \underset{\sim}{M} \times \frac{d\underset{\sim}{M}}{dt} \tag{42}$$

Separating Eq.42 into its two constituent parts, we obtain the equations of motion:

$$\dot\theta - r\dot\psi\, sin\, \theta = \frac{\gamma_{mc}}{M_s\, sin\, \theta} \left(\frac{\partial E}{\partial \psi}\right) \tag{43}$$

and

$$\dot\psi\, sin\, \theta + r\dot\theta = \frac{\gamma_{mc}}{M_s} \left(\frac{\partial E}{\partial \psi}\right) \tag{44}$$

Assuming ψ is a constant ($\psi = \psi_0$) and that the wall moves steadily, we obtain:

$$v_W = \frac{\gamma_{mc} H}{r} \sqrt{\frac{A}{K}} \left\{ 1 + \frac{\pi M_s^2}{K} \left(1 - \sqrt{1 - \left(\frac{H}{2\pi M_s r}\right)^2} \right)^{-\frac{1}{2}} \right\} \tag{45}$$

where v_W is the wall velocity in the y direction. As $H \to 0$:

$$v_W \to \frac{\gamma_{mc} H}{r} \sqrt{\frac{A}{K}} \qquad (46)$$

A comparison of Eqs. 46 and 36 shows that in the limit of small applied field, the damped wall behaves like an undamped wall with respect to the wall parameter $\sqrt{\frac{A}{K}}$. For $H > 2\pi M_s r$, v_W becomes imaginary, implying the existence of a critical field value at:

$$H_{CRD} = 2\pi r M_s . \qquad (47)$$

Finally, the shape of the moving wall is such that for bi-axial anistropy:

$$log \; tan \; \theta = -y \sqrt{\frac{K}{A}} \left\{ 1 + \frac{\pi M_s^2}{K} \left(1 - \sqrt{1 - \left(\frac{H}{2\pi M_s r}\right)^2} \right)^{\frac{1}{2}} \right\} \qquad (48)$$

which for $H \to 0$ is:

$$log \; tan \; \theta = -y \sqrt{\frac{K}{A}} \quad \text{which agrees with Eq.36 for a stationary}$$

wall.

Thin Domain Walls. We have shown that the domain walls in Gd just below T_c can be expected to be thin due to the small value of the wall parameter $\sqrt{\frac{A}{K}}$. A 180° wall 45 atoms thick would, on the average, be expected to have 4° between neighbouring spins. The continuum approach, which relied on this angle being small, might not be applicable to Gd just below T_c.

The phenomenon of thin domain walls has been the subject of studies by Zijlstra and Van den Broek (1970, 1971); it has been cited as a possible cause of the intrinsic magnetic after-effect studied by Taylor (1971) and Hunter (1973). Zijlstra considered a thin domain wall to have a central region where the moment directions change abruptly; this region is bounded by regions of more gradual change. The model enables the central moments to be anti-parallel for $\frac{K}{A} \to \frac{2}{3}$, and predicts a sharp energy barrier if the central moment lies perpendicular to the easy direction of magnetization. From Eqs. 27 and 38 it is seen that the

domain wall mass is proportional to $(\frac{K}{A})^{\frac{1}{2}}$, and so will be large for a thin wall. This has been called the "intrinsic coercivity".

Egami (1973) has applied quantum mechanical and thermal activation theories to the barrier, based on pinning mechanisms. Taylor (1972) has devised a more successful model by assuming a different magnetization rate dependence on the applied field. Experimental studies by Barbara et al (1972) and Taylor et al (1972) have shown that the intrinsic coercivity in the rare earths does not completely pin the domain walls.

2.3   The Magnetization Curve

The shapes of both the "virgin curve" and the subsequent hysteresis cycle on a H vs M plot are well-known. The initial part of the virgin curve is reversible; it rises steeply in the irreversible region, and then levels out as the process of reversible domain wall rotation begins to dominate. Finally, M becomes independent of H when saturation is reached. The initial part of the hysteresis cycle is again reversible, followed by the same irreversible and reversible processes until the sample reaches saturation under a large reversed field. The non-zero magnetization at zero field is known as the remanance and the reverse field necessary to reduce the magnetization to zero is called the coercive force. The area inside the hysteresis loop represents the work done by the field in progressing through one cycle.

The total process is called "technical magnetization" because it involves changes in the sizes and directions of domains rather than in the intrinsic magnetization of the domains. The initial reversible region consists mainly of reversible domain wall displacements, with domains whose direction is similar to that of the applied field, growing at the expense of others. In the irreversible region, both

irreversible domain wall displacement and irreversible domain wall
rotation take place; a fine examination reveals that the magnetization
changes by discrete steps called "Barkhaussen steps".

Reversible Displacement Magnetization. Reversible domain
wall displacement dominates in the initial reversible region. It can
only take place when irregularities are present which cause variations
in energy for the domain wall displacement; of itself, displacement
will not cause variations in the surface energy of the wall in a uniform
material, so that the removal of a field in such an environment would
not cause the wall to return to its original position.

We assume that the energy of a domain wall is changing with
displacement as shown in Figure 1.
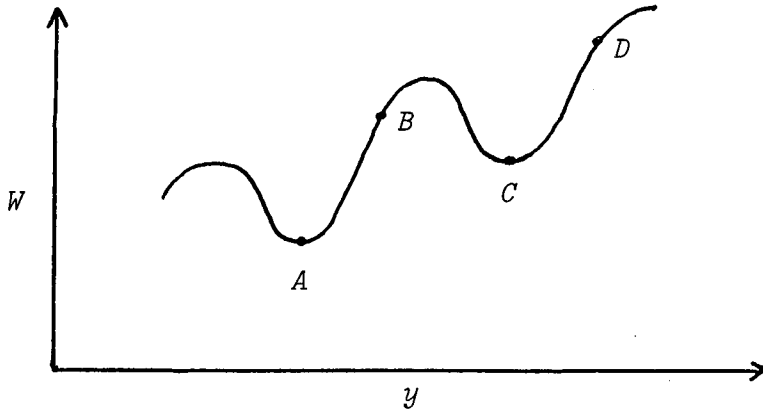
FIG. 1 : VARIATION OF WALL ENERGY WITH DISPLACEMENT

In the absence of a magnetic field the wall stays at some minimum point
A where $\frac{\partial W}{\partial y} = 0$. The energy can be expressed as an approximation

$$W \simeq \tfrac{1}{2} \alpha_{curv} y^2 \tag{49}$$

in the vicinity of A, where α_{curv} is the second derivative of the wall
energy at A. The application of a field $\underset{\sim}{H}$ in a direction at θ to $\underset{\sim}{M}_s$,
adds the usual magnetostatic energy to Eq.49, and equilibrium is reached
when:

$$y = \frac{2M_s H \cos \theta}{\alpha_{curv}} \tag{50}$$

The magnetization in the direction of $\underset{\sim}{H}$ is increased by this displacement, and:

$$\chi_{in} = \frac{4M_s{}^2 y}{3\alpha_{curv}} \tag{51}$$

To account for the fluctuations in energy of a domain wall, Chikazumi (1964) has slightly altered Kernsten's work (1938). He applied a stress theory with a sinusoidal variation in stress:

$$S_T = S_{TO} \cos \left(\frac{2\pi \ Area}{\ell} \right) \tag{52}$$

where ℓ is the wavelength of the spatial variation of the internal stress. He obtains for a domain wall:

$$\chi_{in} = \frac{2M_s{}^2 \ell}{\pi^2 \lambda S_T \delta} \tag{53}$$

When the specimen cools through T_c, the stresses that occur may be as low as that given by Eq.30 so that:

$$\chi_{in} \simeq \frac{2M_s{}^2}{9\lambda^2 E_{YM}} \tag{54}$$

for $\ell \simeq \delta$. An order of magnitude calculation for Gd at 290K using $M_s \simeq 0.5 \ wb/m^2$, $\lambda \simeq 10^{-5}$, and $E_{YM} \simeq 4 \times 10^{10} \ N/m^2$, gives $\chi_{in} \simeq 0.015$ H/m. An alternative mechanism is based on the pinning of the domain walls at their extremities. The pressure exerted by the field causes a bulging of the wall. If the radius of curvature remains less than ½ the separation between the pinning points, this movement will be reversible. This gives:

$$\chi_{in} = \frac{2M_s{}^2 \ell_1}{9W} \tag{55}$$

where ℓ_1 is the distance between constraining points. For $\ell_1 \simeq 10^{-4} \ m$, $W = 1.2 \times 10^{-3} \ J/m^2$ and $M_s \simeq 0.5 \ wb/m^2$, $\chi_{in} \simeq 0.5$ H/m.

Reversible Rotation Magnetization. This process is most evident in relatively high fields just below saturation. If the field H makes an angle θ_0 with the easy axis, equilibrium is reached when the magnetization makes an angle θ with the field such that:

$$\frac{sin\ 2\ (\theta - \theta_0)}{sin\ \theta} = \frac{2M_sH}{K} \tag{56}$$

In a very weak field, where $H \ll \frac{K}{M_s}$, θ is nearly equal to θ_0 because the magnetization will remain near the easy axis. The initial susceptibility from the reversible rotation is:

$$\chi_{in} = \frac{M_s^2\ sin^2\theta_0}{2K} \tag{57}$$

An order of magnitude calculation yields a maximum contribution from this source of $\chi_{in} \simeq 6 \times 10^{-6}$ H/m in Gd immediately below T_c. This is much less than the contributions from the reversible displacement mechanisms.

Irreversible Domain Wall Displacement. The shape of the hysteresis curve at the onset of irreversibility is generally leaf-like. Rayleigh expressed this portion of the curve as:

$$M = \chi_{in}H + \tfrac{1}{2}\eta H^2 \tag{58}$$

where η is the Rayleigh constant. The first term of Eq.58 describes reversible magnetization to a good approximation, and the second term results from irreversibility. The resultant leaf-like loop is called the Rayleigh loop.

Given that the energy variation with domain wall displacement is as shown in Figure 1, under the action of an applied field the wall will attain an equilibrium position where:

$$2HM_s = \frac{dW}{dy} \tag{59}$$

If H is increased until $2HM_s$ is greater than the maximum value of $\frac{dW}{dy}$, the wall will move spontaneously and irreversibly to the point D.

If the field is then decreased, the wall will go to C, giving rise to hysteresis.

The strain theory, which was first suggested by Becker (1932) as a possible mechanism for the variation of domain wall energy with displacement, predicts a critical field for the transition to irreversibility of:

$$H_{CRR} = \frac{\pi \lambda S_T}{M_s} \qquad (60)$$

Using Eq.27 with $E_{YM} \simeq 4 \times 10^{10}$ N/m^2, we obtain $H_{CRR} \simeq 25$ A/m for Gd at 290K.

The inclusion theory proposed by Kernsten (1943) is based on variations in domain wall energy brought about by changes in domain wall area with position due to the presence of non-magnetic inclusions. It predicts a critical field for irreversibility of:

$$H_{CRR} = \frac{W \pi d}{2 M_s \alpha^2} \qquad (61)$$

Using $d \simeq 0.8 \times 10^{-10} m$, one can obtain for Gd just below T_c, $H_{CRR} \simeq 1.8 \times 10^6$ A/m. Thus one would expect the predominant mechanism for irreversibility to be the stress mechanism.

Kernsten (1956) used the pinning model described previously to explain the coercive force dependence on the composition of iron-nickel alloys. When the wall expands beyond the point where its radius of curvature is greater than one-half the distance separating the constraining points, the wall expands discontinuously. The critical field for this discontinuous expansion is given by:

$$H_{CRR} = \frac{W}{M_s \ell_1 \cos \theta} \qquad (62)$$

where θ is the angle between the applied field and the direction of easy magnetization. Based on previously stated figures, $H_{CRR} \simeq 25$ A/m, in good agreement with the critical field for the stress mechanism. On the other hand, the critical field necessary to break the wall ends free of the constraining points is:

$$H_{CRR} \simeq \frac{1.5 \times 10^5 M_s r^2}{\ell_1 \cos \theta} \tag{63}$$

where r is the radius of curvature of the wall when it breaks free.

For $r \simeq 10^{-5} m$, $H_{CRR} \simeq 7.5 \times 10^4$ A/m, and it is clear that the discontinuous expansion will take place long before the wall leaves its pinning points (Chikazumi 1964).

Irreversible Rotation. This process occurs mainly in relatively high fields. Consider a uniaxial anisotropy whose easy axis makes an angle θ_0 with the field. Let θ be the angle through which the magnetization is rotated by the field. Equilibrium will occur when $\frac{d\mathcal{E}}{d\theta} = 0$, whence:

$$H_c \simeq \frac{K \sin 2(\theta - \theta_0)}{M_s \sin \theta} \tag{64}$$

If this equilibrium condition is stable, $\frac{\partial^2 \mathcal{E}}{\partial \theta^2} > 0$, while it is unstable if $\frac{\partial^2 \mathcal{E}}{\partial \theta^2} < 0$. Thus for stability, the critical field is given by:

$$H_{CRR} = \frac{2K \cos 2(\theta - \theta_0)}{M_s \cos \theta} \tag{65}$$

The minimum value for this critical field is obtained for $\theta = 45°$ whence,

$$H_{CRR_{min}} = \frac{K}{M_s} \tag{66}$$

while the maximum field is required for $\theta = 0$ or $90°$, whence:

$$H_{CRR_{max}} = \frac{2K}{M_s} \tag{67}$$

The minimum value for H_{CRR} in Gd just below Tc would be of the order of 8×10^4 A/m.

In randomly oriented polycrystalline materials with uniaxial anisotropy, rotational processes cannot be distinguished from domain wall displacement to the same extent as for cubic materials. It seems possible only to assume that the earlier stages of magnetization are

primarily due to the motion of walls aligned nearly parallel to the field direction, and the latter stages to rotation together with the motion of walls which make large angles with the field direction (Tebble and Craik 1969).

Intrinsic Coercivity. In Section 2.2 we noticed that for thin domain walls there is a sharp energy barrier if the central moment of the wall lies perpendicular to the easy direction of magnetization. It will thus be more energetically favourable for the wall to adopt a configuration where no spin lies in this position. This results in the material having an "intrinsic coercivity". In the limit of $\frac{K}{A} \rightarrow \infty$, the intrinsic coercive force approaches the magnitude of the anisotropy field $\frac{2K}{M_s}$. In Gd, $\frac{K}{A} \simeq 5 \times 10^{15} m^{-2}$ at 290K, and $\frac{2K}{M_s} \simeq 8 \times 10^4 A/m$.

2.4 Magnetic After-Effect

Magnetic after-effect is the general name given to the retarding mechanism by which the change in magnetization is delayed with respect to a change in field. Eddy currents are excluded as are magnetization changes accompanying structural change or aging of the material. Consider a linear system acted upon by an external "force":

$$X = X_0 e^{i\omega t} \qquad (68)$$

with the resulting displacement Y being given by:

$$Y = Y_0 e^{i\omega t} \qquad (69)$$

Between Y_0 and X_0 there exists a relation of the form:

$$Y_0 = \varepsilon(\omega) X_0 \qquad (70)$$

where ε is a constant for variations in the amplitudes X_0 and Y_0, but may depend on ω. $\varepsilon(\omega)$ may be complex in which case energy is dissipated. The most complex case is met when ε consists of an independent constant part and a part which has a phase lag because of the delay:

$$\varepsilon = \varepsilon_0 + \frac{\varepsilon_1}{1+j\omega} \qquad\qquad (71)$$

where $\varepsilon = \varepsilon_0 + \varepsilon_1$ for $\omega = 0$ (static measurements), and $\varepsilon = \varepsilon_0$ for

$\omega \gg \frac{1}{\tau}$. τ is called the response time. The loss angle is given by:

$$tan\ \phi = \frac{\varepsilon_1}{\varepsilon_0}\ \frac{\omega\tau}{1+\omega^2\tau^2} \qquad\qquad (72)$$

Generally, *tan* ϕ is called the loss factor. *Tan* ϕ becomes zero in the

limits of $\omega\tau \to 0$ and $\omega\tau \to \infty$ (Snoek 1949).

When a magnetic field is suddenly changed this type of

behaviour is found in the magnetization. It changes abruptly by an

amount M_I, and then gradually by an amount M_n characterized by the

response time τ. The character of M_n depends both on M_I and on the

final stage of magnetization, being fast in the reversible rotation

region and slow in the irreversible region. Usually the relaxation times

are well distributed throughout the sample.

<u>Jordan Lag</u>. (Jordan 1924). For very large τ, *tan* ϕ should

tend towards zero. However, if for example, τ is distributed over a

very wide range, there remains a finite loss factor which is independent

of frequency and temperature. If the range of τ extends from τ_1 to τ_2,

we can obtain an expression for the fractional change in M_n as a function

of time:

$$\frac{\Delta M_n}{M_n} = Const - \beta\ log\ t \qquad\qquad (73)$$

the validity of which has been demonstrated in Alnico V by Street and

Woolley (1949).

<u>Magnetic After-Effect Mechanism</u>. Snoek (1949) considered that

the magnetic after-effect could be caused by the diffusion of carbon or

nitrogen atoms in the lattice. Impurities could distort the lattice

and increase the depth of the potential minima between lattice points.

Néel (1952) considered that the interstitial impurities change the

intensity of the pseudo-dipolar interaction between atoms of the
parent lattice.

For domain wall displacement, the impurities rearrange their
positions after the wall reaches equilibrium, and affect the wall
energy through a change in anisotropy energy in a way such that $\frac{\partial \mathscr{E}_{cf}}{\partial t}$
is not constant with time. On the other hand, it is assumed that
impurities do not greatly affect the anisotropy energy for reversible
rotation magnetization, so that $\frac{\partial \mathscr{E}_{cf}}{\partial t}$ is constant to a good approximation
and the anisotropy is described by a single response time (Chikazumi 1964).

Thermal Fluctuation After-Effect. This process, caused by the
thermal fluctuation of domain magnetization, was first proposed by
Néel (1949). If the size of a single domain particle is small enough so
that the potential energy barrier to spontaneous rotation in zero field
is of the same order as the coherent rotation of the spins in the domain
due to the thermal agitation $\frac{kT}{2}$ per degree of freedom, the domain
magnetization will rotate due to the thermal fluctuations. An applied
field will cause a redistribution of the spins in a time characteristic
of the precessional speed of coherent rotation caused by thermal
distortion of the crystal lattice. The history of magnetization
distribution with the thermal after-effect is not retained upon a change
in magnetic state, so that it does not obey the superposition principle
as does the diffusion after-effect previously described.

Disaccommodation. Disaccommodation is a gradual decline in
permeability after the application of a magnetic field or mechanical
stress. It refers to the time change in the ease of magnetization, and
not, as do the usual magnetic after-effects, to the change in the
intensity of magnetization. With respect to rotation processes, the
impurity atoms diffuse into favourable sites and stabilize the domain
magnetization direction; with wall displacement processes, the
impurities diffuse to the new positions of the walls, and stabilize the

spins via local anisotropy. This mechanism can give up to a 90% change in susceptibility for displacement less than the domain wall thickness (Chikazumi 1964).

Intrinsic Magnetic After-Effect. Taylor (1971) has observed that in the pseudobinary series Dy (Co, Ni)$_2$ the magnetization increases more rapidly above a critical field than below it, and that it is time-dependent above this critical field. He found that the critical field was dependent on the composition of the specimen and on the rate at which the field was applied. He called the phenomenon the intrinsic magnetic after-effect, and it has been attributed to thin domain walls, some of the theory of which has been discussed earlier in this chapter.

CHAPTER 3

CRITICAL PHENOMENA

3.1   Introduction

In 1869, T. Andrews carried out experiments near the critical temperature of CO_2.   J.D. van der Waals published a classical theory of the pressure-volume isotherms of Andrews in 1873; this was the first, and still one of the most successful, phenomenological theories of phase transitions.   In many cases the various phases of matter seem quite dissimilar and separate, and transitions between them are abrupt.   Nevertheless, by varying the temperature or other thermodynamic parameters, two distinct phases can frequently be made more and more similar in their properties, until ultimately, at a certain critical point, all differences vanish.   Beyond this point only one homogeneous equilibrium phase can exist, and all changes are continuous and smooth. There are many examples of phase changes.   In this work we are concerned with the Curie temperature or critical point of a ferro-magnetic crystal at which the spontaneous magnetization vanishes to zero, but it has become evident that there are quite marked similarities between apparently very different phase transitions. This general principle is embodied in the Law of Corresponding States.

3.2   The Order Parameter

The most fundamental idea which helps elucidate the behaviour near a critical point is the concept that the transition is describable by an order parameter.   This parameter is a numerical measure of the amount and kind of ordering which is built up in the neighbourhood of the critical points.   In a ferromagnet the convenient ordering

parameter is the zero field magnetization $M_{\underset{\sim}{s}}(T)$. A qualitative

representation of magnetic order may be obtained by considering

a system as a fluid of spins, either up or down; at temperatures

well above the critical temperature there is a rapid and random

"flipping" of the magnetic moments from one orientation to the

other. However, as the temperature is lowered towards the critical

point, small "droplets" of correlated spins appear. As the critical

point is approached still further, the droplets grow in dimension;

nevertheless, the net order throughout the system remains at zero

until one reaches T_c. Below T_c, however, the net order of a single

domain particle, the spontaneous magnetization $M_{\underset{\sim}{s}}(T)$ comes into

existence and grows as the temperature is lowered, until at $T = 0$

there is total order. Most of this ordering will occur just below

T_c. Notice that even though above T_c the net magnetization is

zero, there nevertheless exists a considerable degree of "order"

in the system, as reflected in the large dimensions of the islands

of aligned spin. This order is frequently called short-range order,

as distinguished from spontaneous magnetization or long-range order.

3.3   First and Higher Order Transitions

Those transitions in which one or more first derivatives of

the relevant thermodynamic potentials change discontinuously as a

function of their variables are called first-order transitions.

In a ferromagnet at constant temperature the intrinsic magnetization

of a single domain particle changes abruptly from $-M_s(T)$ to $M_s(T)$ as

the field passes through zero. On the other hand, transitions in

which the first derivatives of the thermodynamic potential remain

continuous while only the higher order derivatives are divergent

are termed continuous transitions or more commonly, second or higher order

transitions. The intrinsic magnetization of a ferromagnetic single

domain particle changes continuously as one proceeds lower in

temperature through the Curie point, while the specific heat and
the susceptibility are divergent at T_c.

3.4   The Requirement for a Model

The calculation, from first principles, using the full
microscopic quantum mechanical description of the constituent
electrons and nuclei for a many-particle system which undergoes a
phase transition, even if feasible, would not necessarily increase
one's understanding of the observed behaviour of the system. The
aim of the theory must be to elucidate the general features of the
Hamiltonian of the system which lead to the most characteristic and
typical observed properties. To achieve this, the study of model
systems has been increasingly used. The recent history of critical
phenomena, has, in the main, followed the course of simplifying the
physical models while improving and strengthening the mathematical
techniques to the stage where fairly accurate theoretical treatments
can be given for models which, while gross oversimplifications of
reality in many respects, nevertheless embody a number of features
of the particles and interactions leading to phase transitions and
critical points.

If we assume that we have a physical system in thermodynamic
equilibrium, or suffering infinitesimal departures from equilibrium,
the appropriate model is that of statistical mechanics, classical
or quantum mechanical according to the dictates of the model. The
appropriate partition function is chosen and the connection is
established with thermodynamics. The intensive thermodynamic
properties derived will depend on the size of the system chosen, the
size and shape of the domain of integration, and for a given domain of
integration, the type of ensemble employed. To produce a phase trans-
ition, singularities are required in the mathematics; no singularities
are found with a finite domain of integration, and so to define a true

singularity we have to deliberately introduce an infinity. Thus

in Onsager's theory of the two-dimensional Ising model (1944), the

final stage is to let $N \to \infty$ where N is the number of particles in

the domain. This assumption is reasonable in that most physical systems

have $N \sim 10^{23}$ and we can say that this is sufficiently large for the

critical point to be well-defined. The usual argument about large

numbers in statistical mechanics is that the absolute fluctuations

are proportional to $\frac{1}{\sqrt{N}}$. Since $\frac{1}{\sqrt{N}}$ is about 10^{-11} or 10^{-12}, it would seem

reasonable enough to assume that fluctuations are, in general, of

little importance, but we find that this may not be so near the

critical point. More general theoretical arguments suggest that one

may typically see departures from ideal limiting behaviour at temperature

deviations from T_c given roughly by $\frac{\Delta T}{T_c} \sim N^{-\frac{1}{3}}$, which for Gd would mean

that measurements would have to be taken within $\sim 3 \times 10^{-6}$K of T_c.

However, present day experiments are probably limited close to T_c by

inhomogeneities, gravitational fields and other interfering factors,

rather than by finite size. These points will be further discussed

towards the end of this chapter.

3.5   Critical Point Exponents

Since much of our discussion will concern the way in which

various physical quantities diverge to infinity or converge to zero

as the temperature approaches a critical value, it is appropriate

to present a few mathematical definitions which enable critical

behaviour to be characterized numerically. Speaking loosely, we may

say that a positive function $f(x)$ varies as x^u when x approaches zero

from above, or we may write:

$$f(x) \sim x^u \text{ as } x \to 0^+ \tag{74}$$

More precisely this will mean that:

$$\underset{x \to 0^+}{Lim} \left\{ \frac{\ln d(x)}{\ln x} \right\} = u \tag{75}$$

This does not mean that $f(x)$ is simply proportional to x^u.

One must always expect correction terms of higher order which it is

hoped will be of the form:

$$f(x)_{x \to 0^+} = A x^u (1 + ax + \dots) \tag{76}$$

However, the correction terms may be large, or of a more singular

form such as $1 + ax^{\frac{1}{4}}$. Other more complex expressions may be

appropriate, and it may be very difficult to estimate the leading

exponent u from numerical data. In critical phenomena theory, the

function $f(x)$ under discussion is the ordering parameter appropriate

to the system being studied. The independent variable x is

$$\varepsilon = \frac{T - T_c}{T_c}$$

3.6 Magnetic Systems

The spontaneous magnetization $M_s(T)$ within each domain of a

ferromagnetic crystal varies as shown in Figure 2:
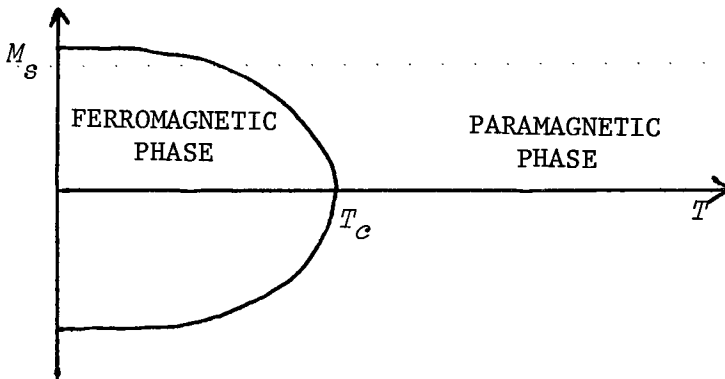
FIGURE 2 : FERROMAGNETIC - PARAMAGNETIC PHASE DIAGRAM

In this oversimplified picture we suppose that the domains are oriented

up or down, as represented by arrows. The original theory of ferromagnetism

proposed by Weiss (1907) assumes that the constituent magnetic moments

interact with one another through an artificial "molecular field"

which is proportional to the average magnetization. More specific

models have since been advanced which have the common features that

they assume the magnetic moments to be localized on fixed lattice

sites and that they influence one another through pairwise interactions

with an energy that achieves its most stable value when the moments

are parallel.

Two particular forms of the interaction have been of special

significance. In the first, the Ising model, the magnetic moments

are assumed to be classical, one-dimensional "sticks" capable of only

two orientations. In the second, the Heisenberg model, the magnetic

moments are regarded as being related to quantum mechanical three-

component spin operators, and one assumes that the energy is proportional

to the scalar product of these operators.

Whereas the Weiss model is exactly soluble, the other two

have not been solved exactly for a three-dimensional lattice.

Nevertheless the models appear to represent reasonable theoretical

descriptions of certain physical systems; and they provide considerable

insight regarding magnetic phase transitions. They belong to what

Stanley calls the "Classical Era of Critical Phenomena" (Stanley 1971).

3.7   The Mean Field Theory of Magnetic Phase Transitions

The post-Heisenberg exchange interaction interpretation

of the Weiss molecular field in terms of the pair-wise exchange

interactions $\mathcal{J}_{ij}$ between spins s_i and s_j situated at the sites i and j

of the lattice has been called the mean field theory. The properties

of a model system in which every magnetic moment interacts with every

other moment with an equal strength have been shown to be identical

to those predicted by the mean field theory.

The critical exponents predicted by the molecular field theory are identical to those of van der Waal's theory for liquids. This is not surprising since van der Waal's theory can be interpreted as an infinite interaction range model also. However most systems in nature have relatively strong, short-range interactions, and the nature of co-operative phenomena observed depends critically on the way in which those interactions "propagate order" from one particle to another. It is evident that the mean field theory provides an inadequate description of phenomena in the critical region.

The theory for a non-interacting system (paramagnetic system) predicts a magnetization of:

$$\underset{\sim}{M}(T) = \underset{\sim O}{M} B_S(Sx) \tag{78}$$

where
$$x = g_J \mu_B H / kT \tag{79}$$

$$\underset{\sim O}{M} = \underset{\sim}{M}(T=0, H=0) = NS \, g_J \mu_B \tag{80}$$

and
$$B_S(y) = \frac{2S+1}{2S} \coth\left(\frac{2S+1}{2S} y\right) - \frac{1}{2S} \coth\left(\frac{y}{2S}\right) \tag{81}$$

is the Brillouin function. Thus, in zero field there is no magnetization in a paramagnetic system. According to the mean field theory of ferro-magnetism, the interactions among the spins give rise to a magnetic field $\underset{\sim w}{H}$ in addition to the external field $\underset{\sim}{H}$. Assume that $\underset{\sim w}{H}$ is proportional to the magnetization:

$$\underset{\sim w}{H} = \lambda \underset{\sim}{M}(T,H) \tag{82}$$

whence the total field is given by:

$$\underset{\sim eff}{H} = \underset{\sim}{H} + \lambda \underset{\sim}{M}(T,H) \tag{83}$$

The parameter λ is called the molecular field parameter. If we now

replace $\underset{\sim}{H}$ by $\underset{\sim}{H}_{eff}$ in the non-interacting model, we find that:

$$\underset{\sim}{M} = \underset{\sim}{M}_O B_S \left\{ \beta g_J \mu_B S(H + \lambda M) \right\} \tag{84}$$

and for $H = 0$:

$$\underset{\sim}{M} = \underset{\sim}{M}_O B_S (\beta g_J \mu_B S\lambda M) \tag{85}$$

In the small argument limit of the Brillouin function we can obtain:

$$\underset{\sim}{M} = \frac{NS^2 g_J^2 \mu_B^2 (S + 1)\lambda}{3SkT} \underset{\sim}{M} \tag{86}$$

for which non-trivial solutions exist if:

$$\left\{ \frac{NSg_J^2\mu_B^2 S(S + 1)}{3k} \right\} \frac{\lambda}{T} < 1 \tag{87}$$

The bracketed term on the left side of the above inequality is the

Curie constant C. That is, non-trivial solutions exist for:

$$T < C\lambda \tag{88}$$

and the critical temperature for the mean field theory is given by:

$$T_c = \lambda C \tag{89}$$

Thus T_c is proportional to the molecular field parameter λ, and as is

to be expected, approaches zero for the paramagnetic limit of $\lambda \to 0$.

Adapting Eq.76 to the magnetic case, we write:

$$\sigma(T) = \frac{|\underset{\sim}{M}_S (T)|}{|\underset{\sim}{M}_S (0)|} = B(-\varepsilon)^\beta \tag{90}$$

In the critical region for small fields, we can obtain:

$$tanh \left\{ \frac{g_J\mu_B H}{2kT} \right\} = \sigma(t) \left(1 - \frac{T_c}{T}\right) + |\sigma(T)|^3 \left\{ \frac{1}{3}\frac{T_c^3}{T^3} + \frac{T_c}{T}\left(1 - \frac{T_c}{T}\right)\right\}$$

$$+ \ ord \ |\sigma(T)|^5 \tag{91}$$

so that for $H = 0$, $\sigma \to 0$, $T \to T_c$:

$$|\sigma(T)|^2 \to \frac{3T^2}{T_c^2} (-\varepsilon) \tag{92}$$

Thus the square of the zero-field magnetization vanishes linearly

with ε, so that $\beta = \frac{1}{2}$ as in the van der Waal theory of a fluid system.

In similar ways, the mean field theory predicts values of the specific

heat exponents to be:

$$\alpha \;=\; \alpha' \;=\; 0 \tag{93}$$

where:

$$C \;\sim\; (-\varepsilon)^{-\alpha'} \quad \text{for} \quad T < T_c \tag{94}$$

and $\qquad C \;\sim\; \varepsilon^{-\alpha} \qquad \text{for} \quad T > T_c$ (95)

while the susceptibility critical exponents are given as:

$$\gamma \;=\; \gamma' \;=\; 1 \tag{96}$$

where

$$\chi \;=\; (-\varepsilon)^{-\gamma'} \quad \text{for} \quad T < T_c \tag{97}$$

and $\qquad \chi \;=\; \varepsilon^{-\gamma} \qquad \text{for} \quad T > T_c$ (98)

3.8   Law of Corresponding States

Eqs. 84 and 89 can be used to eliminate the molecular field

parameter λ from the equation of state:

$$\sigma(t) \;=\; B_S \left\{ \frac{g_J \mu_B S H}{kT} \;+\; \frac{3S}{S+1} \; \frac{T_c \sigma(T)}{T} \right\} \tag{99}$$

The critical-point exponents are the same for all values of spin

quantum number S, but the coefficients in Eq.99 do depend on S. We

see from Eq.99 that even if we measure field, magnetization and

temperature in the proper critical units, two materials will behave

differently if they have different spin quantum numbers. The Law of

Corresponding States would seem to be mainly applicable to the value of

the critical point exponent.

3.9   The Mean Field Theory as an Approximation for the Heisenberg Model

The above treatment assumed nothing concerning the nature of the

coupling constant λ. Further, it does not give a microscopic argument

for the introduction of the effective molecular field. This can be done

through the Heisenberg model for a magnetic system. The basic idea is

encompassed in the exchange interaction dealt with in previous

chapters. In the mean field approximation of the Heisenberg

Hamiltonian we treat exactly only the interactions among the spins

within a cluster, whereas for the remaining spins in the system, we

set $S_{iZ} = <S_Z>$ and $S_{ix} = S_{iy} = 0$. In this case we choose the cluster

to consist of a single spin so that the cluster Hamiltonian is simply

$$\mathcal{H}_i = (-2 \sum_j \mathcal{J}_{ij} <S_Z> - g_J\mu_B H) \, S_{iZ} \tag{100}$$

The dynamics of Eq.100 are those of a single spin situated in a

magnetic field of magnitude:

$$H_{eff} = H + 2 \left\{ (\sum_j \mathcal{J}_{ij})/g_J\mu_B \right\} <S_Z> \tag{101}$$

and we have effectively replaced the molecular field parameter such

that:

$$\lambda = 2 \, (\sum_j \mathcal{J}_{ij})/Ng_J{}^2\mu_B{}^2 \tag{102}$$

while:
$$T_c = \frac{2 \, (\sum_j \mathcal{J}_{ij}) \, S(S + 1)}{3k} \tag{103}$$

In the case of nearest neighbour interaction only, with

two nearest neighbours, assume an average interaction   such that:

$$\sum_j \mathcal{J}_{ij} = z\mathcal{J} \tag{104}$$

whence:
$$T_c = \frac{2z\mathcal{J}S(S + 1)}{3k} \tag{105}$$

Experimental results on materials that are thought to be described

reasonably well by the Heisenberg model show that Eqs.103 and 105

overestimate the value of T_c by as much as 50%. Further, Eq.105

predicts that two lattices will have the same critical temperature for

the same value of Z.

3.10 Landau's Theory for a Ferromagnet

Landau's theory concerning the possible general form of a thermodynamic potential near T_c can be obtained from several of his works (1937 a,b,c,d, 1965, Landau and Lifschitz 1960, 1969). It is the basic classical theory which finds its expression in other approximations (Kadanoff et al 1967).

Consider a single domain ferromagnet with an "easy" axis of magnetization along the geometric z axis (strictly speaking, an isolated single domain particle would have no particular easy direction). Take the order parameter to be $<M_{sZ}(r)>$ which is non-zero for $T < T_c$, and approaches zero continuously as $T \to T_c^-$. The basic assumption is that we can expand the Gibb's free energy G in a power series in the order parameter. We write:

$$G = \int d^3 r g(r) \tag{106}$$

where:

$$g(r) = g_O(T) + H_Z(r) M_{sZ}(r)$$

$$+ a(T) |M_{sZ}(r)|^2 + b(T) |M_{sZ}(r)|^4$$

$$+ c(T) |\nabla M_{sZ}(r) \cdot \nabla M_{sZ}(r)| \tag{107}$$

The first term $g_O(T)$ represents the free energy per unit volume in the absence of magnetization. The second term is the direct magnetostatic contribution. The remaining terms arise from the internal interactions between the spins. This says nothing about the forms of the interactions, only that they exist. Only even powers are present because if we change the sign of M_{sZ}, we do not change the spin-spin interactions. The final term makes the free energy larger when $M_{sZ}(r)$ varies in space, and serves to reduce spatial variations in $M_{sZ}(r)$.

By minimizing G with respect to $M_{\sim SZ}$ we can find the most likely value of M_{SZ}. One can obtain:

$$H_Z(\underset{\sim}{r}) + 2a\, M_{SZ}(\underset{\sim}{r}) + 4b\, M_{SZ}{}^3(\underset{\sim}{r}) - 2c\, \nabla^2 M_{\underset{\sim}{S}} = 0 \qquad (108)$$

The coefficients b and c must both be greater than zero, otherwise there is no minimum for G. If $b < 0$, the transition is first order. If $c < 0$ the magnetization is never uniform because the final term of Eq.107 would have a negative sign and the free energy could be indefinitely minimised by independently increasing $\Delta M_{SZ}(\underset{\sim}{r})$, ignoring any atomic structure in the problem.

Consider some solutions to Eq.108. Let $H_Z(\underset{\sim}{r}) = H_Z$; then there is no spatial variation of $M_{SZ}(\underset{\sim}{r})$, and, dropping the Z subscript, we have:

$$H = (2a + 4b\, M_s{}^2)M_s \qquad (109)$$

When $H = 0$ this has the solutions:

$$M_s = 0 \qquad (110)$$

and

$$M_s = \pm(-\frac{a}{2b})^{\frac{1}{2}} \qquad (111)$$

We want M_s to be non-zero for $T < T_c$. Eq.110 is obviously the solution for $T > T_c$. So from Eq.111:

$$a < 0 \quad \text{for} \quad T < T_c \qquad (112)$$

and since M_s must vanish at T_c:

$$a = 0 \quad \text{for} \quad T = T_c \qquad (113)$$

Obviously then, if Eq.110 is the only solution for $T > T_c$:

$$a > 0 \quad \text{for} \quad T > T_c \qquad (114)$$

The simplest form of the parameter a which satisfies the above conditions is:

$$a(T) = (T - T_c)a' \qquad (115)$$

where a' is a constant.

The preceding arguments hold only for $T \simeq T_c$. Near T_c, because $a(T)$ is small, $g \simeq b\,M_s^4$, which is small even though substantial changes may occur in M_s. This means that near T_c large fluctuations in M_s need little free energy. T_c is characterized by a large tendency towards fluctuations - possibly this could even be infinite; the present theory may not be valid here. Indeed, the basic assumption resting at the foundation of the Landau theory that one can expand the thermodynamic potential as a power series about T_c is unrealistic. Landau, however, points out that there will be singularities in the higher-order coefficients of the power series expansion. He supposes that the singular coefficients are of higher order than that of the terms of the expansion used in the calculation, and proceeds on this basis to examine the lower-order coefficients in order to obtain the predictions regarding the critical region.

From Eqs.111 and 115:

$$M_s \sim (T_c - T)^{\frac{1}{2}} \tag{116}$$

whence $\beta = \frac{1}{2}$ as in the mean field theory. Also, using

$$\chi_T = \left(\frac{\partial M}{\partial H} \right)_T \tag{117}$$

we find:

$$\chi_T = \mid T - T_c \mid^{-1} \tag{118}$$

whence $\gamma = \gamma' = 1$, again in agreement with the mean field theory. Similarly $\alpha = \alpha' = 0$ for the specific heat variation, with the same discontinuity of $\frac{3Nk}{2}$ predicted at the Curie point. That the Landau theory gives these results which are incompatible with experimentally determined results points once again to the unrealistic assumption of convergence of the free energy around T_c.

3.11 The Correlation Length

The arranging of the order parameter over a suitable region of space removes to some extent the fluctuations near T_c; all our usual

deductions from thermodynamics are based upon the assumption that fluctuations are zero, even if a canonical or grand canonical ensemble is used, so that we expect the deductions from thermodynamics and statistical mechanics to be in good agreement, giving well-behaved, non-singular functions. Such an arrangement of the order parameter, however, cannot cover too large a range without ruining the local nature of the Landau theory of the second-order phase transition. The largest range over which we can average without ruining the theory is the correlation length ξ. The true correlation length of the Landau theory is:

$$\xi(T) = \lambda_{COH} |\varepsilon|^{-\frac{1}{2}} \tag{119}$$

where λ_{COH} is the extrapolated zero-temperature coherence length.

3.12 Exponent Inequalities

There are some rigorous results concerning the critical exponents which can be proved from thermodynamics. These include:

(a)   The Rushbrooke inequality (Rushbrooke 1963).

For $T < T_c$,

$$\alpha' + 2\beta + \alpha' \geqslant 2 \tag{120}$$

(b)   The Coopersmith inequality (Coopersmith 1968):

For $T = T_c$, $H \to 0^+$,

$$\Phi + 2\psi - \frac{1}{\delta} \geqslant 1 \tag{121}$$

where:

$$C_H \sim H^{-\psi} \quad \text{for} \quad T = T_c$$

$$S(H) \sim -H^{\psi} \quad \text{(entropy at } T_c\text{)}$$

and $H \sim M_s{}^\delta$ for $T = T_c$

(c)   The Griffiths inequalities (Griffiths 1965 a,b):

$$\alpha' + \beta(1 + \delta) \geqslant 2 \tag{122}$$

$$\gamma' \geqslant \beta(\delta - 1) \tag{123}$$

$$\gamma(\delta + 1) \geqslant (2 - \alpha)(\delta - 1) \tag{124}$$

There are many others, and a comprehensive list appears on p.61 of Stanley's book (1971).

3.13   The Scaling Law Hypothesis

Much experimental and theoretical work in critical point phenomena appears to support the exponent inequalities discussed in the last section. Moreover, the inequalities are in many cases satisfied as equalities, and it would be advantageous to obtain some explanation for this if it is true in general. The static scaling law hypothesis involves making a simple assumption concerning the basic forms of the thermodynamic potentials (Widom 1965 a,b, Domb and Hunter 1965). Although no rigorous justification has been given for this hypothesis, the predictions of the static scaling hypothesis are somewhat less specific than the predictions of the Landau theory. Because the scaling hypothesis gives rise to functional interdependence amongst the critical-point exponents, the number of independent critical point exponents is restricted in number. In addition, the scaling hypothesis makes specific predictions concerning the form of the equation of state. Both these predictions seem to be supported by experimental findings.

The static scaling hypothesis for the Gibbs potential $G(T,H)$ of a magnetic system, asserts that $G(\varepsilon,H)$ is a generalised homogeneous function, assuming any non-singular terms of $G(\varepsilon,H)$ have been subtracted off. That is:

$$G(\lambda^{a_\varepsilon} \varepsilon, \lambda^{a_H} H) = \lambda G(\varepsilon,H) \tag{125}$$

where λ is the scaling parameter and λ can have any value. The parameters a_ε and a_H are not specified, corresponding to the fact that

the scaling hypothesis does not determine the values of the critical

point exponents. On the other hand, the fact that all the critical-

point exponents can be expressed in terms of only two parameters

α_ϵ and α_H, means that if two critical point exponents are specified,

all others can be determined. Furthermore, it can be shown that the

assumption that $G(\epsilon,H)$ is a generalised homogeneous function implies

that the Helmholtz potential, the internal energy, and the enthalpy

are also generalised homogeneous functions.

By differentiating both sides of Eq.125 with respect to H,

and using:

$$M_s = -\left(\frac{\partial G}{\partial H} \right)_T \tag{126}$$

we can obtain:

$$M_s(\epsilon,0) = \lambda^{\alpha_H - 1} M_s(\lambda^{\alpha_\epsilon} \epsilon,0) \tag{127}$$

Because of the properties of a homogeneous function, Eq.127 must be

valid for all values of λ. Therefore it must be valid for:

$$\lambda = \left(-\frac{1}{\epsilon}\right)^{\frac{1}{\alpha_\epsilon}} \tag{128}$$

Therefore, since as $\epsilon \to 0^-$, $M_s(\epsilon,0) \sim (-\epsilon)^\beta$,

$$\beta = \frac{1 - \alpha_H}{\alpha_\epsilon} \tag{129}$$

Similarly: $\quad \delta = \dfrac{\alpha_H}{1 - \alpha_H} \tag{130}$

and $\quad \gamma' = \dfrac{2\alpha_H - 1}{\alpha_\epsilon} \tag{131}$

A combination of the latter three equations yields:

$$\gamma' = \beta(\delta - 1) \tag{132}$$

which, with reference to relationship 123, is one of the Griffith's

inequalities expressed as an equality. Many others of the inequalities

are similarly predicted to be equalities, including the Rushbrooke

inequality.

3.14 Scaled Magnetization and Scaled Magnetic Field

The scaling hypothesis makes specific predictions concerning the form of the magnetic equation of state which are supported by experimental work in both insulating and metallic ferromagnetic systems (Weiss and Forrer 1926   Kouvel and Rodbell 1967, Arrott and Noakes 1967, Kouvel and Comly 1968). Using Eqs. 127 and 128, we can write:

$$M_s(\varepsilon, H) = |\varepsilon|^{(1-a_H)/a_\varepsilon} M_s \left(\frac{\varepsilon}{|\varepsilon|}, \frac{H}{|\varepsilon|^{a_H/a_\varepsilon}} \right) \tag{133}$$

which, from Eqs.129, 130 and 131 yields:

$$\frac{M_s(\varepsilon, H)}{|\varepsilon|^\beta} = M_s \left(\frac{\varepsilon}{|\varepsilon|}, \frac{H}{|\varepsilon|^{\beta\delta}} \right) \tag{134}$$

Define the scaled magnetization:

$$m = |\varepsilon|^{-\beta} M_s(\varepsilon, H) \tag{135}$$

and the scaled magnetic field:

$$h = |\varepsilon|^{-\beta\delta} H(\varepsilon, M_s) \tag{136}$$

also define:

$$F \pm (h) = M_s(\pm 1, h) \tag{137}$$

and Eq.134 becomes simply:

$$m = F \pm (h) \tag{138}$$

or in terms of the inverse of $F \pm (h)$:

$$h = f \pm (m) \tag{139}$$

Eqs. 138 and 139 predict that if we scale M_s by dividing by $|\varepsilon|^\beta$ and H by dividing by $|\varepsilon|^{\beta\delta}$, plots of m vs h should be the same regardless of temperature. The experiments of Kouvel and Comly (1968) and Ho and Litster (1969) show that for small m, h appears to be linear in m, and $\frac{h}{m}$ in m^2. Therefore one might expect $f \pm (m)$ to be of the form:

$$h = f \pm (m) = b_1 m + b_3 m^3 + b_5 m^5 \tag{140}$$

3.15   Models

The modern era of critical phenomena has seen the development
of various models for the explanation of observed behaviour of physical
systems. The "lattice gas" model was formulated by Yang and Lee in 1952.
The position vectors of the atoms are restricted to the sites of a
regularly spaced lattice   , and the partition functions are defined in
terms of an occupation variable $t_{\underset{\sim}{r}}$ which is unity if the site is
occupied and zero if the site is not occupied.

The Ising and Heisenberg models are constructed in terms of
localized magnetic spins. When the crystal has a single axis of
magnetization they can be combined with the lattice-gas model to form
a single Hamiltonian:

$$\mathcal{H} \;=\; 2 \sum_{\underset{\sim}{r}\underset{\sim}{r}'} \Big\{ \mathcal{J}_{11}\; (\underset{\sim}{r} - \underset{\sim}{r}')\; S_{\underset{\sim}{r}}{}^{z} S_{\underset{\sim}{r}'}{}^{z}$$

$$+\; \mathcal{J}_{\perp}\; (\underset{\sim}{r} - \underset{\sim}{r}')\, (S_{\underset{\sim}{r}}{}^{x}\, S_{\underset{\sim}{r}'}{}^{x} + S_{\underset{\sim}{r}}{}^{y}\, S_{\underset{\sim}{r}'}{}^{y})\; \Big\}$$

$$-\; g_{J}\mu_{B} \sum_{r} S_{\underset{\sim}{r}} \cdot H_{\underset{\sim}{r}} \qquad\qquad (141)$$

the unique axis being defined as the z axis with $\mathcal{J}_{11}$ referring to
the exchange parallel to this axis and $\mathcal{J}_{\perp}$ to the exchange in the
x-y plane. The pure isotropic Heisenberg Hamiltonian corresponds to
exchange interactions satisfying $\mathcal{J}_{11}(\underset{\sim}{r}) = \mathcal{J}_{\perp}(\underset{\sim}{r}) = \mathcal{J}(\underset{\sim}{r})$. However,
most real materials have some magnetic anisotropy which, in a uniaxial
case would usually correspond to:

$$|\mathcal{J}_{11}| \;>\; |\mathcal{J}_{\perp}| \qquad\qquad (142)$$

so that in a zero field, the spins order parallel to the z axis. The
extreme anisotropic limit of $\mathcal{J}_{\perp}(\underset{\sim}{r}) = 0$ corresponds to the Ising model.

As a model for ferromagnetism in real materials, the Ising
model is not very adequate because of its requirement of complete
anisotropy. More important than any possible application, however,

is the realization that the model is the simplest one which has been devised for describing phase transitions. For its relevance, we rely on the assumption that statistical mechanics will be able to describe the singularities that represent phase transitions.

The original work of Ising (1925) used combinatorial analysis and he deduced the solution in one dimension. He incorrectly argued that since there was no phase transition in one dimension, there would also be none in three dimensions. The molecular field theory approximation corrected this. In 1944, Onsager presented the first exact solution in two dimensions. Whereas the ordered state is not stable in one dimension, this is not true in two dimensions or three dimensions, and a phase transition is predicted. Onsager's exact solution gives:

$$kT_c = 2\mathcal{J}/\ell n \; (1 + \sqrt{2}) \qquad\qquad (143)$$

No exact solution has yet been found for three-dimensional models. Recent theoretical work has centred around the use of approximations and the development of mathematical techniques to handle the approximations. Diagramatic techniques have been increasingly used. Some effort has also been directed towards accounting for the dynamical aspects of critical phenomena, and dynamic scaling laws have been developed. Although they lead to specific predictions about time-dependent critical phenomena, these predictions do not include all the information we would like to know; more fundamentally, the scaling hypothesis has not yet been fully justified. Another theory, called the mode-mode coupling theory, (Fixman 1962), succeeds in many cases where the dynamic scaling hypothesis has not been successful.

3.16   Susceptibility Critical Exponent Values Above the Critical Point

The theoretical values for γ predicted from the classical theories is unity. This has been pointed out in previous sections of this chapter. An approximation for the three-dimensional Ising magnet

for a simple cubic lattice with $S = \frac{1}{2}$ yields $\gamma = 1.25 \pm 0.001$.

An approximation for the three-dimensional Heisenberg ferromagnet

with $S = \frac{1}{2}$ yields $\gamma = 1.43 \pm 0.04$, while the infinite-spin model

yields $\gamma = 1.33 \pm 0.01$. A summary of experimental determinations

by various workers appears in Heller's article (1967). Values for

iron are 1.33 (Arajs and Colvin 1964), 1.33 $\pm$ 0.03 (Develey 1965),

and 1.333 $\pm$ 0.015 (Noakes et al 1966). For nickel they are 1.35 $\pm$ 0.02

(Weiss and Forrer 1926 analysed by Kouvel and Fisher 1964), 1.32 $\pm$ 0.02

(Develey 1965), and 1.29 $\pm$ 0.04 (Arajs 1965). For cobalt, Colvin and

Arajs (1965) reported $\gamma = 1.21 \pm 0.04$ although the data may have been

affected by anisotropy. In 1965 Graham used a fluxmeter method for Gd

with extrapolations to zero field. He reported a ferromagnetic Curie

temperature of 292.5 $\pm$ 0.5K with $\gamma = 1.3 \pm 0.1$ up to 20K above Tc.

3.17   Experimental Aspects of Ferromagnetic Critical Phenomena

One of the first experimental techniques used in ferromagnetic

critical studies was employed by Weiss and his co-workers (Weiss and

Forrer 1926). The sample was suddenly introduced into a gap in a

magnetic pole piece and the magnetization was computed from the

deflection of a ballistic galvanometer. Other methods include the

vibrating sample magnetometer (Forrer 1956), and the Faraday technique

of weighing the sample in a vertical field having a known gradient. In

addition to these bulk techniques, the more microscopic Mössbauer and

nmr studies have been carried out (see Heller's 1967 review article for

a summary of the results using the latter two techniques).

In the present work the sample under investigation is the core

of a transformer; the output of the transformer depends on the suscept-

ibility of the sample in a way which is to be described in the next

chapter. All of the techniques mentioned are essentially concerned

with making magnetization or susceptibility measurements as a function

of temperature. However, various problems arise in the interpretation of the data.

The first problem lies in the correct determination of T_c and of the range of temperature away from T_c for which the exponent law holds. The critical region is defined as that region where the exponent law behaviour dominates. Molecular field theory fails for $\varepsilon < \frac{1}{Z}$ where Z is the number of nearest neighbours. This would mean that the critical region should extend for $\varepsilon \simeq 10^{-1}$. In fact, Graham's (1965) data extended to $\varepsilon \simeq 6 \times 10^{-2}$, and in general experimental evidence suggests a range of $\varepsilon < 10^{-2}$ to 10^{-1} (Kadanoff et al 1967).

Measurements in an applied field require extrapolation to zero field to fix T_c and to correct the data to obtain intrinsic behaviour. Noakes et al (1966) have taken some of this uncertainty into account by assuming a power-law-temperature dependence and then fitting to the best values of T_c and the critical exponent. Our work seems to indicate the correctness of this philosophy ie, that unacceptable errors can be introduced by evaluating T_c from independent criteria and then using this T_c to find the critical exponent; rather, it is better to calculate T_c and the exponent from the same criteria by assuming the power law holds in the critical regions (refer to Chapter 7).

Domains present a problem to experimental magnetic critical phenomena studies. The theory described in this chapter has applied only to a single-domain particle, ie to a uniformly saturated sample. In this work we find that critical ferromagnetic behaviour cannot be observed for $T < T_c$ in a polycrystalline sample of Gd because of the dominating presence of domains in that region. In principle, much of the difficulty should be overcome by using a single crystal and

applying the field along the easy axis. However, even then problems will arise unless extremely pure single-crystal samples are used which are, moreover, fashioned into a controlled shape (Noakes et al 1967).

The microscopic techniques of nmr and Mössbauer can be inherently more accurate in determining the intrinsic magnetization of a material, in that they are not affected by anisotropy, and the measured quantities can be determined with a high precision. However, magnetostriction presents a problem as the coupling between the nuclear and electron spin systems depends on the lattice parameters which themselves undergo anomalies near T_c. Further, the field set up by the nuclei at the electron spins can appreciably tip the electronic magnetization and cause an error in the measurement of the local resonant field. Also, if the magnetization is due partly to spin and partly to orbital angular momentum, and if the ratio of these contributions is not independent of temperature, the nuclear magnetic resonance frequency need not be proportional to either. This should present little problem where Gd is concerned. Lastly, fluctuations will cause deviations from the true resonance frequency, and we have seen previously that a system is very susceptible to fluctuations near T_c.

Of these problems associated with the microscopic techniques, only that caused by magnetostriction is apt to be serious. It has been estimated, however, that errors of only about 1% will be caused by it, and this is not likely to alter the critical behaviour (Heller 1967).

CHAPTER 4

THERMOMAGNETIC MODULATION THEORY

4.1   Introduction

The experimental work outlined in this thesis has

centred about the use of modulation techniques to study the

susceptibility of Gd near T_c. Both conventional AC susceptib-

ility techniques and thermal modulation techniques have been used,

either separately or in conjunction. In Chapter 6 it will be

shown that non-equilibrium effects due to domains have been

observed below T_c in polycrystalline Gd; the following treatment

will outline the equilibrium theory and extend it to include the

effects of non-equilibrium in the domain properties.

4.2   Thermal Modulation Theory

Consider a sample in a cool environment, heated by an

oscillatory power source $P \cos \omega_T t$. Suppose that at any time t

the temperature is the same at any point in the sample, and that

the difference between the temperature at any such point and that

of the environment is θ. Assume that convection is the dominant

mechanism of heat loss from the sample to its environment. Then,

by Newton's law of cooling:

$$mC \frac{d\theta}{dt} + b\theta = P \cos \omega_T t \qquad (144)$$

where m and C are the mass and specific heat respectively of the

sample, and b is the Newton's law of cooling constant for the

sample in its environment. The solution of Eq. 144 leads in the

steady state to a temperature modulation:

$$\theta = \overline{\theta} + \Delta \cos (\omega_T t + \phi_T) \qquad (145)$$

where $\overline{\theta}$ is the mean difference between the temperature of the sample and that of the movement:

$$\overline{\theta} = \overline{P}/b \qquad (146)$$

where $\overline{P}$ is the average heater power and from this, values of b may be obtained by plotting the mean steady state temperature vs $\overline{P}$. The modulation amplitude is:

$$\Delta = P(b^2 + \omega_T^2 m^2 C^2)^{-\frac{1}{2}} \qquad (147)$$

and there is a thermal phase lag given by:

$$\phi_T = -\arctan \omega_T m C / b \qquad (148)$$

Thermal Skin Depth Effects Using Plane Geometry

Consider a sample whose thickness is so large compared with the thermal skin depth that plane geometry can be used. The formulation of the problem gives:

$$\frac{\partial \underset{\sim}{\theta}}{\partial t} = a \frac{\partial^2 \underset{\sim}{\theta}}{\partial x^2} \qquad (149)$$

at depth x in the sample, where:

$$a = \frac{K}{\rho C} \qquad (150)$$

K being the thermal conductivity of the sample, and ρ being the density of the sample. In general the steady state solution to Eq. 149 is of the form:

$$\underset{\sim}{\theta} = \underset{\sim}{B} e^{i \omega_T t - (i + 1) k_T x} \qquad (151)$$

where
$$k_T = \left(\frac{\omega_T}{2a}\right)^{\frac{1}{2}} = \frac{1}{\delta_T} \qquad (152)$$

δ_T being the thermal skin depth. The phasor $\underset{\sim}{B}$ gives the amplitude and phase of the thermal oscillation and is determined from the boundary condition:

$$P' \cos \omega_T t = b'\theta(0, T) - K \left(\frac{\partial \theta}{\partial x}\right)_{x=0} \tag{153}$$

which relates the heater power to the heat loss to the surroundings and the heat entering unit surface area of the sample. Here P' and b' are normalized so that $P' = P/A$ and $b' = b/A$ where A is the surface area of the sample. From Eqs. 151 and 153, the steady state solution is given by:

$$\theta = \overline{\theta} + \Delta e^{-k_T x} \cos(\omega_T t - k_T x + \theta_T) \tag{154}$$

where the surface modulation amplitude and phase are given by

$$\Delta = P'(b'^2 + 2b'k_T K + 2k_T^2 K^2)^{-\frac{1}{2}} \tag{155}$$

and

$$\phi_T = -artan\left\{ k_T K / (b' + k_T K) \right\} \tag{156}$$

The average modulation is given by:

$$<\theta - \overline{\theta}> = A \int_0^\infty (\theta - \overline{\theta}) dx \tag{157}$$

leading to

$$<\theta - \overline{\theta}> = (A \delta_T / \sqrt{2}) \cos(\omega_T t + \phi_T - \frac{\pi}{4}) \tag{158}$$

The main differences between this and the result given by Eq. 145 for the case of a large skin depth are the effective volume factor $(A \delta_T / \sqrt{2})$ in the amplitude, the difference between Eqs. 148 and 156 for ϕ_T, and the additional phase lag of $\pi/4$ resulting from the integration over the thermal wave. The dependence of phase upon the specific heat is now such that as

$$(\rho \omega_T CK/2)^{\frac{1}{2}} / \{b' + (\rho \omega_T CK/2)^{\frac{1}{2}}\}$$

tends to zero and unity, the total phase $\phi_T - \frac{\pi}{4}$ will tend to $-\frac{\pi}{4}$ and $-\frac{\pi}{2}$ respectively compared with the case of a large skin depth where the phase θ_T tends to zero and $-\frac{\pi}{2}$ as $\omega_T mC/b$ tends to zero and infinity respectively. It is of interest to examine the behaviour of the

total phase lag θ as one shifts from one model to the other. Order

of magnitude calculations for the sample used in our experiments yield

$$\frac{\omega_T mC}{b} \sim 10^3$$

while $\qquad (\rho\omega_T CK)^{\frac{1}{2}} / \sqrt{2} \, b' \simeq 0.3.$

It can be seen that while $artan \; \dfrac{\omega_T mC}{b} \simeq \pi/2$, $artan \; (\omega_T \rho CK/2)^{\frac{1}{2}} / \{b' +$

$(\rho\omega_T CK/2)^{\frac{1}{2}}\}$ can be less than $\pi/4$ by a reasonable amount. Thus

it might be expected that ϕ might decrease with a decrease in skin

depth. Physically this can be attributed to a lowering of the

effective mass being modulated; where the thermal skin depth is

less than the thickness of the sample, the effective modulated

mass per unit area of the sample is $\sim \delta_T\rho/2$. The foregoing

discussion is of relevance here since the specific heat of a

ferromagnetic crystal diverges at T_C, and a simple application

of either Eq. 148 or Eq.156 would lead us to expect an increase

in the phase lag near T_C. A further examination of these points

will appear in Chapter 6.

We have approached this problem from the stand point of

the large – and small – skin depth models in the interests of

simplicity, and we have seen the apparent difficulties arising

in this treatment when the thermal skin depth is comparable to

the sample thickness. This difficulty is bound to arise of

course, because strictly speaking neither model is applicable

in this case. It behoves us, therefore, to proceed to the more

general, but complicated model of cylindrical geometry.

Thermal Skin Depth Effects Using Cylindrical Geometry.

For the more general case of cylindrical geometry with a

cylindrical or toroidal sample, the relevant differential

equation is:

$$\frac{\partial \theta}{\partial t} = a \left(\frac{\partial^2 \theta}{\partial r^2} + \frac{1}{r} \frac{\partial \theta}{\partial r} \right) \tag{159}$$

where θ is the temperature difference between the environment

and a point at a radial distance r from the axis of the cylinder

of radius R. The steady state oscillatory term in θ may be

written as (e.g., Arpaci 1966):

$$\underset{\sim}{\theta}(r,t) = \underset{\sim}{B} e^{i\omega_T t} \left\{ J_0(i\sqrt{2} \ \overline{i} k_T r) \ / \ J_0(i\sqrt{2i} \ k_T R) \right\} \tag{160}$$

J_ν are the Bessel functions of the first kind whose

properties are elaborated on in Section 4.4 prior to the treatment

of a general thermomagnetic theory. It will be shown there that

when the argument of the Bessel function is $xe^{\pm i \, 3\pi/4}$ it may be

expressed in terms of the ber and bei functions $R_\nu(x)$ and $M_\nu(x)$

respectively:

$$J_\nu(xe^{\pm i \ 3\pi/4}) = R_\nu(x) \pm M_\nu(x) \tag{161}$$

The phasor $\underset{\sim}{B}$ in Eq. 160 is determined from the boundary condition:

$$P'e^{i\omega_T t} = b'\theta(R,t) + K \left(\frac{\partial \underset{\sim}{\theta}}{\partial r} \right)_{r \, = \, R} \tag{162}$$

leading to:

$$\theta(r,t) = P'e^{(i\omega_T t \, + \, \phi)} J_0(i \sqrt{2i} \ k_T r)(X^2 + Y^2)^{-\frac{1}{2}} \tag{163}$$

where

$$X = b'R_O + K \, k_T(M_1 + R_1) \tag{164}$$

and

$$Y = b'M_O + K \, k_T(M_1 - R_1) \tag{165}$$

the R_J and M_J being calculated for $x = \sqrt{2} \ k_T R$.

The phase is given by:

$$\phi = - \, artan \ Y/X \tag{166}$$

with a surface oscillation phase:

$$\phi_T = \phi + artan \ (M_O/R_O) \qquad (167)$$

The average modulation is then:

$$<\theta - \bar{\theta}> = L \int_O^R (\theta - \bar{\theta}) \ 2\pi r \ dr \qquad (168)$$

where L is the sample length. Hence:

$$<\theta - \bar{\theta}> = \sqrt{2} \ \pi RL \ \delta_T P' \ \{ \ (R_1{}^2 + M_1{}^2)/(X^2 + Y^2) \ \}^{\frac{1}{2}}$$
$$cos \ (\omega_T t + \phi_T + \phi') \qquad (169)$$

where ϕ' is the additional phase shift associated with the integration and is given by:

$$\phi' = artan \ \{ \ (M_1 + R_1)/(R_1 - M_1) \ \} - artan\left(\frac{M_O}{R_O}\right) \qquad (170)$$

In the limit $x \to 0$ (ie, $\delta_T >> R$), Eq. 169 becomes identical to Eq. 145 in both amplitude and phase. For $x \to \infty$ (ie, $\delta_T << R$) it becomes identical to Eq. 154 for the plane wave solution as is also expected (Wilson et al 1975).

4.3   Thermal Modulation in a Static Magnetic Field – The DC Technique

The application of the above theory to the study of the susceptibility in a static magnetic field is relatively simple. The field $\underset{\sim}{H}$ creates a sample magnetization of magnitude $M(T)$ in the field direction; the temperature modulation produces a small oscillation in M, and a voltage is induced in a pick-up coil. We treat this in terms of the oscillation in the susceptibility $\chi = \frac{M}{H}$ where H is the field magnitude in the direction perpendicular to the plane of the pick-up coil. χ is defined here for any value of H. By means of a Taylor expansion, the time dependence is:

$$\chi(T) = \chi(\overline{T}) + \Delta\chi^{\mathbf{1}}(\overline{T}) \; cos \; (\omega_T t + \phi) \tag{171}$$

where ϕ is the total thermal phase lag. $\overline{T}$ is the mean sample

temperature, and $\chi^{\mathbf{1}}(\overline{T}) = \left(\dfrac{d\chi(T)}{dT} \right)_{\overline{T}}$. The voltage induced in

the pick-up coil is given by:

$$v = \xi V dM/dt = \xi V H d\chi/dt \tag{172}$$

where V is the sample volume and ξ is determined by the number

of turns, the coil dimensions and the sample filling factor.

Hence:

$$v = \xi V \Delta \; \omega_T \; H\chi^{\mathbf{1}}(\overline{T}) \; cos \; (\omega_T t + \phi - \frac{\pi}{2}) \tag{173}$$

If, as is usual, $b << \omega_T mC$, and we assume that the thermal skin

depth is large compared to the sample thickness, we obtain from

Eq. 147:

$$v = \left[\; \xi V P H \chi^{\mathbf{1}}(\overline{T})/mC \; \right] \; cos \; (\omega_T t + \phi_T - \frac{\pi}{2}) \tag{174}$$

and ϕ_T is given by Eq. 148. We see, therefore, that the signal

is independent of the modulation frequency. Generally only very

small modulation amplitudes ($\sim mK$) have been used in our

experiments, so that Eq. 171 is valid. If larger values are used

so that the signal leads to a modulation-broadened curve, Eq. 171

should be replaced by a Fourier integral (Wilson 1963).

Where the thermal skin depth is small compared to the

sample thickness, plane geometry can be used and Eqs. 155 to 158

may be employed to obtain v and ϕ, while for the more general

case of cylindrical geometry we make use of Eqs. 162 to 170. We

must recall that the behaviour of the phase is likely to be

complicated, and the considerations expressed following Eq. 158

should be borne in mind as they are directly applicable here.

4.4 Thermal Modulation in an Alternating Magnetic Field - The AC Technique

The preceding section dealt with thermal modulation in a static field. This will be referred to in this thesis as the DC technique. It was noted that the signal produced in the pick-up coil is independent of modulation frequency when the thermal skin depth is larger than the sample thickness. This section will treat thermal modulation in an alternating field, and will be referred to as the AC technique. It will be seen that the signal is enhanced by a factor of order the ratio of the electromagnetic frequency to the thermal frequency.

Suppose the thermally modulated sample is the core of a transformer operating at a carrier frequency ω_C, where $\omega_C \gg \omega_T$. If the amplitude of the magnetic field produced by the primary coil is H_O, the sample magnetization at any point in the sample is:

$$M(t) = \chi(T) \, H_O \, cos \, \omega_C t \qquad (175)$$

and the Taylor expansion leads to:

$$M(t) = H_O \{ \chi(\overline{T}) + \Delta\chi^{\pm}(\overline{T}) \, cos \, (\omega_T t + \phi_T)\}$$
$$cos \, \omega_C t \qquad (176)$$

The signal produced in the secondary coil is given by:

$$v_{total} \; \alpha \; \frac{dB}{dt} = const \, \frac{dH}{dt} - \xi V \frac{dM}{dt} \qquad (177)$$

where B is the total magnetic induction. The portion of v_{total} arising from $\frac{dH}{dt}$ is not due to the ferromagnetic susceptibility of the sample, and so is not temperature dependent. Consider only the latter term of Eq. 177. When the sample thickness is small compared to either the electromagnetic or thermal skin depths, it is given by:

$$v = \xi V H_o \omega_C \chi(\overline{T}) \ cos \ (\omega_C t - \frac{\pi}{2})$$

$$+ \ \xi V H_o \Delta \chi^1 (\overline{T}) \ \{ \ \omega_C \ cos \ (\omega_T t + \phi_T) \ sin \ \omega_C t$$

$$+ \ \omega_T \ sin \ (\omega_T t + \phi_T) \ cos \ \omega_C t \ \} \tag{178}$$

The first term is the carrier wave. We see that under these conditions it has the same temperature dependence as the susceptibility of the sample. This forms the basis of the simple AC technique which we use often in this work and which we call the "zero harmonic technique". We have taken care to operate in a region of field frequency where the carrier amplitude is proportional to ω_C so that it can be assumed that the electromagnetic skin depth is larger than the sample thickness.

The latter two terms of Eq. 178 are $\frac{\pi}{2}$ out of phase in ω_T and ω_C and since $\omega_C \gg \omega_T$ it is safe to assume that the third term is much smaller than the second and causes little interference to it. If the signal is demodulated and phase-sensitive detected at ω_T, the resulting modulation is:

$$v_T = \xi V H_o \Delta \omega_C \chi^1 (\overline{T}) \ cos \ (\omega_T t + \phi_T) \tag{179}$$

or, assuming $b \ll \omega_T mC$:

$$v_T = \frac{\xi P H_o V \omega_C \chi^1 (\overline{T})}{m \omega_T C} \ cos \ (\omega_T t + \phi_T) \tag{180}$$

and it is seen that: $\qquad |v_T| \ \alpha \ \frac{\omega_C}{\omega_T} \tag{181}$

which represents an enhancement of the modulation signal when compared to Eq. 174.

If the signal given by Eq. 178 is detected at the nth harmonic of the thermal modulation, one obtains the nth derivative of $\chi(\overline{T})$ because of the expansion (Russell and Torchia 1962):

$$\chi(t) = \chi(\overline{T}) + \sum_{n=1}^{\infty} \Delta^n (2^{1-n}/n!) \chi^{(n)} (\overline{T}) \cos \left[n(\omega_T t + \phi_T) \right] \tag{182}$$

where $\chi^{(n)}$ represents the nth derivative. It can be seen that the amplitude of the second harmonic signal versus $\overline{T}$ will be equal to $\frac{1}{4}\Delta$ multiplied by the derivative of the corresponding first harmonic curve (Wilson et al 1975).

The AC technique for Plane Geometry

Consider a sample of area A, whose thickness is large compared to both the electromagnetic and thermal skin depths. Take the applied field to be $H_0 \cos \omega_C t$ and the applied heating power to be such that the surface thermal fluctuations are given by $\Delta \cos (\omega_T t + \phi_T)$. Then the solutions to the plane wave problems are such that the equation corresponding to Eq. 178 is:

$$v = \xi A H_0 \chi(\overline{T}) \omega_C \int_0^{\infty} e^{-k_C x} \sin (\omega_C t - k_C x) dx$$

$$+ \xi A H_0 \chi^1(\overline{T}) \Delta \omega_C \int_0^{\infty} e^{-kx} \cos (\omega_T t - k_T x + \phi_T) \sin (\omega_C t - k_C x) dx$$

$$+ \xi A H_0 \chi^1(\overline{T}) \Delta \omega_T \int_0^{\infty} e^{-kx} \sin (\omega_T t - k_T x + \phi_T) \cos (\omega_C t - k_C x) dx$$

$$\tag{183}$$

where

$$k_C = 1/\delta_C = (\omega_C \sigma_C \mu/2)^{\frac{1}{2}} \tag{184}$$

σ_C being the conductivity and μ being the permeability of the sample material, and:

$$k = k_C + k_T \tag{185}$$

The first term of Eq. 183 is the carrier wave. Let this term be T_1:

$$T_1 = \xi A H_O \chi(\overline{T}) \omega_C \int_0^\infty e^{-k_C x} \left[sin\ (\omega_C t)\ cos\,(k_C x) - cos\ (\omega_C t)\ sin\,(k_C x) \right] dx$$

$$(186)$$

We make use of the following integrals:

$$\int_{x_1}^{x_2} e^{-ax}\ cos\ bx\,dx = \frac{e^{-ax}}{a^2 + b^2} \left[-a\ cos\ bx + b\ sin\ bx \right]_{x_1}^{x_2}$$

$$(187)$$

and

$$\int_{x_1}^{x_2} e^{-ax}\ sin\ bx\,dx = \frac{e^{-ax}}{a^2 + b^2} \left[-a\ sin\ bx - b\ cos\ bx \right]_{x_1}^{x_2}$$

$$(188)$$

and we find that:

$$T_1 = \frac{\xi A H_O \chi(\overline{T}) \omega_C}{\sqrt{2}\ k_C}\ cos\ (\omega_C t - \frac{3\pi}{4})$$

$$(189)$$

$A/k_C = A\delta_C$ is the effective volume in Eq. 189. A comparison with the first term of Eq.178 shows that in the limit $k_C \to 0$ these terms become equal in magnitude apart from the attenuation factor $\frac{1}{\sqrt{2}}$ due to the integration over the electromagnetic skin depth; this integration is also responsible for the extra phase lag of $\frac{\pi}{4}$ contained in Eq. 189.

Once again, the third term of Eq. 183 will cause little interference to the second term. Then:

$$v_T \simeq \xi A H_O \chi^4 (\overline{T}) \Delta \omega_C \int_0^\infty e^{-kx}\ cos\ (\omega_T t - k_T x + \phi_T)\ sin\ (\omega_C t - k_C x)dx$$

$$(190)$$

Let $\qquad \xi A H_O \chi^4 (\overline{T}) \Delta \omega_C = X$ $\qquad\qquad\qquad$ (191)

$$\therefore\ v_T = X \int_0^\infty e^{-kx}\{cos\ (\omega_T t + \phi_T)\ cos\ k_T x + sin\ (\omega_T t + \phi_T)\ sin\ k_T x\}\ X$$

$$\{sin\ \omega_C t\ cos\ k_C x - cos\ \omega_C t\ sin\ k_C x\}dx$$

$$(192)$$

$$= X\{ \cos (\omega_T t + \phi_T) \sin \omega_C t \int_0^\infty e^{-kx} \cos k_T x \cos k_C x \, dx$$

$$- \cos (\omega_T t + \phi_T) \cos \omega_C t \int_0^\infty e^{-kx} \cos k_T x \sin k_C x \, dx$$

$$+ \sin (\omega_T t + \phi_T) \sin \omega_C t \int_0^\infty e^{-kx} \sin k_T x \cos k_C x \, dx$$

$$- \sin (\omega_T t + \phi_T) \cos \omega_C t \int_0^\infty e^{-kx} \sin k_T x \sin k_C x \, dx\} \tag{193}$$

Utilize Eqs. 187 and 188; if we bear in mind the usual relationships giving the products of trigonometrical functions we obtain:

$$v_T = \frac{X}{2} \{\cos (\omega_T t + \phi_T) \sin \omega_C t \left(\frac{1}{2k} + \frac{k}{k^2 + (\Delta k)^2} \right)$$

$$- \cos (\omega_T t + \phi_T) \cos \omega_C t \left(\frac{1}{2k} - \frac{\Delta k}{k^2 + (\Delta k)^2} \right)$$

$$+ \sin (\omega_T t + \phi_T) \sin \omega_C t \left(\frac{1}{2k} + \frac{\Delta k}{k^2 + (\Delta k)^2} \right)$$

$$+ \sin (\omega_T t + \phi_T) \cos \omega_C t \left(\frac{1}{2k} - \frac{k}{k^2 + (\Delta k)^2} \right) \} \tag{194}$$

where

$$\Delta k = k_T - k_C \tag{195}$$

Let:

$$D = \left(\frac{1}{2k} - \frac{k}{k^2 + (\Delta k)^2} \right) \sin (\omega_T t + \phi_T) - \left(\frac{1}{2k} - \frac{\Delta k}{k^2 + (\Delta k)^2} \right) \cos (\omega_T t + \phi_T) \tag{196}$$

and let:

$$B = \left(\frac{1}{2k} + \frac{k}{k^2 + (\Delta k)^2} \right) \cos (\omega_T t + \phi_T) + \left(\frac{1}{2k} + \frac{\Delta k}{k^2 + (\Delta k)^2} \right) \sin (\omega_T t + \phi_T) \tag{197}$$

So that:

$$v_T = \frac{X\sqrt{D^2 + B^2}}{2} \ cos \ (\omega_C t - \alpha_T) \tag{198}$$

where $\alpha_T = artan \left(\frac{B}{D}\right)$ (199)

Refer to Eqs. 183 and 189. Let:

$$Y = \frac{\xi A H_O \chi(\overline{T})\omega_C}{\sqrt{2} \ k_C} \tag{200}$$

Then:

$$v = Y \ cos \ (\omega_C t - \frac{3\pi}{4}) + \frac{X\sqrt{D^2 + B^2}}{2} \ cos \ (\omega_C t - \alpha_T) \tag{201}$$

With $\omega_C \gg \omega_T$, we will now express the signal in its amplitude-modulated carrier wave form where the modulation is multiplied by the cosine of the phase difference between the terms of Eq. 201.

$$v = cos \ (\omega_C t - \frac{3\pi}{4}) \ \{Y + \frac{X\sqrt{D^2 + B^2}}{2} \ cos \ (\frac{3\pi}{4} - \alpha_T)\} \tag{202}$$

The modulation is thus:

$$v_T = \frac{X\sqrt{D^2 + B^2}}{2} \ cos \ (\frac{3\pi}{4} - \alpha_T) \tag{203}$$

$$= \frac{X\sqrt{D^2 + B^2}}{2\sqrt{2}} \ \frac{B-D}{\sqrt{D^2 + B^2}} \tag{204}$$

$$= \frac{X(B-D)}{2\sqrt{2}} \tag{205}$$

which, using Eqs. 191, 196 and 197 gives:

$$v_T = \frac{\xi A H_O \chi^1(\overline{T}) \Delta\omega_C}{2(k_T + k_C)} \sqrt{\frac{(k_T + k_C)^2 + k_C^2}{k_T^2 + k_C^2}} \ cos \ (\omega_T t + \phi_T - \phi_{TC}) \tag{206}$$

where $\phi_{TC} = artan \left\{\frac{k_T^2 + k_T k_C}{k_T^2 + 2k_C^2 + k_T k_C}\right\}$ (207)

In the limit $k_T \ll k_C$ (ie, $\delta_T \gg \delta_C$) we have:

$$v_T \to \frac{\xi A H_O \chi^1(\overline{T}) \Delta \omega_C}{\sqrt{2}\, k_C}\ \cos\ (\omega_T t + \phi_T) \tag{208}$$

which, with the effective volume being $A/k_C = A\delta_C$ is equivalent

to Eq. 180 apart from the attenuation factor of $1/\sqrt{2}$ due to the

integration over the electromagnetic skin depth.

In the opposing limit $k_T \gg k_C$ $(\delta_C \gg \delta_T)$, we find

$$v_T \to \frac{\xi A H_O \chi^1(\overline{T}) \Delta \omega_C}{2 k_T}\ \cos\ (\omega_T t + \phi_T - \frac{\pi}{4}) \tag{209}$$

This is equivalent to a combination of Eqs. 158 and 179 with an

extra attenuation factor of $1/\sqrt{2}$ due to the $\pi/4$ phase difference

between the carrier wave and the modulation.

General Theory of the AC Technique for Cylindrical Geometry

The solution to the general problem for cylindrical geometry

is complicated and lengthy; it involves a large number of

mathematical expressions which can render it very confusing to the

reader. In the interests of clarity we will first present the

necessary mathematical formulae together with a number of definitions

which enable the solution to be presented in a more succint form.

Following this we will define the problem and present the final

solution; then we will examine the limits. The section will conclude

with an outline of the mathematical method we have used to obtain the

solution. To present the full derivation would occupy some thirty

pages of this thesis, and would detract from the important work

contained in the following three chapters. Furthermore, from an

experimental point of view, the general solution has proven thus far

to be of theoretical interest only, as the important information can

be elucidated from the models which have been presented previously

in this chapter.

We make use of the Bessel functions of the first kind:

$$J_\nu(mx) = \sum_{n=0}^{\infty} \frac{(-1)^n \left(\frac{mx}{2}\right)^{2n+\nu}}{n!\,\Gamma(k + \nu + 1)} \tag{210}$$

where Γ is the gamma function:

$$\Gamma(n+1) = n! \text{ for } n \text{ an integer} \tag{211}$$

$$\Gamma(n)\Gamma(n-1) = \pi/sin\,(n\pi) \text{ for fractional } n$$

We require the Ber and Bei functions, $R_\nu(y)$ and $M_\nu(y)$ respectively where:

$$J_\nu(i\sqrt{i}\,y) = R_\nu(y) + i\,M_\nu(y) \tag{212}$$

and

$$J_\nu(\sqrt{i}\,y) = R_\nu(y) - i\,M_\nu(y) \tag{213}$$

The following are directly applicable:

$$R_0(y) = \sum_{n=0}^{\infty} \left\{ \frac{(-1)^n \left(\frac{y}{2}\right)^{4n}}{(2n!)^2} \right\} \tag{214}$$

$$M_0(y) = \sum_{n=0}^{\infty} \left\{ \frac{(-1)^n \left(\frac{y}{2}\right)^{4n+2}}{[(2n + 1)!]^2} \right\} \tag{215}$$

$$R_1(y) = \sum_{n=0}^{\infty} \left\{ \frac{cos\,[\frac{(2n + 3)\pi}{4}]\left(\frac{y}{2}\right)^{2n+1}}{n!\,(n+1)!} \right\} \tag{216}$$

$$M_1(y) = \sum_{n=0}^{\infty} \left\{ \frac{sin\,[\frac{(2n + 3)\pi}{4}]\left(\frac{y}{2}\right)^{2n+1}}{n!\,(n+1)!} \right\} \tag{217}$$

In the problem we consider a cylinder of radius R. We let r be the distance of any point on the cylinder from the axis of the cylinder.

We let:

$$A = \sqrt{2}\, k_C R \qquad\qquad (218)$$

$$a = \sqrt{2}\, k_C r \qquad\qquad (219)$$

$$B = \sqrt{2}\, k_T R \qquad\qquad (220)$$

$$b = \sqrt{2}\, k_T r \qquad\qquad (221)$$

where A is not to be confused with the surface area used elsewhere in this chapter. The surface area of the cylinder will be defined in terms of its length and diameter. We now define the following:

$$D \equiv R_O(A)\, R_O(B) \qquad\qquad (222)$$

$$E \equiv R_O(A)\, M_O(B) \qquad\qquad (223)$$

$$F \equiv M_O(A)\, R_O(B) \qquad\qquad (224)$$

$$G \equiv M_O(A)\, M_O(B) \qquad\qquad (225)$$

$$H \equiv R_O(B)\{R_1(A) - M_1(A)\} \qquad\qquad (226)$$

$$I \equiv R_O(A)\{R_1(B) - M_1(B)\} \qquad\qquad (227)$$

$$J \equiv M_O(A)\{R_1(B) + M_1(B)\} \qquad\qquad (228)$$

$$K_C \equiv \{ [R_O(A)\, R_O(a) + M_O(A)\, M_O(a)]^2$$
$$+ [M_O(A)\, R_O(a) - R_O(A)\, M_O(a)]^2 \}^{\frac{1}{2}} \qquad\qquad (229)$$

$$K_T \equiv \{ [R_O(B)\, R_O(b) + M_O(B)\, M_O(b)]^2$$
$$+ [M_O(B)\, R_O(b) - R_O(B)\, M_O(b)]^2 \}^{\frac{1}{2}} \qquad\qquad (230)$$

$$N \equiv R_O(B)\, \{R_1(A) + M_1(A)\} \qquad\qquad (231)$$

$$P \equiv R_O(A)\, \{R_1(B) + M_1(B)\} \qquad\qquad (232)$$

$$Q \equiv M_O(B)\, \{R_1(A) + M_1(A)\} \qquad\qquad (233)$$

$$S \equiv M_O(A) \{M_1(A) - R_1(A)\} + R_O(A) \{M_1(A) + R_1(A)\} \qquad (234)$$

$$T \equiv R_O(A) \{M_1(A) - R_1(A)\} - M_O(A) \{M_1(A) + R_1(A)\} \qquad (235)$$

$$U \equiv R_O^2(A) + M_O^2(A) \qquad (236)$$

$$V \equiv R_O^2(B) + M_O^2(B) \qquad (237)$$

$$X \equiv \frac{\xi \chi^1(\overline{T}) 2\pi L \omega_C \Delta}{UV} \qquad (238)$$

L being sample length.

$$Y \equiv M_O(B) \{R_1(A) - M_1(A)\} \qquad (239)$$

$$Z \equiv M_O(A) \{R_1(B) - M_1(B)\} \qquad (240)$$

where none of the above symbols is to be identified with those used elsewhere in this thesis, such as for example the magnetic field and thermal conductivity symbols.

Finally, let:

$$k'_T = \frac{k_T^2 + k_C^2}{\sqrt{2}\, k_T} \qquad (241)$$

and $\quad k'_C = \dfrac{\sqrt{2}\, k_C^2}{(k_T + k_C)(k_T^2 + k_C^2)} \qquad (242)$

The sample is a cylinder of radius R and length L. As before, the applied field is $H_O \cos \omega_C t$ and the surface thermal oscillations are $\Delta \cos (\omega_T t + \phi_T)$.

The solution for the carrier wave is:

$$T_1 = \frac{\xi H_O \chi(\overline{T}) 2\pi R L \omega_C}{\sqrt{2}\, k_C} \sqrt{\frac{R_1^2(A) + M_1^2(A)}{R_O^2(A) + M_O^2(A)}}\ \cos (\omega_C t + \phi_C) \qquad (243)$$

where

$$\tan \phi_C = \frac{T}{S} \qquad (244)$$

The solution for the modulation is:

$$v_T = X \left\{ \frac{(TI_1 - SI_2)^2 + (TI_3 - SI_4)^2}{(T^2 + S^2)} \right\}^{\frac{1}{2}} \cos\ (\omega_T t + \phi_T - \mu) \qquad (245)$$

$$\tan \mu = \frac{TI_3 - SI_4}{TI_1 - SI_2} \qquad (246)$$

where I_1, I_2, I_3 and I_4 are integrals such that:

$$TI_1 - SI_2 = \frac{R}{2\sqrt{2}} \left\{ \frac{1}{k'_C} \left[\begin{array}{l} Q(ES - TG) - H\ (TD + SF) \\ + N(SD - TF) - Y\ (TE + SG) \end{array} \right] \right.$$

$$\left. + \frac{1}{k'_T} \left[\begin{array}{l} -\ I(TD + SF) + J\ (SE - TG) \\ -\ P(TE + SG) + Z\ (SD - TF) \end{array} \right] \right\} \qquad (247)$$

$$TI_3 - SI_4 = \frac{R}{2\sqrt{2}} \left\{ \frac{1}{k'_C} \left[\begin{array}{l} Q(TF - SD) - H\ (TE + SG) \\ + N(SE - TG) + Y\ (TD + SF) \end{array} \right] \right.$$

$$\left. + \frac{1}{k'_T} \left[\begin{array}{l} -\ I(TE + SG) + J\ (TF - SD) \\ +\ P(TD + SF) + Z\ (SE - TG) \end{array} \right] \right\} \qquad (248)$$

When examining the behaviour of the solution in the various limits, the following are used:

$$\underset{x \to o}{Lim}\ R_O(x) = 1 \qquad (249)$$

$$\underset{x \to o}{Lim}\ M_O(x) = \frac{x^2}{4} \qquad (250)$$

$$\underset{x \to o}{Lim}\ R_1(x) = -\frac{x}{2\sqrt{2}} \qquad (251)$$

$$\underset{x \to o}{Lim}\ M_1(x) = \frac{x}{2\sqrt{2}} \qquad (252)$$

$$\lim_{x \to \infty} R_O(x) = \frac{e^{x/\sqrt{2}} \cos (x/\sqrt{2} - \pi/8)}{(2\pi x)^{\frac{1}{2}}} \tag{253}$$

$$\lim_{x \to \infty} M_O(x) = \frac{e^{x/\sqrt{2}} \sin (x/\sqrt{2} - \pi/8)}{(2\pi x)^{\frac{1}{2}}} \tag{254}$$

$$\lim_{x \to \infty} R_1(x) = \frac{-e^{x/\sqrt{2}} \sin (x/\sqrt{2} - \pi/8)}{(2\pi x)^{\frac{1}{2}}} \tag{255}$$

$$\lim_{x \to \infty} M_1(x) = \frac{e^{x/\sqrt{2}} \cos (x/\sqrt{2} - \pi/8)}{(2\pi x)^{\frac{1}{2}}} \tag{256}$$

In the limit $k_C R = \frac{R}{\delta_C} \to 0$ ($\delta_C \gg R$) we find that Eq. 243

becomes identical to the first term of Eq.178, ie, we obtain the

expression for the carrier wave when the magnetic field is the same

for every point in the sample. In the limit $k_C R \to \infty$ ($\delta_C \ll R$) we

find that Eq.243 becomes identical with Eq.189 corresponding to the

plane wave solution for the carrier signal.

In the limit of $k_C R \simeq k_T R = 0$ ($\delta_C \simeq \delta_T \gg R$) Eq. 245 for the

modulation signal becomes Eq.179 which was the solution for both

δ_C and δ_T being larger than the sample thickness. In the limit of

$R \to \infty$ for finite k_C and k_T, Eq.245 becomes Eq.206 for the plane wave

thermomagnetic solution.

For $k_C \ll k_T$ Eq.245 becomes an expression independent of

k_C and involving the thermal modulation amplitude of Eq.169:

$$v_T = \xi V H_O <\theta - \overline{\theta}> \omega_C \chi'(\overline{T}) \tag{257}$$

In the opposing limit of $k_C \gg k_T$ the amplitude and phase terms

become equivalent expressions in k_C to the former limit in k_T.

The derivation of the general thermomagnetic solution follows

closely that of the plane wave thermomagnetic solution. The general

solutions to the electromagnetic and the thermal waves are the same after one has adjusted the relevant parameters. For example, the electromagnetic solution for cylindrical geometry is:

$$H(r,t) = \frac{H_O K_c}{U} \cos (\omega_C t - \alpha) \tag{258}$$

where

$$\tan \alpha = \frac{M_O(A)R_O(a) - R_O(A) M_O(a)}{R_O(A)R_O(a) + M_O(A) M_O(a)} \tag{259}$$

In a similar way to the derivation of Eq.183, the induced signal in the secondary coil is given by:

$$v \simeq \xi H_O \chi(\overline{T}) 2\pi L \omega_C \int_O^R \frac{K_c}{U} r \sin (\omega_C t - \alpha) dr \tag{260}$$

$$+ \xi H_O \chi'(\overline{T}) 2\pi L \omega_C \Delta \int_O^R \frac{K_c K_T}{UV} r \cos (\omega_T t + \phi_T - \beta)$$

$$\sin (\omega_C t - \alpha) dr$$

where

$$\tan \beta = \frac{M_O(B)R_O(b) - R_O(B)M_O(b)}{R_O(B)R_O(b) + M_O(B)M_O(b)} \tag{261}$$

As before, the first term of Eq.260 describes the carrier wave at ω_C. To evaluate the integral we use the following relationships (see for example the "Handbook of Mathematical Functions with Formulas, Graphs and Mathematical Tables" p.380).

$$\int_O^R rR_O(a)dr = \frac{R}{2k_C} [M_1(A) - R_1(A)] \tag{262}$$

$$\int_O^R rM_O(a)dr = -\frac{R}{2k_C} [M_1(A) + R_1(A)] \tag{263}$$

and we can obtain Eq.243.

In evaluating the second term of Eq.260, we find that:

$$v_T = X \{ \cos (\omega_T t + \phi_T) \sin \omega_C t \int_O^R r \cos \beta \cos \alpha \ K_m \ K_c \ dr$$

$$- \cos (\omega_T t + \phi_T) \cos \omega_C t \int_O^R r \cos \beta \sin \alpha \ K_m \ K_c \ dr$$

$$+ \sin (\omega_T t + \phi_T) \sin \omega_C t \int_O^R r \sin \beta \cos \alpha \ K_m \ K_c \ dr$$

$$- \sin (\omega_T t + \phi_T) \cos \omega_C t \int_O^R r \sin \beta \sin \alpha \ K_m \ K_c \ dr \ \} \qquad (264)$$

This is similar in many respects to Eq.193. If we now represent each of the integrals of Eq.264 by I_1, I_2, I_3, and I_4 respectively and we let:

$$A_\theta = I_1 \cos (\omega_T t + \phi_T) + I_3 \sin (\omega_T t + \phi_T) \qquad (265)$$

and

$$B_\theta = I_2 \cos (\omega_T t + \phi_T) + I_4 \sin (\omega_T t + \phi_T) \qquad (266)$$

Then:

$$v_T = X\sqrt{A^2 + B^2} \ \cos(\omega_C t - \eta) \qquad (267)$$

where

$$\tan \eta = \frac{A_\theta}{B_\theta} \qquad (268)$$

As in the plane solution, this modulation must be weighted by the cosine of the phase difference between the carrier wave and the modulation. This phase difference is $\phi_C + \eta$. Therefore the modulation signal is given by:

$$v_T = X\sqrt{A_\theta^2 + B_\theta^2} \ \cos (\phi_C + \eta) \qquad (269)$$

which results in Eq.245.

To evaluate the integrals I_1, I_2, I_3 and I_4 we use the following relationships:

$$\int x \ (- R_O(a) \ R_O(b) \ - \ M_O(a) \ M_O(b))dx \ =$$

$$\frac{x}{2\sqrt{2}} \ \{ \ M_O(b)[R_1(a) \ + \ M_1(a)] \ + \ R_O(b)[R_1(a) \ - \ M_1(a)]$$

$$- \ R_O(a)[M_1(b) \ - \ R_1(b)] \ + \ M_O(a)[M_1(b) \ + \ R_1(b)] \ \} \quad\quad (270)$$

and

$$\int x \ (\ R_O(a) \ M_O(b) \ - \ M_O(a) \ R_O(b) \ )dx \ =$$

$$\frac{x}{2\sqrt{2}} \{ \ R_O(b)[R_1(a) \ + \ M_1(a)] \ - \ M_O(b)[R_1(a) \ - \ M_1(a)]$$

$$- \ R_O(a)[R_1(b) \ + \ M_1(b)] \ + \ M_O(a)[R_1(b) \ - \ M_1(b)] \ \} \quad\quad (271)$$

By using Eqs.259 and 261, we find that:

$$I_1 \ = \ \int_O^R r\{DR_O(a) \ R_O(b) \ + \ GM_O(a) \ M_O(b)\}dr$$

$$+ \ \int_O^R r\{ER_O(a) \ M_O(b) \ + \ FM_O(a) \ R_O(b)\}dr \quad\quad (272)$$

The complicating factor is the existence of the coefficients

D, E, F and G in Eq.272. No corresponding coefficients appear in

Eqs.270 and 271. To obtain the coefficients in I_1 we use

generalized coefficients k'_C and k'_T which are each functions of

both k_C and k_T. We use the expansions of Eqs.214 to 217 to match

equal powers of k_C and k_T between, for example, Eq.272 and the

combination of the right hand sides of Eqs.270 and 271.

For example, writing only powers of k_C and k_T, we have:

$$DR_O(a) \ R_O(b) \ \rightarrow \ D(1 \ - \ k_T^4 \ + \ k_T^8 \ - \ ... \ - \ k_C^4 \ + \ k_C^4 k_T^4 \ - \ ...)$$

$$(273)$$

and
$$GM_O(a) \ M_O(b) \ \rightarrow \ G(k_C^2 k_T^2 \ - \ k_C^2 k_T^6 \ + \ k_C^2 k_T^{10} - \ ...$$

$$- \ k_C^2 k_T^2 \ ...) \quad\quad (274)$$

while

$$M_O(B)\left(R_1(A) + M_1(A)\right) \rightarrow (k_C{}^3 k_T{}^2 - k_C{}^3 k_T{}^6 + k_C{}^3 k_T{}^{10} + \ldots - k_C{}^7 k_T{}^2 \ldots)$$

$$(275)$$

and

$$- R_O(B)\left(R_1(A) - M_1(A)\right) \rightarrow (k_C - k_C k_T{}^4 + k_C k_T{}^8 \ldots) \qquad (276)$$

We therefore take $\dfrac{D}{k_C'}$ of Eq. 276 to introduce a degree of compatability

with Eq. 273 and $\dfrac{G}{k_C'}$ of Eq. 275 to correspond in some way to

Eq. 274. We treat I_2, I_3 and I_4 in the same way, the task being

simplified by the high degree of symmetry between the integrals.

Finally, we tailor the generalized coefficients k_C' and k_T' so that

in the limit $k_C R \rightarrow \infty$, $k_T R \rightarrow \infty$, the solutions match the corresponding

solutions in the plane wave case. In this way we obtain Eqs. 241 and 242.

The complexity of the solution makes it difficult to absolutely verify

its correctness, but the fact that it corresponds to the other models

in the limits described is encouraging.

4.5   Relaxation Effects

We have seen evidence of relaxation effects in the domain

properties below T_c (refer to Ch. 6, and Sydney et al 1975 a, b).

In this treatment we will assume that there is a uniform temperature

and applied field at all points in the sample at any given time.

The treatment of relaxation effects in both static and alternating

fields will be identical, involving only the time dependence of the

susceptibility (Wilson et al 1975).

Simple Relaxation

For "simple relaxation" it is assumed that, as the temperature is modulated, χ is always relaxing exponentially towards its equilibrium value $\chi_e(T)$ with a relaxation time τ:

$$\frac{d\chi}{dt} = \frac{-[\chi(t) - \chi_e(T)]}{\tau} \qquad (277)$$

Such simple behaviour would not be expected below T_c, but a comparison of the observed behaviour with that expected for simple relaxation will still be worthwhile. Simple relaxation would be expected in temperature modulation experiments on low temperature nuclear magnetizations.

By substituting a Taylor expansion of $\chi_e(T)$ into Eq. 277 it follows that:

$$\chi(t) = \chi_e(\overline{T}) + \sum_{n=1}^{\infty} \{\Delta^n (2^{1-n}/n!)\, \alpha_n \chi_e^{(n)}(\overline{T}) \cos\, [n(\omega_T t + \phi_T) - \phi_n]\}$$

$$(278)$$

where $\phi_n = \arctan\, n\omega_T \tau$ and $\alpha_n = (1 + n^2\omega_T^2\tau^2)^{-\frac{1}{2}}$. Comparing this with Eq. 182, we see that the relaxation will result in a reduction of the nth harmonic signal amplitude by a factor α_n and an additional phase lag of ϕ_n.

Relaxation of Domain Properties

In applying temperature modulation techniques to study a ferromagnetic material near T_c, applied fields which are small in comparison with the exchange fields will generally be used so that the intrinsic magnetic ordering is observed. Above T_c exchange-enhanced paramagnetism with a field-independent susceptibility is expected; below T_c the response to the applied field will be determined by the intrinsic magnetization $M_S(T)$ and by the domain

properties. We treat here the case where the response of M_S

to the temperature modulation is fast enough for it to be always

in thermal equilibrium but with relaxation effects arising from

the domain properties.

We write for the equilibrium susceptibility:

$$\chi_e(H,T) = G_e(H,T) \; \chi_N(H,T) \tag{279}$$

where χ_N is the susceptibility which would be observed if there

were no domains present. Hence G_e represents the effects of the

domains upon the thermal equilibrium susceptibility. Writing

$\chi_N(H,T) = M_S(T)/H$, it follows that the equilibrium magnetization

is:

$$M_e(H,T) = M_S(T) \; G_e(H,T) \tag{280}$$

When the applied field is large enough to magnetically saturate the

sample, i.e. there are no domains present, Eq. 280 shows that $G_e = 1$.

On the other hand, when H is sufficiently low for the linear,

reversible domain wall displacement to dominate the susceptibility,

M_e will be proportional to H and we may write from Eq. 280:

$$G_e(H,T) = g_e(T)H \tag{281}$$

where $g_e(T)$ represents the temperature dependence of the domain wall

mobility. Then, defining in the same way an instantaneous g, it

follows that in a temperature modulation experiment the time dependence

of χ is given by:

$$\chi(t) = g(t) \; M_S(T) \tag{282}$$

We assume that when the temperature is changing g undergoes

exponential relaxation with a time constant τ:

$$\frac{dg}{dt} = - \left\{ \frac{g(t) - g_e(T)}{\tau} \right\} \tag{283}$$

and hence, as for χ in Eq. 278:

$$g(t) = g_e(\overline{T}) + \sum_{n=1}^{\infty} \{\Delta^n (2^{1-n}/n!) \ g_e^{(n)}(\overline{T})\alpha_n \ cos \ [n(\omega_T t + \phi_T) - \phi_n]\}$$

(284)

Assuming that M_S is always in thermal equilibrium, then:

$$M_S(t) = M_S(\overline{T}) + \sum_{n=1}^{\infty} \Delta^n (2^{1-n}/n!) M_S^{(n)}(\overline{T}) \ cos \ n \ (\omega_T t + \phi_T)$$

(285)

For nth harmonic detection we consider only the terms in the
product $g(t)M_S(t)$ which have a frequency $n\omega_T$. For first harmonic
detection this leads to:

$$\chi_1(t) = \Delta \ \{g_e M_S' \ cos \ (\omega_T t + \phi_T) + M_S g_e' \ \alpha_1 \ cos \ (\omega_T t + \phi_T - \phi_1)\}$$

(286)

where the values of M_S, g_e and their derivatives all correspond to
the mean temperature $\overline{T}$. For slow modulation ($\omega_T \tau \to 0$):

$$\chi_1(t) \to \Delta \chi_e^1(\overline{T}) \ cos \ (\omega_T t + \phi_T)$$

(287)

which, as expected, is the same as Eq. 171 for no relaxation effects.
For fast modulation ($\omega_T \tau \to \infty$):

$$\chi_1(t) \to \Delta \ g_e(\overline{T})M_S'(\overline{T}) \ cos \ (\omega_T t + \phi_T)$$

(288)

and here also there is no phase shift caused by the relaxation,
g remaining equal at all times to $g_e(\overline{T})$ with the signal being
produced solely by the oscillations in M_S. Eq. 286 may also be
written as:

$$\chi_1(t) = \Delta \ \{(g_e M_S' + M_S g_e' \ \alpha_1^2)^2 + (g_e' M_S \omega_T \ \tau \alpha_1^2)^2\}^{\frac{1}{2}} cos \ (\omega_T t + \phi_T + \phi_r)$$

(289)

where the phase shift ϕ_r due to the relaxation is given by:

$$tan \ \phi_r = -M_S g_e' \ \omega_T \tau / (\chi_e^1 + g_e M_S' \ \omega_T^2 \tau^2)$$

(290)

At temperatures just below T_c the terms $g_e \ M_S'$ and $g_e' \ M_S$ will be
of opposite signs with amplitudes much greater than that of their
sum χ_e' so that:

$$\tan \phi_r \simeq -M_S \, g_e'/g_e \, M_S' \, \omega_T \tau \qquad (291)$$

and it follows that the domain relaxation will produce a phase lead

($\phi_r > 0$) as we have observed. At lower temperatures g_e' may have

either sign so that either a phase lead or lag is possible.

For second harmonic detection, collection of terms in

$g(t)\dot{M}_S(t)$ with a frequency $2\omega_T$ leads to:

$$\chi_2(t) = \tfrac{1}{4}\Delta^2 \Big\{ \, \alpha_2 \, M_S \, g_e'' \, \cos \, [2(\omega_T t + \phi_T) - \phi_2]$$

$$+ \, 2\alpha_1 \, g_e' \, M_S' \, \cos \, [2(\omega_T t + \phi_T) - \phi_1]$$

$$+ \, g_e \, M_S'' \, \cos \, 2(\omega_T t + \phi_T) \, \Big\} \qquad (292)$$

For slow modulation ($\omega_T \tau \to 0$):

$$\chi_2(t) \to \tfrac{1}{4}\Delta^2 \, \chi_e''(\overline{T}) \, \cos \, 2 \, (\omega_T t + \phi_T) \qquad (293)$$

in agreement with Eq. 182. For fast modulation ($\omega_T \tau \to \infty$) we have

$$\chi_2(t) \to \tfrac{1}{4}\Delta^2 \, g_e(\overline{T}) M_S''(\overline{T}) \, \cos \, 2(\omega_T t + \phi_T) \qquad (294)$$

Note that, as the mean temperature is varied, in the limits

of both slow and fast modulation, a phase reversal of the second

harmonic signal is expected near T_c.

90.

CHAPTER   5

EXPERIMENTAL TECHNIQUE

5.1   General

Apart from the sophisticated nature of the individual items

of equipment used in this research, the experimentation is simple.

To some extent this may be attributed to the selection of Gd as the

subject of study since its Curie point is at room temperature.

However, this simplicity is mostly due to the simple concept of the

experiments. The inductance technique of measuring AC susceptibility

is standard : the sample under study constitutes the core of a

transformer, and the output of the transformer is measured as a

function of the sample temperature (see eg, Casimir 1940, Heller

1967). Furthermore, the technique of measuring the temperature-

differential of the magnetic susceptibility of a ferromagnetic

material near T_c has been used before : Chynoweth (1958) used

temperature modulation in a static field to ascertain the Curie point

in gadolinium iron garnet; Chynoweth called the effect the pyromagnetic

effect and Walser et al (1971) used it for the detection of infra-red

radiation.

In this work we have combined these two techniques to produce

the AC modulation technique which leads to an enhancement of the

modulation signal as we have seen in Chapter 4.

5.2   Analogue Computer Simulation of Thermal Modulation

The flowchart given in Fig. 3 shows the analogue computer

logic which was used to simulate the thermal response of a sample to

a sinusoidal power waveform in a heater coil. The investigation was

carried out on the simple model wherein at any time every point in

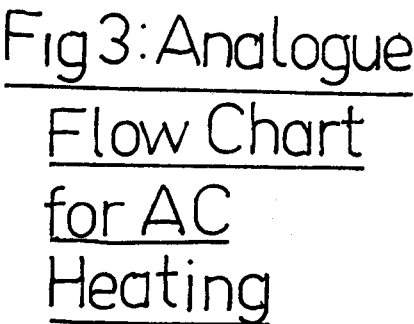the sample is assumed to be at the same temperature. The

$$\frac{d\theta_T}{dt} + \frac{b\theta_T}{mc} = \frac{V_o^2}{Rmc}\sin^2\omega t \parallel \frac{d\theta_{THCP}}{dt} + \frac{b\theta_{THCP}}{mc} = \frac{V_o^2}{2Rmc} \parallel \theta = \theta_T - \theta_{THCP}$$

OPERATING BUS

$\div 0.8$

DISTRIBUTOR

3302 A TRIG. GEN

MULTIMODE
NEG. PHASE
ZERO ANGLE
EXTERNAL

3300A OSC.

CH.A $\quad \frac{V_o}{\sqrt{R}}\sin\omega t$

CH.B $\quad -\frac{V_o}{\sqrt{R}}\sin\omega t$

X -1

X -1

MULT.-INT.

$-\frac{V_o^2}{10R}\sin^2\omega t$

X -10

$\frac{V_o^2}{R}\sin^2\omega t$

X -1

$\div 10mC$

$-\frac{V_o^2}{10Rmc}\sin^2\omega t$

INT -1

$\frac{b\theta_T}{10mC}$

$\frac{\theta_T}{10}$

$\div 10$

$\frac{-mC}{10b}$

X -1

$-\frac{\theta}{100}$

$-\frac{\theta_{THCP}}{100}$

X 10

SOLUTION $\frac{\theta}{10}$

10 V

$\div 100$

$\frac{V_o^2}{200Rmc}$

INT

$-\frac{b\theta_{THCP}}{100mC}$

$\frac{-mC}{10b}$

$\div 10$

Fig 3: Analogue Flow Chart for AC Heating

solutions were thus obtained to Eq. 144.

5.3   Sample Assembly

Figure 4 gives a schematic diagram of the sample assembly. The polycrystalline gadolinium ingot from which the bulk samples were made was supplied by Rare Earths Products Limited. While the ingot was quoted by the suppliers to be 99.9% pure, it is thought to be somewhat futile to place reliance on impurity figures in Gd when assessing our results, since Gd is an extremely good absorber of gaseous impurities, especially oxygen and nitrogen. Minimal precautions were taken to keep our sample surfaces "clean", but the samples were taken directly from the ingot supplied without any further processing, and the experiments were performed in the atmosphere apart from the layers of wire, binding and insulation which constituted the remainder of the sample assembly. However, the major part of the impurities should have occurred relatively close to the surface of the sample, and as our results will show, care was taken to ensure that measurements came from the bulk of the sample. Moreover, we have studied the effects of impurities on our measurements; where required, we have tailored our experimental conditions to minimize these effects. For example, we have not endeavoured to obtain the susceptibility critical exponent for Gd below T_c. We found that domain properties made it impossible to do so in the ferromagnetic region. One such domain property is a magnetic after effect (refer to Chapter 6) which we have attributed to gaseous impurities. Domains have been found not to be present more than ~ 1K above T_c and we have thus used our techniques to obtain a measurement for γ.

For the majority of experiments the sample was in the form of a toroid (OD 2.4 cm, ID 1.8 cm). Where DC magnetic

HEATER COIL

PRIMARY COIL   SECONDARY COIL

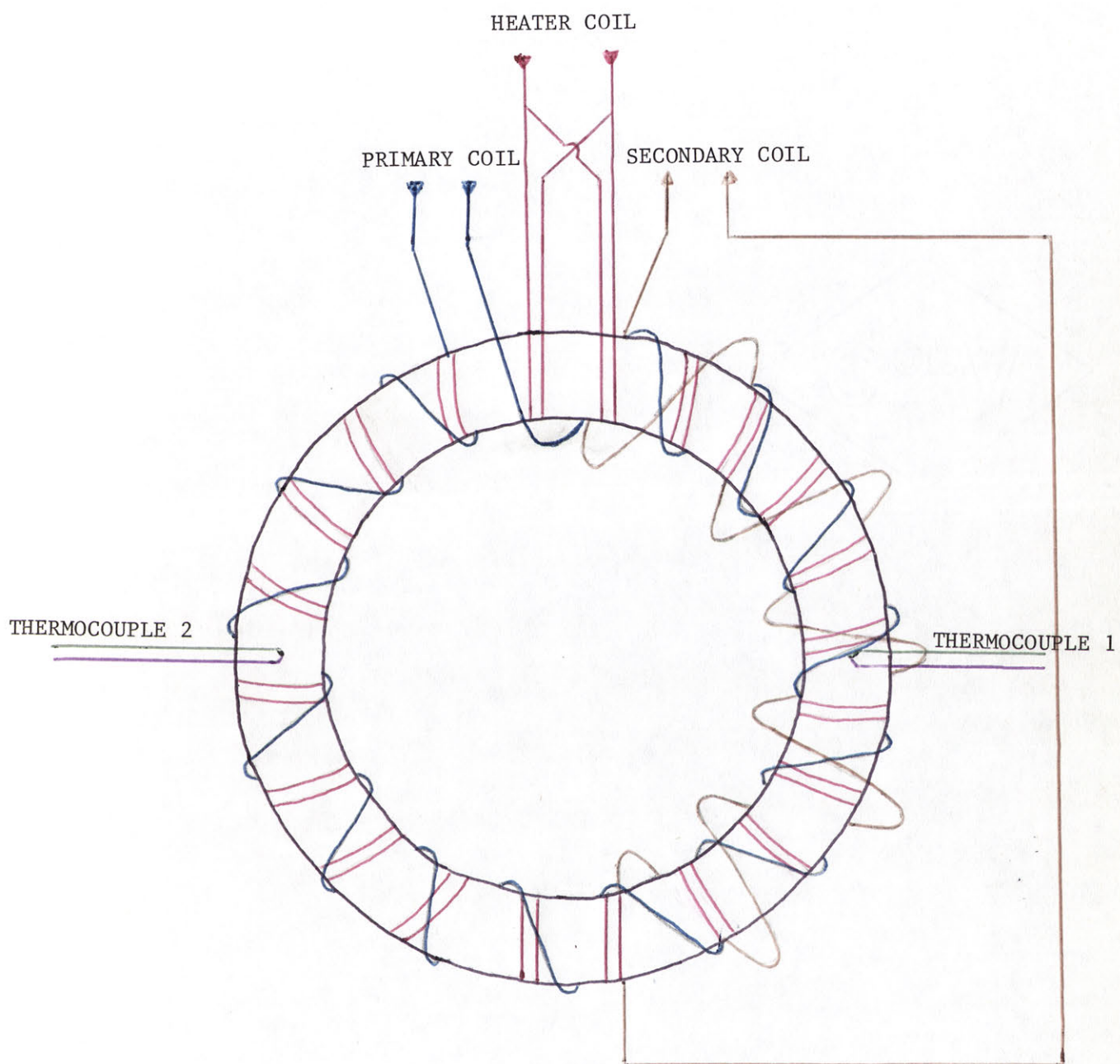THERMOCOUPLE 2   THERMOCOUPLE 1

FIGURE 4   SAMPLE ASSEMBLY

fields greater than 850 A/m were required, cylindrical samples were used (length 2.5 cm, diameter 3mm). Experiments were also performed on Gd foil samples supplied by Metals Research Limited. Once again, these samples were quoted as being 99.9% pure, but the effects of gaseous absorption are thought to be more prominent with foil and the broadened results we observed were attributed to these impurities. Consequently, none of the quantitative results quoted in this thesis have come from the experiments on Gd foil.

The effects of annealing have not been studied here. It is felt that without undue concentration on this aspect of sample preparation, gaseous absorption could render the results of annealing inconclusive.

The large number of phenomena observed in this work on polycrystalline gadolinium have pushed studies on single crystal samples beyond the scope of this thesis. Such studies, however, should be an important area for continuation in this field of research.

Thermometry. Copper-constantan thermocouples constructed from 48 SWG plastic-coated wires and calibrated against the freezing point and boiling point of distilled water were used. The thermo-couple heads were placed in small holes drilled into the samples. For the toroidal sample, two thermocouples were used, one on each side of the toroid; for the cylindrical samples, one thermocouple was placed midway along the length of the sample and the other at the end of the sample. The use of very fine thermocouple wires to prevent heat conduction along them was one of the main precautions taken to prevent temperature inhomogeneities in the samples. Depending on heating and cooling rates, temperature differentials of up to 10K could be introduced between the positions of the thermocouple heads; however, with the 48 SWG wires used, no measurable temperature inhomogeneity could be found for heating and cooling rates up to ~ 0.1K/sec. A

Kaye Instruments Ice-Point Reference device was used to supply to cold junction reference temperature for the thermocouples.

Temperature Control. An AC heater of "moleculoy" wire (75% Ni, 20% Cr, 3% Al, 2% Co) was wound non-inductively over the whole sample for the majority of the experiments. For the cylindrical samples it was found necessary to have compensating heater coils near the sample ends to allow for heat loss from the ends. Usually, the thermal environment was supplied by a Lauda K4R electronic thermostatic bath; it has a large thermal capacity, and provided the heater power did not exceed ~ 0.3 W, temperature variation throughout the sample was less than 0.1K. Where large DC magnetic fields were required, the physical dimensions of the thermostatic bath were not compatible with those of the field-generating devices. In these cases (none of which apply to the accurate quantitative assessments based on temperature measurement) a rectangular cold dewar was used to provide the heat sink for the sample assembly. This was of suitable dimensions for the field-generating devices, but temperature control could only be guaranteed to ± 0.5K.

Coil Assembly and Magnetic Field Control. For the toroid assembly, a primary coil of 500 turns of copper wire was wound tightly over the sample and the heater coils so as to uniformly cover the whole of the sample. This was followed by a secondary coil of 1500 turns of copper wire wound over half the sample, one of the thermocouple heads being centrally placed to this coil. This arrangement serves to minimize the effects of any thermal and magnetic irregularities on the secondary output. The proximity effect for these coils was found to be negligible in the frequency range used.

With the cylindrical samples, the transformer was built separately
on a plastic former and the sample assembly with the heater and
the thermocouple heads incorporated, was placed into the centre
cavity of the transformer.

In the DC experiments with fields up to $\simeq$ 850 A/m, a DC
current was passed through the primary coil so as to generate a
static field along the circular axis of the toroid. This field
could be calculated from the current and the known turns
configuration, and for our assembly was 7.5 A/m for each mA of
current. The secondary coil acted as the pick-up coil. For
higher fields, external field-generating devices were used to
avoid excessive heating in the primary coil. Helmholtz coils
were used to generate DC fields between 850 A/m and 2400 A/m,
while an electromagnet was employed when larger fields were
required. An esr probe was used to calibrate both these devices.

5.4   General Experimental Design

Photographs of the major items of equipment can be seen in
Fig. 5. Two Princeton lock-in amplifiers (phase sensitive detectors,
PSDs) a model 124 and a model 124AL, together with a Princeton model
127 two-phase unit formed the core of the measuring apparatus. The
124AL can detect at frequencies down to 0.2 Hz, although, as stated
in the specifications, deviations from linearity occur in phase and
amplitude measurements for frequencies below about 2 Hz. Where
this was likely to cause difficulties, a separate calibration against
a waveform of known phase and amplitude was carried out before each
measurement. Where possible, a differential input was used, and at
low frequencies it was found to be beneficial to connect 1000 Ω
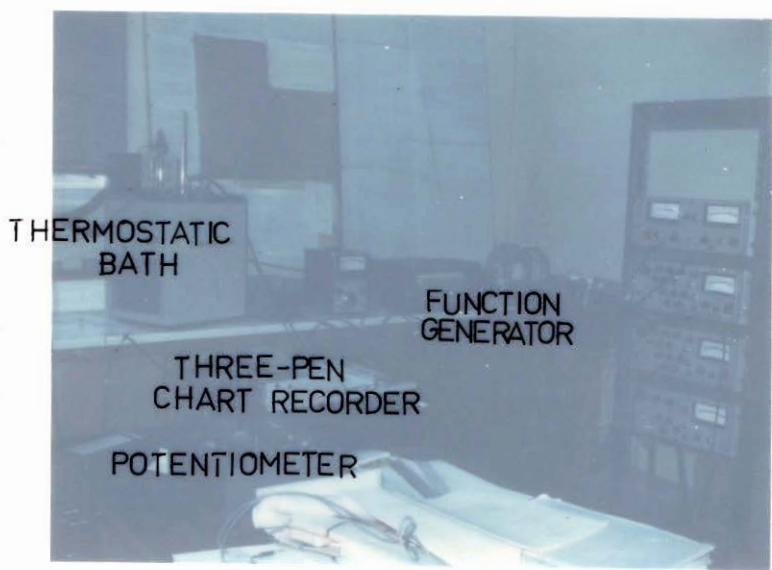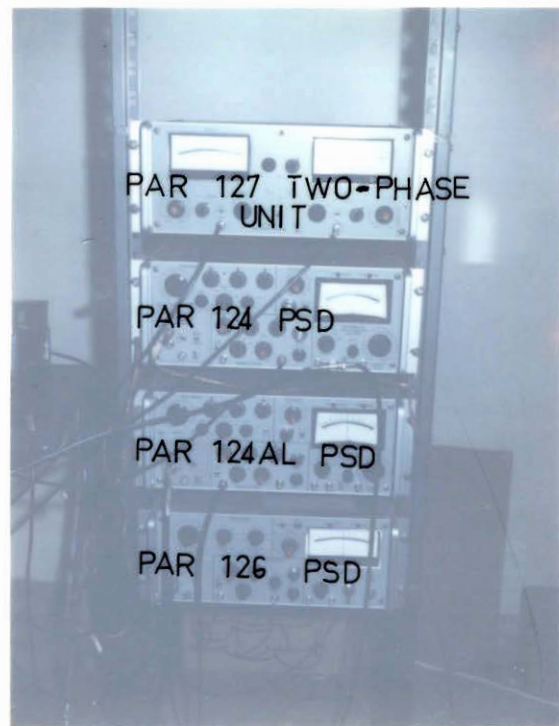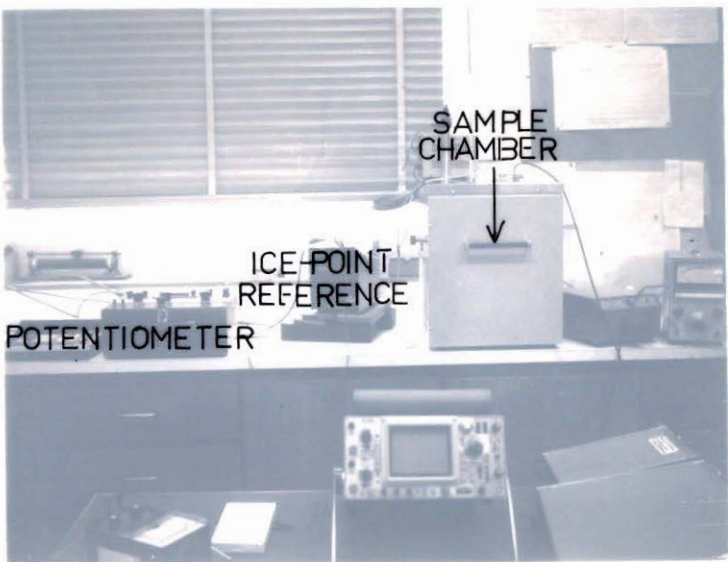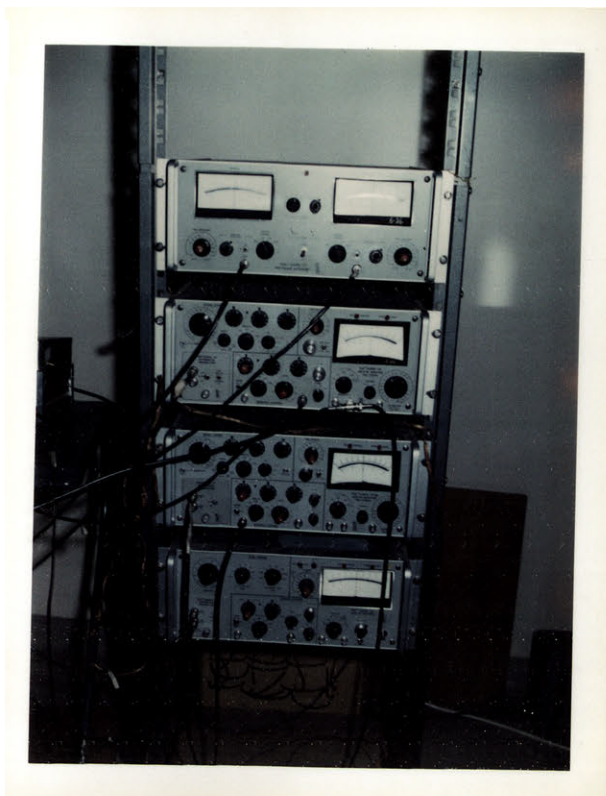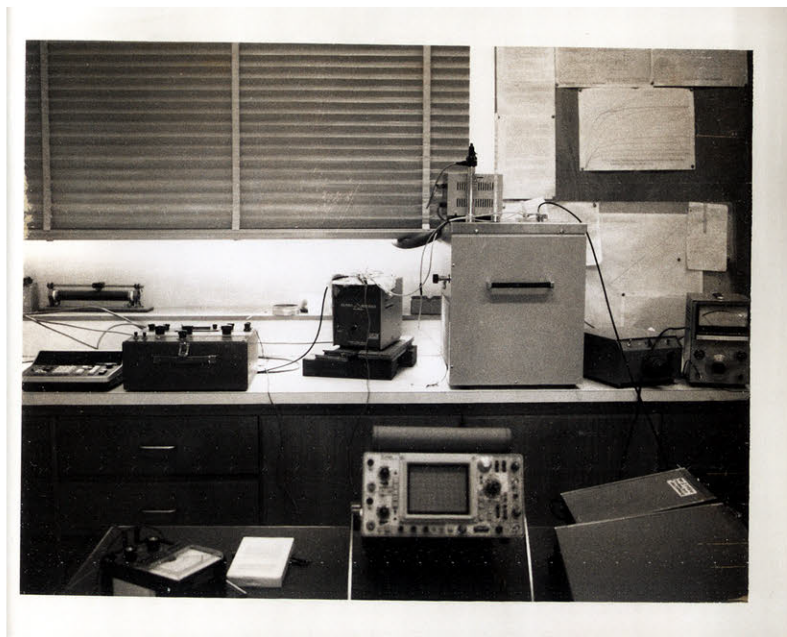from each input to ground to aid in common-mode rejection : the

FIG 5: EQUIPMENT

sample assembly output impedance was about $7\,\Omega$ while the common-mode source resistance was found to be $\sim 10^4\,\Omega$.

The primary current in the majority of the AC experiments was taken from the internal oscillator of that PSD which was being used to monitor the secondary output at the field frequency. This allowed the PSD to be used in the internal reference mode which facilitated greater signal-to-noise ratio at low frequencies. The output resistance of this generator was $600\,\Omega$, so that the arrangement closely approximated a constant-current circuit. Nevertheless, a Princeton model 126 PSD was used to accurately monitor the voltage across a standard resistance placed in the primary circuit; in this way, corrections were made for changes in primary current with temperature.

Where higher currents than could be supplied by the PSD internal oscillator were required, a Systron-Donner/Datapulse 410 sweep-function generator with either a $600\,\Omega$ or a $50\,\Omega$ output resistance was used. With a $50\,\Omega$ output resistance, significant corrections were required to account for primary current changes.

The heater power was supplied by the 410 generator with a $50\,\Omega$ output resistance. The resistance of the heater was approximately $50\,\Omega$. The gating, variable DC offset and variable waveform capabilities of the model 410 generator, together with its low-frequency characteristics made it useful for many of the experiments performed in this work.

Other items of equipment used consistently during this work include a Leeds and Northrups 8686 millivolt potentiometer for temperature measurement and a Rikidenki three-pen chart recorder.

5.5 AC Susceptibility Measurements

The experimental layout for this standard technique is shown in Fig. 6. With the sample forming the core of the transformer, the secondary output is given according to the theory in Chapter 4:

$$v = N H_O \omega_C [(\mu_0 + \xi\chi') \sin \omega_C t - \xi\chi'' \cos \omega_C t] \qquad (295)$$

where N is the number of secondary turns, ξ is a sample filling factor, χ' and χ'' are the real and imaginary (dispersive and absorptive) components of the AC susceptibility χ, and the applied field is $H = H_O \cos \omega_C t$. The secondary coil voltage was monitored by the 124AL PSD in conjunction with the 127 two phase unit, enabling both χ' and χ'' to be measured.

Magnetic Hysteresis Measurements. The experimental layout for the magnetic hysteresis measurements is shown in Fig. 7. The primary current was generated by a Hewlett Packard model 203A function generator which has two outputs one of whose phase can be altered. The two PSDs were employed as AC amplifiers. An RC filter arrangement of suitable time constant was placed between the PSDs to act as an integrator, and the integrated output was placed onto the Y plates of a CRO operating in the X-Y mode. The X plate voltage representing the field came from the variable phase output of the function generator; this output was adjusted so that the X and Y voltages were in phase when the sample temperature was well above T_c. This procedure was necessary since it was found that the 124 PSD introduces a phase error for frequencies less than about 70 Hz. The relative magnetic resonance and the relative minor loop coercive force were then measured as a function of temperature from the Lisajous figure on the CRO.
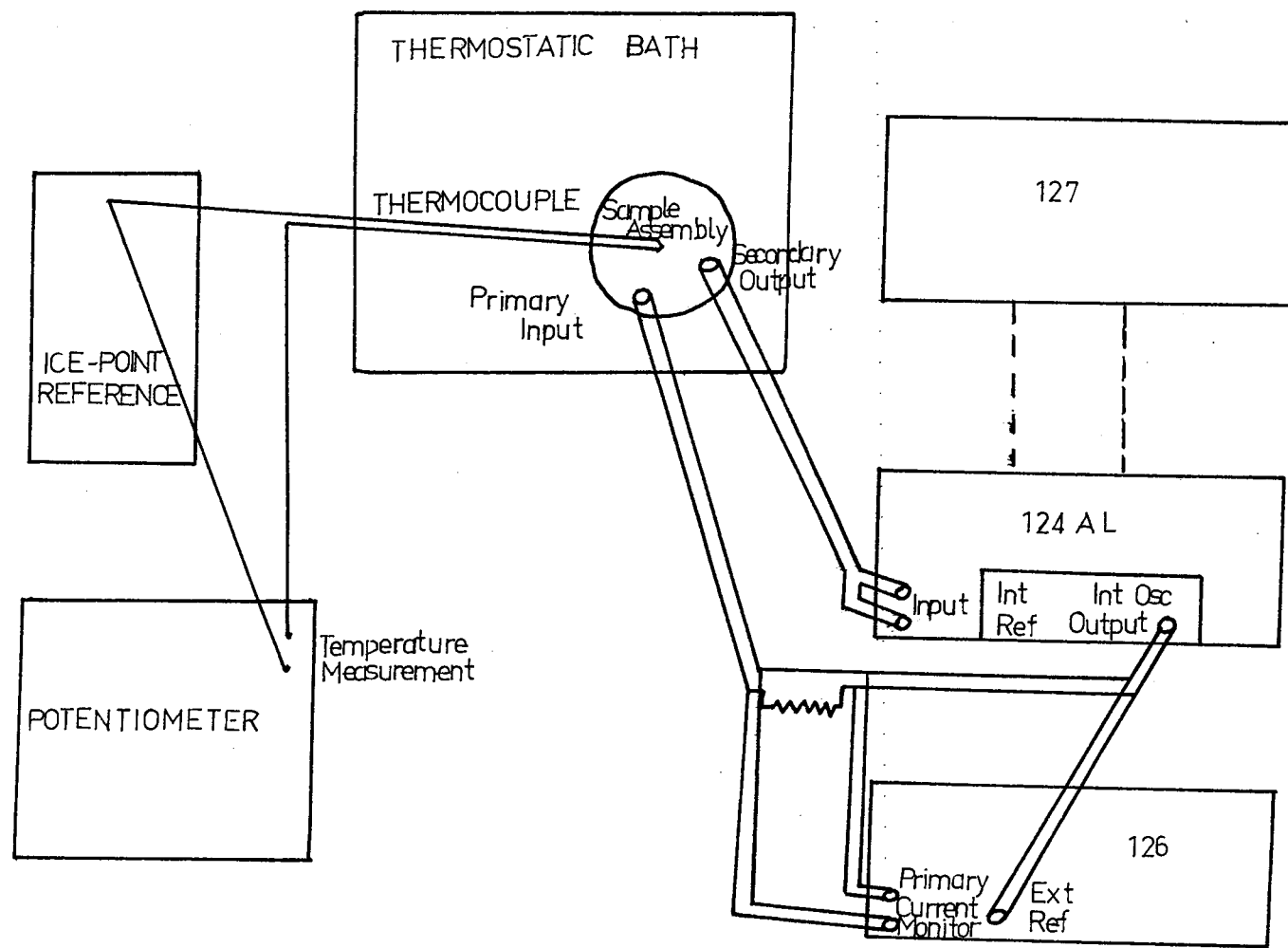
THERMOSTATIC BATH

THERMOCOUPLE

Sample Assembly

Secondary Output

Primary Input

ICE-POINT REFERENCE

127

124 A L

Input | Int Ref | Int Osc Output

Temperature Measurement

POTENTIOMETER

126

Primary Current Monitor | Ext Ref

FIG.6: AC SUSCEPTIBILITY TECHNIQUE

THERMOSTATIC BATH

VARIABLE PHASE FUNCTION
GENERATOR

ICE-
POINT
REFERENCE

THERMOCOUPLE

Sample
Assembly

Secondary
Output

Primary
Input

Fixed
Phase

Variable
Phase

124 AL

Input

Output

Temperature
Measurement

OSCILLOSCOPE

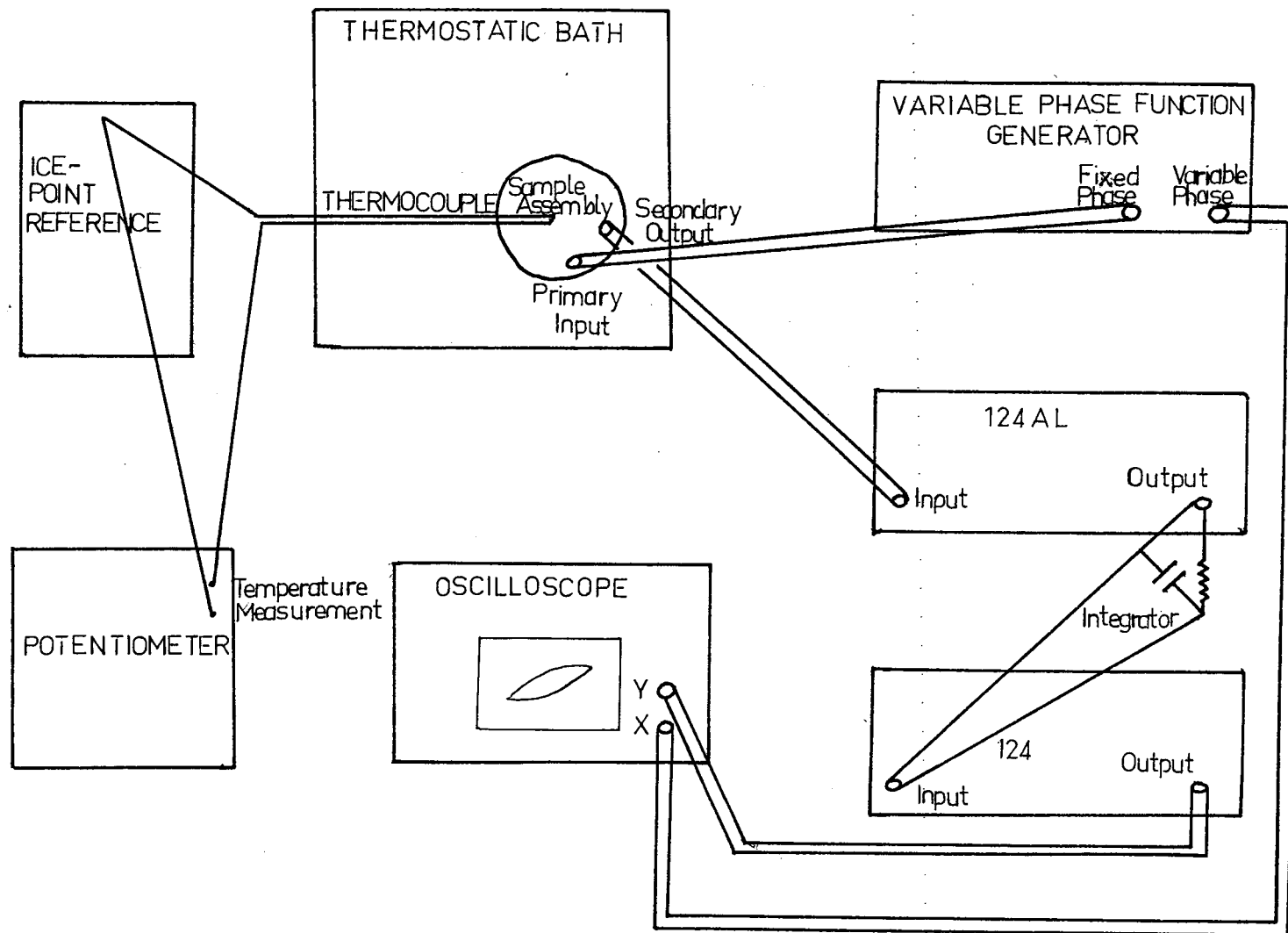Integrator

POTENTIOMETER

Y
X

124

Input

Output

FIG. 7 : MAGNETIC HYSTERESIS TECHNIQUE

Thermal Relaxation Experiments on the Susceptibility. By

applying square wave voltage pulses to the heater coil the temperature

of the sample could be alternately raised and lowered with a response

time ~ 0.2 sec. The secondary voltage and the thermocouple voltage

were monitored on the chart recorder and the response of the

susceptibility to sudden temperature changes was observed. That

the slow-response observed just below T_c was due to relaxation

processes was supported by the observation of fast response of the

secondary voltage at temperatures above T_c.

5.6   DC Temperature Modulation Studies

The experimental layout for the DC temperature modulation

technique is shown in Fig. 8. A sinusoidal current with frequency

$\omega_T/2$ was passed through the heater coil producing temperature

modulation of frequency ω_T. The modulation amplitude ΔT was

typically a few mK. Modulation frequencies from 0.3 to 10 Hz were

used. A DC magnetic field was applied along the sample axis. The

induced signal in the secondary coil was measured using the 124AL PSD

operating in the second harmonic mode. The technique of using a

heater current with frequency $\omega_T/2$ and detecting the modulation

signal at ω_T has the advantage of rejecting any spurious signals

resulting from pick-up from the heater coil.

5.7   AC Temperature Modulation Experiments

Figure 9 shows the experimental layout for an AC temperature

modulation experiment at the first harmonic of the heater power

waveform. No DC field is necessary. The sample formed the core of

an AC transformer as in the conventional AC susceptibility techniques

described in Sec. 5.5. Temperature modulation then results in an

amplitude modulated secondary output voltage. The 124 PSD operating

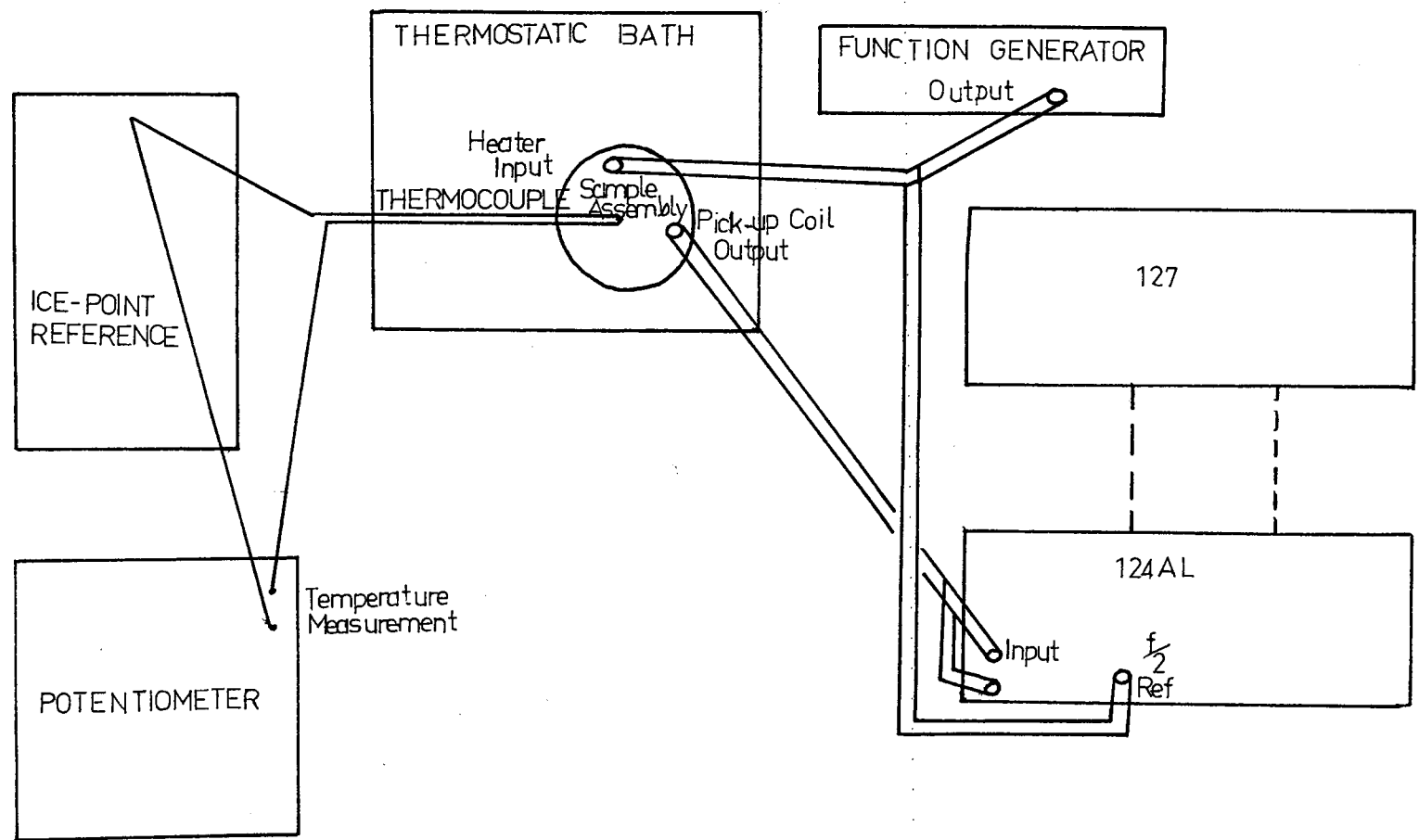at f_C was used to give an output proportional to the permeability.

THERMOSTATIC BATH

FUNCTION GENERATOR
Output

Heater
Input

THERMOCOUPLE Sample
Assembly

Pick-up Coil
Output

ICE-POINT
REFERENCE

127

124 AL

Input

$\frac{f}{2}$
Ref

Temperature
Measurement

POTENTIOMETER

FIG. 8 : DC MODULATION TECHNIQUE

THERMOSTATIC BATH

FUNCTION GENERATOR
Output

Heater Input

Sample
THERMOCOUPLE Assembly

Secondary
Output

Primary
Input

ICE-POINT
REFERENCE

Temperature
Measurement

POTENTIOMETER

127

124

Int
Ref

Int
Osc Out

Output

Input

124AL
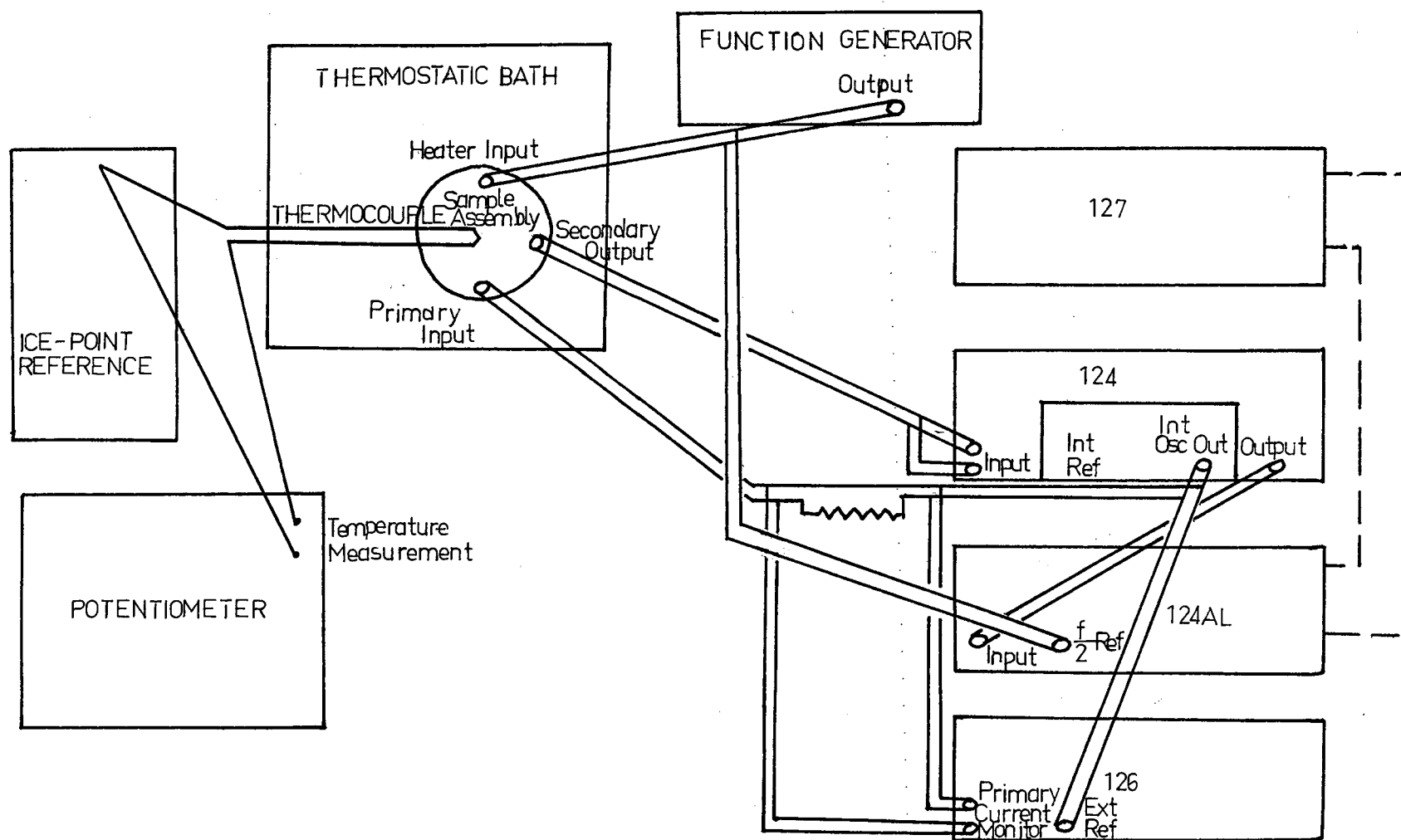
Input

f
2 Ref

Primary
Current
Monitor

Ext
Ref

126

FIG. 9: AC MODULATION TECHNIQUE

The output time constant tc used here was such that $\omega_C^{-1} \ll tc \ll \omega_T^{-1}$ so that signals at the carrier frequency were smoothed without removal of the temperature modulation signal. This output was then fed into the 124AL PSD with the 127 two-phase unit operating in the second harmonic mode at frequency f_T.

As shown in Chapter 4, phase-sensitive detection at the nth harmonic of the temperature modulation yields a signal which is proportional to the nth temperature derivative of the susceptibility, $\chi^{(n)}$, so that both this arrangement and the DC modulation technique described in the previous section yield the first derivative $\chi^1\ (\overline{T})$. By doubling the frequency of the input reference signal and also operating with the 124AL in the second harmonic reference mode, it was possible to detect the second harmonic signal at frequency $2\omega_T$. The rapid decrease in signal-to-noise ratio as the order of the detected harmonic was increased made it impracticable to detect signals at higher harmonics.

Relaxation of the First Harmonic Signal. Here a sinusoidal current with frequency ω_T plus a DC offset were passed through the heater coil. If the total voltage is $V_{DC} + V_{AC}\ sin\ \omega_T t$, then the power waveform is related to $V_{DC}^2 + 2\ V_{DC}\ V_{AC}\ sin\ \omega_T t + (V_{AC})^2\ sin\ ^2\omega_T t$. Thus modulation is produced at ω_T as well as $2\ \omega_T$. The 124AL PSD was operated in the external reference (first harmonic) mode to detect the modulation at ω_T. By suddenly changing the DC offset current V_{DC} with a compensating change in V_{AC} so as to keep $V_{DC}\ V_{AC}$ constant, it was possible to make rapid changes in the mean temperature of the sample without any change in the actual modulation amplitude. The time-dependence of the in-phase and quadrature modulation signals and of the sample temperature were then monitored on the 3-pen chart recorder.

5.8   Measurement of Modulation Amplitudes

Since both the DC and the AC temperature modulation signals
are proportional to the modulation amplitude Δ,   any variations
in Δ must be allowed for in obtaining $\chi(T)$ curves from these
techniques.   Such a variation is expected with Gd near T_c because
of the divergence of the specific heat.   The temperature dependence
of the modulation amplitude and phase were determined by measuring
the output of the thermocouple on the 124AL PSD.   To perform these
measurements, low modulation frequencies and a modulation amplitude
of ~ 35 mK were used.

CHAPTER   6

DOMAIN RESULTS AND DISCUSSION

In this chapter it is intended to deal with the experimental results exclusive of those relating to the critical exponent γ which will be left to the following chapter.

6.1   Analogue Computer Simulation

Figure 10 contains the results of the simulation of the thermal modulation of the sample. The simulation was performed under conditions of constant power input with the important changing factors being mC, the product of the sample mass and the specific heat of the material, and b, the Newton's law of cooling constant. In accordance with Eq. 146, varying b while holding mC constant causes the mean sample temperature to rise at similar rates to different equilibrium temperatures; varying mC and holding b constant causes the mean temperature to rise at different rates to the same equilibrium temperature. The conditions have been chosen such that $b \ll \omega_T mC$ to conform to observed behaviour in our experiments, and in accordance with Eq. 147 it can be seen that the oscillations are relatively independent of b, but are dependent on mC.

6.2   AC Susceptibility Studies

Figure 11 shows $\chi(T)$ curves obtained with a frequency of 100 Hz. The curves are qualitatively similar to the 2 KHz data we have published previously (Sydney et al 1974) except that in higher fields at lower temperatures where the permeability is highest, it was found that the 2 KHz curves were somewhat distorted as the electromagnetic skin depth was no longer far greater than the sample
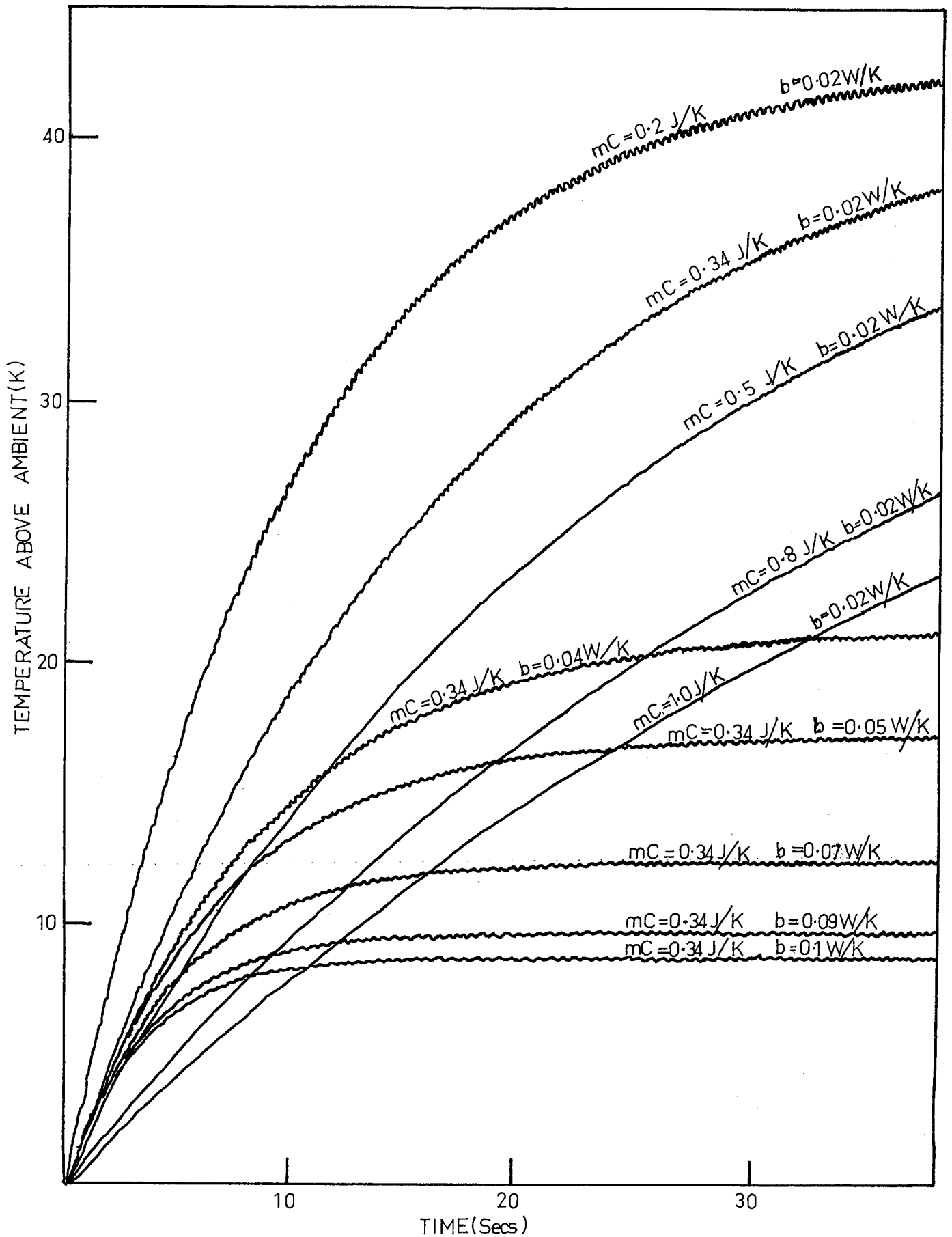
FIGURE 10:   ANALOGUE TEMPERATURE DEPENDENCE ON COEFFICIENT OF CONVECTIVE
HEAT TRANSFER b, MASS m, SPECIFIC HEAT C; INPUT POWER 2 WATT;
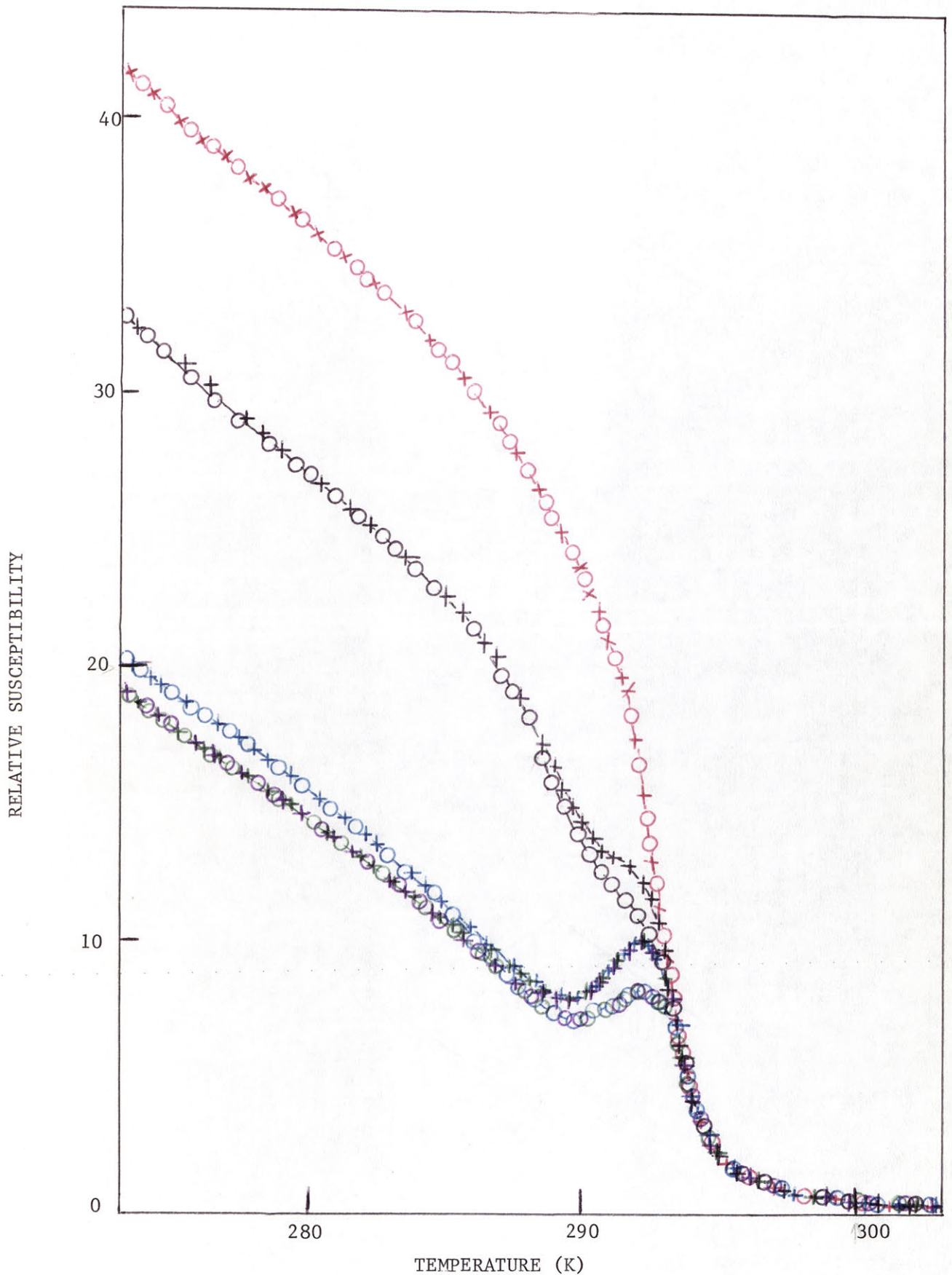FREQUENCY 2 Hz.

FIGURE 11: TEMPERATURE DEPENDENCE OF THE SUSCEPTIBILITY OF GADOLINIUM.
FIELD FREQUENCY 100 Hz; RMS FIELDS: RED 750 A/m;
BLACK 75 A/m; BLUE 7.5 A/m; GREEN 7.5 x 10^{-1} A/m;
PURPLE 7.5 x 10^{-2} A/m; + COOLING; O WARMING.

diameter. As shown below, distortion of the curves by eddy current effects was negligible at 100 Hz. For high ($\gtrsim$ 700 A/m) AC fields there is little evidence of structure in an essentially monatonically varying $\chi(T)$. In low fields, $\chi(T)$ exhibits a peak below T_c with a minimum at about 290.5K; also there is a significant difference in $\chi(T)$ obtained over a few degrees below T_c depending on whether the sample was being cooled from above T_c or warmed from about 10K below T_c. For intermediate fields there was still some significant thermal hysteresis, and $\chi(T)$ exhibited an inflection in the temperature range corresponding to the structure in the low field $\chi(T)$ curves. Whilst the cooling curves were always highly reproducible, the warming curves showed some rate dependence for warming rates greater than 0.2K/min; however, no rate dependence was observed for lower rates. In one low-field experiment the sample was warmed to 291.4K where there is the largest difference between the warming and cooling curves, and no time dependence was observed while the temperature was held constant for two hours. Above T_c there was no temperature hysteresis, and a field independent exchange enhanced paramagnetic susceptibility was observed.

Figure 12 shows the temperature dependence of the phase lag, $\phi = \arctan \left(\frac{\chi''}{\chi'} \right)$ caused by the presence of the absorptive component of χ. In most respects, these measurements reflect the qualitative details of the coercive force measurements; however, they also permit more accurate measurements of the absorption at low fields than is possible from magnetic hysteresis measurements. In the paramagnetic region the primary current and the secondary voltage were observed to be exactly in quadrature corresponding to $\phi = 0$ and hence $\chi'' = 0$ for all values of applied field used. This indicates that above T_c there are no relaxation effects on the time scale of the 100 Hz
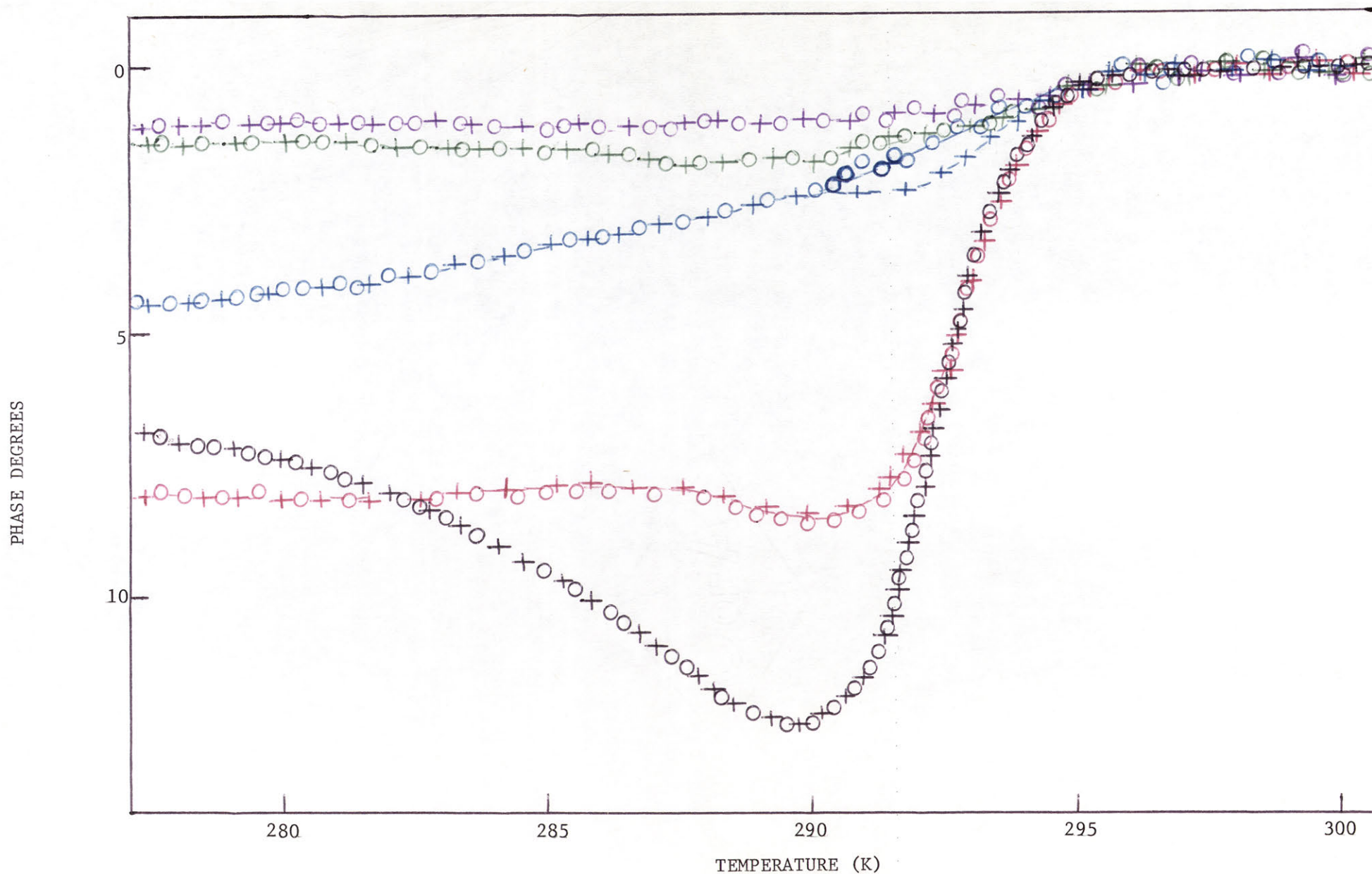
FIGURE 12: TEMPERATURE DEPENDENCE OF THE PHASE OF THE COMPLEX SUSCEPTIBILITY. FIELD FREQUENCY 100 Hz; RMS FIELD AMPLITUDES: RED 750 A/m; BLACK 75 A/m; BLUE 7.5 A/m; GREEN 7.5×10^{-1} A/m; PURPLE 7.5×10^{-2} A/m; + COOLING; 0 WARMING.

frequency used. At temperatures $\leqslant 296 \pm 0.3$K phase lags were observed at both low and high fields.

In Fig. 13 the dependence of χ at 100 Hz upon the RMS applied field amplitude is shown. At temperatures above T_c the susceptibility is field independent over the wide range of applied fields used. Below T_c the susceptibility is accurately field-independent for applied fields ranging over three decades below about 8 A/m. This appears to be the first observation of an initial field-independent susceptibility for a rare earth ferromagnet. For larger applied fields χ increases with increasing fields reaching a maximum at about 375 A/m which corresponds to the inflection in the virgin magnetization curve as the sample approaches saturation. The corresponding dependence of the phase lag ϕ upon field is shown in Fig. 14. It is seen that at fields below $\sim$ 8 A/m ϕ is effectively field-independent; the onset of irreversible processes in higher fields is well indicated by the abrupt increase in ϕ for fields above 8 A/m.

The dependences of χ and ϕ upon frequency both above T_c and also below T_c for several different values of the applied field are given in Figures 15 and 16. The data obtained above T_c shows a frequency-independent χ and an almost zero phase lag for frequencies up to $\sim$ 1 KHz; at higher frequencies the effects of the finite skin depth appear. Below T_c skin depth effects begin to occur at lower frequencies because of the higher susceptibility and this is most marked for larger applied fields where χ is largest. Otherwise, for large fields χ is almost frequency independent whereas for lower fields the frequency dependences of both χ and ϕ are characteristic of a small magnetic after-effect. In Fig. 17 the temperature dependence of the low-field susceptibility is shown for a variety of frequencies from 0.2 to 100 Hz. A tendency to smooth out the trough in the region of 290K as the frequency is lowered, is indicated.
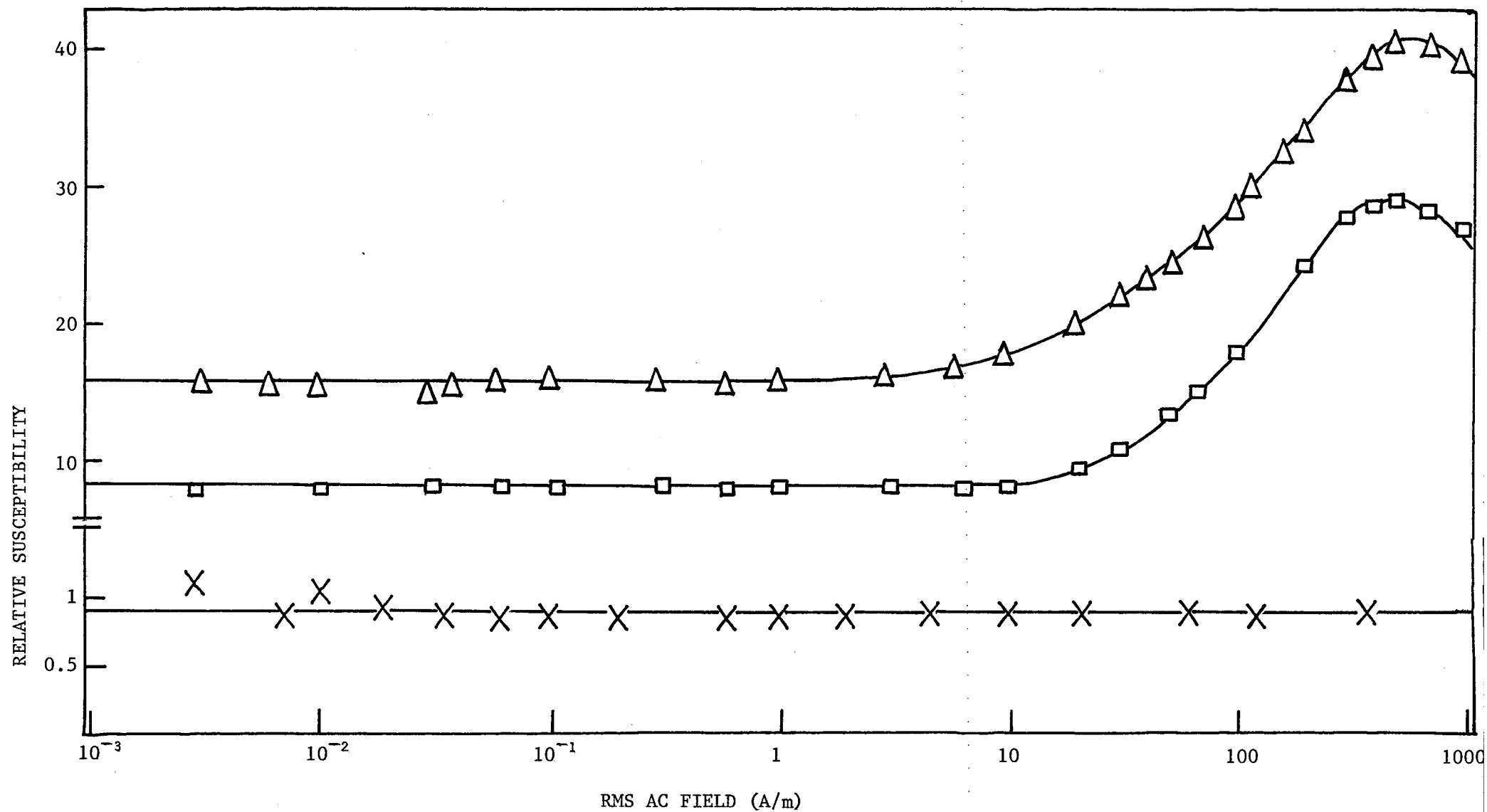
FIGURE 13: DEPENDENCE OF THE AC SUSCEPTIBILITY ON APPLIED AC FIELD AT 100 Hz FOR VARIOUS TEMPERATURES :
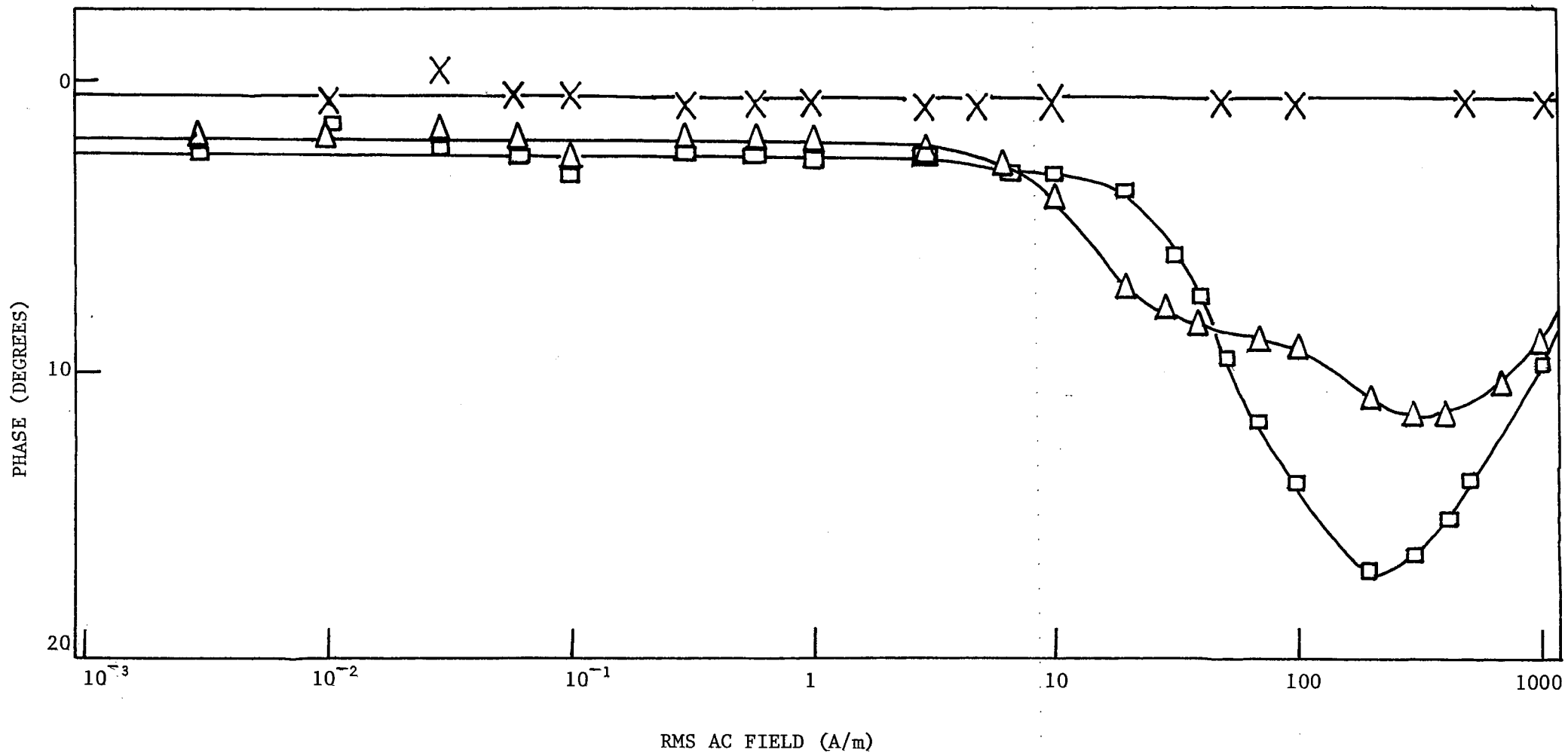✕ 296.8K; ☐ 289.7K; △ 280.3K.

FIGURE 14:   DEPENDENCE ON APPLIED AC FIELD OF THE PHASE OF THE COMPLEX SUSCEPTIBILITY FOR VARIOUS TEMPERATURES :
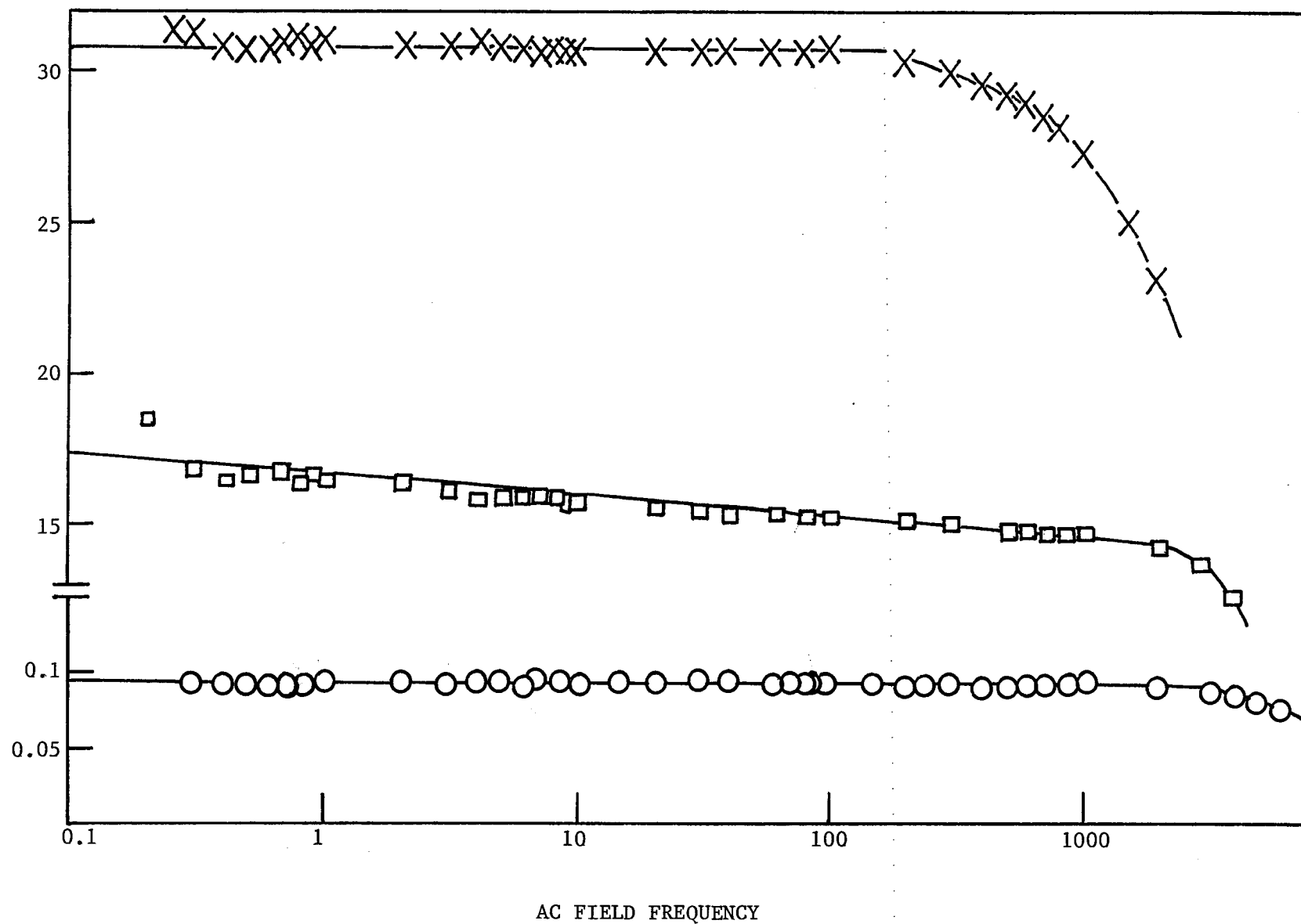
X 296.8K;   □ 289.7K;   △ 280.3K.

FIGURE 15: DEPENDENCE OF THE AC SUSCEPTIBILITY ON THE APPLIED AC FIELD FREQUENCY FOR VARIOUS CONDITIONS OF TEMPERATURE AND RMS AC FIELD : × 100 A/m at 277.9K; □ 0.75 A/m at 278.2K; 0 100 A/m at 319.3K.
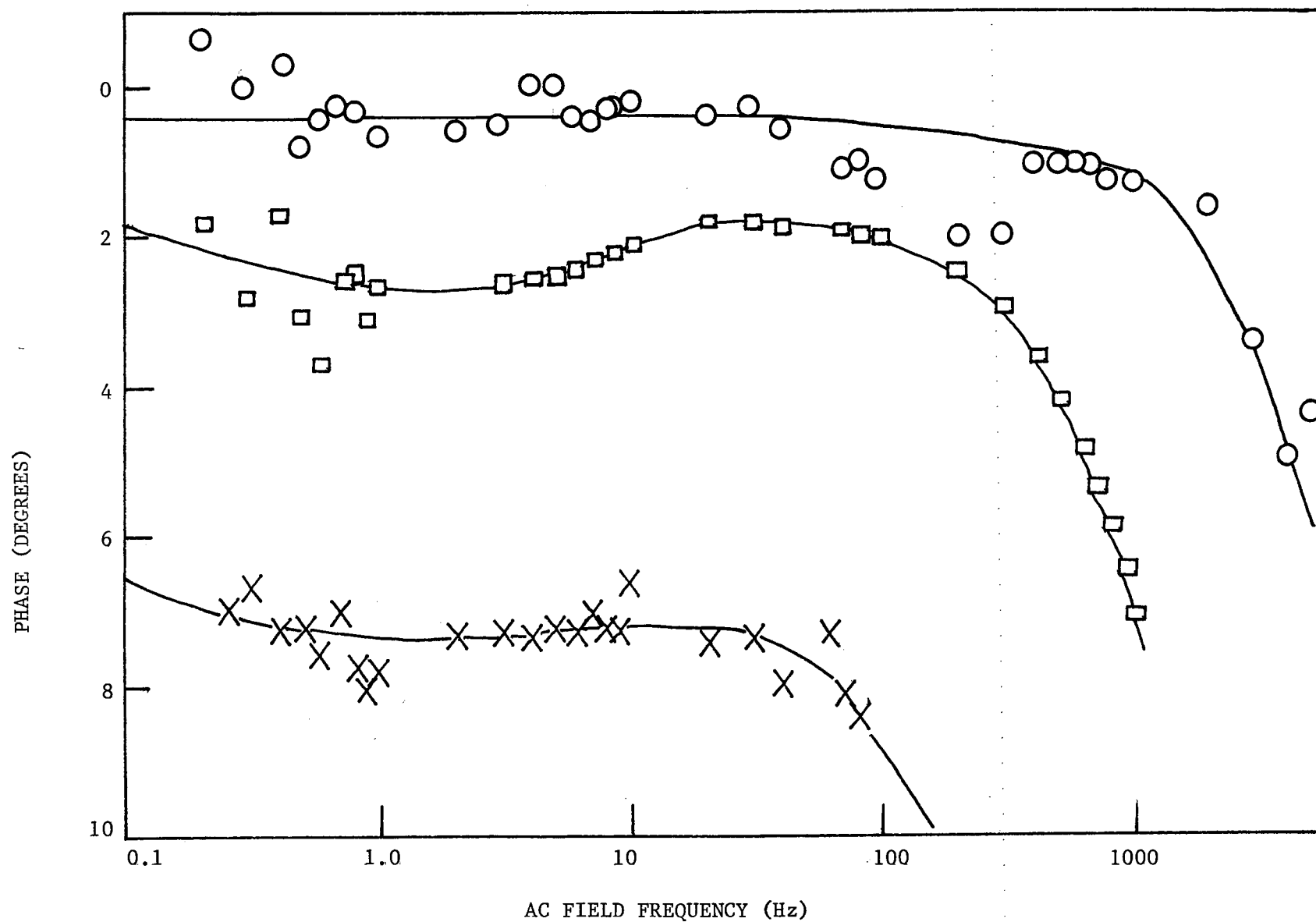
FIGURE 16: DEPENDENCE ON APPLIED AC FIELD FREQUENCY OF THE PHASE OF THE COMPLEX SUSCEPTIBILITY FOR VARIOUS CONDITIONS OF TEMPERATURE AND RMS AC FIELD : ✕ 100 A/m AT 277.9K; □ 0.75 A/m AT 278.2K; O 100 A/m AT 319.3K.
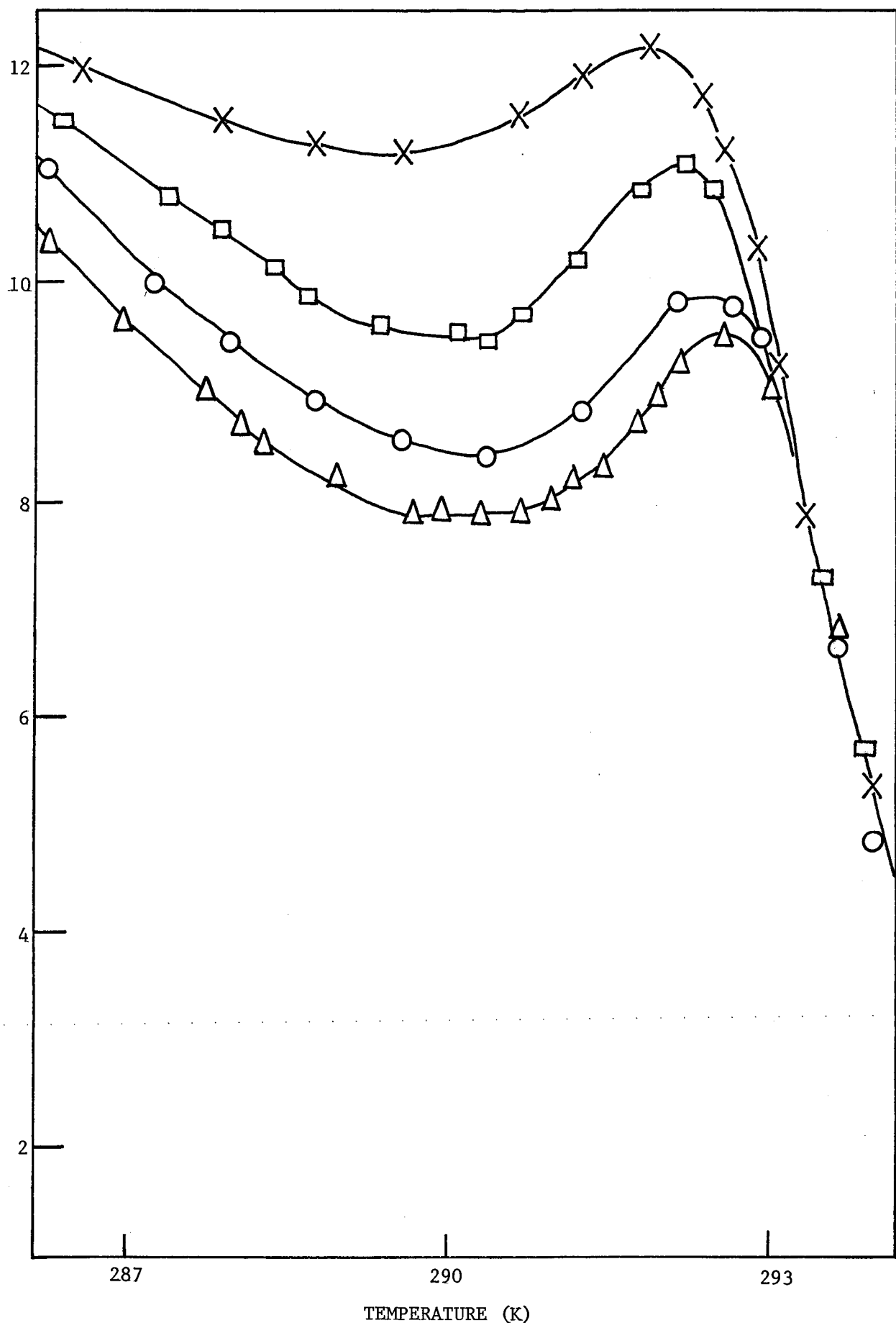
FIGURE 17: TEMPERATURE DEPENDENCE OF THE AC SUSCEPTIBILITY OF GADOLINIUM
NEAR THE CURIE TEMPERATURE FOR COOLING EXPERIMENTS IN AC FIELDS
OF 0.38 A/m RMS WITH VARIOUS FREQUENCIES: ✕ 0.2 Hz; □ 0.5 Hz;
0 1.0 Hz; △ 100 Hz.

The experiments on the gadolinium foil also showed similar structure in $\chi(T)$ in low fields, as shown in Fig. 18. This confirms that this structure is not due to electromagnetic skin depths. This was further indicated by the retention of the structure with field frequencies down to 0.2 Hz for the toroidal sample.

The experiments performed on the cylinder were mainly supplementary in nature being carried out to complete the experimental study via this technique. The low-field AC $\chi(T)$ curves showed the same structure as for the toroid, and were relatively unaffected by the presence of a 2400 A/m DC field along the cylindrical axis (Sydney et al 1974).

Magnetic Hysteresis Measurements. The magnetic hysteresis studies performed below T_c indicated that for applied fields less than ~ 8 A/m the domain magnetization processes are effectively reversible with a magnetization which is proportional to the field, in agreement with the susceptibility measurements. For larger fields, magnetic hysteresis was observed. Figure 19 shows the temperature dependence of the minor loop coercive field for various applied fields. The form of these results bears some resemblance to those of Bates and Pacey (1961) and Belov et al (1961) but their results are not as sharply defined in temperature as those of Fig. 19; the minimum for their coercive force data occurred at ~ 210K in agreement with the theory of Goodenough (1954).

Thermal Relaxation Results. When carrying out the thermal relaxation experiments, currents ~ 30 mA were suddenly switched on or off in the heater. This gave rise to significant temperature inhomogeneities. The temperature differential between the two thermo-couples on either side of the toroid grew at the rate of ~ 1.5K min. when the heater was switched on, and fell at the rate of ~ 1K/min. when
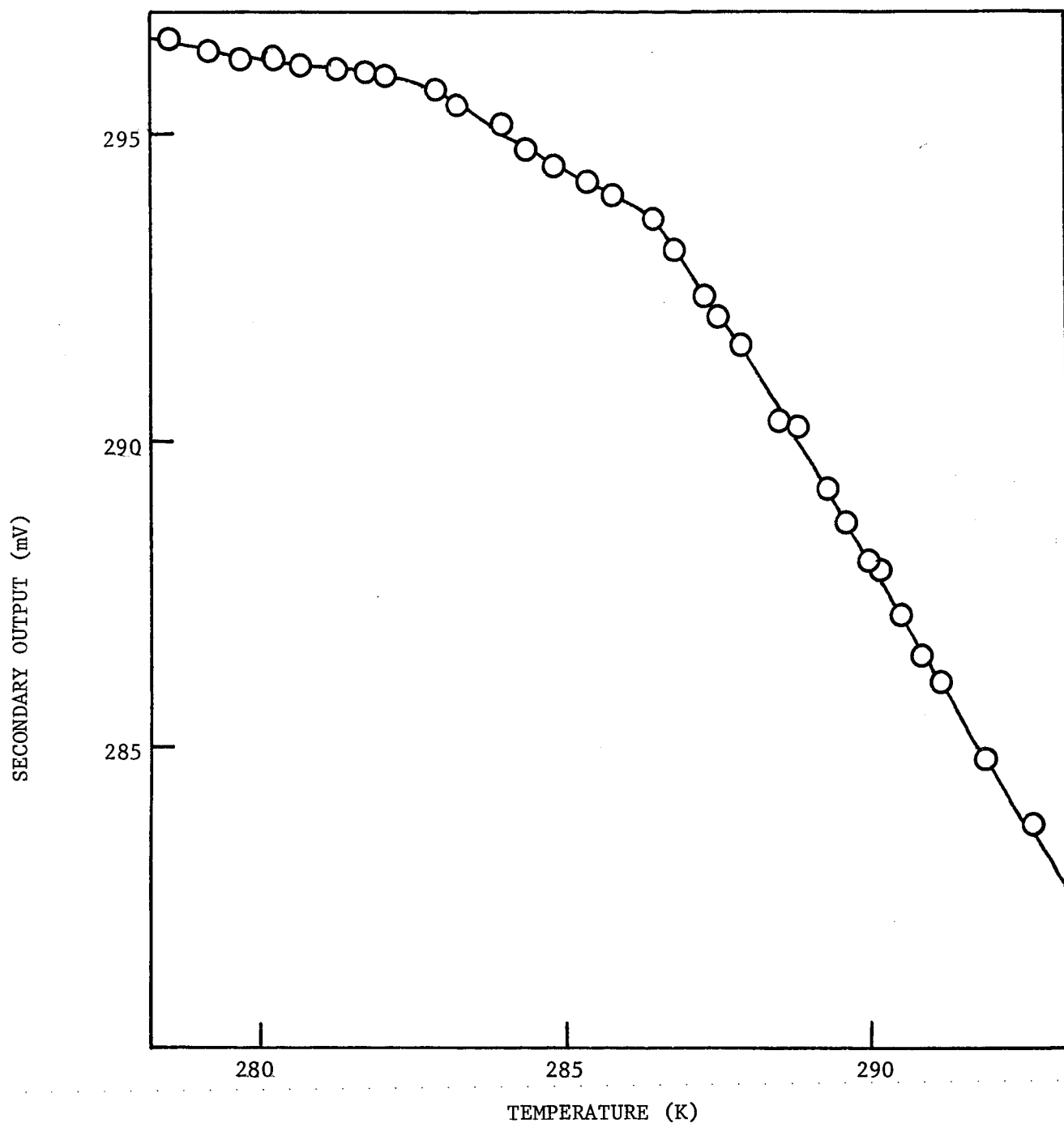
FIGURE 18: TEMPERATURE DEPENDENCE OF THE SECONDARY COIL OUTPUT
IN A COOLING EXPERIMENT FOR A FOIL SAMPLE.
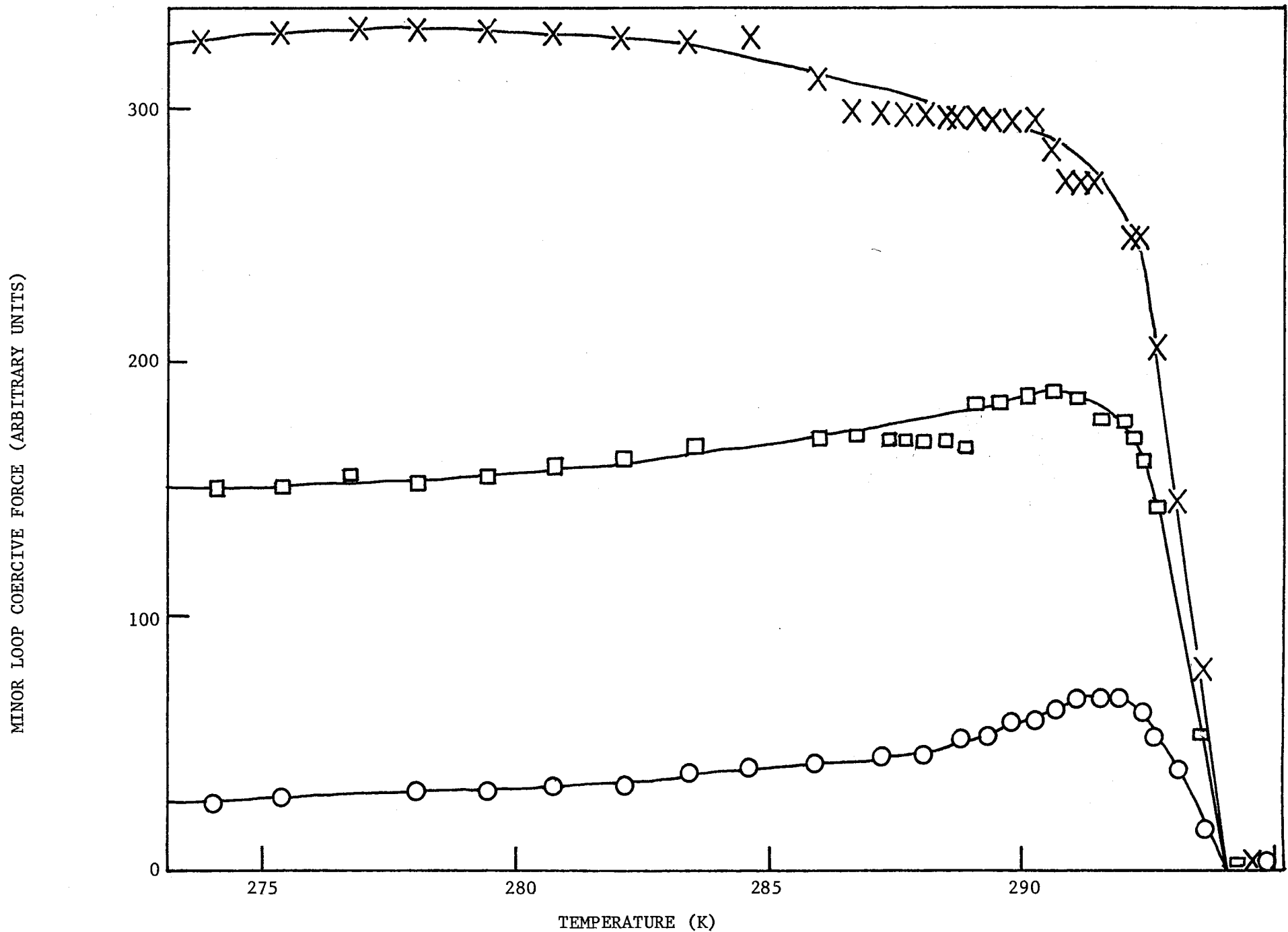AC FIELD FREQUENCY 2000 Hz; RMS AC FIELD 80 A/m.

FIGURE 19: TEMPERATURE DEPENDENCE OF THE MINOR LOOP COERCIVE FORCE FOR AC FIELDS OF FREQUENCY 40 Hz AND VARIOUS RMS AMPLITUDES: ✗ 840 A/m; ☐ 375 A/m; ◯ 126 A/m.

the heater was switched off, these rates being dependent on the
relative temperatures of the sample and the environment. However,
by measuring the broadened heating and cooling $\chi(T)$ curves with
these large heating currents on, we were able to gain a qualitative
approximation to the "equilibrium" transition secondary voltage
curve which would result when the heater was switched on or off in
the absence of non-equilibrium effects in the sample. Figure 20(a)
shows the time dependence of the sample temperature (measured at
the centre of the secondary coil) after suddenly switching off the
heater. The initial temperature was 293.1K, at the peak of the
equilibrium low-field $\chi(T)$ curve. Figure 20(b) shows the response
of the secondary voltage in a low field, together with the
approximate equilibrium curve described above. It can be seen that
a rise took place in the secondary output over a period ~ 2 sec.
during which time the inhomogeneous temperature differential across
the sample would have fallen only about 0.03K, insufficient to give
any effect. The susceptibility then fell slowly back to the
equilibrium curve. After allowing for the continual change of
temperature and the curvature of the equilibrium curve, we ascertained
a characteristic time of 2 - 6 secs for the relaxation of the
secondary output. Similarly, Fig. 21 shows the results of sudden
heating of the sample in the region of the trough in $\chi(T)$. The
output stayed below the equilibrium curve, and then rose back to it;
however, the output did not fall rapidly during the initial part of
the temperature change.

In the paramagnetic region no such non-equilibrium effects
were observed; χ always followed the equilibrium curve regardless of
the rate of temperature change. This may be seen from Fig. 22A which

FIGURE 20(a): TIME DEPENDENCE OF THE SAMPLE TEMPERATURE

FIGURE 20(b): TIME DEPENDENCE OF THE SECONDARY COIL OUTPUT ($\times$) SUPERIMPOSED ON THE EQUILIBRIUM $\chi(T)$ CURVE (O).

FIGURE 20:   RELAXATION RESULTING FROM SUDDEN COOLING FROM THE PEAK IN THE EQUILIBRIUM AC $\chi(T)$ CURVE IN A FIELD OF 0.75 A/m RMS AT 1000 Hz.

FIGURE 21(a): TIME DEPENDENCE OF THE SAMPLE TEMPERATURE

FIGURE 21(b): TIME DEPENDENCE OF THE SECONDARY COIL
OUTPUT (χ) SUPERIMPOSED ON THE EQUILIBRIUM
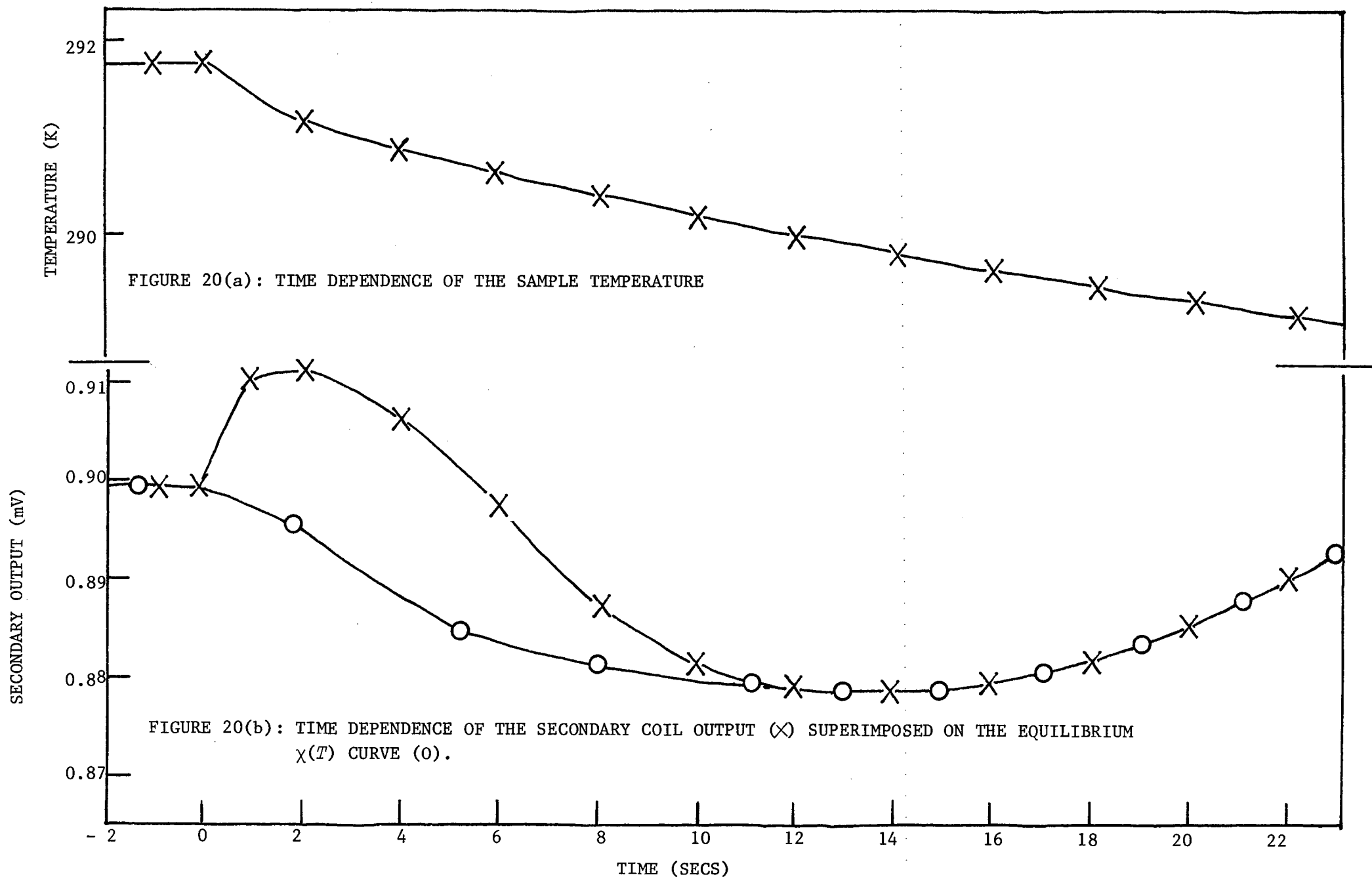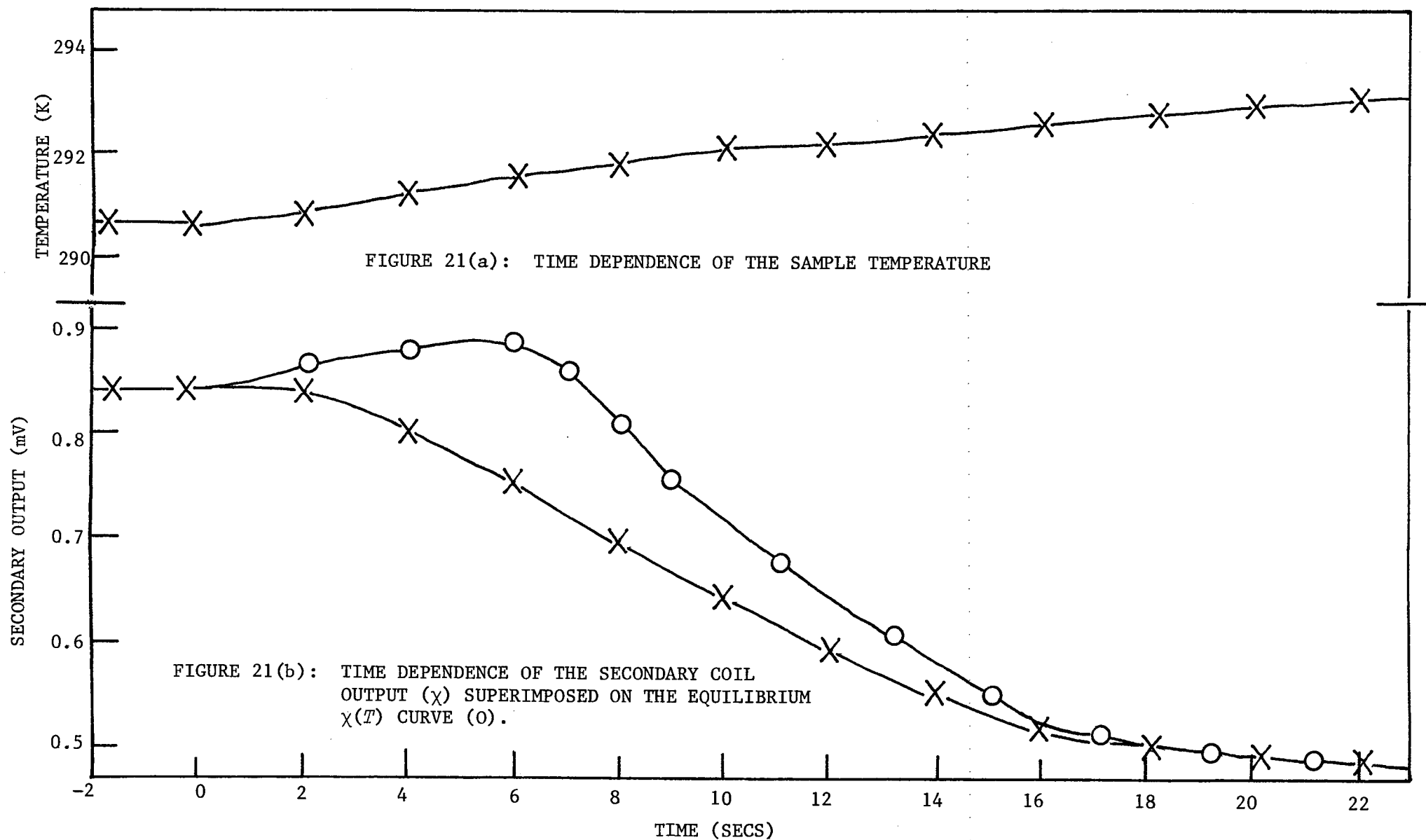$\chi(T)$ CURVE (O).

FIGURE 21: RELAXATION RESULTING FROM SUDDEN WARMING FROM THE TROUGH IN THE EQUILIBRIUM AC $\chi(T)$ CURVE IN A FIELD OF
0.75 A/m RMS AT 1000 Hz.

FIGURE 22A(a): TEMPERATURE
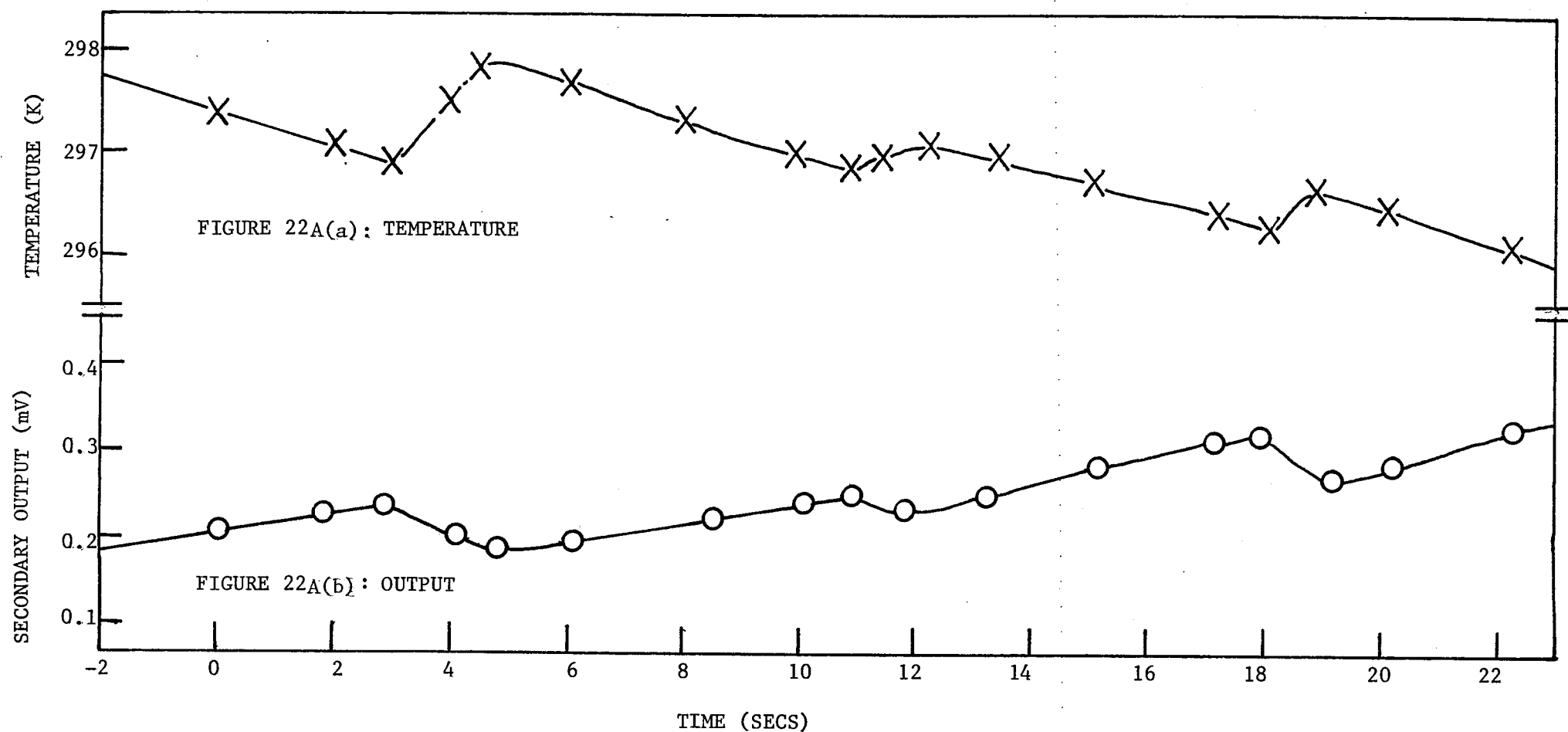
FIGURE 22A(b): OUTPUT

TIME (SECS)

FIGURE 22A: RESPONSE OF THE SECONDARY OUTPUT TO LARGE TEMPERATURE OSCILLATIONS IN THE PARAMAGNETIC REGION.
AC FIELD 0.75 A/m RMS AT 1000 Hz.

shows the result of switching the heating current on and off over

many cycles. Reversal of the thermal direction causes reversal of

the output change. Figure 22B shows that this is not the case on

the region of the structure in the $\chi(T)$ curves in low fields.

Discussion. Above T_c the susceptibility is independent of

applied field for the range of fields used here, and is also

frequency independent apart from the effects of eddy currents at

frequencies $\gtrsim$ 100 Hz.

If the Curie point were to be defined to be the temperature

at which domain nucleation commences then, from the sharp onset of

hysteresis we obtain a value T_c = 294.1 ± 0.2K. Alternately, from

the temperature for which $\frac{d\chi}{dT}$ is a maximum we obtain T_c = 293.7 ± 0.2K

in reasonable agreement with the results of the temperature modulation

experiments contained in the following section. Below T_c there is

a transition region of several degrees in which the low initial field

susceptibility actually decreases with temperature and there is

considerable temperature hysteresis. We believe that this is

associated with the domain nucleation and this is supported by the

observed relaxation effects and by the rapid temperature variation of

the coercive field. Below T_c the initial-field-independent

susceptibility is observed for applied fields up to ~ 8 A/m, this

value decreasing very slightly as the temperature is lowered. Both

the strain theory (Eq. 57) and the pinning theory (Eq. 59) outlined

in Chapter 2 would appear to describe the observed behaviour

reasonably accurately. The decrease of the critical field with

temperature would be explained from Eqs. 57 and 59 by the increase in

M_S. On the other hand, both the inclusion theory and the thin domain

wall theory seem to predict critical fields some orders of magnitude

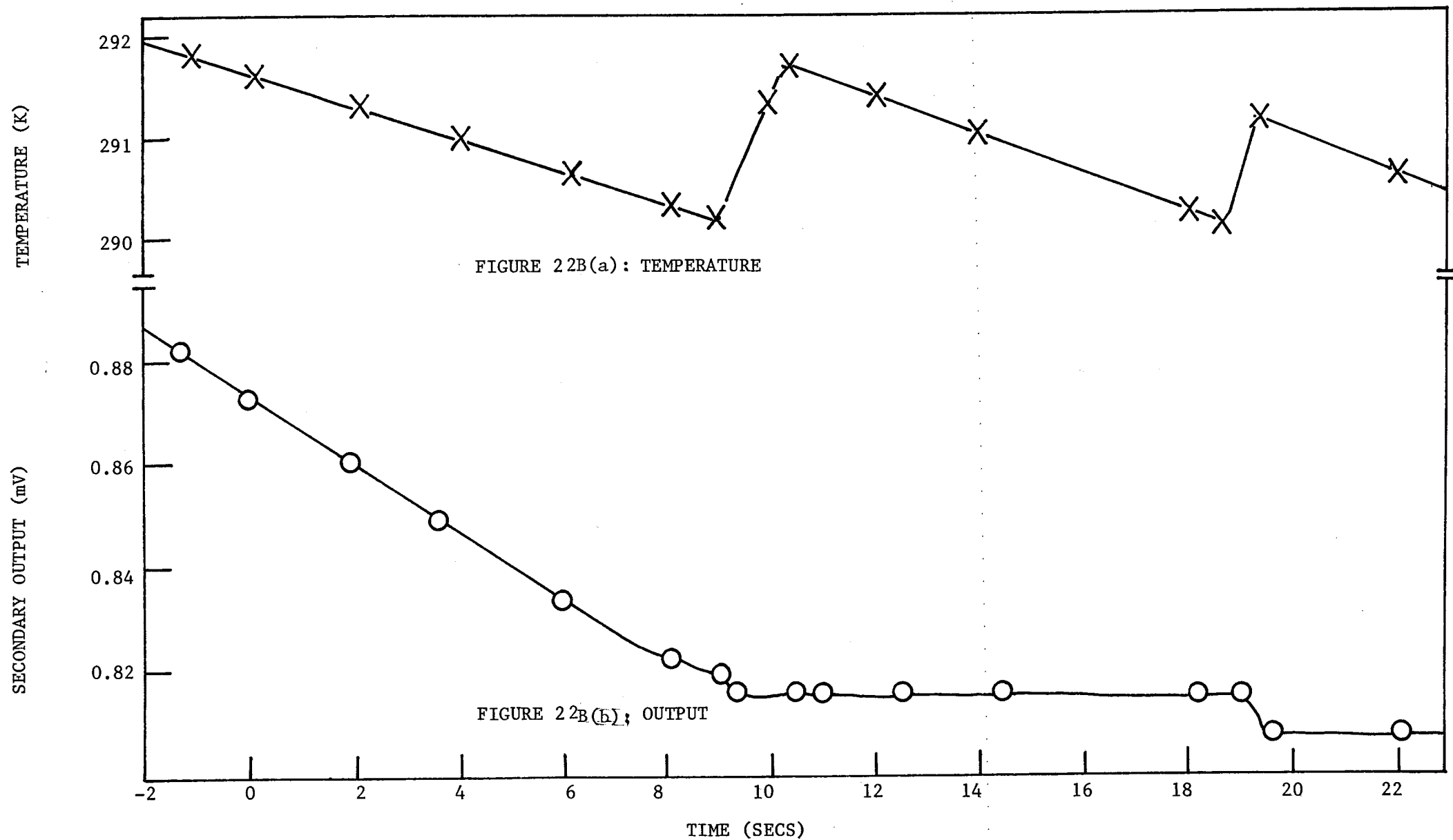FIGURE 22B(a): TEMPERATURE

FIGURE 22B(b): OUTPUT

FIGURE 22B: RESPONSE OF THE SECONDARY OUTPUT TO LARGE TEMPERATURE OSCILLATIONS IN THE REGION 290-292K. AC FIELD 0.75 A/m RMS AT 1000 Hz.

too large, and similarly the transition to irreversible rotation

would seem to occur in fields much larger than 8 A/m.

The large difference between the initial and higher field

susceptibilities below T_C may in part be due to anisotropy in the

contribution of reversible domain wall displacement to the low-field

susceptibility. In the temperature range used here, the easy axis

of magnitization is the c axis and a uniaxial domain structure is

expected. The domain wall displacement contribution will then be

zero for applied fields in the basal plane and, for a polycrystalline

sample, the average contribution should be one third of that for

applied fields parallel with the c axis. Higher field processes

such as irreversible wall displacement and rotation should be more

isotropic. Whether the susceptibility should actually rise or fall

as the temperature is lowered in the region of T_C as domains

nucleate is not obvious. As outlined in Chapter 4 there will be

two competing effects − the intrinsic magnetization will rise while

the nucleation of domains will tend to lower the susceptibility.

Anisotropic effects will cause the low field susceptibility to be

considerably less than that in high fields, so that it is not too

surprising to observe a decrease in low fields and an increase in

higher fields as the temperature is lowered through the transition

region. Several other ferromagnetic metals such as iron and nickel

also show a decrease in the low-field susceptibility with decreasing

temperature in the region of T_C (Bates 1963, Chikazumi 1964). This

is, however, due to the expected proportionality of χ with $\dfrac{M_S}{\sqrt{K}}$

(Kernsten 1956) and the fact that $K \rightarrow 0$ as $T \rightarrow T_C$ in these metals.

As has been pointed out in Chapters 1 and 2, this is not the case

for Gd where K remains almost temperature independent in the vicinity

of the Curie point (Corner et al 1962) so that this cannot be the origin of the behaviour in low fields in the transition region.

The thermal relaxation experiments show that when sudden changes of temperature are made in the transition region, the time dependence of the observed susceptibility is significantly different to that expected from the equilibrium curve and, in some cases, initially moves in the opposite direction to that for equilibrium. This fits well with the theory given in Chapter 4; the intrinsic magnetization is assumed to always remain in equilibrium while the contribution from the domain structure to the susceptibility exhibits relaxation. This work indicates that in the transition region the relaxation times are $\simeq$ 2 to 6 secs in the region of the peak of the low-field $\chi(T)$ curves.

The maximum in the phase lag which occurs for fields ~ 370 A/m as shown in Fig. 14 corresponds to the greatest percentage of irreversibility near the point in the $M(H)$ curves where χ reaches a maximum as in Fig. 13. It is known that reversible rotation mechanisms can dominate in a sample between the point of inflection in the $M(H)$ curve and saturation (see e.g., Chikazumi 1964). For low fields there is a residual phase lag which is field-independent; Fig. 12 shows that this is also temperature-independent and from Fig. 16 it is shown to be almost frequency independent, apart from a weak minimum at about 1 Hz. This behaviour is typical of the diffusion after-effect described in Chapter 2 (Snoek 1949) with a wide range of relaxation times. The minimum in phase at 1 Hz could indicate a weak peak in the distribution of relaxation times at about 1 sec. The steady decrease in the low field susceptibility as the frequency is increased from 0.5 to above 100 Hz is in agreement with this and, as expected, is not observed for high

applied fields or for temperatures above T_c. The origin of this after-effect is probably associated with the presence of gaseous impurities in the samples (see e.g., Chikazumi 1964, p.310). The low-frequency $\chi(T)$ curves of Fig. 17 also indicate the presence of an after-effect. The filling of the trough in $\chi(T)$ as the frequency is lowered is probably due to the expected increase in χ just below T_c with no corresponding change in χ above T_c. The absence of any low temperature satellite peak in the DC temperature modulation signal versus temperature curves given in the following section also suggests that the low field DC $\chi(T)$ curve does not exhibit any trough.

While the results presented here are in general qualitative agreement with those of Gerstein and Olander (1971) there are significant differences in detail. Firstly the 150 A/m fields they used are thought to be too large to observe initial-field behaviour in Gd. Also, we consider that the theory of domain wall dynamics which they have used to interpret data in the very low frequency region to be inapplicable for that region in Gd. This view is supported by the fact that in our measurements $\dfrac{\chi'}{|\chi|^2}$ rose by about 10% from 0.2 Hz to 50 Hz at 0.8 A/m, with a positive intercept at the zero frequency axis, whereas, if we were above the resonant frequency $\dfrac{\chi'}{|\chi|^2}$ should be falling with frequency and a negative intercept would be required. Finally, we have seen no significant temperature hysteresis in the magnetic losses (Figs. 12 and 16), whereas Gerstein and Olander reported temperature hysteresis in both χ' and χ'', the larger being in χ''.

Originally we suspected that the large difference in the

$\chi(T)$ curve for low and high AC fields below T_c may have been due

to field-cooling effects in which the domain structure is

influenced by the presence of the applied field while cooling

through T_c. To test for this possibility some additional experiments

were performed on the toroidal sample. In one, the sample was cooled

to 289.9K in an AC field of 75 A/m and thereafter in 0.5 A/m. The

susceptibility changed abruptly to the low-field curve when the field

was decreased. In other such studies cooling experiments in high or

low AC fields were followed by warming in low or high fields

respectively; no changes were observed from the results of warming

experiments presented elsewhere in this chapter. These indications

of the absence of field cooling effects are in agreement with our

previous observation (Sydney et al 1974) that the low-field AC

$\chi(T)$ curve was not significantly affected by the presence of a large

DC field.

6.3   Modulation Studies

Measurement of b. As shown in Fig. 23 a linear relationship

was found between the mean equilibrium temperature and the applied

heater power, proving the applicability of the Newton's law of

cooling term used in the modulation theory contained in Chapter 4.

The value of b was found to be $\sim 10^{-2}$ W/K, much smaller than $\omega m C$.

For a modulation frequency of 1 Hz, $\omega m C \sim 10$ W/K at room temperature.

DC Results. Figure 24 shows the temperature dependence of

the signal amplitude for DC experiments over a wide range of applied

fields. The curves exhibit a single peak centred at about 292.9K.

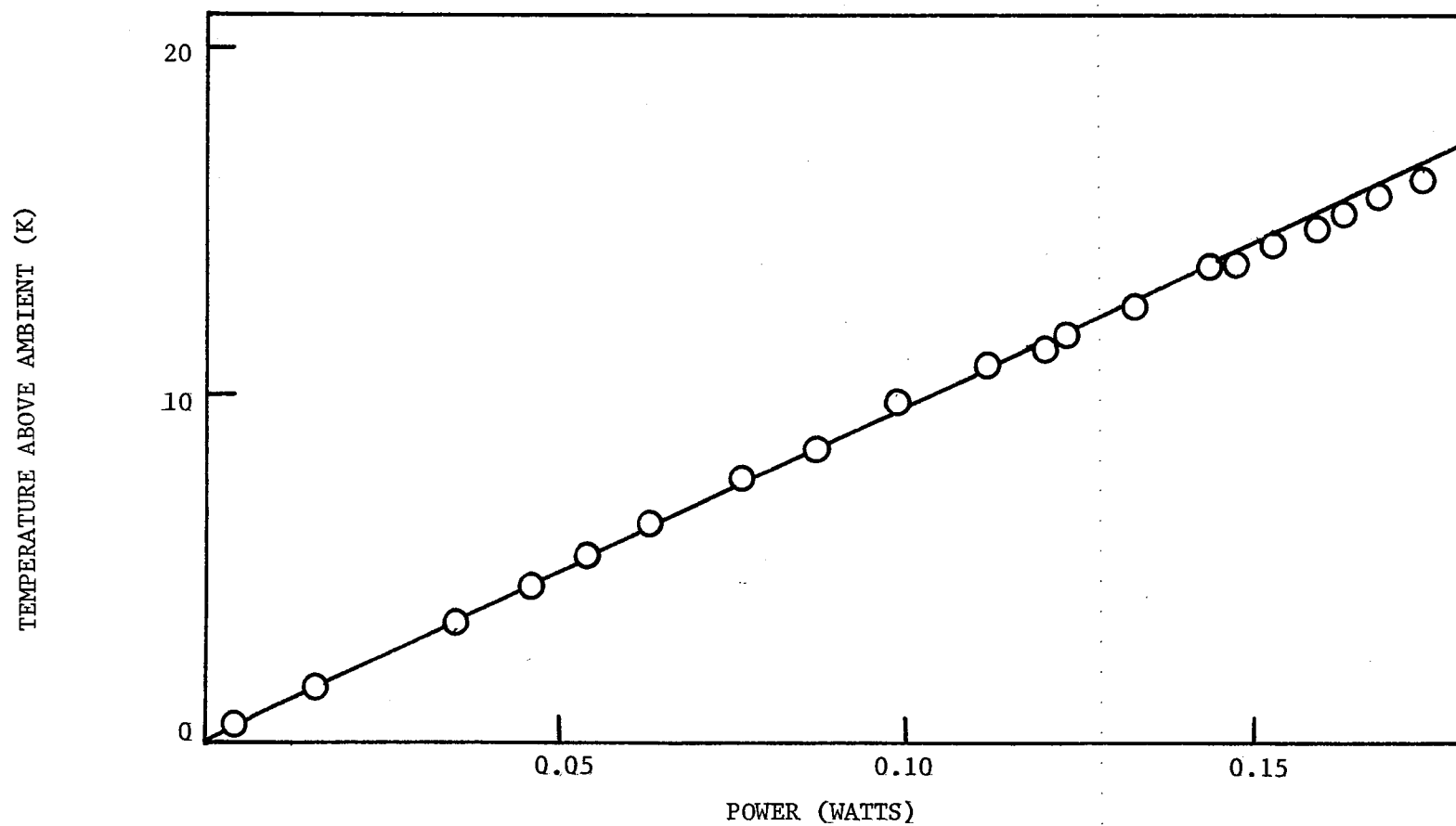FIGURE 23: TEMPERATURE OF THE SAMPLE ABOVE AMBIENT VERSUS HEATER POWER TO SHOW THE
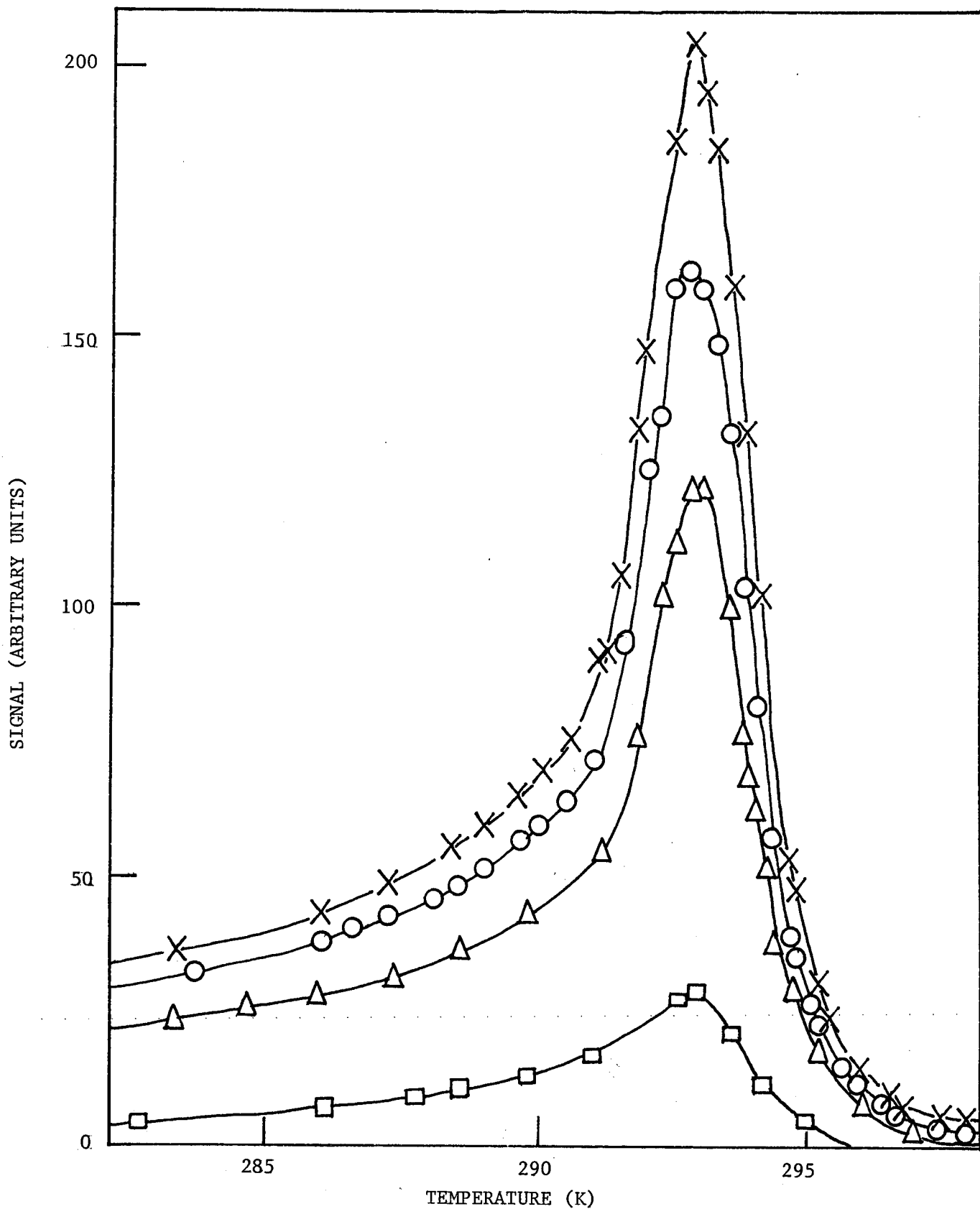APPLICABILITY OF NEWTON'S LAW OF COOLING TO THE SAMPLE ASSEMBLY.

FIGURE 24: TEMPERATURE DEPENDENCE OF THE DC FIELD, TEMPERATURE MODULATION
SIGNAL FOR COOLING EXPERIMENTS. MODULATION FREQUENCY 0.3 Hz.
MODULATION AMPLITUDE $\simeq$ 6 mK. VARIOUS APPLIED DC FIELDS:
$\times$ 750 A/m; O 600 A/m; $\triangle$ 375 A/m; $\square$ 75 A/m.

For all fields used there is no other structure apparent in the

$S(T)$ curves. Supplementary experiments performed on cylindrical

samples in DC fields showed that the peaks begin to broaden for

fields $\gtrsim$ 1000 A/m in agreement with previous observations of the

temperature dependence of the DC magnetization (Nigh et al 1963).

The dependence of the maximum signal amplitude upon applied fields

is shown in Fig. 25; this indicates the low sensitivity of this

technique in small applied fields. Figure 26 shows the temperature

dependence of the signal phase with respect to the second harmonic

of the heater current waveform; no strong structure is apparent.

Also, unlike the AC experiments, no temperature hysteresis effects

were observed in the DC signal amplitude or phase.

AC Experiments. The AC technique is most sensitive in

zero DC field although it can be used in the presence of DC fields.

Figure 27 shows a typical set of curves for the temperature

dependence of the signal amplitude for a modulation frequency of

2 Hz and various AC magnetic field strengths. A well-defined peak

at 293.2 ± 0.2K for low fields with a small shift at lower

temperatures in larger fields is seen. On the low temperature side

of the main peak a satellite peak is observed. The form of the

curves was not altered for modulation frequencies down to 0.3 Hz as

shown in Fig. 28. For frequencies above about 6 Hz the curves

tended towards a single broad peak at about 291.5K as shown in Fig.

29. The form of the curves was found to be independent of field

frequency provided skin depth effects were not present. As shown

previously in this chapter, when modulation amplitudes $\gtrsim$ 30 mK

were used, the $S(T)$ curves broadened because of inhomogeneity in
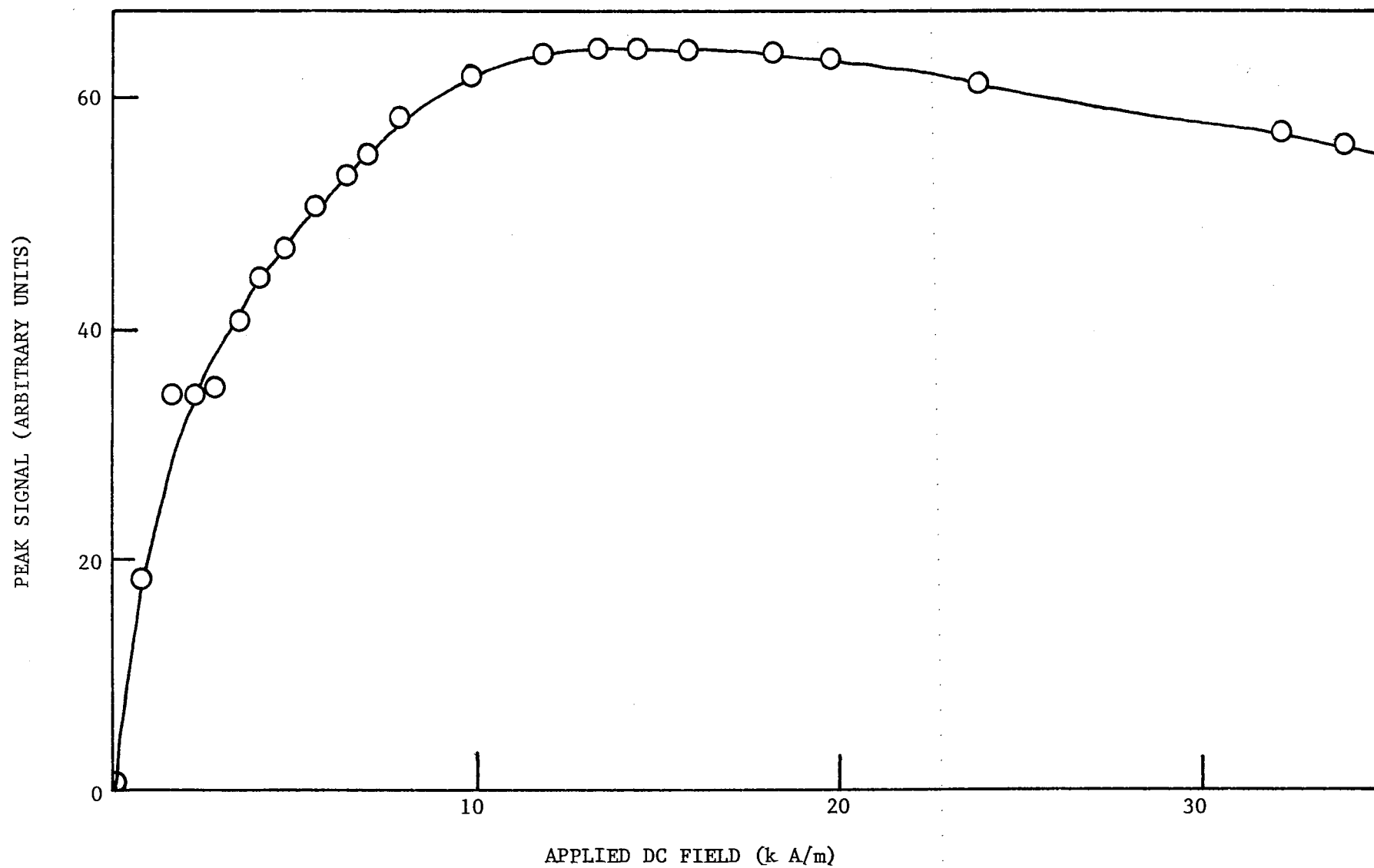
FIGURE 25: DEPENDENCE OF THE PEAK DC FIELD, TEMPERATURE MODULATION SIGNAL ON DC FIELD.
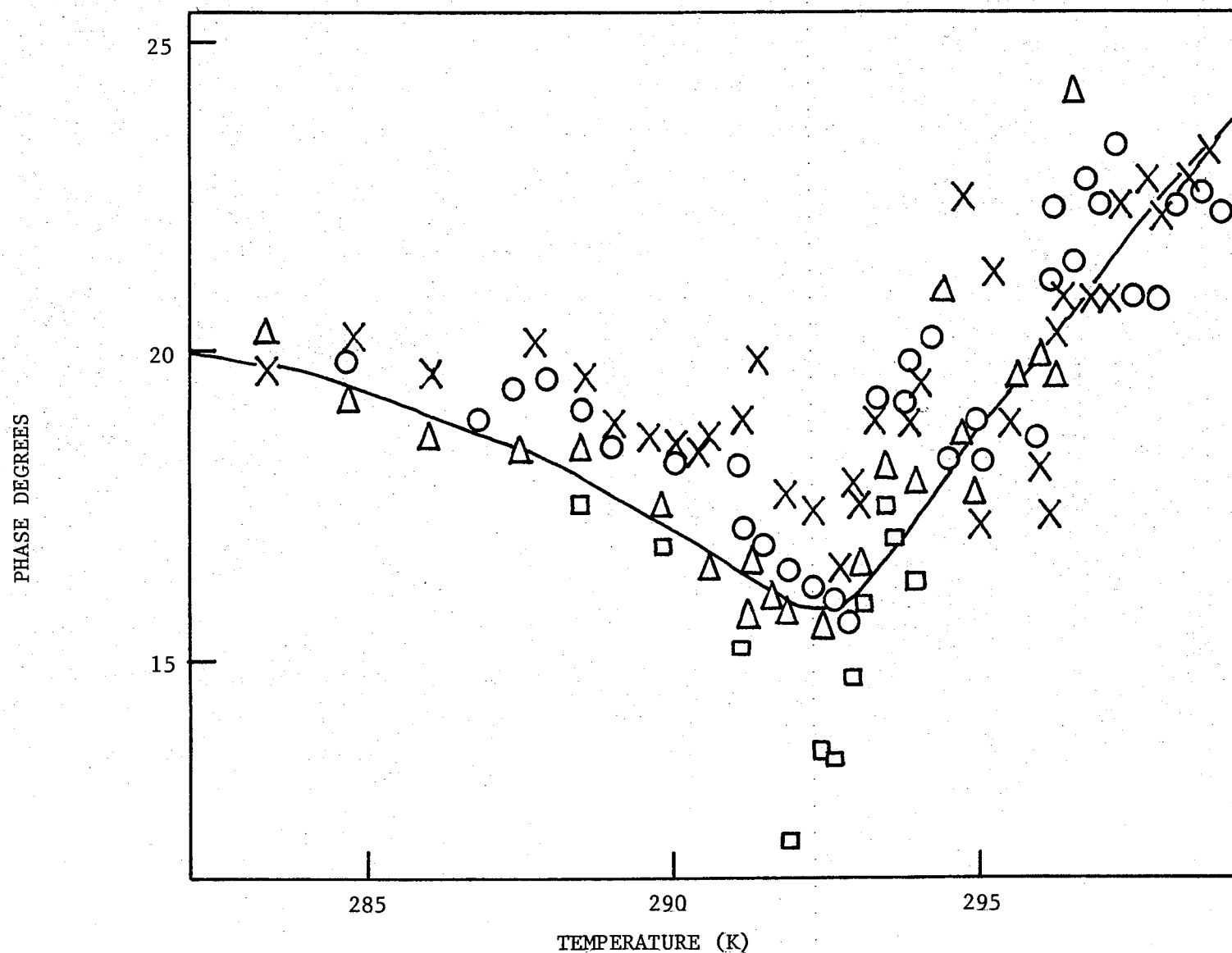
FIGURE 26 : TEMPERATURE DEPENDENCE OF THE PHASE OF THE DC FIELD, TEMPERATURE MODULATION SIGNAL WITH
RESPECT TO THE HEATER POWER WAVEFORM FOR COOLING EXPERIMENTS. MODULATION FREQUENCY
0.3 Hz. MODULATION AMPLITUDE $\simeq$ 6 mK. VARIOUS APPLIED DC FIELDS : $\times$ 750 A/m; 0 600 A/m;
$\triangle$ 375 A/m; $\square$ 75 A/m.
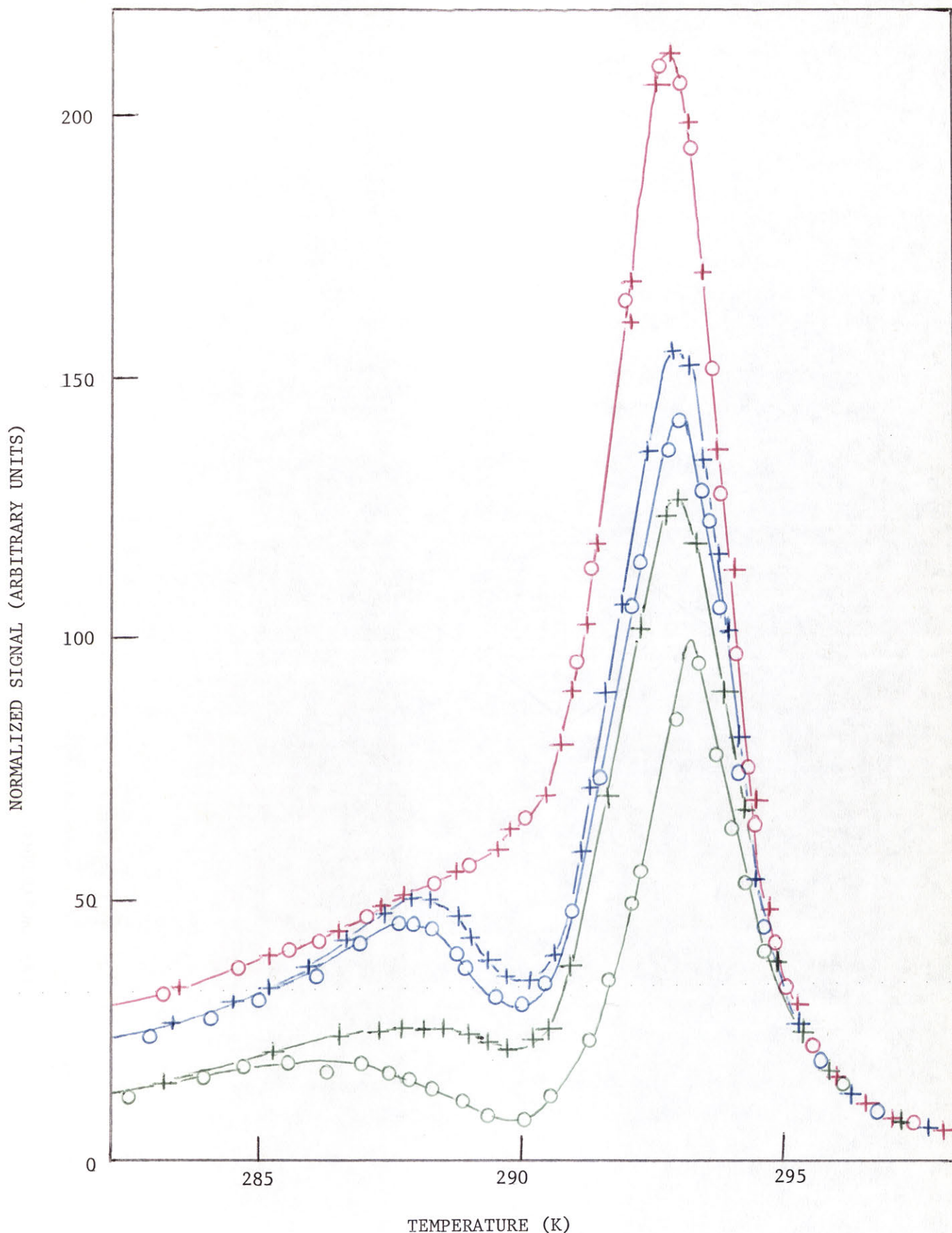
FIGURE 27: TEMPERATURE DEPENDENCE OF THE AC FIELD, TEMPERATURE MODULATION
SIGNAL NORMALIZED WITH RESPECT TO THE AC FIELD. MODULATION
FREQUENCY 2 Hz. AC FIELD FREQUENCY 100 Hz. MODULATION AMPLITUDE
$\simeq$ 6 mK. RMS AC FIELDS: RED 750 A/m; BLUE 75 A/m; GREEN 10 A/m;
+ COOLING; 0 WARMING.
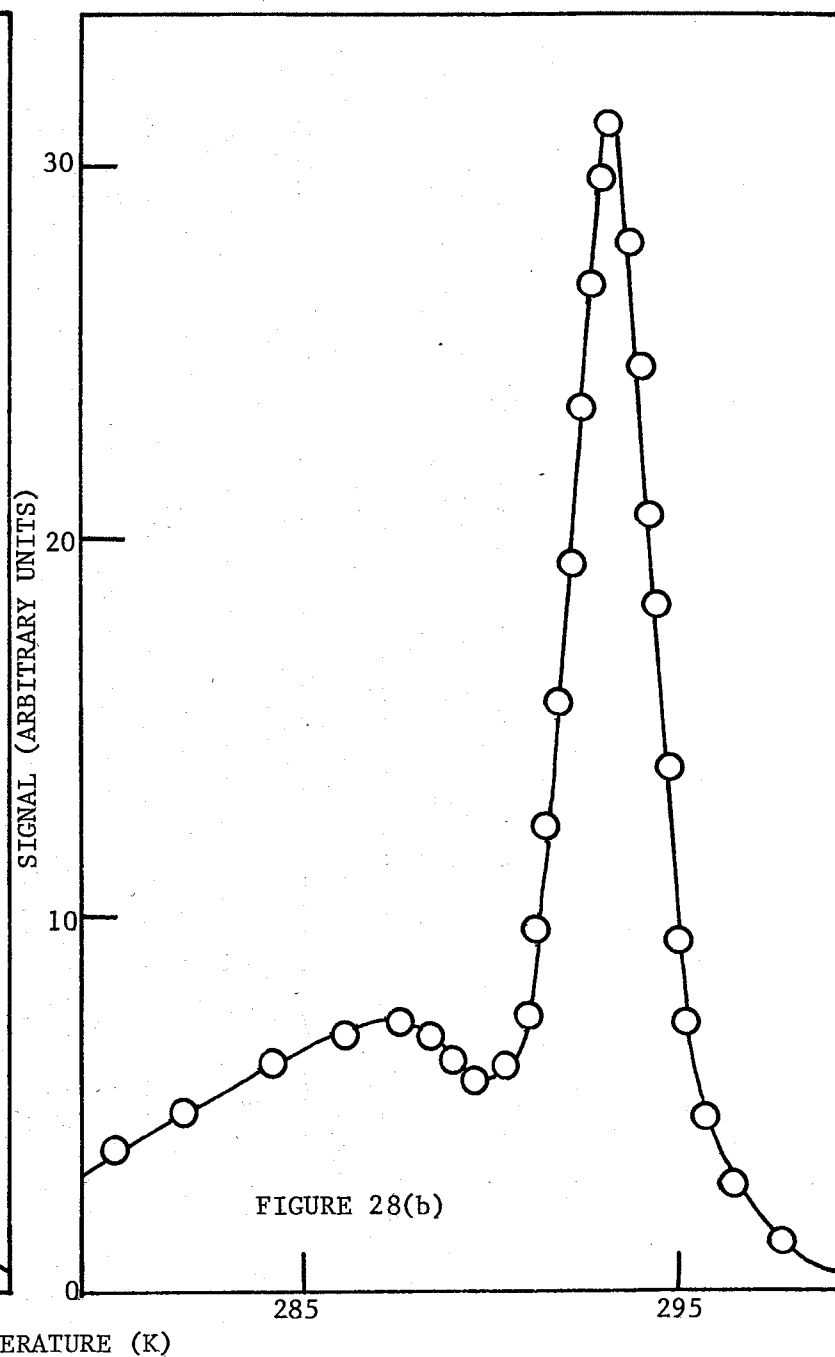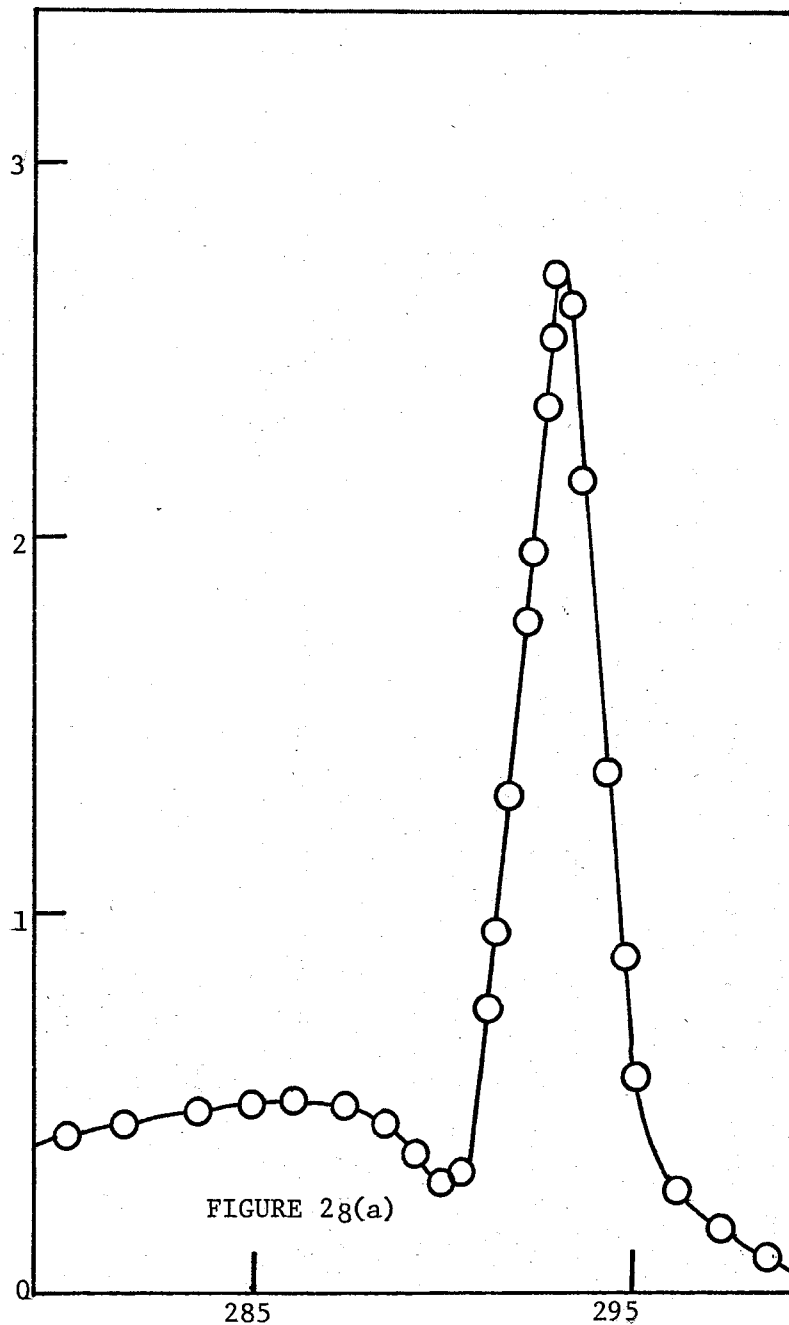
FIGURE 28: TEMPERATURE DEPENDENCE OF THE AC FIELD, TEMPERATURE MODULATION SIGNAL FOR TWO DIFFERENT
MODULATION FREQUENCIES. AC FIELD 7.5 A/m RMS. AC FIELD FREQUENCY 1000 Hz. (a) MODULATION
FREQUENCY 0.3 Hz, MODULATION AMPLITUDE ≃ 40 mK. (b) MODULATION FREQUENCY 2 Hz, MODULATION
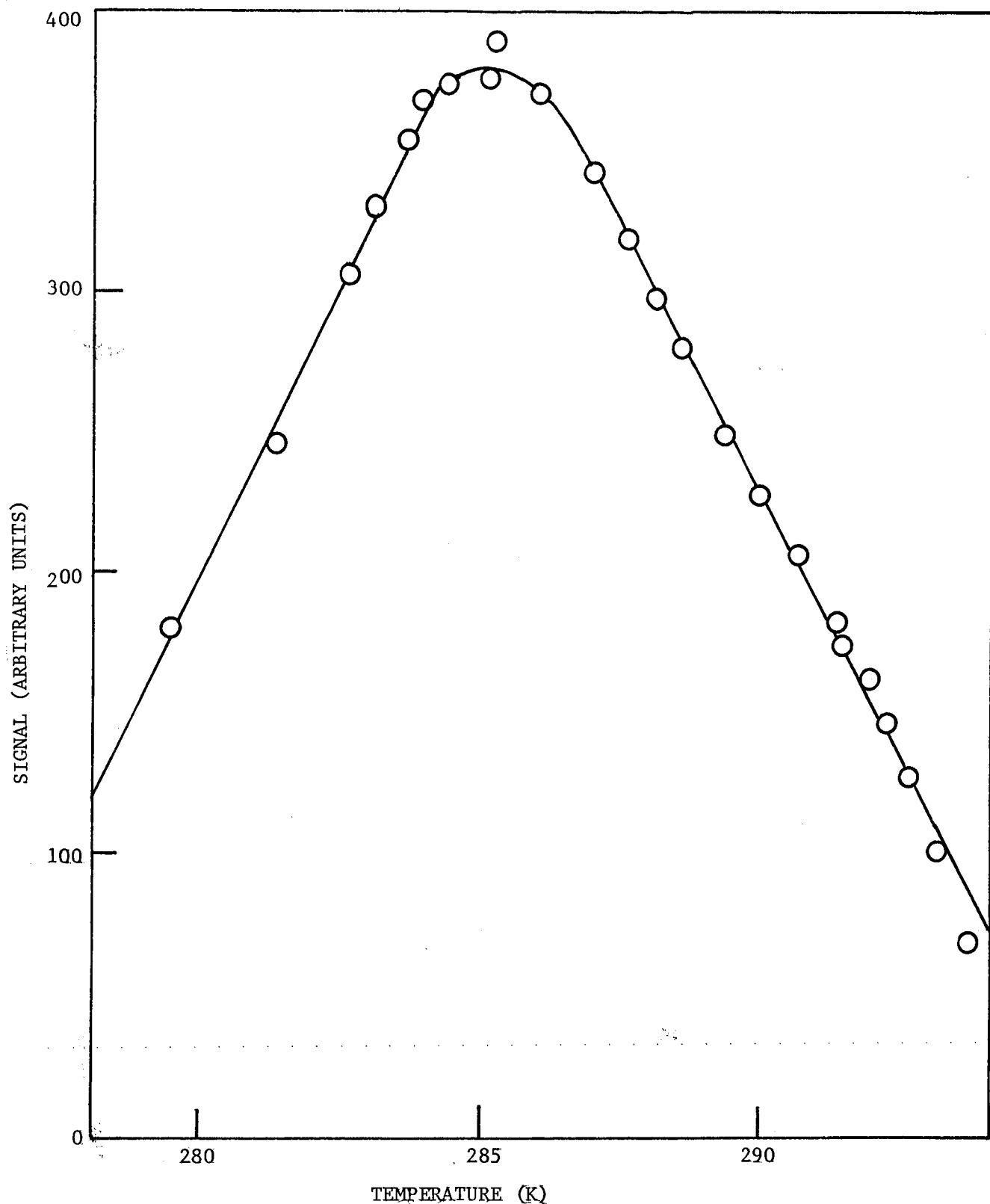
FIGURE 29: TEMPERATURE DEPENDENCE OF THE AC FIELD TEMPERATURE MODULATION SIGNAL FOR A MODULATION FREQUENCY OF 20 Hz. FIELD FREQUENCY 1000 Hz. RMS FIELD 7.5 A/m; MODULATION AMPLITUDE ≃ 1 mK.

the sample temperature. For smaller amplitudes however the distortion was not significant. As shown in Fig. 27, except for AC fields as large as about 700 A/m, the signal amplitude exhibited considerable temperature hysteresis, with the signals for the warming curves being less than those for the cooling curves.

The variation with temperature of the signal phase is shown in Fig. 30. Of particular significance is the marked peak corresponding to the relative phase lead at 290.7 ± 0.2K in the region of the trough between the two peaks of Fig. 27 and of the trough in the low-field $\chi(T)$ curves given in Fig. 11. This phase peak exhibits an extremely large degree of temperature hysteresis being far smaller in the cooling experiments. No significant changes in the phase results were found for modulation frequencies down to 0.3 Hz as shown in Fig. 31. Reliable measurements of the modulation signals were not made below that frequency.

Some AC temperature modulation experiments were carried out for a cylindrical sample. The temperature dependences of both the signal and the phase were very similar to those for the toroidal sample, except that the satellite structure, though certainly present, was less pronounced. For this assembly, AC field experiments were also carried out with DC fields applied parallel to the cylindrical axis. The presence of a DC field produced little change in the shape of the $S(T)$ curves. Large DC fields, as expected, greatly reduced the actual signal amplitudes.

AC temperature modulation experiments with detection at the second harmonic of the modulation were found to be very dependent on the rates of cooling and warming. Above about 0.2K/min., very

FIGURE 30: TEMPERATURE DEPENDENCE OF THE PHASE OF THE AC FIELD, TEMPERATURE MODULATION
SIGNAL WITH RESPECT TO THE HEATER POWER WAVEFORM. MODULATION FREQUENCY 2 Hz.
AC FIELD FREQUENCY 100 Hz. MODULATION AMPLITUDE $\simeq$ 6 mK. RMS AC FIELD :
RED 750 A/m; BLUE 75 A/m; GREEN 10 A/m. + COOLING; O WARMING.

FIGURE 31(a)

FIGURE 31(b)

FIGURE 31: TEMPERATURE DEPENDENCE OF THE PHASE OF THE AC FIELD, TEMPERATURE MODULATION SIGNAL WITH RESPECT TO THE HEATING POWER WAVEFORM FOR TWO MODULATION FREQUENCIES. AC FIELD 7.5 A/m RMS. AC FIELD FREQUENCY 1000 Hz. X COOLING, O WARMING. (a) MODULATION FREQUENCY 0.3 Hz, MODULATION AMPLITUDE $\simeq$ 40 mK. (b) MODULATION FREQUENCY 2 Hz, MODULATION AMPLITUDE $\simeq$ 6 mK.

complex behaviour was found, the most significant feature being

a very sudden appearance of the signal at 294.6K when cooling.

For rates ~ 0.1 K/min. a single broad minimum at 292.9K was

observed in the second harmonic signal without any other signific-

ant structure. Because there was still some rate dependence even

for rates ~ 0.1K/min., it was not possible to determine if any

temperature hysteresis was present. A typical warming curve is

given in Fig. 32; a modulation amplitude of $\Delta \simeq 35$ mK was used,

with the modulation and carrier frequencies being 0.3 and 1000 Hz

respectively, with an applied field of 8 A/m RMS. The correspond-

ing temperature dependence of the phase is shown in Fig. 33. A

fairly sharp peak occurred at about 292.9K with a total phase

variation of about $20°$.

Relaxation Results. Figure 34 shows the approximate

initial directions of the first harmonic signal change during the

relaxation experiments superimposed on an equilibrium $S(T)$ curve.

A close analysis of these changes revealed qualitative conformity

with the second harmonic results outlined above: below the peak

in $S(T)$ the first harmonic signal initially moves upwards in

response to sudden cooling. Therefore we do not find the $180°$

phase change in the second harmonic signal which is otherwise

expected near the peak in the first harmonic signal in the absence

of relaxation effects (Wilson et al 1975, and refer to Chapter 4).

Measurement of the Modulation Amplitude. The variation with

temperature of the modulation amplitude as determined from phase-

sensitive detection at 0.6 Hz of the thermocouple output is shown

in Fig. 35. The minimum in Δ occurs at 291.3 $\pm$ 0.2K, below the
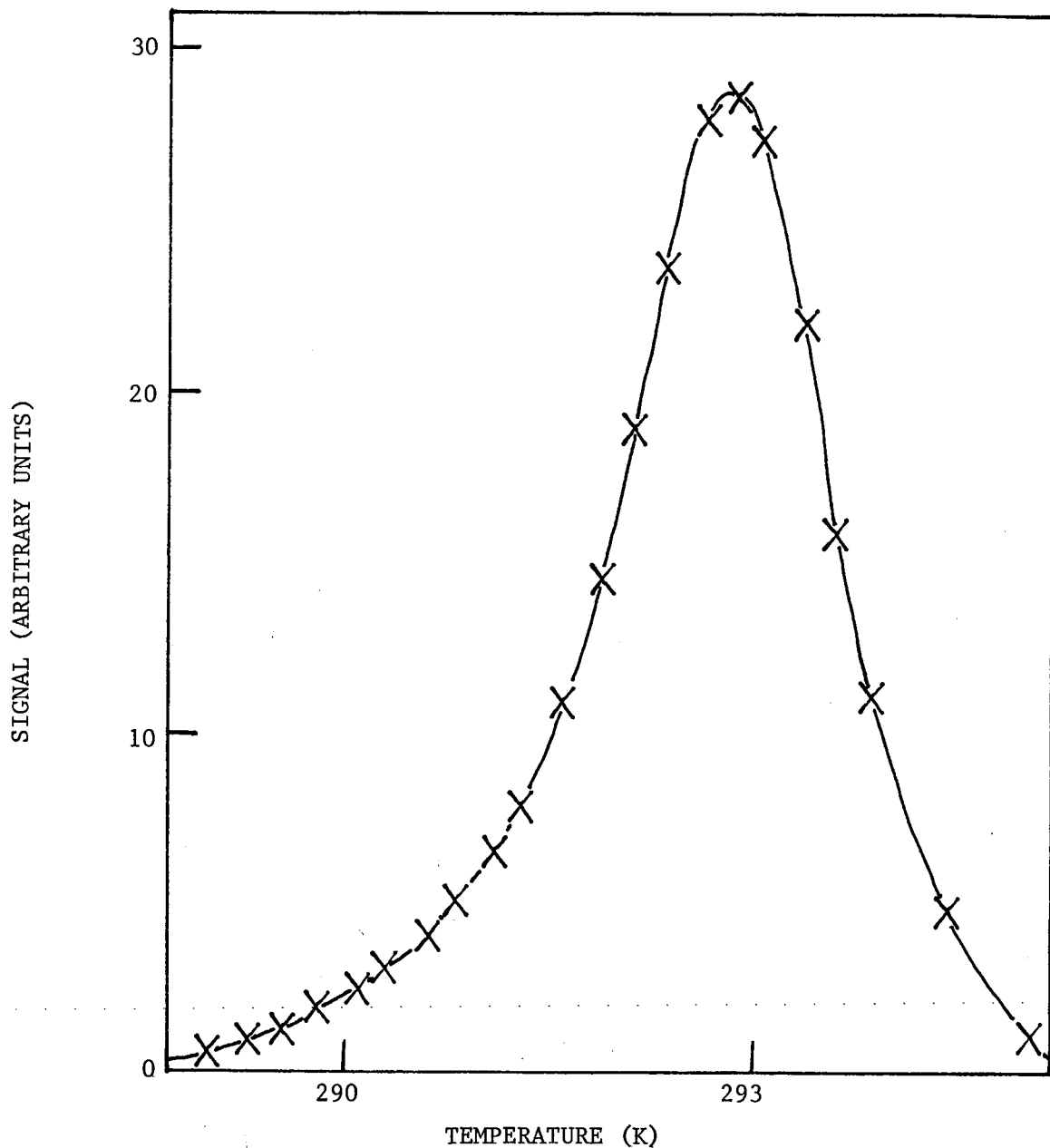
FIGURE 32: TEMPERATURE DEPENDENCE OF THE AC FIELD, TEMPERATURE MODULATION
SECOND HARMONIC SIGNAL FOR A WARMING EXPERIMENT. MODULATION
FREQUENCY 0.3 Hz. MODULATION AMPLITUDE $\simeq$ 40 mK. RMS AC FIELD
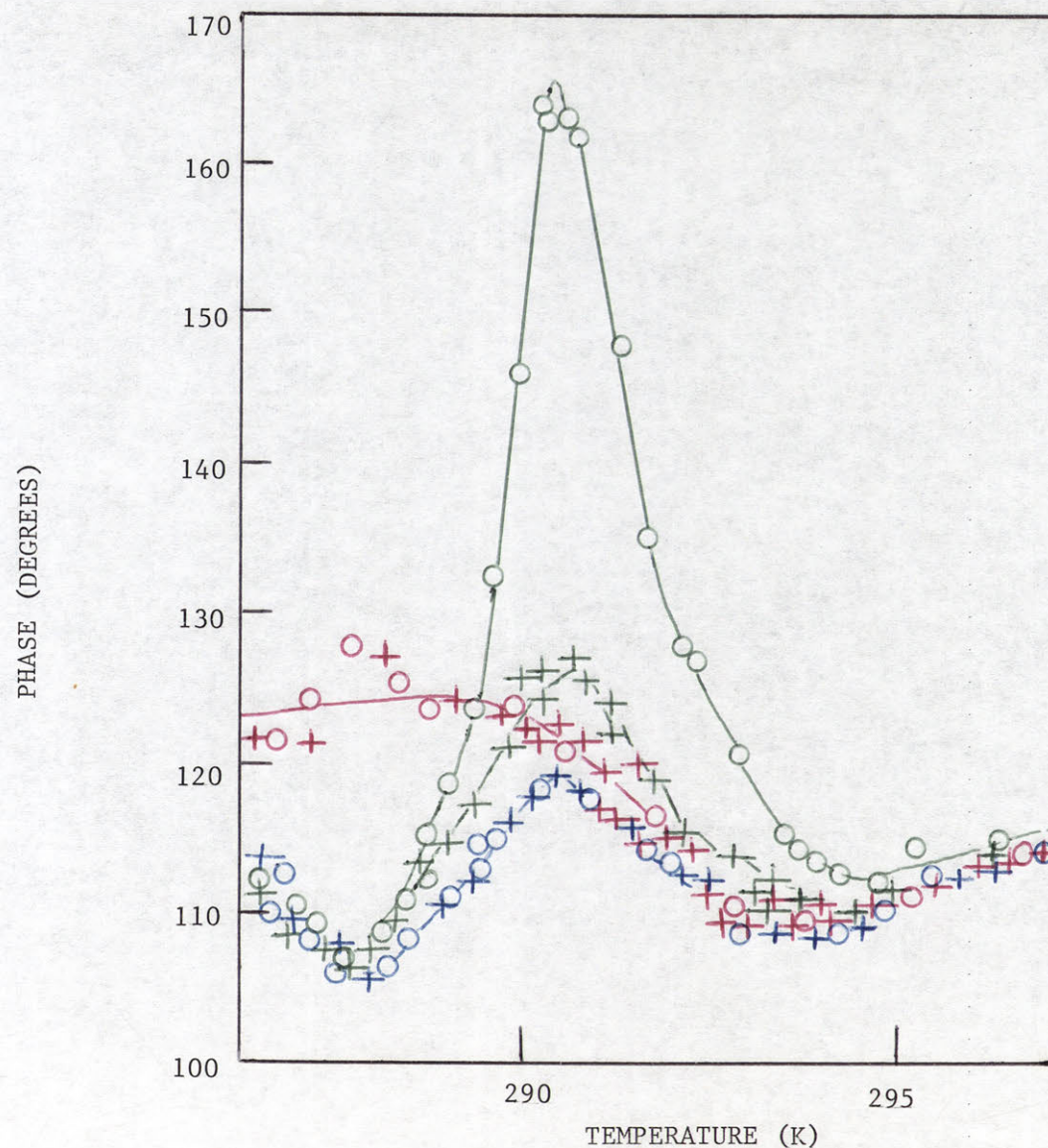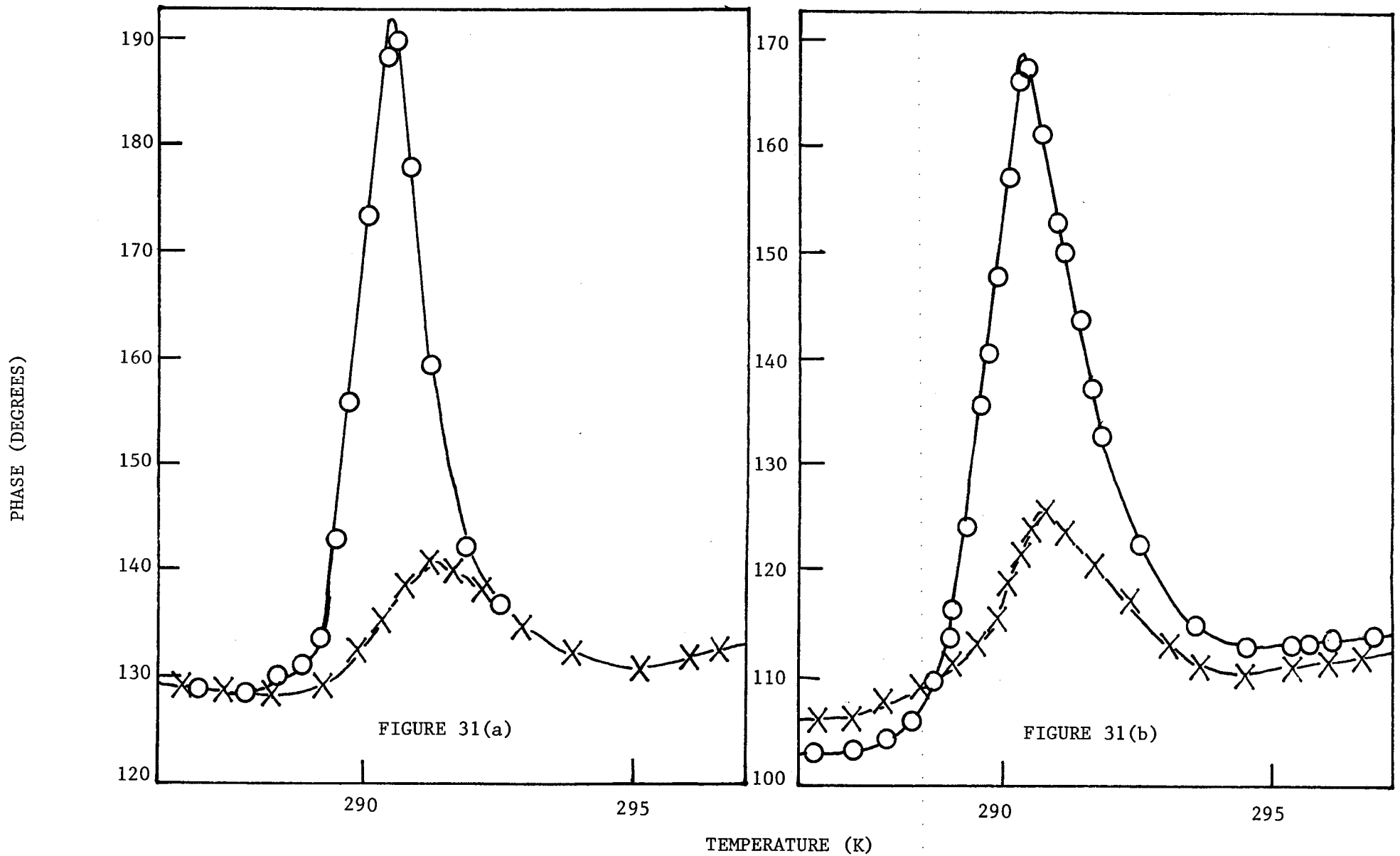8 A/m. AC FIELD FREQUENCY 100 Hz.

FIGURE 33: TEMPERATURE DEPENDENCE OF THE PHASE OF THE AC FIELD, TEMPERATURE MODULATION SECOND HARMONIC SIGNAL WITH RESPECT TO THE HEATER POWER WAVEFORM FOR A WARMING EXPERIMENT. MODULATION FREQUENCY 0.3 Hz. MODULATION AMPLITUDE $\simeq$ 40 mK. RMS AC FIELD 8 A/m. AC FIELD FREQUENCY 1000Hz.
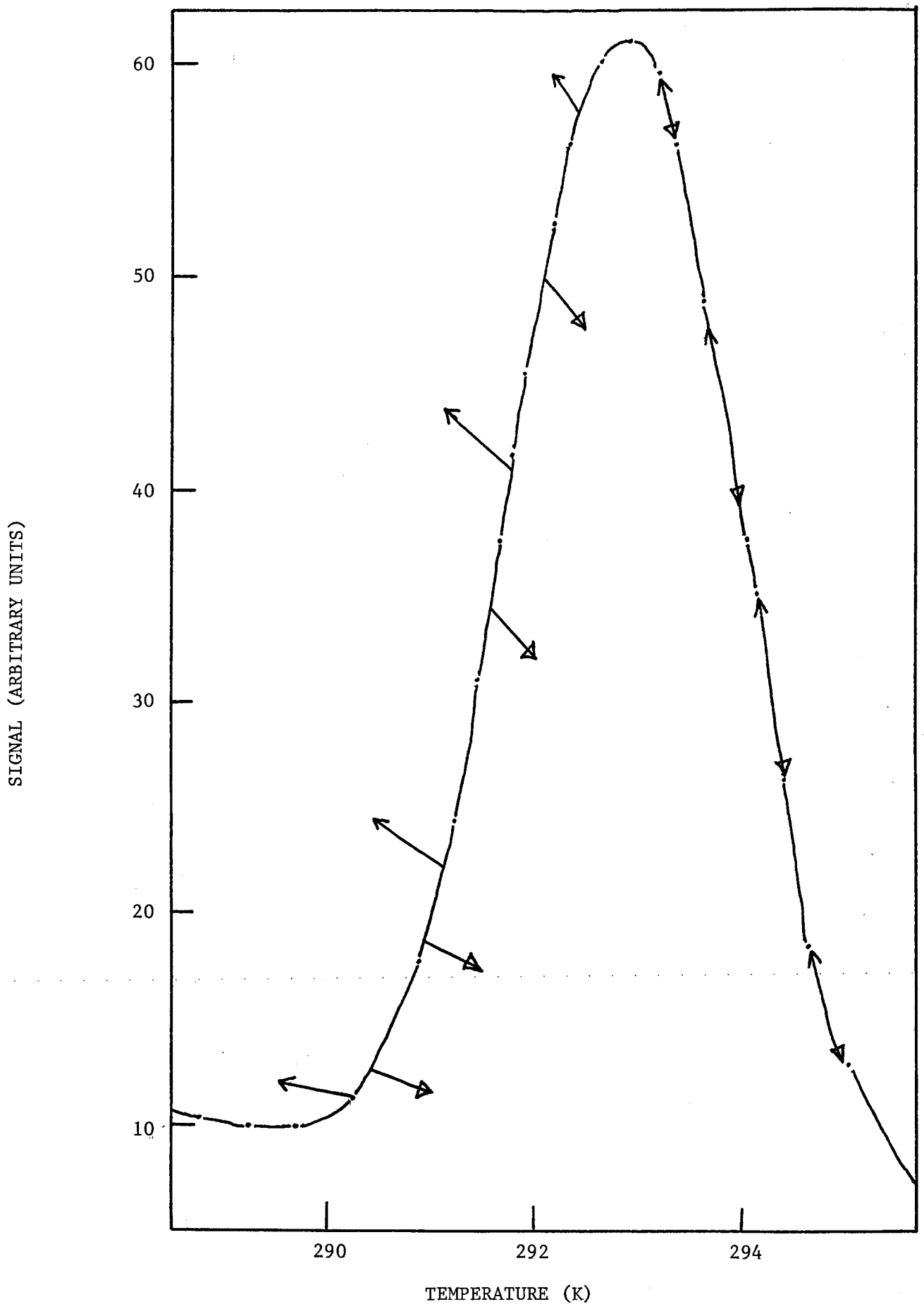
FIGURE 34: APPROXIMATE DIRECTIONS OF THE CHANGES IN THE AC FIELD, TEMPERATURE
MODULATION SIGNAL IN RESPONSE TO SUDDEN CHANGES IN TEMPERATURE,
SUPERIMPOSED ON AN EQUILIBRIUM AC MODULATION CURVE. MODULATION
FREQUENCY 0.3 Hz. AC FIELD FREQUENCY 1000 Hz. MODULATION AMPLITUDE
≃ 35 mK. RMS AC FIELD 75 A/m.   ◄── COOLING;   ──▷ WARMING.
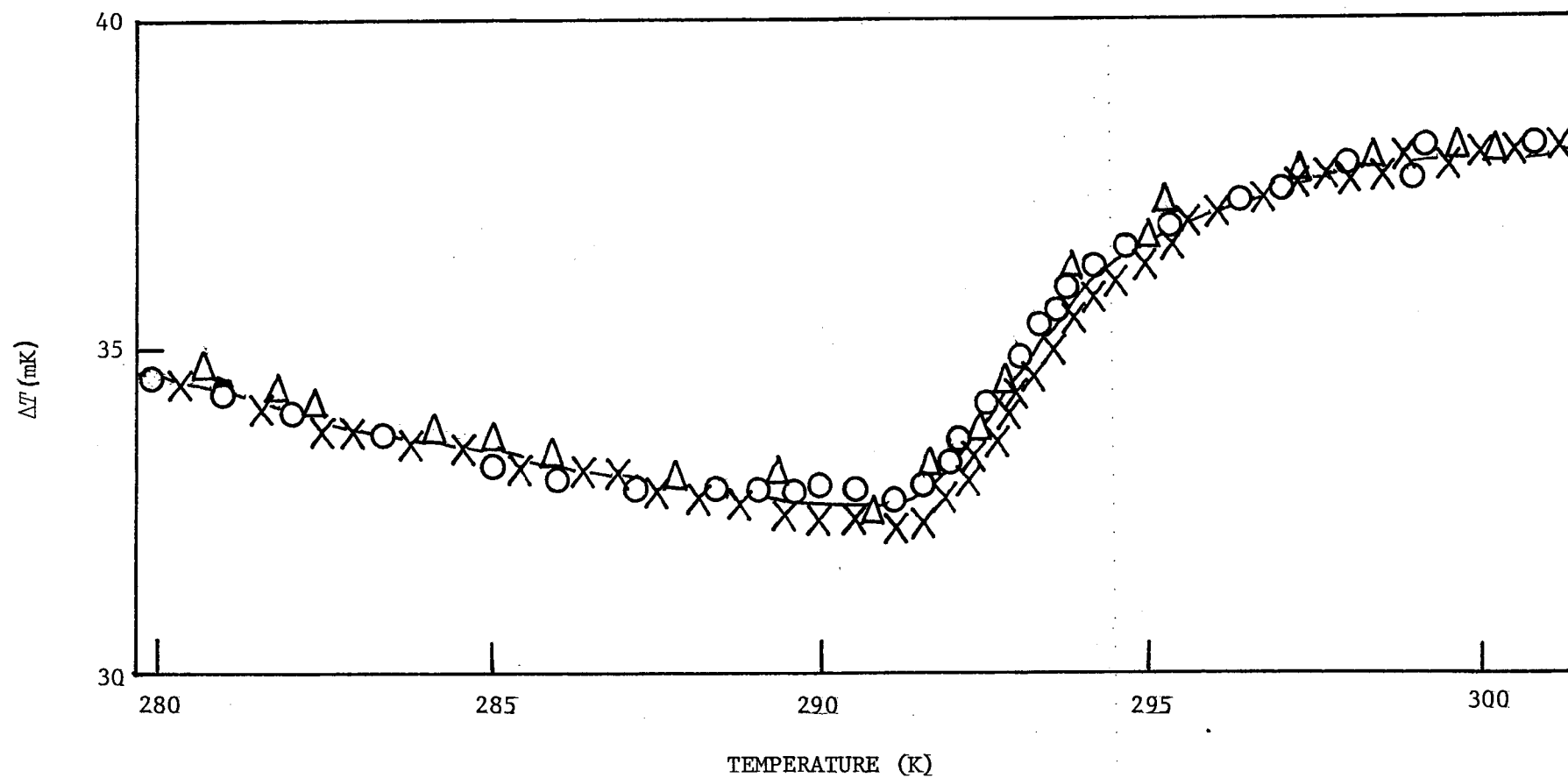
FIGURE 35:   TEMPERATURE DEPENDENCE OF THE TEMPERATURE MODULATION AMPLITUDE. MODULATION FREQUENCY 0.6 Hz.
X COOLING IN ZERO MAGNETIC FIELD.   O WARMING IN ZERO MAGNETIC FIELD.   Δ COOLING IN 750 A/m
DC FIELD.

peak in the first harmonic $S(T)$ curve. Figure 36 shows the corresponding temperature dependence of the phase of the modulation. It peaks where the amplitude modulation is a minimum. The presence of a DC magnetic field of 750 A/m appears to have no significant effect on the amplitude or phase of the temperature modulation.

Discussion. The temperature dependence of the modulation amplitude as given in Fig. 35 indicates a maximum in specific heat at 291.3 ± 0.2K, in good agreement with the maximum observed at 291.8K by Griffel et al (1954); however, this agreement may be somewhat fortuitous in view of the dependence of T_C upon sample purity. This temperature is significantly lower than the value of 293.7 ± 0.2K corresponding to the largest value of $\chi^2(T)$ as in the previous section and the largest signal amplitudes in both the AC and DC modulation experiments. This is not surprising as the specific heat maximum should occur when $M_S \dfrac{dM_S}{dT}$ is a maximum whereas the results given both in this section and in the previous one indicate that domain properties strongly influence the temperature dependence of the susceptibility. The observed temperature dependence of the phase of the temperature modulation given in Fig. 36 is very different to the expected behaviour of a minimum at 291.3K; the thermocouple measures the modulation from only part of the sample, and the observed temperature dependence may be due to the dependence of the thermal skin depth δ_T upon temperature. Here $\delta_T \simeq 1mm$, which is comparable with the sample radius. This may explain the difference between the phase results for the DC field, temperature modulation experiments and those for the temperature modulation measurements. Further careful studies of the temperature dependences of the modulation amplitude and phase are being carried out. A conventional
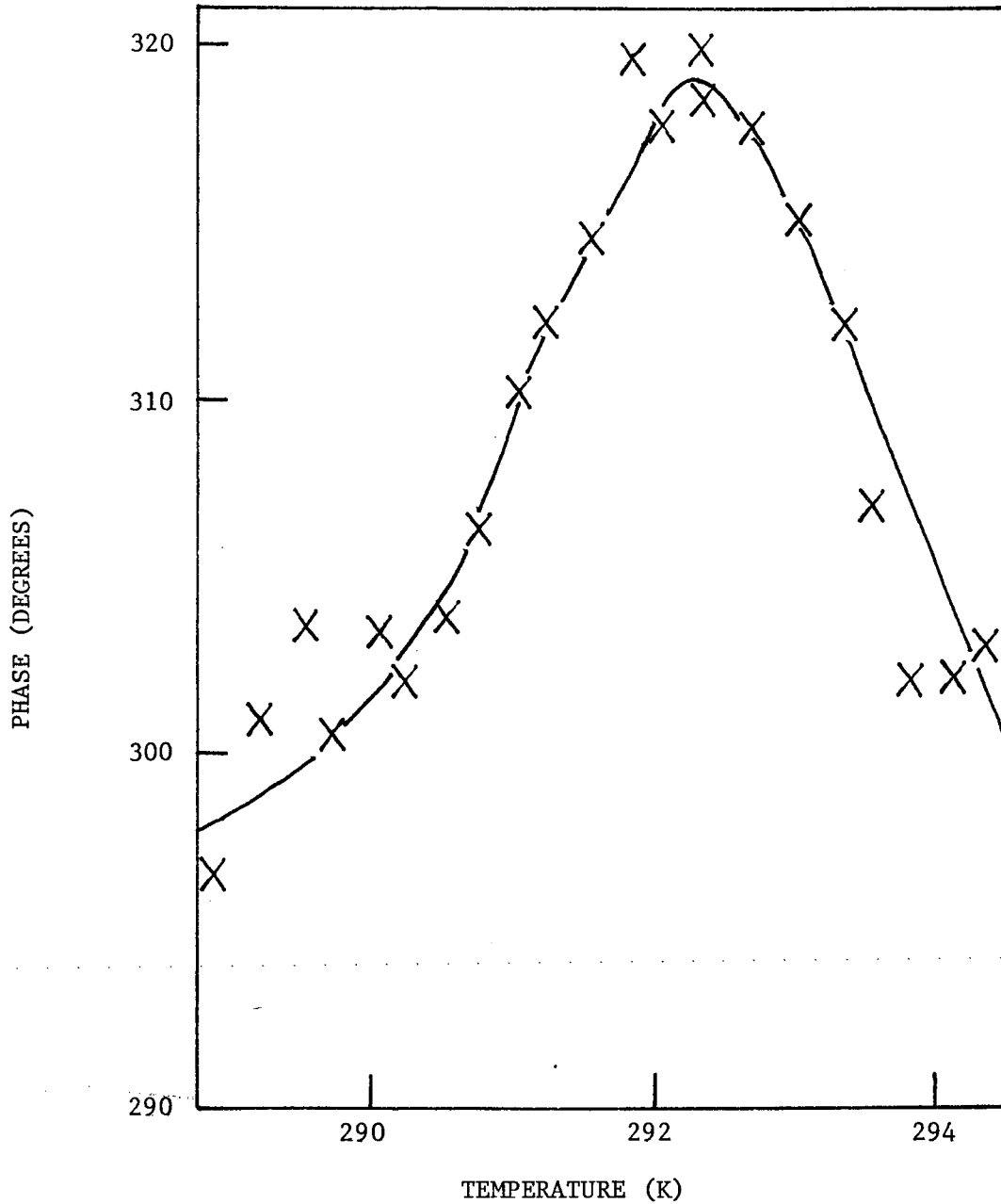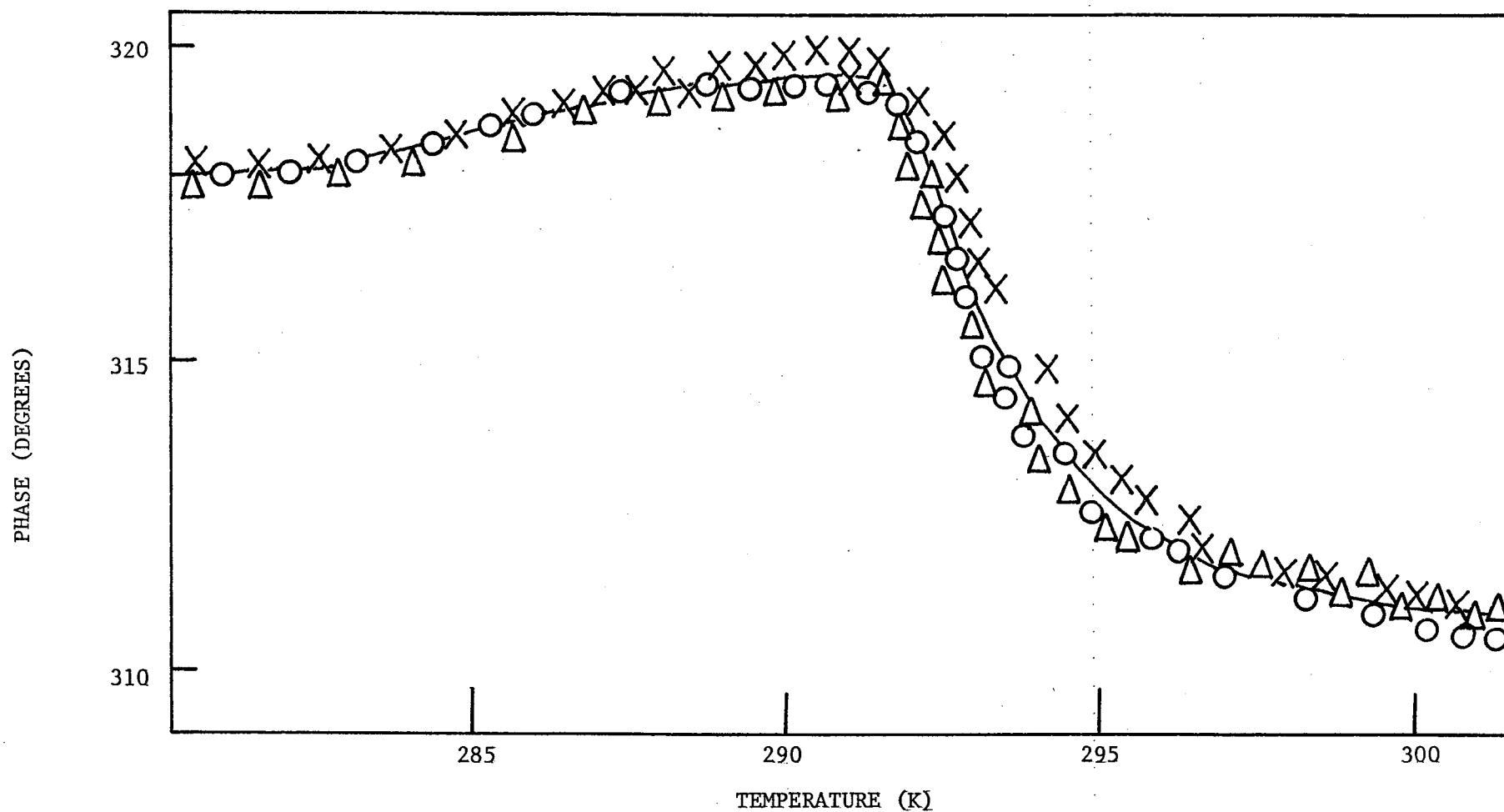
FIGURE 36: TEMPERATURE DEPENDENCE OF THE PHASE OF THE TEMPERATURE MODULATION WITH RESPECT TO THE
HEATER POWER WAVEFORM. MODULATION FREQUENCY 0.6 Hz. ✕ COOLING IN ZERO MAGNETIC FIELD.
O WARMING IN ZERO MAGNETIC FIELD. △ COOLING IN 750 A/m DC FIELD.

calorimetric study of the specific heat of the samples is also in progress.

To facilitate discussion of the effects of relaxation on the low-field AC experiments, curves showing the temperature variations of the AC susceptibility and the signal amplitude and phase of the temperature modulation signals for a low-field warming experiment are given together in Fig. 37. Further, it is instructive to examine the effects of relaxation (as presented in Chapter 4) at temperatures where χ_e^1 is zero. Here, in the absence of any relaxation effects ($\omega_T \tau = 0$), the first harmonic signal should be zero. Zero values of χ_e^1 will occur when the contributions from the temperature dependences of M_S and g cancel, i.e., when $gM_S{}' = - M_S g'$. Relaxation of $g(t)$ will introduce an imbalance and Eq. 289 and 290 show that the signal amplitude will then be non-zero with a phase lead given by:

$$tan \; \phi_r \; = \; 1/(\omega_T \tau) \qquad\qquad (296)$$

For slow modulation ($\omega\tau \ll 1$) small signal amplitudes with a large phase lead will result. For fast modulation ($\omega_T \tau \gg 1$) there will be large, almost in-phase signals.

The results shown in Fig. 37 demonstrate well the main features of the above theory. The quantity χ_e^1 is zero at 291.9 ± 0.2 and 290.0 ± 0.4K. At 291.9K there is a large modulation signal and small phase lead which is to be expected for slow relaxation ($\omega_T \tau \gg 1$). At 290K there is a small signal amplitude and large phase lead corresponding to relatively fast relaxation ($\omega_T \tau \lesssim 1$). One concludes that the domain properties responsible for these effects relax very slowly at T_C where nucleation is commencing and faster at lower temperatures.
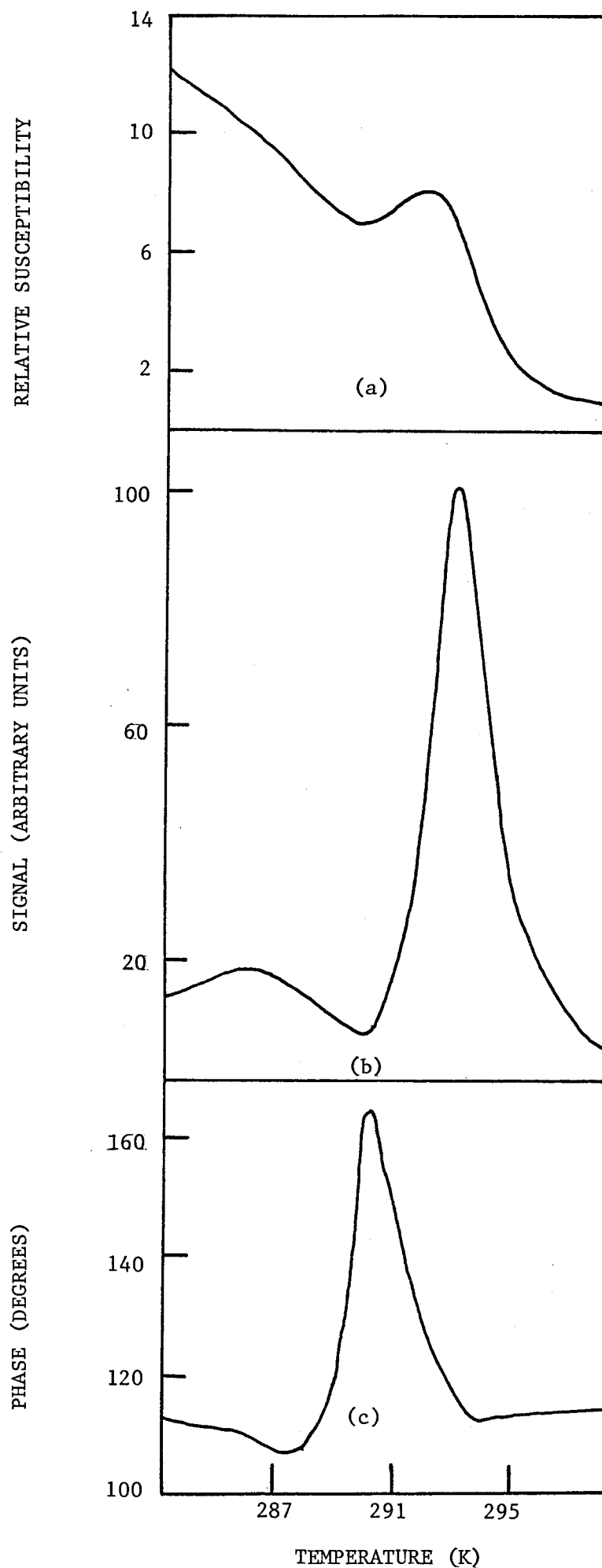
FIGURE 37: TEMPERATURE DEPENDENCES OF THE RELATIVE AC SUSCEPTIBILITY(a), AC FIELD, TEMPERATURE MODULATION SIGNAL (b), AND PHASE OF THE AC FIELD, TEMPERATURE MODULATION SIGNAL (c).WARMING EXPERIMENT. AC FIELD FREQUENCY 100 Hz. MODULATION FREQUENCY 2 Hz. MODULATION AMPLITUDE ≃ 6 mK. RMS AC FIELD 10 A/m.

Writing $\chi = gM_S$ and ascribing the relaxation effects to

the domain g term requires that the same effects be observed in

both AC and DC experiments : in low fields the same process of

reversible domain displacement will dominate in both the AC and DC

susceptibilities. Hence, we now consider the implications of our

observation that there are no significant relaxation or temperature

hysteresis effects in the DC experiments; that is, there are no

such effects in the temperature dependence of the DC susceptibility.

This is quite feasible in view of the variation of the $\chi(T)$ curves

with the frequency of the AC field as shown in Fig. 17. The trough

in the AC $\chi(T)$ curves together with their temperature hysteresis

must then be due to the magnetic after-effect. The lack of anomalous

behaviour in the DC experiments indicates that there is no significant

temperature hysteresis or slow relaxation in the actual domain

nucleation; rather, the temperature hysteresis and relaxation effects

in the low-field AC susceptibility must be caused by hysteresis and

relaxation in the after-effect at temperatures where domains nucleate

and de-nucleate. An impurity after-effect is not expected to affect

the DC susceptibility but, because of a damping of domain wall motion

it produces a reduction of the AC susceptibility as observed in the

frequency dependence of the susceptibility as in the previous section.

The relaxation theory of Chapter 4 is easily extended to cover these

results by again writing $\chi = g\sigma$ for the low-field susceptibility and

putting:

$$g = g_0 - (\Delta g) \tag{297}$$

where (Δg) is the decrease in g due to the after-effect; (Δg) is

frequency-dependent tending to zero at very low frequencies so that

the DC susceptibility is $g_0 M_S$. As the frequency is increased (Δg)

will increase tending to an almost frequency-independent value at high frequencies. It is assumed that g_0 does not exhibit relaxation or temperature hysteresis effects and that (Δg) satisfies a relaxation equation:

$$\frac{d(\Delta g)}{dt} = -\frac{[(\Delta g) - (\Delta g)_e]}{\tau} \tag{298}$$

where the equilibrium value $(\Delta g)_e$ is a function of temperature. Above T_c there are no domains, and as expected, there are no relaxation effects so that $(\Delta g)_e = 0$. As the temperature is lowered below T_c, $(\Delta g)_e$ will increase and, as indicated by Fig. 17, will then become approximately temperature-independent. In the region of T_c, $(\Delta g)_e$ exhibits temperature hysteresis with a polarity such that, from Fig. 11, it is greater on warming than on cooling. This polarity is in agreement with an impurity after-effect in which the pinning of walls by impurities is stronger on warming than on cooling at temperatures in the nucleation region. This model leads to results which are of the same form as the corresponding equations of Chapter 4. Equations 287 and 290 of Chapter 4 for the first harmonic oscillation $\chi_1(t)$ and for the resultant phase become:

$$\chi_1(t) = \Delta \ \{M_S g_0' + M_S' g_e) \ \cos \ (\omega_T t + \phi_T)$$

$$- M_S(\Delta g)_e' \ \alpha_1 \ \cos \ (\omega_T t + \phi_T - \phi_1)\} \tag{299}$$

and

$$\tan \phi_r = \frac{M_S(\Delta g)_e' \ \omega_T \tau}{\chi_e^2 + \omega_T^2 \tau^2 (M_S' g_e + M_S g_0')} \tag{300}$$

where $\tan \phi_1 = \omega\tau$ and $\alpha_1 = (1 + \omega_T^2 \tau^2)^{-\frac{1}{2}}$ $\tag{301}$

These are the same as in Chapter 4, except that the relaxing term $M_S g_e'$ has become $-M_S(\Delta g)_e'$ and the "fast" term $M_S' g_e$ has become

$(M_S' g_e + M_S g_0')$. Note that the sign of $(\Delta g)_e'$ is opposite to that of g_e', and the minus sign in the new "slow" term is thus cancelled with respect to the corresponding term for Chapter 4. Equation 300 can be simplified to

$$tan \ \phi_r \ = \ \beta \omega_T \tau / (1 \ - \ \beta \ + \ \omega_T^2 \tau^2) \tag{302}$$

where $$\beta \ = \ M_S (\Delta g)_e' / (M_S' g \ + \ M_S g_0') \tag{303}$$

is the ratio of the relaxing and fast components of $\chi^i(T)$. At temperatures where $\chi^i(T) = 0$, $\beta = 1$ and:

$$tan \ \phi_r \ = \ 1/(\omega_T \tau) \tag{304}$$

as in Eq. 296. As above, a consideration of such points shows that in the nucleation region, τ decreases as the temperature is lowered. Curves of ϕ_r versus $\omega \tau$ are given in Fig. 38 for several values of β. For $\beta < 1$ the relaxing term is always less than the fast term in Eq. 299 and the phase lead is less than it would be for $\beta = 1$. For $\beta > 1$ the signal amplitude passes through zero at points where $\omega_T \tau = \sqrt{\beta - 1}$ and the phase then changes discontinuously between $\pm \dfrac{\pi}{2}$. This corresponds to exact cancellation of the relaxing and fast terms in Eq. 299. Such effects were not observed in our experiments but certainly would be if extremely low modulation frequencies were used.

We now discuss the features of the three curves in Fig. 37 in terms of the above relaxation theory. Above T_c no domain effects are expected and, apart from the variation of Δ, the signal amplitude should vary as the derivative $\chi^i(T)$. The maximum signal amplitude occurs at 293.2K, where ϕ_r is still small and this is just a little below the temperature at which $\chi^i(T)$ is a maximum. Here the domains are just beginning to nucleate. The relaxation of (Δg) will be extremely slow ($\omega_T \tau \gg 1$), and the large signal will be given by:
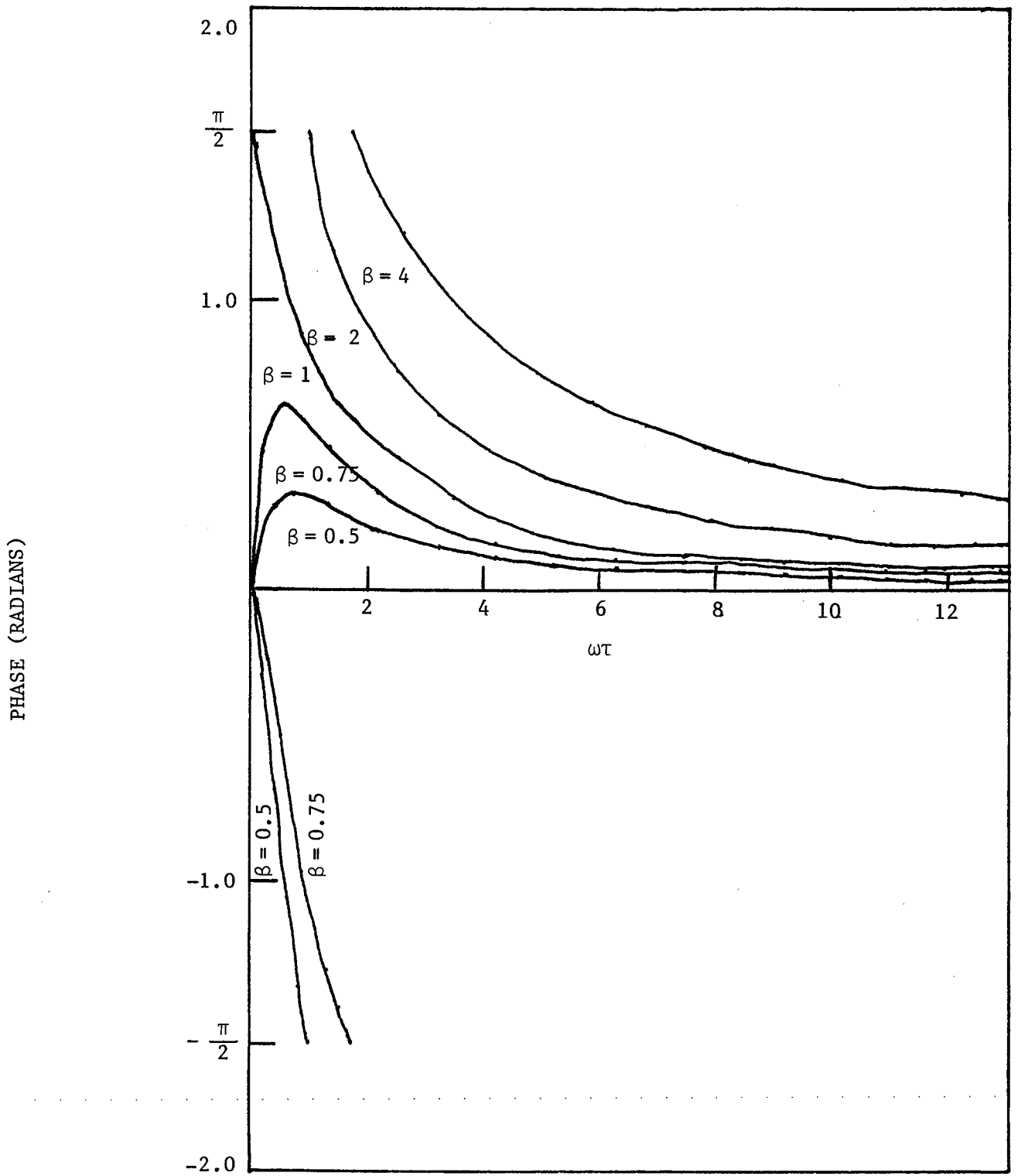
FIGURE 38: DEPENDENCE ON $\omega_T \tau$ OF THE PHASE

$$\phi_r = artan \left\{ - M_S g'_e \ \omega_T \tau / (\chi'_e + g_e M'_S \ \omega_T^2 \tau^2) \right\}$$

FOR VARIOUS VALUES OF $\quad \beta = \dfrac{-M_S g'_e}{g_e M'_S}$

$$\chi_1(t) \simeq \Delta \ (M_S g_0' + M_S' g) \ cos \ (\omega_T t + \phi_T) \tag{305}$$

the relaxing term in Eq. 299 being effectively zero because of the small value of α_1. At 291.9K, where $\chi^1(T) = 0$, the large signal amplitude requires that still $\omega_T \tau \gg 1$ and this is in agreement with the observation in the previous section that here $\tau \sim$ 2-6 secs. Between the two temperatures where $\chi^1(T) = 0$, $\beta > 1$ since $(\Delta g)_e'$ is always negative in the nucleation region, and the phase lead will increase as $\omega_T \tau$ decreases. The maximum phase lead occurs at 290.7 $\pm$ 0.2K, just above the trough in $\chi(T)$, since below this β will decrease below 1. Figure 38 shows that when $\beta < 1$ and $\omega_T \tau \to 0$ the phase lead tends to zero. The large phase maximum must also occur at a point where the modulation signal amplitude is a minimum and this agrees well with the results.

In Figs. 28 and 31 it was pointed out that the signal amplitude and phase for modulation frequencies of 0.3 Hz and 2 Hz are almost identical. This requires that at any one temperature there is a broad range of relaxation times; it is interesting that a similar conclusion was reached in the previous section with respect to the results of Fig. 16 for field frequency.

The difference between the cooling and warming curves will be partly due to a difference in $(\Delta g)(T)$; as above, at any temperature in the nucleation region (Δg) will be greater on warming than on cooling and, in the region of the phase peak $|(\Delta g)_e'|$ will be greater on cooling than on warming; therefore, between the two points where $\chi^1(T) = 0$, β will be larger on cooling as can be seen from Fig. 11. However, this is quite obviously not the whole explanation since this would by itself, predict a larger phase lead on cooling (as can be seen from Fig. 38 and in contradiction to the results of Fig. 30) and a smaller modulation signal on cooling. The latter observation can be

deduced from Eq. 299 and an analysis of the DC results of Fig. 24.

Since the DC field temperature modulation signal involves only g_0,

it is clear that:

$$|M_S' g_e| > |M_S g_0'|$$ (306)

and so the fast and relaxing terms of Eq. 299 oppose each other.

Therefore, a larger $|(\Delta g)_e'|$ on cooling would favour a smaller signal

amplitude for cooling than warming: this is not the case as can be

seen from Fig. 27.

It is therefore necessary to postulate that the average

relaxation time during warming is considerably shorter than during

cooling. This is in agreement with the observation in the previous

section that the effects of relaxation in the susceptibility

following sudden temperature changes were much weaker during warming

experiments. Probably the slow relaxation caused during cooling is

associated with the diffusion of impurities to the newly-nucleated

walls, whereas in warming from lower temperatures, more stable

impurity-wall configurations have been set up.

One result of relaxation effects in any experiment in which

modulation and phase-sensitive detection is used is that the signal

amplitude is not, even for sufficiently small modulation amplitudes,

proportional to the appropriate derivative. In Fig. 39 $\chi(T)$ curves

for cooling experiments with low (12.8 A/m) and high (850 A/m) RMS

applied AC fields are given together with suitably normalized curves

obtained by integrating the signal amplitudes of the corresponding

temperature modulation signal amplitudes, starting at high temperatures.

Correction was made for the temperature dependence of ΔT. Above T_C

there is good agreement between $\chi(T)$ and the integrated curves, as

expected for slow modulation ($\omega_T \tau \ll 1$). Below T_C the two curves
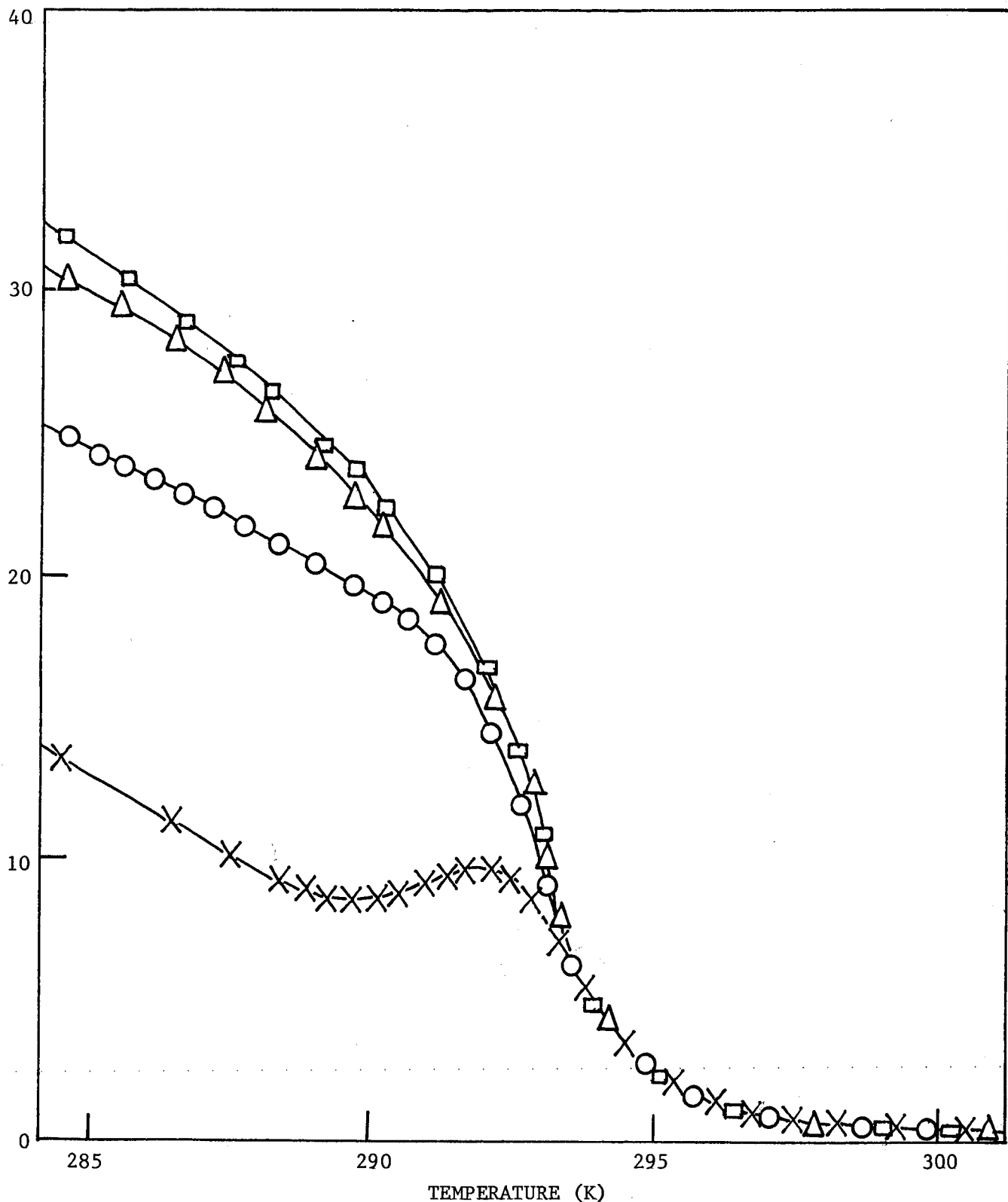
FIGURE 39: INTEGRATED AC FIELD, TEMPERATURE MODULATION COOLING CURVES SUPERIMPOSED ON $\chi(T)$ COOLING CURVES WITH THE INTEGRATED CURVES NORMALIZED TO MAKE THE RESULTS COINCIDE AT 299.2K. MODULATION FREQUENCY 2 Hz. AC FIELD FREQUENCY 100 Hz. MODULATION AMPLITUDE $\simeq$ 6 mK. X $\chi(T)$ WITH 12.8 A/m RMS AC FIELD; 0 INTEGRATED $S(T)$ WITH 12.8 A/m RMS AC FIELD; Δ $\chi(T)$ WITH 850 A/m RMS AC FIELD; $\square$ INTEGRATED $S(T)$ WITH 850 A/m RMS AC FIELD.

are also very similar for the large AC field, and this was expected

since in large AC fields the susceptibility will not be greatly

affected by the impurity – diffusion after-effect, $(\Delta g \ll g)$.

However, in lower fields the integrated curve is considerably greater

than $\chi(T)$. This requires that the relaxing component is one which

reduces the equilibrium AC susceptibility, in agreement with the

assumptions of our relaxation theory.

As the AC field is increased above the initial field-independent

susceptibility region, the theory must be formulated in terms of

$G(H,T)$. In the ferromagnetic region, G is expected to increase and

$\left| {}^{dG}e/_{dT} \right|$ is expected to decrease with increasing field. From Eq.299

it can be seen that this will result in a shift of the peak of the

modulation signal lower towards the temperature at which $\left| {}^{dM}s/_{dT} \right|$

is a maximum. This prediction is borne out in the results of Fig.27.

Also, the decreasing contribution from the after-effect in high

fields explains the decrease of structure in the high AC field signal

and phase temperature dependences, the reduced significance of the

trough in the high field AC $\chi(T)$ curves, and relative absence of

temperature hysteresis in high AC fields in both the $\chi(T)$ and

modulation signal measurements. It is also the reason for the marked

similarity between the DC field, temperature modulation phase results

and those for high AC fields, and predicts the relative lack of

temperature hysteresis in the latter results.

For fast modulation, it was shown in Chapter 4 that:

$$\chi_1(T) \to \Delta \ g_e \ (\overline{T}) \ M_S' \ (\overline{T}) \ cos \ (\omega_T t + \phi_T) \qquad (307)$$

so that the peak in the modulation signal for fast modulation would be

expected to occur closer to the maximum of dM_S/dT (presumably at T_c)

than for slower modulation experiments. The peak in the 20 Hz data

of Fig. 29 at about 291.5K agrees well with the position of the

minimum in Δ in Fig. 35 at 291.3 ± 0.2K.

The results of relaxation experiments in which the effects

of sudden temperature changes on the first harmonic signal amplitude

are studied for low AC fields are in agreement with the observation

of a single peak in the temperature dependence of the second harmonic

signal amplitude.

Finally, we comment on the sensitivities of the DC field

and AC field, temperature modulation techniques. As shown in

Fig. 25, the sensitivity of the DC technique is small in very small

applied DC fields; by contrast, the AC technique is most sensitive

in zero DC field. The two techniques are thus complementary in

nature with respect to field strength.

6.4   A New Manifestation of the Magnetic After-Effect in the

         AC Susceptibility

During the studies of the AC modulation technique, one of

the thermocouples was at one stage connected to an earth point on

the chart recorder. Anomalous amplitude and phase results were

found in the AC modulation signal at temperatures lower than about

288K. The dependences of the amplitude and phase of the AC

modulation signal on AC field amplitude in these instances under

several experimental conditions are shown in Figs. 40 and 41

respectively. It can be seen that the normalized amplitude in low

AC fields increases rapidly below about 8 A/m, while the phase

exhibits marked structure in this critical region of field.

Further investigation of these phenomena has revealed that

they are due to a magnetic after-effect which causes the low field

AC susceptibility to be enhanced by an additional time varying
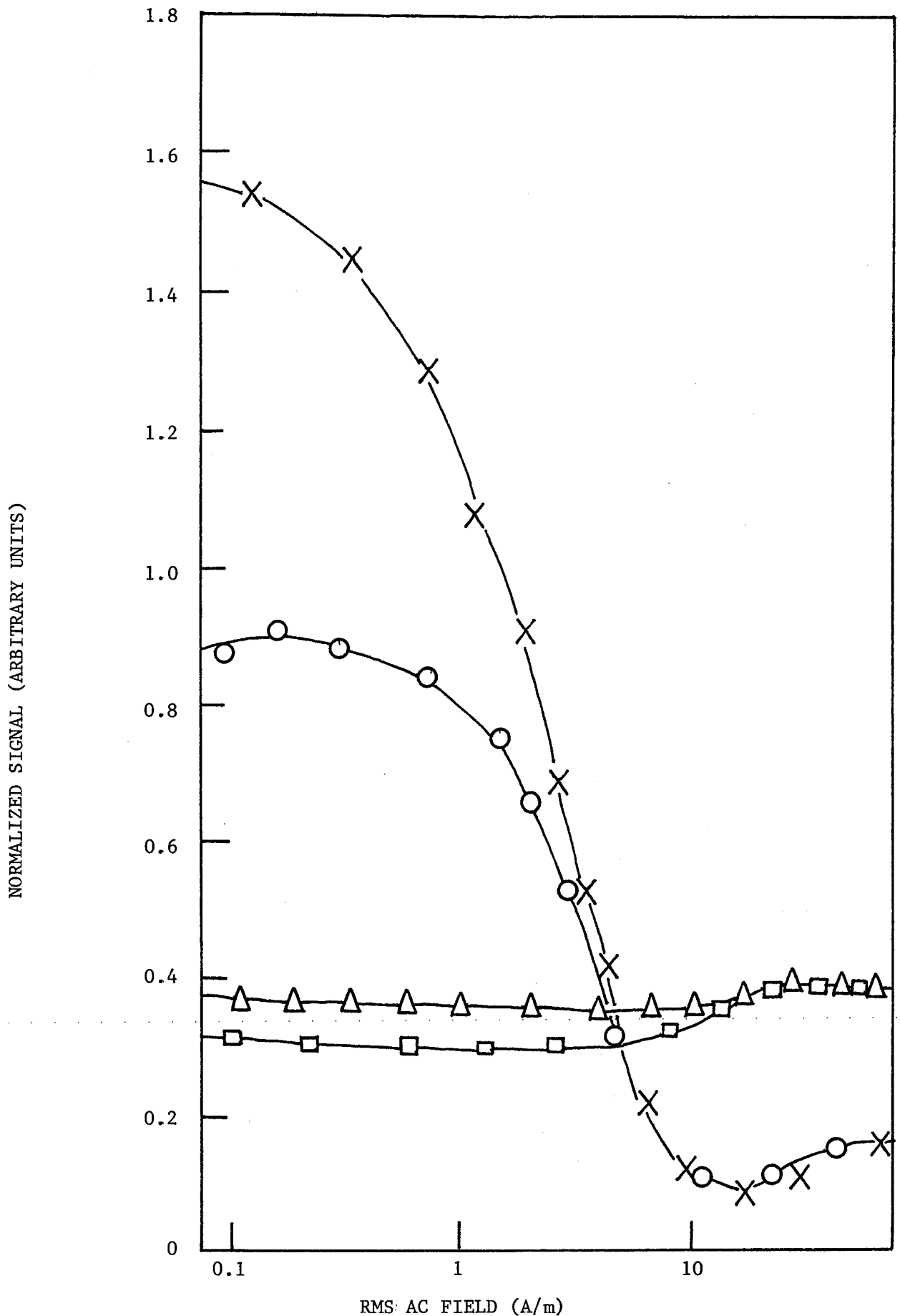
FIGURE 40: FIELD DEPENDENCE OF THE AC FIELD TEMPERATURE MODULATION SIGNAL
NORMALIZED WITH RESPECT TO AC FIELD AMPLITUDE DISTORTED BECAUSE
OF THE TRANSIENT FIELD-ENHANCEMENT MAGNETIC AFTER-EFFECT.
TEMPERATURE 274.6K. AC FIELD FREQUENCY 1000 Hz. VARIOUS
CONDITIONS OF MODULATION FREQUENCY AND AMPLITUDE: X 2 Hz AT
$\simeq$ 1 mK. 0 2 Hz AT $\simeq$ 6 mK. $\triangle$ 0.3 Hz AT $\simeq$ 6 mK. $\square$ 0.3 Hz AT
$\simeq$ 36 mK.
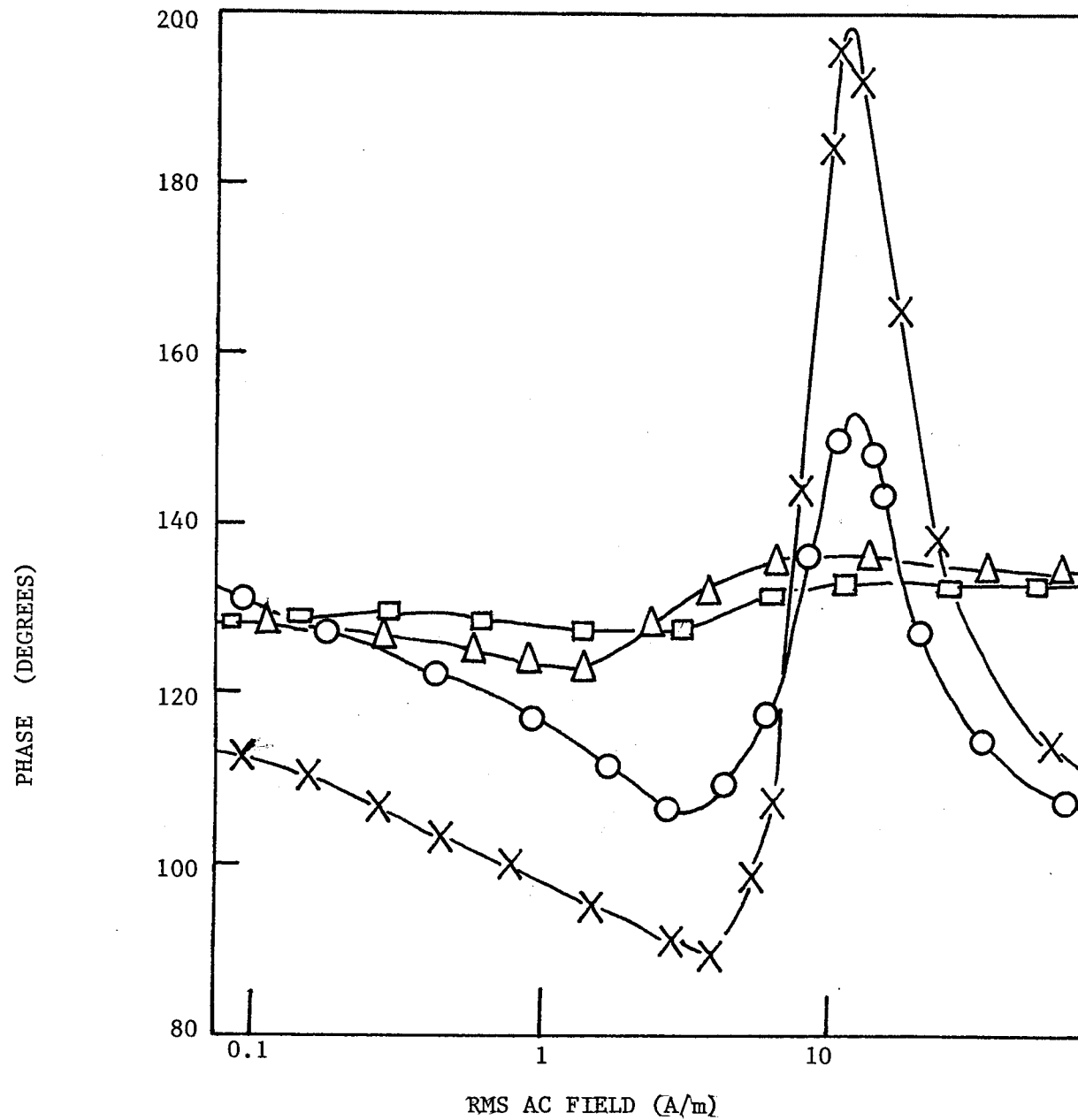
FIGURE 41: FIELD DEPENDENCE OF THE PHASE OF THE AC FIELD TEMPERATURE MODULATION SIGNAL WITH RESPECT
TO THE HEATER POWER WAVEFORM DISTORTED BECAUSE OF THE TRANSIENT FIELD ENHANCEMENT MAGNETIC
AFTER-EFFECT. TEMPERATURE 274.6K. AC FIELD FREQUENCY 1000 Hz. VARIOUS CONDITIONS OF
MODULATION FREQUENCY AND AMPLITUDE: X 2 Hz AT $\simeq$ 1 mK. 0 2 Hz AT $\simeq$ 6 mK. $\triangle$ 0.3 Hz AT
$\simeq$ 6 mK. $\square$ 0.3 Hz AT $\simeq$ 36 mK.

field. A small leakage current from the heater through the sample and the thermocouple to earth gave rise to a magnetic field at the frequency of the heater current. This caused enhancement of the AC susceptibility in a way which is to be described below.

It is beyond the scope of this thesis to fully discuss the research carried out on this effect. We have confirmed that the effect is associated with a biassing magnetic field by super-imposing low frequency square, triangular and sinusoidal pulses of current on the 1000 Hz or 100 Hz primary current of the transformer. The output of the PSD monitoring the secondary output was connected to a CRO. Note that because the PSD is a narrow-band instrument, there is little likelihood of detecting other than a small amount of transient pick-up from the low-frequency biassing pulses. By comparing the results obtained in the ferromagnetic region with those in the paramagnetic region, we were able to show that the results we will present here have not been significantly affected by transient noise.

Figure 42 shows the effect on the susceptibility at 1000 Hz in an AC field of amplitude 2.3 A/m RMS of a 1.4 A/m square pulse of biassing field lasting 9.6 secs. The baseline before A has been DC shifted. The first peak corresponds to the switching on of the biassing field, the second to the switching off. It can be seen that two similar peaks are produced; in both cases the AC susceptibility enhancement produced by a change in the biassing field decreases to zero after the change has ceased, with a relaxation time of about 1.6 secs.

The percentage enhancement decreases rapidly for primary fields greater than ~ 8 A/m. The relative enhancement as a function
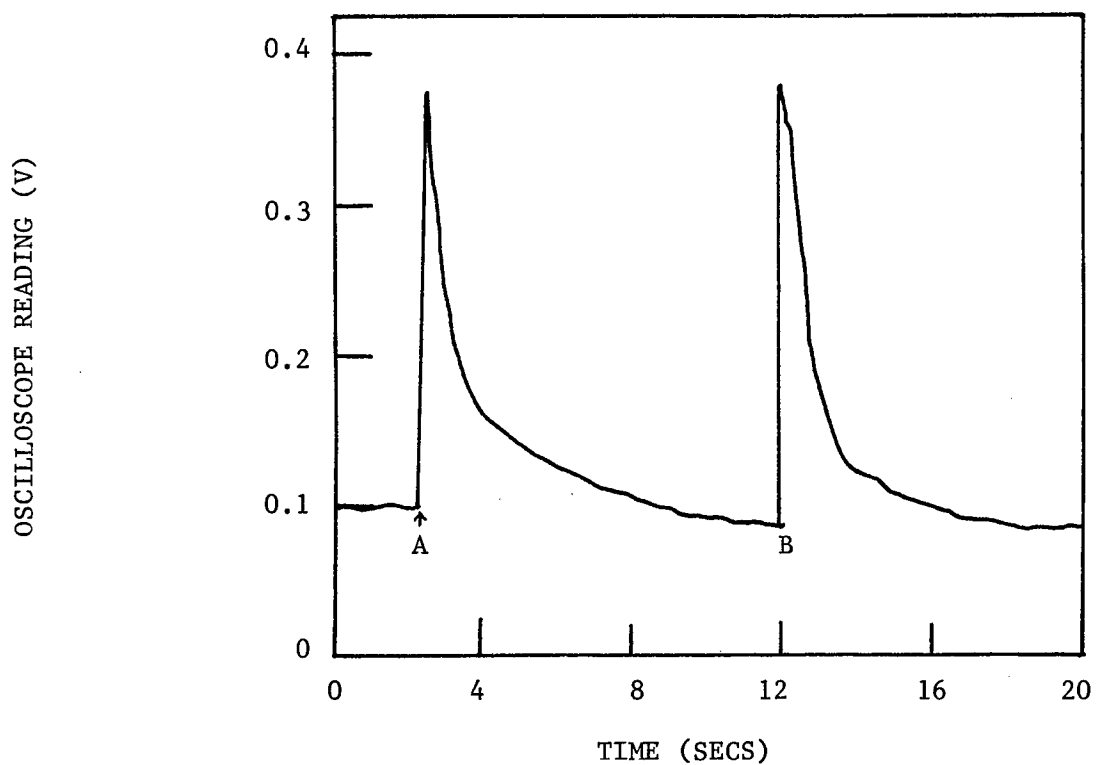
FIGURE 42: TRANSIENT-FIELD ENHANCEMENT OF THE AC SUSCEPTIBILITY.
A - FIELD ON, B-FIELD OFF. TEMPERATURE 278.2K.AC
FIELD FREQUENCY 1000 Hz. RMS AC FIELD 2.3 A/m.
BIASSING FIELD 1.4 A/m.

of AC field amplitude is shown in Fig. 43. The similarity with

Fig. 40 can be seen. In accordance with observations presented

previously in this chapter, it is therefore thought that this

after-effect must be associated with the low-field reversible

domain wall translation processes.

The temperature dependence of the relative magnitude of

this effect is shown in Fig. 44 for a low biassing field. It is

seen that the magnitude achieves a broad maximum in the region of

280K. The data of Corner et al for Gd (1962) reveals a similar

broad maximum in the anisotropy at about 280K.

The susceptibility enhancement has been shown to be

associated with the time derivative of the biassing field. More-

over, under none of the experimental conditions employed (biassing

fields from 0.7 A/m to 750 A/m, and primary fields of 100 Hz and

1000 Hz from 10^{-2} A/m RMS to 850 A/m RMS) was the effect seen to

be additive; this can be seen, for example, from the result shown

in Fig. 45. Here the square biassing pulse was of a duration less

than the relaxation time of the enhancement. Furthermore, the

dependence of the enhancement with the rise-time of the biassing

field has been investigated. It was found that the effect was

greatly diminished for rise times $\gtrsim$ the relaxation time of the

enhancement.

Experiments were also performed with biassing fields

$\simeq$ 750 A/m acting on a primary field $\simeq$ 5 A/m. It was found that

the majority of the enhancement fell rapidly after the biassing

field had stopped changing. However, a close analysis of the final

small part of the enhancement revealed that it relaxed back to zero

with the same characteristic time as that of the enhancement

produced by low biassing fields. This is similar to the behaviour
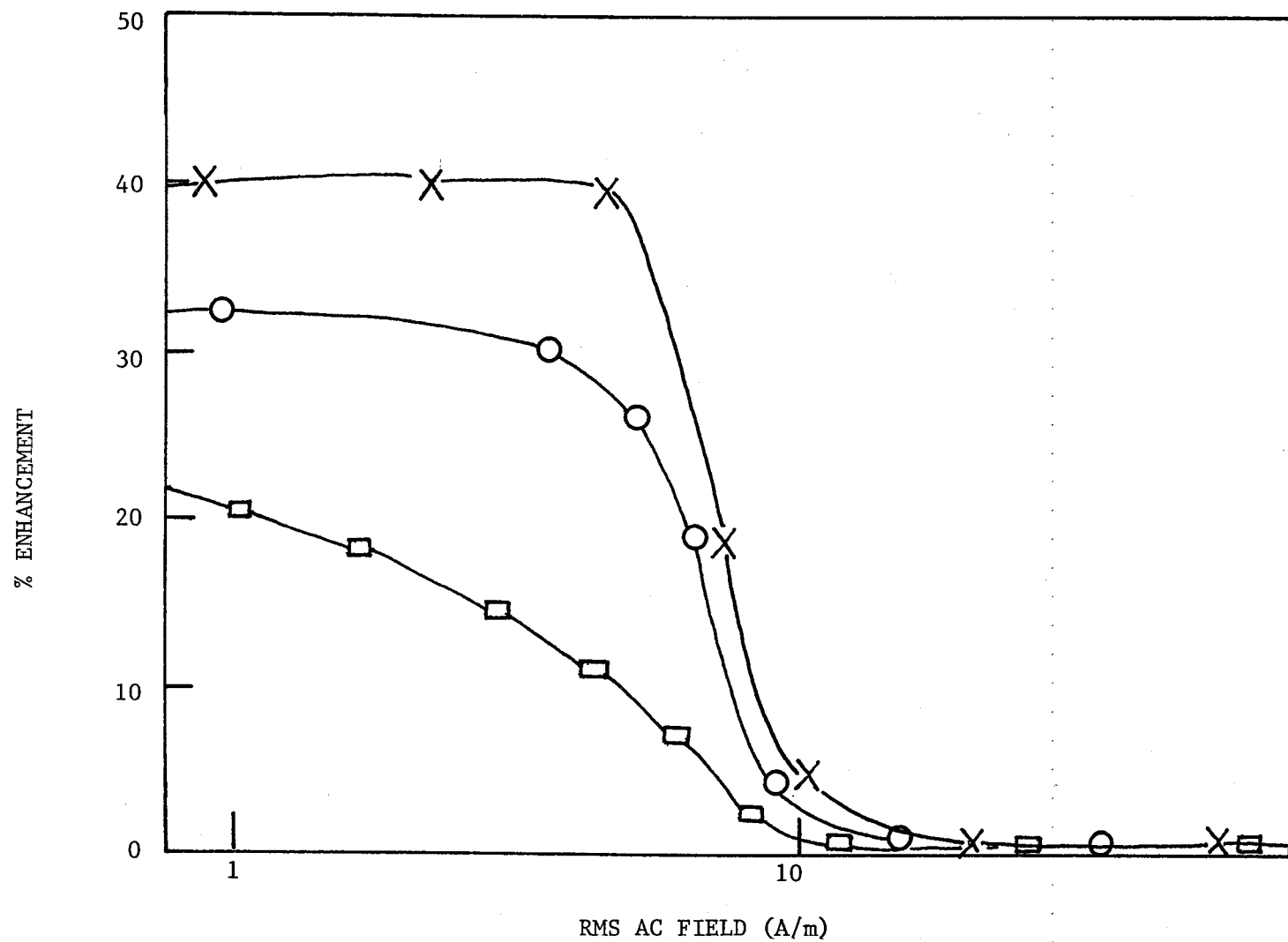
FIGURE 43: FIELD DEPENDENCE OF THE TRANSIENT FIELD ENHANCEMENT OF THE AC SUSCEPTIBILITY. AC FIELD FREQUENCY 1000 Hz. TEMPERATURE 278.2K. STEP-FUNCTION OFFSET FIELDS: X 450 A/m; 0 300 A/m; □ 150 A/m.
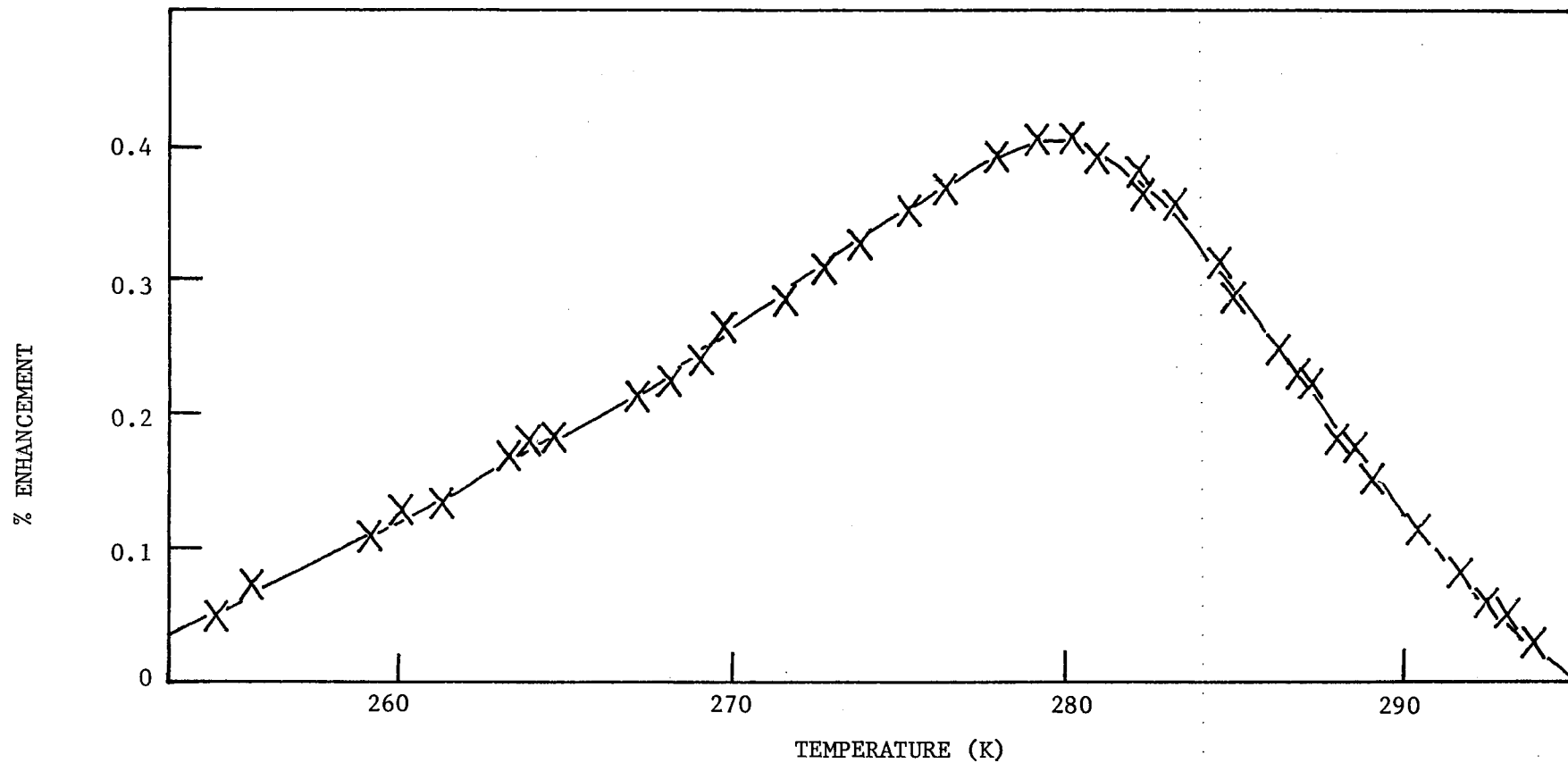
FIGURE 44: TEMPERATURE DEPENDENCE OF THE TRANSIENT FIELD ENHANCEMENT OF THE AC SUSBEPTIBILITY. AC FIELD FREQUENCY 1000 Hz. RMS AC FIELD 4.5 A/m. AC BIASSING FIELD OF 4.5 A/m RMS AT 20 Hz.

OSCILLOSCOPE READING (V)
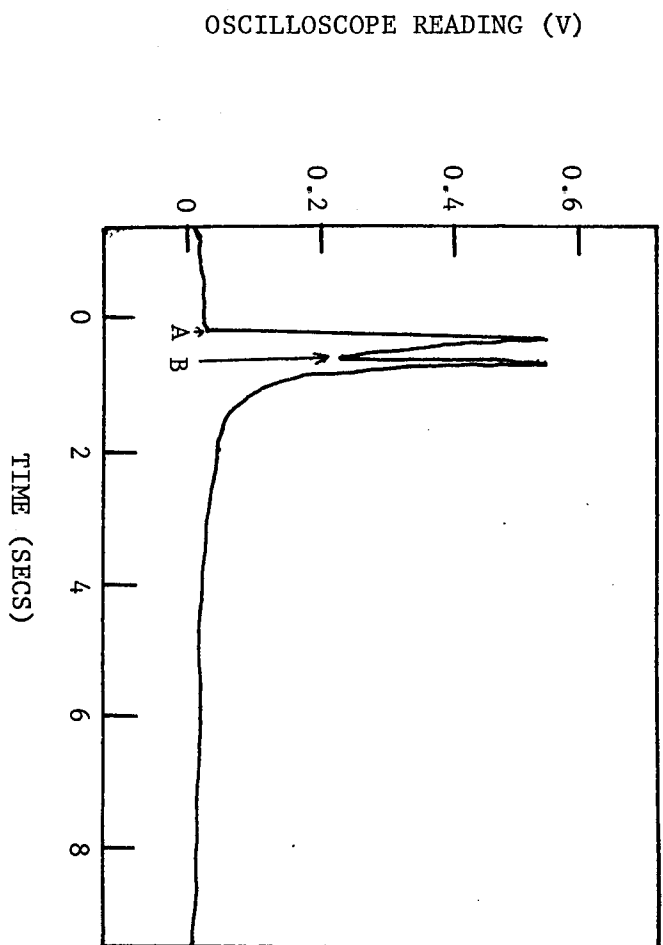
FIGURE 45: TRANSIENT FIELD ENHANCEMENT OF THE AC SUSCEPTIBILITY FOR A FAST
RECTANGULAR PULSE OF BIASSING FIELD. A - FIELD ON. B - FIELD OFF.
TEMPERATURE 278K. AC FIELD FREQUENCY 1000 Hz. RMS AC FIELD 2.3 A/m.
BIASSING FIELD 1 A/m.

of the normal magnetic diffusion after-effect in the DC magnetiz-
ation, wherein the magnetic change consists of a fast portion
associated with high fields, and a slow part due to low fields
(see e.g., Bozorth 1951, Chikazumi 1964, and refer to Chapter 2).

Work is proceeding with a view to presenting a fuller
account of this phenomenon at a later date. Preliminary attempts
to explain it have centred around Snoek's (1949) approach to the
diffusion magnetic after-effect. A sudden change in field could
have the effect of temporarily removing the domain wall from the
immediate influence of the impurity causing an increase in the
differential domain wall mobility and a consequential AC
susceptibility enhancement. Over the period of the relaxation
time of the enhancement it is envisaged that the impurities diffuse
to the new site of the wall causing the AC susceptibility to
gradually decrease. A difficulty seems to be, however, that if the
biassing field was such that the wall displacement caused by it was
less than the dimensions of the potential well due to the impurity,
one would not expect to see the same enhancements produced by
switching the biassing field on and off within the time of relaxation.
For none of our experimental conditions have we seen evidence that
different enhancements can be so produced. This difficulty could
be overcome if we were to postulate that these potential wells are
very localized and square in nature, and that we have not been able
to detect the enhancements due to biassing displacements within the
wells.

The fast-response enhancement produced by a high biassing
field could be explained in terms of the finite rise or fall-time

of the biassing field: it would traverse the region of high differential susceptibility in the M versus H curve. In view of our findings in Sec. 6.2 that a large DC field has little effect on the low AC field susceptibility, one would need to propose that there is a transient differential susceptibility in medium fields near the point of inflection in the M versus H curve; this transient susceptibility would be higher than the equilibrium value of the low AC field susceptibility in DC fields of this magnitude.

CHAPTER 7

SUSCEPTIBILITY CRITICAL EXPONENT ANALYSIS

ABOVE THE CURIE POINT

In Chapter 3 it was seen that amongst the most important problems confronting experimentalists in bulk critical exponent evaluations are sample purity and configuration, the effect of finite magnetic field, the accurate determination of T_c, and the definition of the temperature range near T_c for which the functional relationship between the relevant ordering parameter and $\varepsilon = \left| \dfrac{T - T_c}{T_c} \right|$ holds.

In this work we have avoided the above difficulties or taken steps to minimize their effects. Although we have studied only polycrystalline samples of Gd, we have attempted to ascertain γ only in the paramagnetic region above those temperatures where anomolous behaviour due to domain nucleation has been reported in Chapter 6. The field-independent nature of the susceptibility in this region of temperature has led us to believe that for the conditions we have used, measurements of γ have not been significantly affected by the finite field.

As stated in Chapter 3, we have adopted the philosophy of Noakes et al (1966) in assuming a power-law temperature dependence of the susceptibility and fitting the data to the best value of T_c as well as the critical exponent. The Curie temperature is then no longer an independent variable in the exponent evaluation, but is simultaneously determined with the exponent.

The experimentation used here is identical with that dis-
cussed in Chapter 5. We combine the data from the AC susceptibility
and the AC modulation techniques. In Chapter 6 we saw that to a good
approximation the temperature dependence of the integrated AC
modulation signal above T_c agrees with that of the susceptibility
after allowing for a suitable normalization constant. Fig. 46
examines this temperature range in more detail, and shows that the
two curves seem to be superimposed. This would imply that the
exponents for the susceptibility and for the modulation amplitude
would differ by unity irrespective of the choice of T_c. However, a
detailed quantitative assessment of this data reveals imperfections
in the analysis which are not apparent on the linear scale of Fig.46.

Following on from Eq. 295 we have, in the paramagnetic
region where $\chi'' = 0$ and in the absence of temperature modulation,
the secondary voltage given by:

$$|v| = N H_O \omega(\mu_0 + \xi\chi) \tag{308}$$

$$\text{Let} \quad N H_O \omega \mu_0 = v_O \tag{309}$$

$$\text{and} \quad K = N H_O \omega \xi \tag{310}$$

so that v_O and K are constants.

$$\text{Then} \quad |v| = v_O + K\chi \tag{311}$$

so that when obtaining a direct functional relationship from the
carrier signal amplitude, one must take care to choose the correct
values of v_O and K. If the exponent is to be evaluated from a
log-log analysis, one plots $\log \left(\dfrac{|v|}{v_O} - 1 \right)$ against $\log \varepsilon$ so that
both T_c and v_O become important parameters.

Critical phenomena theory requires that the exponent law
holds between χ and ε only for the correct value of T_c. Because
the temperature derivative of the susceptibility will diverge near
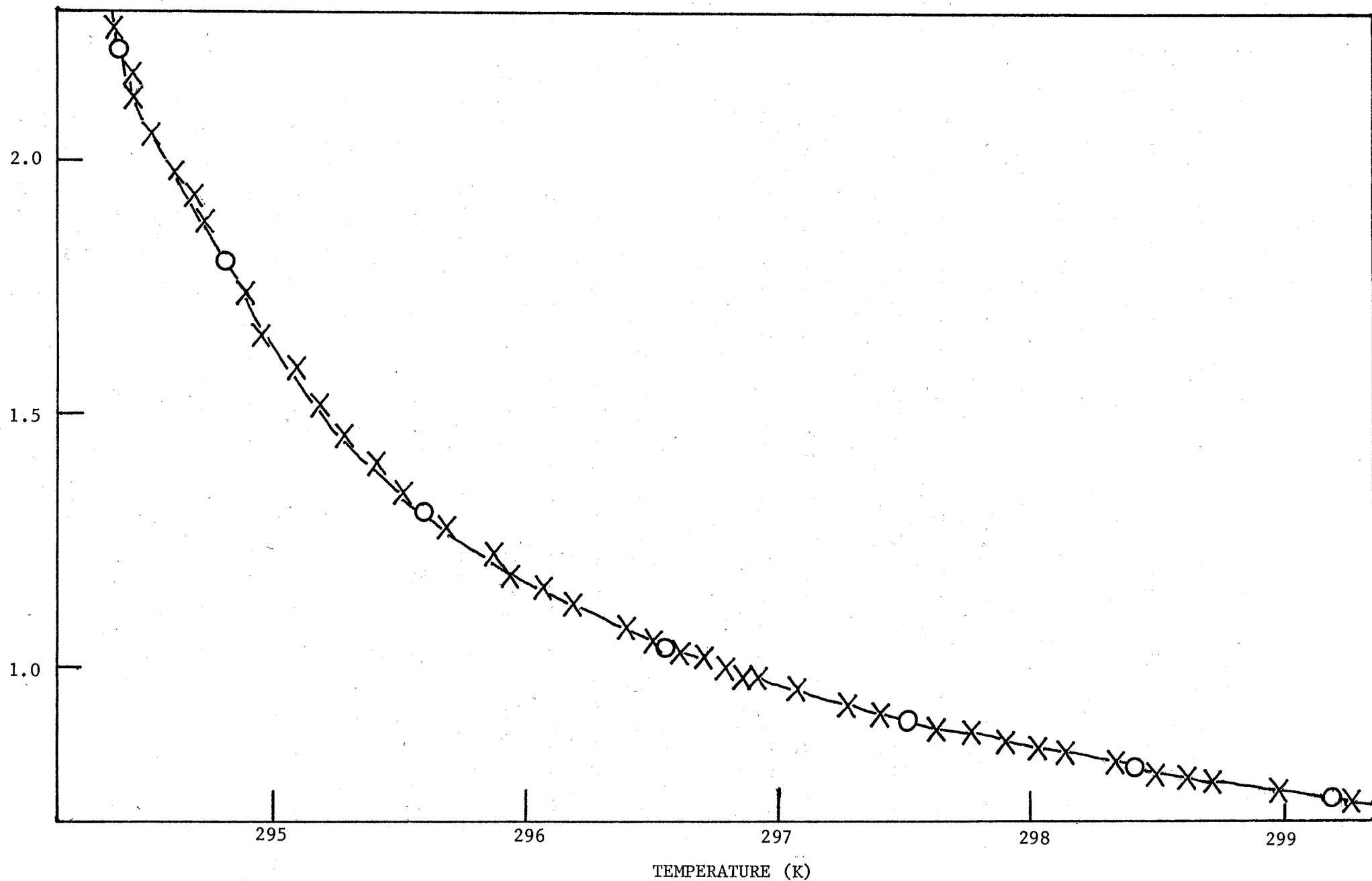
FIGURE 46: TEMPERATURE DEPENDENCE OF THE AC SUSCEPTIBILITY AND INTEGRATED $S(T)$ RESULTS IN THE PARAMAGNETIC REGION. RMS AC FIELD 1.5 A/m. AC FIELD FREQUENCY 1 kHz. MODULATION FREQUENCY 2 Hz. MODULATION AMPLITUDE $\simeq$ 8 mK. X $\chi(T)$. O INTEGRATED $S(T)$.

T_c more quickly than the susceptibility itself, the straight-line plot of $\chi/\left|\frac{d\chi}{dT}\right|$ versus temperature will have a positive intercept on the temperature axis which is uniquely, T_c (Heller 1967). In principle, this affords a method of obtaining T_c from our data, but in practice experimental noise and uncertainties related to how close to T_c the exponent law fits the experimental data made it an inaccurate way of doing so.

In this chapter, when quoting values of exponents determined from modulation data, it will be assumed that the observed exponent in the signal has been decreased by unity because of the proportionality between the signal and $\frac{d\chi}{dT}$. In view of the above considerations, it is not surprising that for a general choice of T_c a small but measurable difference was obtained between the exponents for the correctly normalized AC susceptibility data and those for the modulation data.

Plots of $\log\left(\frac{v}{v_0} - 1\right)$ versus $\log \epsilon$ and $\log \{\text{modulation signal}\}$ versus $\log \epsilon$ are shown in Fig.47. In practice, evaluations have been carried out by computer least-squares fit analyses of the respective logarithms. For each choice of T_c, v_0 was varied to give the best straight line fit of $\log\left(\frac{v}{v_0} - 1\right)$ versus $\log \epsilon$. Calculated exponents for both the techniques were plotted against T_c as shown in Fig. 48. The value of v_0 required for the best straight line of $\log\left(\frac{v}{v_0} - 1\right)$ versus $\log \epsilon$ increases with decreasing T_c; an increase in v_0 and a decrease in T_c both lead to an increase in the exponent evaluated for those parameters. Thus, if the chosen T_c is above the Curie point, γ evaluated from the carrier signal data will be less than that for the modulation data. The opposite will be true if the chosen T_c is above the Curie point. The point of intersection of the two plots is taken for the correct values of T_c and γ.

FIGURE 47(a)
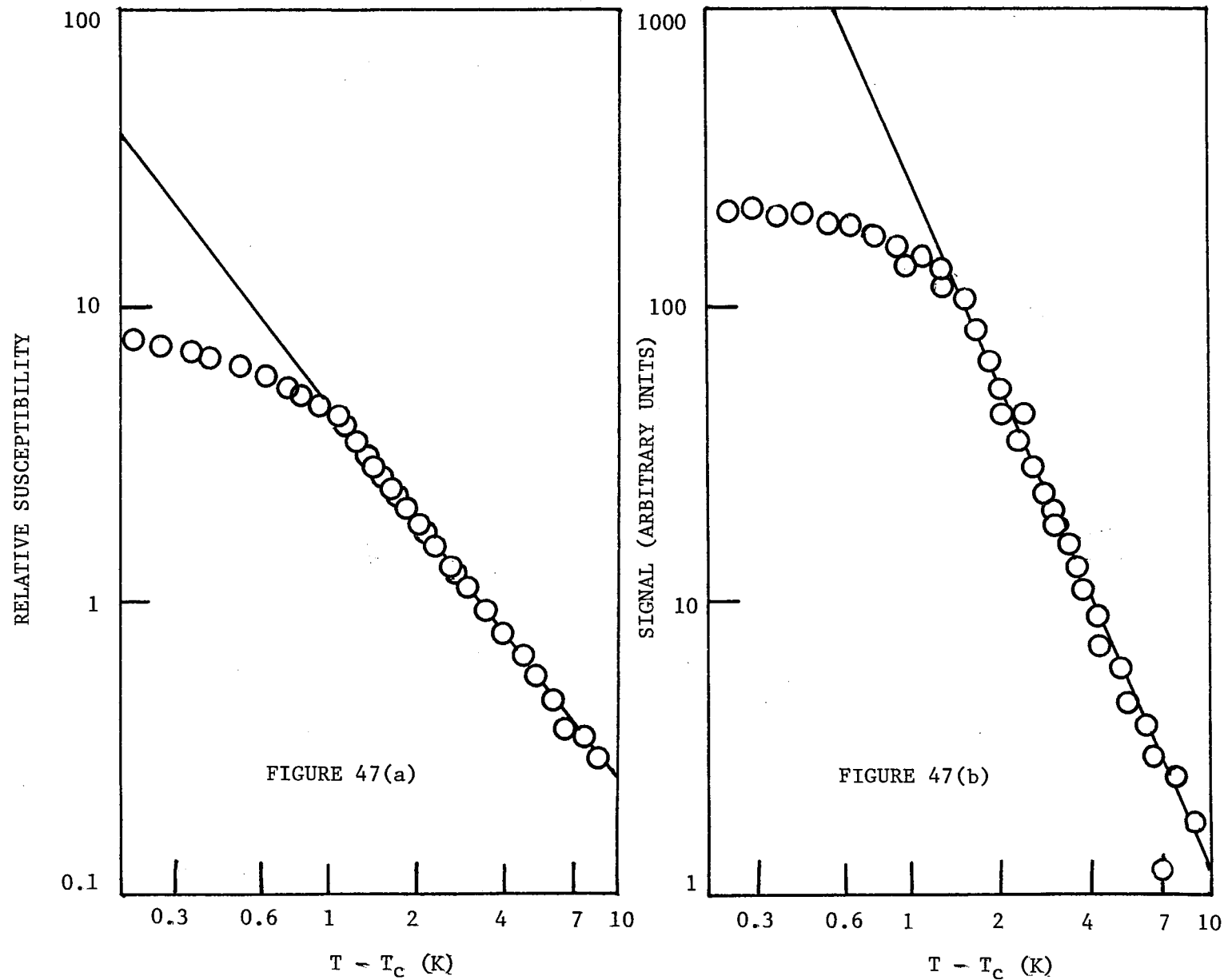
FIGURE 47(b)

FIGURE 47: CRITICAL EXPONENT ANALYSES. (a) SUSCEPTIBILITY FROM AC $\chi(T)$. (b) AC FIELD, TEMPERATURE
MODULATION SIGNAL. RMS AC FIELD 1.5 A/m. AC FIELD FREQUENCY 1000 Hz. MODULATION AMPLITUDE
0.5 mK. MODULATION FREQUENCY 2 Hz.
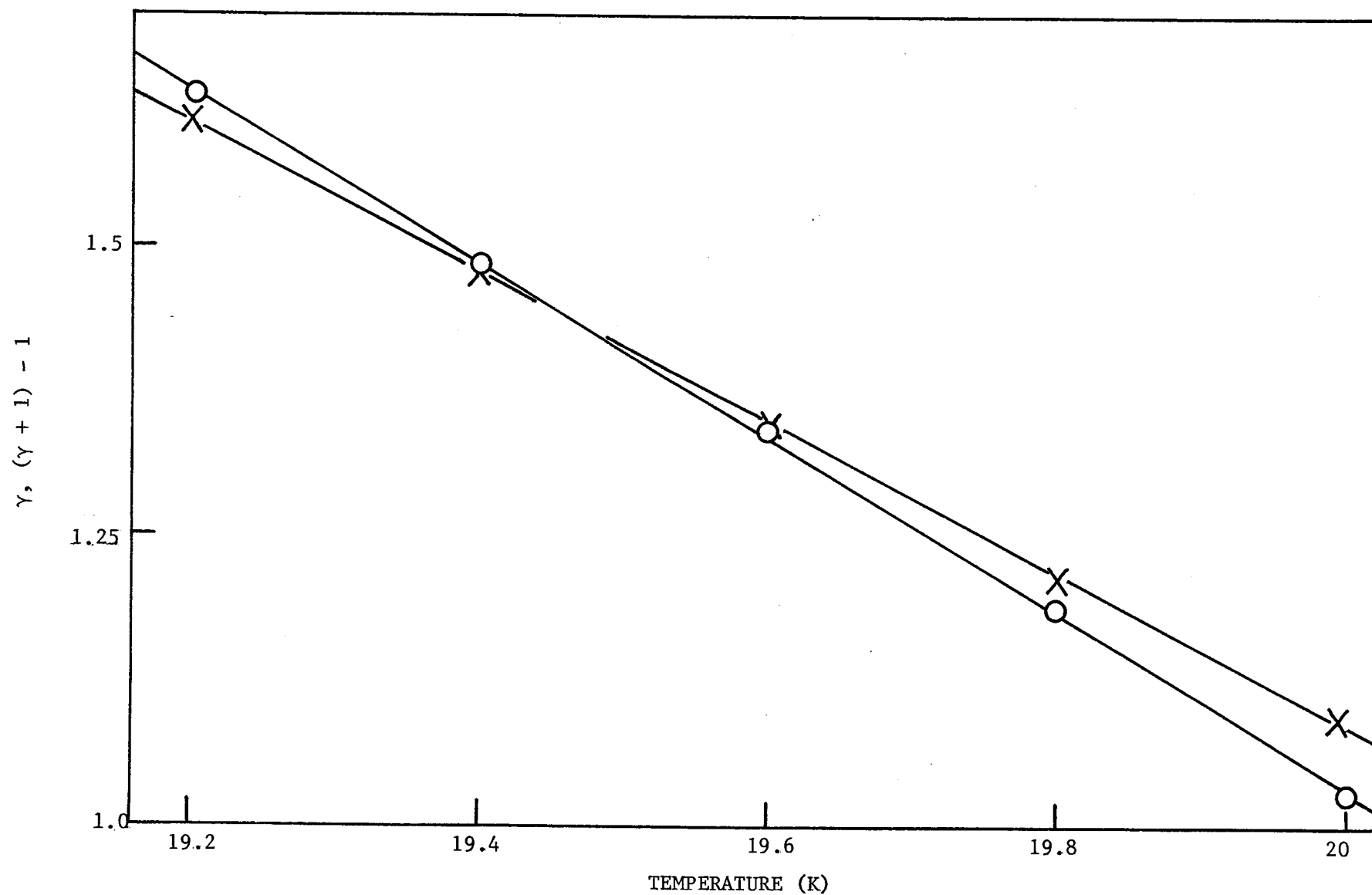
FIGURE 48: DEPENDENCES OF THE EVALUATED EXPONENTS ON THE CHOICE OF CURIE TEMPERATURE. O SUSCEPTIBILITY MEASUREMENTS. X AC FIELD, TEMPERATURE MODULATION MEASUREMENTS. RMS AC FIELD 1.5 A/m. DC FIELD FREQUENCY 1000 Hz. MODULATION AMPLITUDE 0.5 mK. MODULATION FREQUENCY 2 Hz.

Values obtained by this technique from a variety of AC field amplitudes and modulation amplitudes are given in Table 1. The field frequency was 1 KHz and the modulation frequency was 2 Hz. The values of v_O shown represent the values of the normalizing voltage used for each experiment multiplied by the ratio of 1.5 A/m to the amplitude of the AC field amplitude employed. Tables 2 and 3 show a breakdown of the results in terms of field amplitude and modulation amplitude respectively.

EXPERIMENTAL CONDITIONS		$T_c (K)$	γ	$v_O (mV)$ (relative to v_O for 1.5 A/m)
RMS AC FIELD AMPLITUDE (A/m)	TEMPERATURE MODULATION AMPLITUDE (mK)			
1.5	0.5	292.6	1.43	0.18
1.5	2	292.4	1.34	0.17
1.5	8	292.6	1.41	0.18
3.8	0.5	293.0	1.29	0.19
3.8	2	292.8	1.40	0.18
3.8	8	292.5	1.51	0.20
7.5	2	293.0	1.34	0.20
7.5	8	293.1	1.23	0.18

TABLE 1 Summary of results for a field frequency of

1 KHz and a modulation frequency of 2 Hz.

RMS AC FIELD AMPLITUDE (A/m)	$T_c(K)$	γ
1.5	292.5 ± 0.2	1.39 ± 0.05
3.8	292.8 ± 0.2	1.40 ± 0.05
7.5	293.0 ± 0.2	1.29 ± 0.05

TABLE 2   Breakdown of the results in Table 1 to

show field dependence.

TEMPERATURE MODULATION AMPLITUDE (mK)	$T_c(K)$	γ
0.5	292.8 ± 0.2	1.36 ± 0.05
2	292.7 ± 0.2	1.36 ± 0.05
8	292.8 ± 0.2	1.38 ± 0.07

TABLE 3   Breakdown of the results in Table 1 to

show dependence on temperature modulation

amplitude.

The exponent evaluations have been carried out in the range

of temperature extending from approximately 301 K to 294 K ie,

from $\varepsilon \simeq 2.8 \times 10^{-2}$ to 4.1×10^{-3}. Graham's (1965) data

extended to $\varepsilon \simeq 6 \times 10^{-2}$; we have seen no evidence to suggest

departure from the exponent law at least up to $\varepsilon \simeq 5.5 \times 10^{-2}$.

Field frequency effects have been investigated in Chapter 6 and are thought to be negligible in this region of temperature for field frequencies $\leq$ 1 KHz. Modulation frequency properties have also been researched, and in the absence of domain relaxation effects, they seem to have little influence on the determinations other than through the modulation amplitude.

The evaluated T_c may increase with increased AC field amplitude, but there seems to be no systematic dependence of γ on field amplitude. It appears that for the modulation amplitudes used, there is no significant effect of different modulation amplitudes on the determinations of either T_c or γ.

The overall result for γ is 1.37 ± 0.05 and, in the absence of any significant dependence of T_c on field amplitude, T_c = 292.8 ± 0.2K. The approximation for the three-dimensional Hiesenberg model gives, as stated in Chapter 3, γ = 1.43 ± 0.04 for spin $S = \frac{1}{2}$, and 1.33 ± 0.01 for an infinite spin model ($S = 7/2$ for Gd). With regard to experimental determinations, we may recall Graham's (1965) determinations of γ = 1.3 ± 0.1 with T_c = 292.5 ± 0.5K. These were obtained from measurements using a fluxmeter in fields down to ~ 4 x 10^4 A/m; T_c was obtained from the temperature for which plots of M^2 versus $\frac{H}{M}$ passed through the origin. For each temperature, $\frac{1}{\chi_0}$ was determined from the horizontal intercept of such a plot. The method thus involves field extrapolation procedures and relies on the use of an independently-chosen T_c for the exponent evaluation. Further our thermocouples were in electrical contact with the sample in contrast to Graham's measurements, and we have been able to reduce the uncertainty in the measurement of T_c.

The value of T_c = 292.8 ± 0.2K is below the peaks in the

low-field AC modulation signal given in Chapter 6, but in good

agreement with the positions of the high AC field peaks, the DC

modulation peaks, and the second harmonic peaks. A full

description of the expected influence of domain properties on the

position of the peak in low AC fields is given in Chapter 6. This

value of T_c is not in agreement with that determined from the

measurement of the temperature dependence of modulation amplitude.

Since there is no equivalent of the carrier signal

involved in the DC modulation technique, it cannot be employed in

conjunction with this method of critical exponent analysis.

However, comparable values of γ are obtained from the two modulation

techniques if the same value of T_c is used. Using T_c = 292.8 K, the

value of γ obtained from the AC modulation technique is 1.30 ± 0.05

while that from the DC modulation technique is 1.25 ± 0.07. Once

again, it is argued that the method of choosing an independent T_c

is not reliable because of the interdependence of T_c and γ shown

in Fig. 48.

CHAPTER   8

CONCLUSION

8.1   Domain Properties

The results of this research indicate the existence of a
unique domain mobility factor g associated with the low field
reversible domain wall translation processes in polycrystalline
gadolinium. Thermal relaxation properties have been seen in the
low-field AC susceptibility; these have been attributed to effects
on the contribution of the magnetic after-effect to g, where domains
are nucleating. Similarly the thermal hysteresis observed in the
low-field AC susceptibility measurements is thought to be due to the
different character of this contribution between warming and cooling
cycles.

Since g is associated with reversible domain wall translation,
its properties will be anisotropic. For a single crystal sample
aligned with its easy axis of magnetization along the field direction,
one might expect that the low-field susceptibility would be little
different from the high field susceptibility for all temperatures.
Presumably then, the relaxation and thermal hysteresis properties
observed for the polycrystalline sample in low fields might not be
significant in such a single crystal. Conversely, these effects
could be far more significant in single crystal samples aligned with
the field direction along the basal plane.

Domains have been seen here to nucleate at about 294K. This
is clearly above the temperature at which dM/dT is a maximum. The
question remains regarding the correct criteria for the definition
of the Curie point. The most consistent value of T_c obtained from

this research seems to be in the vicinity of 292.8K; this value

was obtained from the critical exponent evaluations of Chapter 7,

and is consistent with values obtained from the DC modulation

technique, the high-field AC modulation technique, and the AC second

harmonic technique. Accepting this, one can see that domains exist

in a finite field above T_c. Darnell and Cloud (1964) have asserted

the existence of a zero-field magnetization for temperatures up to

~ 305K, although Graham (1965) saw no evidence of this. On the

basis of our results, it is feasible that intrinsic order exists

up to ~ 294K.

Above this temperature, however, our measurements indicate

that there is no zero-field magnetization. For all regions of

temperature we have observed field-independent susceptibility for

fields $\lesssim$ 8 A/m, indicating that there is no <u>net</u> magnetization in

zero field. In the presence of domains, zero net magnetization is

not indicative of any lack of intrinsic magnetic order within each

domain; however, where no domains are present, zero net magnetiz-

ation in a sample results from the absence of intrinsic order : ie,

the sample is paramagnetic.

Further research is being carried out on the transient-field

enhancement of the AC susceptibility via magnetic after-effects

reported at the conclusion of Chapter 6. While we seem to have

characterised it well experimentally, gaps still exist in our

theoretical explanation of it. It is hoped to publish a full account

of it in the near future.

8.2   Temperature Modulation Techniques

The temperature modulation techniques will find ready

application when studying any quantity which varies rapidly with

temperature. This is particularly so when the quantity itself is
small. Thus we have seen here that while the susceptibility of a
ferromagnet is relatively small in the vicinity of its Curie
temperature adding difficulty to bulk magnetization methods of
measurement, the modulation techniques are most sensitive here due
to the rapid variation of the susceptibility with temperature.

To some extent this general principle might not appear to
have been followed in the research presented here, since a large
portion of our results have been obtained using the conventional AC
inductance technique. However, most of the phenomena discussed in
this thesis were first discovered via the modulation techniques.
Having seen these manifestations, it behoved us to attempt to explain
them via the more conventional technique; given the sensitivity of
our equipment we were able to do this once we knew what effects could
be expected, and, since the results of the conventional technique are
less difficult to interpret, this seems the logical method of research.
More importantly, since the AC modulation technique is new, it is in
need of fundamental reinforcement. The results from the AC suscept-
ibility technique and the temperature modulation techniques have
corresponded, and have demonstrated the validity of the theory given
in Chapter 4.

Thus the satellite structure seen in the temperature
dependence of the modulation data was associated with the structure
later found in the low field AC $\chi(T)$ curves. Yet, the modulation
curves were not the true derivatives of the $\chi(T)$ curves; this, plus
the phase lead seen in the phase dependence of the AC modulation
phase led us to a search for thermal relaxation effects in $\chi(T)$.
The thermal hysteresis properties in low AC fields were first seen in

the AC modulation data, and the new magnetic after-effect

discussed in the concluding section of Chapter 6 was discovered

as a result of anomalous behaviour in the AC modulation data

under circumstances outlined in that section.

In the majority of our modulation studies we have used an

electric current heater without DC offset so that the sample was

modulated at twice the frequency of the current waveform. Phase-

sensitive detection at ω_T has the advantage of rejecting direct

inductance noise at $\omega_T/2$.

More importantly however, AC modulation techniques should

result in better signal-to-noise ratios than DC methods. As pointed

out in Chapter 4, the modulation amplitude in our case was enhanced

by a factor $\sim \dfrac{\omega_C}{\omega_T}$, but in general the technique affords the use of

AC amplifiers in the detection process rather than DC amplifiers.

Thus for example, one could study a resistance discontinuity at a

phase transition by passing a constant current through a sample,

modulating the temperature, and detecting the modulation of the

voltage across the sample; it would be more advantageous to use a

constant amplitude AC current for the constant sample current than

a DC current, and make the frequency of the AC current much greater

than that of the modulation (R. Street, private communication 1975).

Because of the domain properties we have seen in polycrystall-

ine Gd, our original aim of simultaneously measuring specific heat

and susceptibility has not been realized. In principle, however, the

modulation techniques provide a means of doing this, and may prove

successful under circumstances where the effects of domains are not

as significant as we have seen here.

The following idea is due to Professor G.V.H. Wilson. At

temperatures of the order of mK when the Boltzmann energy $\sim kT$ is

of the same order of magnitude as the energy of interaction between
the magnetic moment of the nucleus and the field acting on the
nucleus, the magnetic contribution from the nuclei will add to the
otherwise saturated magnetization curve from the electrons. In
principle, this small transition which has not been seen directly
by bulk techniques, could be detected using the thermal modulation
techniques. It can, at present, be detected for a limited number
of nuclei by microscopic techniques such as nuclear orientation,
Mössbauer and nmr techniques, but in principle the only nuclei
which could not be studied by the modulation techniques would be
those with zero magnetic moments. Note that at these low temper-
atures the electronic contribution to the modulation signal would
be negligible as only the nuclear magnetization would exhibit any
significant temperature dependence.

8.3 Critical Exponent Evaluation

In terms of experimental method, the combination of the
conventional AC susceptibility technique and the AC temperature
modulation technique represents the culmination of this research.
It has found ready application in the measurement of γ presented
in Chapter 7. No independent determination of the Curie temperature
is necessary; the two techniques provide the two indpendent criteria
for the simultaneous determination of T_c and γ. The value of
$\gamma = 1.37 \pm 0.05$ for Gd conforms well to the three-dimensional
approximation to the Heisenberg model for a ferromagnet as has been
shown in Chapter 7. Further work is being carried out to confirm
this result using other techniques of analysis. It is intended also
to apply these modulation techniques to the study of other magnetic
transitions and other materials including single crystals.

REFERENCES

Aharoni, A., Rev.Mod.Phys., 34, 227 (1962).

Alstad, J. and Legvold, S., J.Appl.Phys., 35, 1752 (1964).

Andrews, T., Phil.Trans.R.Soc., 159, 575 (1869).

Arajs, S. and Colvin, R.V., J.Appl.Phys., 32, 3368 (1961).

Arpaci, V.S., Conduction Heat Transfer, Addison-Wesley, U.S.A. (1966).

Arrott, A. and Noakes, J.E., Phys.Rev.Lett., 19, 786 (1967).

Banister, J.R., Legvold, S. and Spedding, F.H., Phys.Rev., 94,
        1140 (1954).

Barbara, B., Fillion, G., Gignoux, D. and Lemaire, R.,
        Sol.Stat.Comm., 10, 1149 (1972).

Barber, N., The Renormalization Group and Critical Phenomena -
        An Introduction, Australian National University (1973).

Barson, F., Legvold, S. and Spedding, F.H., Phys.Rev., 105, 418 (1957).

Bates, L.F. and Pacey, A.J., Proc.Phys.Soc., 78, 878 (1961).

Bates, L.F., Modern Magnetism, 4th ed., Cambridge University Press (1963).

Becker, R., Phys.Zeits., 33, 905 (1932).

Belov, K.P., Levitin, R.Z., Nikitin, S.A. and Ped'ko, A.V.
        J.Exptl.Theoret.Phys.(U.S.S.R.), 40, 1562 (1961).
        [Engl. Trans. - Sov.Phys. - JETP, 13, 1096 (1961)].

Belov, K.P. and Ped'ko, A.V., J.Exptl.Theoret.Phys. (U.S.S.R.),
        42, 87 (1962) [Engl. Trans. - Sov.Phys. - JETP, 15,
        62 (1962)].

Belov, K.P., Proc.Intl.Conf. on Magnetism, Institute of Physics and
        The Physical Society, London (1965) p.266.

Birss, R.R. and Wallis, P.M., Proc.Intl.Conf. on Magnetism, Institute
        of Physics and The Physical Society, London (1965) p.266.

Bloch, F., Zeit.für Phys., 74, 295 (1932).

Bolton, H.C., The Australian Physicist, Sept.1972, p.136.

Bozorth, R.M., Bell System Tech.J., 19, 1 (1940).

Bozorth, R.M., Ferromagnetism, D.Van Nostrand, Princeton (1951).

Bozorth, R.M. and Wakiyama, T., J.Phys.Soc. Japan, 17, 1669 (1962).

Bozorth, R.M. and Wakiyama, T., J.Phys.Soc. Japan, 18, 97 (1963).

Brown, W.F., Rev.Mod.Phys., 17, 15 (1945).

Brown, W.F., Phys.Rev., 105, 1479 (1957).

Cable, J.W. and Wollan, E.O., Phys.Rev., 165, 733 (1968).

Callen, E.R. and Callen, H.B., Phys.Rev., 129, 578 (1963).

Callen, E.R. and Callen, H.B., Phys.Rev., 139, A455 (1965).

Callen, E.R., J.Appl.Phys., 39, 519 (1968).

Carey, R. and Isaac, E.D., Magnetic Domains and Techniques for
        Their Observation, English Universities Press, London
        (1966).

Casimir, H.B.G., Magnetism and Very Low Temperatures, Cambridge,
        New York (1940).

Chaplin, D.H., Sydney, K.R. and Wilson, G.V.H., Phys.Lett., 46A,
        55 (1973). (Included after this thesis.)

Chikazumi, S., Physics of Magnetism, Wiley, New Work (1964).

Chynoweth, A.G., J.Appl.Phys., 29, 563 (1958).

Cooper, B.R., Phys.Rev.Letters, 19, 900 (1967).

Cooper, B.R., Solid State Phys., 21, 393 (1969).

Cooper, B.R. in Magnetic Properties of Rare Earth Metals, (R.J. Elliot
        ed.), Plenum, London (1972).

Coopersmith, M.H., Phys.Rev., 167, 478 (1968).

Corner, W.D., Roe, W.C. and Taylor, K.N.R., Proc.Phys Soc., (London),
        80, 927 (1962).

Craik, D.J. and Tebble, R.S., Rep.Prog.Phys., 24, 116 (1961).

Darby, M.I. and Taylor, K.N.R., Proc.Intl.Conf. on Magnetism,
        Institute of Physics and The Physical Society, London
        (1965) p.742.

Darnell, F.J. and Cloud, W.H., J.Appl.Phys., 35, 935 (1964).

Dillon, J.F., in Magnetism, Vol.III, (G.T. Rado and H. Suhl, eds.),
        Academic Press, New York (1963).

Dimmock, J.O. and Freeman, A.J., Phys.Rev.Lett., 13, 750 (1964).

Dimmock, J.O., Freeman, A.J. and Watson, R.E., J.Appl.Phys., 36,
        1142 (1965).

Domb, C. and Hunter, D.L., Proc.Phys.Soc., (London), 86, 1147 (1965).

Egami, T., Phys.Stat.Sol.b, 57, 211 (1973a).

Egami, T., Phys.Stat.Sol.a, 20, 157 (1973b).

Eisberg, R.M., Fundamentals of Modern Physics, Wiley, New York
        (1961).

Elliot, R.J., in Magnetism, Vol.III, (G.T. Rado and H. Suhl, eds.),
        Academic Press, New York (1963).

Elliot, R.J., in Magnetic Properties of Rare Earth Metals,
        (R.J. Elliot, ed.), Plenum, London (1972).

Enz, V., Physica, 26, 698 (1960).

Evenson, W.E. and Lui, S.H., Phys.Rev., 178, 783 (1969).

Fisher, M.E., Rep.Prog.Phys., 30, 615 (1967).

Fixman, M., J.Chem.Phys., 36, 310 (1962).

Foner, S., Rev.Sci.Instrum., 27, 548 (1956).

Freeman, A.J., Dimmock, J.O. and Watson, R.E., Phys.Rev.Lett., 16,
        94 (1966).

Freeman, A.J. in Magnetic Properties of Rare Earth Metals,
        (R.J. Elliot, ed.), Plenum, London (1972).

Frei, E.H., Shtrikman, S. and Treves, D., Phys.Rev., 106, 45 (1957).

Gerstein, B.C. and Olander, F., J.Appl.Phys., 42, 3438 (1971).

Gilbert, T., Phys.Rev., 100, 1243 (1955).

Goodenough, J.B., Phys.Rev., 95, 917 (1954).

Graham, C.D., J.Phys.Soc. Japan, 17, 1310 (1962).

Graham, C.D., J.Appl.Phys., 34, 1341 (1963).

Graham, C.D., J.Appl.Phys., 38, 1375 (1967).

Griffel, M., Skochdopole, R.E. and Spedding, F.H., Phys.Rev., 93,
        657 (1954).

Griffiths, R.B., Phys.Rev.Lett., 14, 623 (1965a).

Griffiths, R.B., J.Chem.Phys., 43, 1958 (1965b).

Handbook of Mathematical Functions with Formulas, Graphs and
        Mathematical Tables, U.S. Department of Commerce,
        National Bureau of Standards Applied Mathematics Series
        55, p.380.

Hegland, D.E., Legvold, S. and Spedding, F.H., Phys.Rev., 131,
        158 (1963).

Heller, P., Rep.Prog.Phys., 30, 731 (1967).

Ho, J.T. and Litster, J.D., Phys.Rev.Lett., 22, 603 (1969).

Hunter, J., Ph.D. Thesis, Durham University (1973).

Ising, E., Z.Phys., 31, 253 (1925).

Jelinek, F.J., Hill, E.D. and Gerstein, B.C., J.Phys.Chem.Solids, 26, 1475 (1965).

Jordan, H., El.Nachr.Techn., 1, 27 (1924).

Kadanoff, L.P., Götze, W., Hamblen, D., Hecht, R., Lewis, E.A.S., Palciauskas, V.V., Rayl, M., Swift, J., Aspnes, D. and Kane, J., Rev.Mod.Phys., 39, 395 (1967).

Kasuya, T., Progr.Theoret.Phys. (Japan), 16, 45 (1956).

Kasuya, T., in Magnetism, Vol.IIB, (G.T. Rado and H. Suhl, eds.), Academic Press, New York (1966).

Kernsten, M., Phys.Zeits., 39, 860 (1938).

Kernsten, M., Grundlagen einer Theorie der Ferromagnetischen Hysterese und der Koerzitivkraft, Hirzel, Lipzig (1943).

Kernsten, M., Z.Agnew.Phys., 7, 313 (1956a).

Kernsten, M., Z.Agnew.Phys., 8, 382 (1956b).

Kernsten, M., Z.Agnew.Phys., 8, 496 (1956c).

Kittel, C. and Galt, J.K., Solid State Phys., 3, 437 (1956).

Kittel, C., Introduction to Solid State Physics, 3rd ed., Wiley, New York (1966) p.436.

Koehler, W.C., Child, H.R., Nicklow, R.M., Smith, H.G., Moon, R.M. and Cable, J.W., Phys.Rev.Lett., 24, 16 (1970).

Koehler, W.C., in Magnetic Properties of Rare Earth Metals, (R.J. Elliot, ed.), Plenum, London (1972).

Kouvel, J.S. and Rodbell, D.S., Phys.Rev.Lett., 18, 215 (1967).

Kouvel, J.S. and Comly, J.B., Phys.Rev.Lett., 20, 1237 (1968).

Kuchin, V.M., Semenkov, V.A., Shil'shtein, S.Sh. and Patrikeev, Yu.B., J.Exptl.Theoret.Phys. (U.S.S.R.), 55, 1241 (1968). [Engl.Trans. - Sov.Phys. - JETP, 28, 649 (1969)].

Landau, L.D., Phys.Z.Sowjun, 11, 26 (1937a).

Landau, L.D., J.Exptl.Theoret.Phys. (U.S.S.R.), 7, 19 (1937b).

Landau, L.D., Phys.Z.Sowjun, 11, 545 (1937c).

Landau, L.D., J.Expt.Theoret.Phys. (U.S.S.R.), 7, 627 (1937d).

Landau, L.D. and Lifshitz, E.M., Electrodynamics of Continuous Media, Permagon Press, Oxford (1960).

Landau, L.D. and Lifshitz, E.M., Statistical Physics, 2nd ed., Permagon Press, Oxford (1969).

Legvold, S., in Magnetic Properties of Rare Earth Metals, (R.J. Elliot, ed.), Plenum, London (1972).

Levy, R.A., Principles of Solid State Physics, Academic Press, New York and London (1968).

Lifshitz, E., J.Phys.U.S.S.R., 8, 337 (1944).

Loucks, T.L., Phys.Rev., 137, A1333 (1965).

Lounasmaa, O.V. and Sundström, L.J., Phys.Rev., 150, 399 (1966).

Lounasmaa, O.V. and Sundström, L.J., Phys.Rev., 158, 591 (1967).

Mackintosh, A.R. and Møller, H.B., in Magnetic Properties of Rare Earth Metals, (R.J. Elliot, ed.), Plenum, London (1972).

Mason, W.P., Phys.Rev., 96, 302 (1954).

Mattheiss, L.F., Phys.Rev., 133, A1399 (1964).

Milstein, F. and Robinson, L.B., Phys.Rev., 177, 904 (1969).

Néel, L., Cahiers de Phys., 12, 1 (1942).

Néel, L., Cahiers de Phys., 13, 18 (1943).

Néel, L., J.Phys.Radium, 5, 241 (1944a).

Néel, L., J.Phys.Radium, 5, 265 (1944b).

Néel, L., Cahiers de Phys., 25, 1 (1944c).

Néel, L., Ann.Géophys., 5, 99 (1949).

Néel, L., J.Phys.Radium, 13, 249 (1952).

Nellis, W.J. and Legvold, S., J.Appl.Phys., 40, 2267 (1969a).

Nellis, W.J. and Legvold, S., Phys.Rev., 180, 581 (1969b).

Nesbitt, E.A. and Wernick, J.H., Rare Earth Permanent Magnets, Academic Press, New York (1973).

Nigh, H.E., Legvold, S. and Spedding, F.H., Phys.Rev., 132, 1092 (1963).

Noakes, J.E., Tornberg, N. and Arrott, A., J.Appl.Phys., 37, 1264 (1966).

Onsager, L., Phys.Rev., 65, 117 (1944).

Patrick, L., Phys.Rev., 93, 384 (1954).

Preisach, F., Z.Physik., 94, 277 (1935).

Rayleigh, Lord, Phil.Mag., 23, 225 (1887).

Rhyne, J.J., in Magnetic Properties of Rare Earth Metals,
          (R.J. Elliot, ed.), Plenum, London (1972).

Robinson, L.B., Milstein, F. and Jayarama, A., Phys.Rev., 134,
          A187 (1964).

Ruderman, M.A. and Kittel, C., Phys.Rev., 96, 99 (1954).

Rushbrooke, G.S., J.Chem.Phys., 39, 842 (1963).

Russell, A.M. and Torchia, D.A., Rev.Sci.Instr., 33, 442 (1962).

Smith, H.G., Moon, R.M. and Cable, J.W., Phys.Rev.Lett., 24, 16 (1970).

Snoek, J.L., New Developments in Ferromagnetic Materials,
          Elsevier, Amsterdam (1949).

Spedding, F.H. and Daane, A.H., J.Am.Chem.Soc., 74, 2783 (1952).

Stanley, H.E., Introduction to Phase Transitions and Critical
          Phenomena, Clarendon Press, Oxford (1971).

Street, R. and Woolley, J.C., Proc.Phys.Soc. (London), A62, 562 (1949).

Sydney, K.R., Wilson, G.V.H., Chaplin, D.H. and McKenna, T.J.,
          J.Phys.F., 4, L98 (1974).

Sydney, K.R., Chaplin, D.H. and Wilson, G.V.H., J.Phys.F.,
          to be published (1975a). (Included after this thesis).

Sydney, K.R., Chaplin, D.H. and Wilson, G.V.H., J.Phys.F.,
          to be published (1975b). (Included after this thesis.)

Taylor, K.N.R., Phys.Lett., 35A, 153 (1971).

Taylor, K.N.R. and Darby, M.I., Physics of Rare Earth Solids,
          Chapman and Hall, U.K. (1972).

Taylor, K.N.R., Melville, D. and Primavesi, G.J., J.Phys.F., 2,
          584 (1972).

Tebble, R.S. and Craik, D.J., Magnetic Materials, Wiley and Sons,
          London (1969).

Tsuya, N., Clark, A.E. and Bozorth, R.M., Proc.Intl.Conf. on Magnetism,
          Institute of Physics and The Physical Society, London
          (1965) p.250.

144.

Unsworth, P.J., J.Phys.B., 2, 122 (1969).

van der Waals, J.D., Ph.D. Thesis, University of Leiden (1873).

Walser, R.M., Benê, R.W. and Caruthers, R.E., I.E.E.E. Transactions
on Electron Devices, ED-18, 309 (1971).

Watson, R.E., Freeman, A.J. and Dimmock, J.O., Phys.Rev., 167,
497 (1968).

Weiss, P., J.Phys.Radium, Paris 6, 667 (1907).

Weiss, P. and de Freudenreich, J., Arch.Sci. (Geneva), 42, 449 (1916).

Weiss, P. and Forrer, R., Annls.Phys., 5, 153 (1926).

Widom, B., J.Chem.Phys., 43, 3892 (1965a).

Widom, B., J.Chem.Phys., 43, 3898 (1965b).

Will, G., Nathans, R. and Alperin, H.A., J.Appl.Phys., 35, 1045 (1964).

Wilson, G.V.H., J.Appl.Phys., 34, 3276 (1963).

Wilson, G.V.H., Chaplin, D.H. and Sydney, K.R., J.Phys.D.,
to be published (1975).

Wybourne, B.G., in Spectroscopic Properties of Rare Earths, Wiley,
New York, London and Sydney (1965).

Wybourne, B.G., Phys.Rev., 148, 317 (1966).

Yang, C.N. and Lee, T.D., Phys.Rev., 87, 404 (1952).

Yang, C.N. and Lee, T.D., Phys.Rev., 87, 410 (1952)

Yosida, K., Phys.Rev., 106, 893 (1957).

Zijlstra, H., I.E.E.E. Transactions on Magnetization, 6, 179 (1970).

Zijlstra, H. and van den Broek, J.J., I.E.E.E. Transactions on
Magnetization, 7, 226 (1971).

LIST OF PUBLICATIONS

PUBLISHED

1.   "Studies of Ferromagnetic Critical Phenomena by Temperature
        Modulation Techniques", D.H. Chaplin, K.R. Sydney and
        G.V.H. Wilson, Phys.Letters, 46A, 55 (1973).

2.   "Effects of Magnetic Domains on the Susceptibility of
        Gadolinium Near the Curie Temperature", K.R. Sydney,
        G.V.H. Wilson, D.H. Chaplin and T.J. McKenna, J.Phys.F.,
        4, L98 (1974).

ACCEPTED FOR PUBLICATION IN J.PHYS.D.

3.   "Theory of Temperature Modulation Studies of Ferromagnetic
        Materials", G.V.H. Wilson, D.H. Chaplin and K.R. Sydney.

TO BE SUBMITTED TO J.PHYS.F.

4.   "Susceptibility Studies of Gadolinium Near the Curie Point",
        K.R. Sydney, D.H. Chaplin and G.V.H. Wilson.

5.   "Thermal Modulation Studies of Gadolinium Near the Curie
        Point", K.R. Sydney, D.H. Chaplin and G.V.H. Wilson.

UNDER PREPARATION

6.   "Observation of Enhancement of Low Field Initial Susceptibility
        by a Magnetic After-Effect", G. Wantenaar, K.R. Sydney,
        D.H. Chaplin and G.V.H. Wilson.

7.   "Determination of the Critical Exponent for Gadolinium
        Above the Curie Point", K.R. Sydney, G. Wantenaar, D.H. Chaplin
        and G.V.H. Wilson.

PUBLISHED PAPERS

STUDIES OF FERROMAGNETIC CRITICAL PHENOMENA
BY TEMPERATURE MODULATION TECHNIQUES

D.H. CHAPLIN, K.R. SYDNEY and G.V.H. WILSON

Department of Physics, Royal Military College, Canberra, Australia.

The application of temperature modulation techniques to determine the temperature dependence of dc magnetisation and ac susceptibility of gadolinium metal near the Curie point is described

We report the application of temperature modulation and phase-sensitive detection to the study of critical phenomena in ferromagnetic metals. Whereas in conventional studies [1–5] of critical phenomena one measures quantities associated with the spontaneous magnetisation σ which is small near the Curie point T_c, the modulation techniques involve the temperature derivative $d\sigma/dT$, so that large signals are observed in the critical region. The experiments yield accurate values of T_c together with accurate and detailed data for the temperature dependences of the dc magnetisation M and the ac susceptibility χ.

So far we have used cylindrical (3.0 mm dia $\times$ 27.4 mm) samples of 99.9% purity gadolinium. An insulated electrical heater is noninductively wound over the sample. A sinusoidal voltage is applied to the heater at a frequency f_m (1.1 to 5 Hz) so that the surface temperature of the sample is modulated at a frequency $2f_m$ with a modulation amplitude ΔT of order a few mK. In the "dc technique" a dc magnetic field is applied along the axis of the sample and the induced voltage, at $2f_m$, in a concentric pick-up coil, is measured using a phase-sensitive detector operating with a second harmonic reference signal. The output signal is proportional to $\Delta T (dM_H/dT)$ where M_H is the sample magnetisation in the applied field H. By slowly varying the ambient temperature, the temperature dependence of the signal is obtained. In the "ac technique" no dc applied field is necessary. The sample, including the temperature modulating heater, is used as the core of a transformer operating at the carrier frequency $f_c \sim 1$ kHz. The signal is here the amplitude modulation at $2f_m$ of the secondary transformer voltage. A constant current generator provides the primary voltage and, by varying the ambient temperature, the temperature
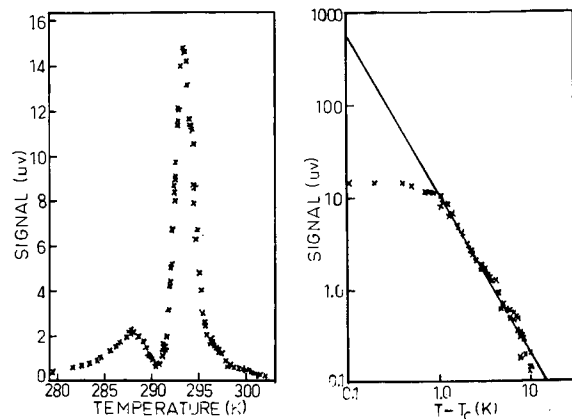
Fig. 1a. Temperature dependence of the signal using ac technique. b. Logarithmic plot for $T > T_c$.

dependence of $(d\chi/dT)$, where χ is the susceptibility of the sample at the carrier frequency, may be deduced. Relative advantages of the ac technique are enhancement of the signal by $\sim f_c/f_m$ and also any additive spurious pick-up signals at $2f_m$ can easily be filtered from the amplitude modulated secondary waveform. While ac susceptibility is not as fundamental (in terms of understanding critical phenomena) as is dc magnetisation, both have been measured in other (conventional) studies [1–5], so that a further advantage of the modulation technique is that it permits a careful comparison of the two quantities and of their relationship to the critical behaviour of the spontaneous order parameter.

Both ac and dc techniques have been applied to the cylindrical samples of gadolinium. A typical curve of signal versus temperature for the ac technique is shown in fig. 1a. For small applied fields (0.5 mT to

10 mT) the dc curves were broadened. Both ac and low field dc techniques yielded a strong peak at 293.1 ± 0.3 K. This corresponds to the point of inflextion in the $\sigma(T)$ curve, and agrees well with earlier values [4—6] for the Curie point of gadolinium. A careful study of the effects of the experimental parameters on the ac $S(T)$ curves has been made. The form of these curves is not significantly affected by varying f_c from 500 to 2.5 kHz, f_m from 1.1 to 5 Hz, ΔT from 0.5 to 18 mK, and the carrier amplitude over a wide range. The temperature dependence of the signal phase was more complex than that expected from the known specific heat anomaly for gadolinium near the Curie point [6].

In fig. 1b a logarithmic plot of the data for $T > T_c$ is given. Analysis of the data from the many ac and dc experiments performed yielded consistent critical exponents of 1.75 ± 0.1 for $T > T_c$ (both techniques) 1.75 ± 0.2 for $T < T_c$ (ac) and 1.04 ± 0.15 for $T < T_c$ (dc). As the present experiments involve the derivative $(d\sigma/dT)$, one is tempted to conclude that the resulting critical exponents are 0.75 ± 0.1 for the susceptibility $(T > T_c)$ and 2.75 ± 0.2 or 2.04 ± 0.15 for $T < T_c$.

However, further work is in progress to relate the exponents observed in these experiments to those for the spontaneous order parameter. In particular the experiments are being extended to toroidal samples to eliminate the effects of demagnetising fields, and to cylindrical foils to eliminate complications from the effects of the thermal and electromagnetic skin depths.

References

[1] F.J. Darnell and W.H. Cloud, J. Appl. Phys. 35 (1964) 935.
[2] C.D. Graham, Jr., J. Appl. Phys. 34 (1963) 1341.
[3] F. Milstein and L.B. Robinson, Phys. Rev. 177 (1969) 904.
[4] L.B. Robinson, F. Milstein and A. Jayaraman, Phys. Rev. 134 (1964) A187.
[5] H.E. Nigh, S. Legvold and F.H. Spedding, Phys. Rev. 132 (1963) 1092.
[6] M. Griffel, R.E. Skochdopole and F.H. Spedding, Phys. Rev. 93 (1953) 657.

LETTER TO THE EDITOR

Effects of magnetic domains on the susceptibility of gadolinium near the Curie temperature

K R Sydney, G V H Wilson, D H Chaplin and T J McKenna

Department of Physics, Royal Military College, Canberra, Australia

Abstract. The temperature dependence of the AC susceptibility and the coercive field of gadolinium has been studied near the Curie temperature.

Recently we reported a new technique involving temperature modulation and phase-sensitive detection to determine the temperature derivatives of the DC magnetization and AC susceptibility (χ) of a ferromagnetic metal near the Curie temperature (Chaplin *et al* 1973). The technique was applied to the study of polycrystalline gadolinium. Always evident in the differential susceptibility curves was a satellite peak corresponding to an inflexion in the $\chi(T)$ curve a few degrees below the Curie point. Variations of the AC field amplitude from 50 to 250 A m^{-1} RMS produced little change in the form of the curves.

In order to determine the origin of the satellite, we have carried out a detailed experimental study of the susceptibility in the vicinity of the Curie point. Conventional AC experiments were performed on a toroidal specimen of gadolinium (Rare Earths Products Ltd, 99·9% pure). This formed the core of a small transformer, the primary of which was connected to a constant-current generator. Gadolinium has often been studied (Milstein and Robinson 1969, Patrick 1954, Robinson *et al* 1964) by such means in investigating pressure-dependent Curie point shifts, but this has always been done at constant and large field amplitudes. A wide range (0·001–850 A m^{-1}) of RMS AC fields was used; magnetic hysteresis curves were also obtained over the same temperature range. Frequencies from 2 Hz to 2 kHz were employed, and in this range, the susceptibility was almost frequency-independent.

Figure 1 illustrates the temperature dependence of the susceptibility normalized with respect to the susceptibility of paramagnetic gadolinium at an arbitrarily chosen high reference temperature. In the high AC field there is little evidence of structure in an essentially monotonically varying $\chi(T)$. At low fields, however, $\chi(T)$ exhibits a peak below the Curie point with a minimum at about 290·5 K. Also at low fields there is a significant difference in $\chi(T)$ obtained over a few degrees below the Curie point, depending on whether the sample was being cooled from above or warmed from about 10 K below the Curie point. For intermediate fields, corresponding to those used in the earlier temperature modulation experiments (Chaplin *et al* 1973), there was still significant temperature hysteresis, and $\chi(T)$ exhibited an inflection at a temperature agreeing well with the satellite peak observed in those experiments. While the cooling curves were always highly reproducible, the warming curves showed some rate dependence for warming rates greater than 0·2 K min^{-1}; however, no rate dependence was observed
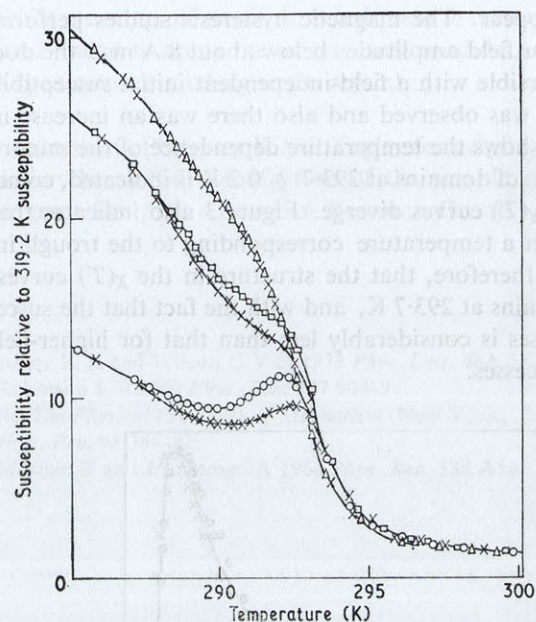
Figure 1. Temperature dependence of the AC susceptibility of gadolinium at 2 kHz for various field amplitudes in the region of the Curie temperature: $\triangle$ cooling in 845 A m^{-1} RMS; $\square$ cooling in 86 A m^{-1} RMS; $\bigcirc$ cooling in 2·8 A m^{-1} RMS; $\times$ corresponding warming curves.
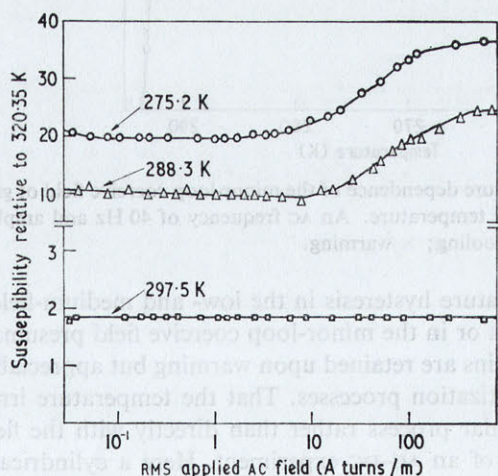
Figure 2. Dependence upon field amplitude of the susceptibility of gadolinium at 2 kHz for various temperatures.

at lower rates, and in one experiment the sample was warmed to 291·4 K, and no time dependence was observed while the temperature was held constant for 2 h. In figure 2 the dependence of χ upon the field amplitude is shown for several temperatures. Above the Curie point, paramagnetism is indicated by the field independence. Below the Curie point, the susceptibility is field-independent for fields below about 8 A m^{-1}, above which it rises significantly. This is also the field at which the structure in the $\chi(T)$ curves

in figure 1 begins to disappear. The magnetic hysteresis studies performed below the Curie point showed that for field amplitudes below about 8 A m⁻¹ the domain magnetization processes were reversible with a field-independent initial susceptibility. At higher fields, magnetic hysteresis was observed and also there was an increase in the slope of the virgin curve. Figure 3 shows the temperature dependence of the minor-loop coercive field. The sudden formation of domains at $293\cdot7 \pm 0\cdot2$ K is indicated, coinciding with the temperature at which the $\chi(T)$ curves diverge. Figure 3 also indicates that the coercive field reaches a maximum at a temperature corresponding to the trough in the low-field $\chi(T)$ curves. It is evident, therefore, that the structure in the $\chi(T)$ curves is associated with the formation of domains at $293\cdot7$ K, and with the fact that the susceptibility from low-field reversible processes is considerably less than that for higher-field irreversible domain magnetization processes.
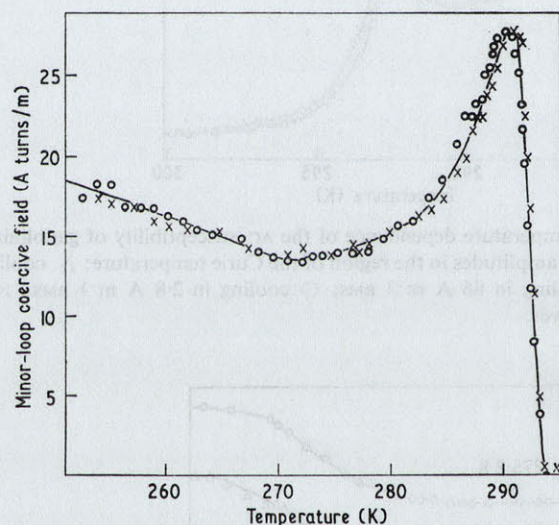
Figure 3. Temperature dependence of the minor-loop coercive field of gadolinium in the region of the Curie temperature. An AC frequency of 40 Hz and amplitude 86 A m⁻¹ RMS was used. ○ cooling; × warming.

The observation of temperature hysteresis in the low- and medium-field $\chi(T)$ curves but not in the high-field curves or in the minor-loop coercive field presumably indicates that some cooling-induced strains are retained upon warming but appreciably affect only the low-field reversible magnetization processes. That the temperature irreversibility is associated with such a particular process rather than directly with the field amplitude used is proved by the results of an AC–DC experiment. Here a cylindrical sample was used with an AC field parallel with its major axis. The low-field AC $\chi(T)$ curves obtained showed the same satellite as for the toroid and were almost unaffected by the presence of a parallel 2400 A m⁻¹ DC field. It is well known that even in the presence of a large DC biasing field the processes responsible for minor AC magnetic hysteresis loops are the same as those in the absence of the DC field (see eg Morrish 1965).

The results show that magnetic domains nucleate at a well defined temperature above which there is well behaved exchange-enhanced paramagnetism. Below this temperature the susceptibility, particularly for low fields, has a complex temperature dependence associated with domain processes. Above this temperature the values of critical exponents

obtained should be meaningful; sensitive techniques are then required. We are continuing these studies, and intend to apply the temperature modulation technique in more detail to a variety of specimens, including single crystals.

References

Chaplin D H, Sydney K R and Wilson G V H 1973 *Phys. Lett.* **46A** 55–6
Milstein F and Robinson L B 1969 *Phys. Rev.* **177** 904–9
Morrish A H 1965 *The Physical Principles of Magnetism* (New York: Wiley) pp 403–4
Patrick L 1954 *Phys. Rev.* **93** 384–92
Robinson L B, Milstein F and Jayaraman A 1964 *Phys. Rev.* **134** A187–92

TO BE PUBLISHED

THEORY OF TEMPERATURE MODULATION STUDIES OF

FERROMAGNETIC MATERIALS

G V H Wilson, D H Chaplin and K R Sydney
Department of Physics, Royal Military College, Canberra
Australia

ABSTRACT: The theory of experiments, in which the temperature

of a ferromagnetic sample is modulated and the voltage induced

in a pick-up coil is phase-sensitive detected, is outlined.

Calculations are made of the effects of magnetic relaxation and

of the thermal skin depth on the signal amplitude and phase.

1.   Introduction

        Recently we reported the application of a new technique

involving temperature modulation and phase-sensitive detection to

determine the temperature derivatives of the DC magnetization M

and AC susceptibility χ of a ferromagnetic metal, gadolinium, near

the Curie temperature (Chaplin et al 1973). The differential

susceptibility curves always exhibited a satellite peak correspond-

ing to an inflection in the $\chi(T)$ curve a few degrees below the

Curie point and, in a further study of the AC susceptibility and

coercive field using conventional techniques (Sydney et al 1974),

it was shown that this satellite peak was associated with the

effects of domain nucleation. A fuller description of the

experimental results for gadolinium is given in two accompanying

papers (Sydney et al 1975, to be referred to as II and III).

Below the Curie point non-equilibrium effects associated with

relaxation of domain properties are important. In this paper we

outline a general theory of temperature modulation experiments

including the effects of magnetic relaxation and of the thermal

skin depth.

        To introduce the bases of the experiments we first neglect

the effects of relaxation and of the skin depths - i.e., it is

assumed that at any time every point in the sample is at the same

temperature T and experiences the same applied field. The

oscillatory term in the temperature is then given by the solution of

$$mC \; \frac{dT}{dt} + bT \;\; = \;\; P \; cos \; \omega t$$

where m and C are the mass and specific heat respectively of the

sample and b is the Newton's law of cooling constant for the sample

in its environment. The oscillatory heat input $P \cos \omega t$ is provided by an electrical heater wound over the sample. If a sinusoidal heater voltage is used without DC offset then ω is at the second harmonic of the voltage whereas by employing a DC offset a power term at the frequency of the voltage waveform is introduced. The solution of (1) leads in the steady state to a temperature modulation

$$T = \overline{T} + \Delta_T \cos (\omega t + \phi_T) \tag{2}$$

where $\overline{T}$ is the mean temperature. The modulation amplitude is

$$\Delta_T = P(b^2 + \omega^2 m^2 C^2)^{-\frac{1}{2}} \tag{3}$$

and there is a thermal phase lag given by

$$\phi_T = - \arctan \omega mC/b \tag{4}$$

The rise δT in the mean temperature above ambient is given by

$$\delta T = \overline{P}/b$$

where $\overline{P}$ is the average heater power and from this, values for b may be obtained by plotting the mean steady state temperature versus $\overline{P}$.

In the DC experiments an applied DC magnetic field $\underset{\sim}{H}$ is used to create a sample magnetization $M(T)$; the temperature modulation produces a small oscillation in M and the resulting voltage induced in a pick-up coil is monitored by phase-sensitive detection. We treat this in terms of the oscillation in the susceptibility $\chi = M/H$ which is defined here for any field H. By means of a Taylor expansion the time dependence is

$$\chi(t) = \chi(\overline{T}) + \Delta_T \chi^1(\overline{T}) \cos (\omega t + \phi_T) \tag{5}$$

where χ^1 is the temperature derivative. The signal – the voltage induced in the pick-up coil, is given by

$$v = - \xi V dM/dt$$

where V is the sample volume and ξ is determined by the number of turns, the coil dimensions and the sample filling factor. Hence

$$v = \xi \Delta_T V \omega H \chi^1(\overline{T}) \cos (\omega t + \phi_T - \frac{\pi}{2}) \qquad (6)$$

When, as is usual, $b \ll \omega m C$, this becomes

$$v = \xi V P H \chi^1(\overline{T})/(mC) \cos (\omega t + \phi_T - \frac{\pi}{2}) \qquad (7)$$

and the signal amplitude is independent of the modulation frequency.

Generally only very small modulation amplitudes ($\sim$ mK) are used so that the expansion (5) is valid. If larger values are used so that the signal leads to modulation-broadened curve, instead of $\chi^1(\overline{T})$ equation (5) should be replaced by a Fourier integral (Wilson 1963).

In the AC experiments the temperature modulated sample is used as the core of an AC transformer operating at a carrier frequency $\omega_c \gg \omega$. If the amplitude of magnetic field produced by the primary coil is H_O the sample magnetization is

$$M(t) = \chi(T) H_O \cos \omega_c t \qquad (8)$$

and the Taylor expansion leads to

$$M(t) = H_O \{ \chi(\overline{T}) + \Delta_T \chi^1(T) \cos (\omega t + \phi_T) \} \cos \omega_c t \qquad (9)$$

Neglecting the contribution $\mu_O dH/dt$ which is not modulated the secondary voltage is then

$$-\xi V dM/dt = \xi V H_O \omega_c \chi(\overline{T}) \sin \omega_c t + \xi V H_O \Delta_T \chi^1(T) \{ \omega_c \cos (\omega t + \phi_T)$$
$$\sin \omega_c t + \omega \sin (\omega t + \phi_T) \cos \omega_c t \}$$

for which the amplitude modulation signal, after detection, is

$$v = \xi V H_O \Delta_T \omega_c \chi^1(\overline{T}) \cos (\omega t + \phi_T) \qquad (10)$$

or, assuming that $b \ll \omega m C$

$$v = \frac{\xi P V H_O \omega_c \chi^1(\overline{T})}{mC\omega} \cos (\omega t + \phi_T) \tag{11}$$

Comparison of equations (7, 11) shows the main advantage of the AC technique - a signal enhancement of order ω_c/ω.

By measuring the modulation amplitude Δ_T as a function of $\overline{T}$, e.g., by detection of the oscillatory emf from a thermocouple, the contribution of the specific heat to the signal amplitude may be allowed for and the derivative $\chi^1(\overline{T})$ obtained. Before carrying out the experiments on gadolinium we had expected to simultaneously obtain accurate data for the specific heat anomaly near the Curie temperature from measurements of the phase lag ϕ_T. However, in a detailed application of both modulation and conventional techniques to study the AC and DC susceptibility in the region of the Curie point in II and III it was observed that relaxation effects dominated the observed signal phase producing a phase lead. These effects are treated in the next section.

The above equations give the signals for DC and AC experiments in which phase-sensitive detection at the modulation frequency is used. In general detection at the nth harmonic of the modulation frequency yields the nth derivative of $\chi(T)$ because of the expansion (Russell and Torchia, 1962)

$$\chi(T) = \chi(\overline{T}) + \sum_{n=1}^{\infty} \Delta_T^n (2^{1-n}/n!) \chi^{(n)}(\overline{T}) \cos [n(\omega t + \phi_T)] \tag{12}$$

where $\chi^{(n)}$ represents the nth derivative. One method of determining the temperature modulation amplitude follows. If experiments are performed by detecting at both the first and second harmonics, the amplitude of the second harmonic signal versus $\overline{T}$ will be equal to $\frac{1}{4}\Delta_T$ multiplied by the derivative of the corresponding first harmonic curve.

2.   Relaxation effects

Here we treat the effects of magnetic relaxation on the signals. It is still assumed that there is a uniform temperature and applied field at all points in the sample at any given time. The treatment of relaxation effects on both the DC and AC experiments will be identical, involving only the time dependence of the susceptibility.

2.1   Simple relaxation: For 'simple relaxation' it is assumed that, as the temperature is modulated, χ is always relaxing exponentially towards its equilibrium value $\chi_e(T)$ with a relaxation time τ,

$$\frac{d\chi}{dt} = -\frac{\chi(t) - \chi_e(T)}{\tau} \tag{13}$$

Such simple behaviour would not be expected for a ferromagnet below the Curie temperature but a comparison of the observed behaviour with that expected for simple relaxation will still be worthwhile. Simple relaxation would be expected in temperature modulation experiments on low temperature nuclear magnetizations.

By substituting a Taylor expansion of $\chi_e(T)$ into (13) it follows that

$$\chi(t) = \chi_e(T) + \sum_{n=1}^{\infty} \Delta_T^n (2^{1-n}/n!)\alpha_n \chi_e^{(n)}(\overline{T}) \, cos \, [n(\omega t + \phi_T) - \phi_n] \tag{14}$$

where $\phi_n = arctan \, n\omega\tau$ and $\alpha_n = (1 + n^2\omega^2\tau^2)^{-\frac{1}{2}}$
Comparing this with (12) we see that the relaxation will result in a reduction of the nth harmonic signal amplitude by a factor α_n and an additional phase lag ϕ_n.

2.2   Relaxation of domain properties: In applying temperature modulation techniques to study a ferromagnetic material near th

Curie temperature T_C applied fields which are small in

comparison with the exchange fields will generally be used

so that the intrinsic magnetic ordering is then observed.

Above T_C exchange-enhanced paramagnetism with a field-

independent susceptibility is then expected; below T_C the

response to the applied field will be determined by the

intrinsic magnetization $\sigma(T)$ and by the domain properties.

We treat here the case where the response of σ to the

temperature modulation is fast enough for it to always be

in thermal equilibrium but with relaxation effects arising

from the domain properties.

We write, for the equilibrium susceptibility

$$\chi_e(H,T) = G_e(H,T)\chi_N(H,T) \tag{15}$$

where χ_N is the susceptibility which would be observed if

there were no domains present. Hence G_e represents the

effects of the domains upon the thermal equilibrium suscept-

ibility. Writing $\chi_N(H,T) = \sigma(T)/H$ it follows that the

equilibrium magnetization is

$$M_e(H,T) = \sigma(T)G_e(H,T) \tag{16}$$

When the applied field is large enough to magnetically

saturate the sample, i.e., there are no domains present,

(16) shows that $G_e = 1$. When, on the other hand, H is

sufficiently low for the linear, reversible domain wall

displacement to dominate the susceptibility then M_e will be

proportional to H and we may write, by (16), $G_e(H,T) =$

$g_e(T)H$ where $g_e(T)$ represents the temperature dependence of

the domain wall mobility. Then, defining in the same way

an instantaneous g, it follows that in a temperature

modulation experiment the time dependence of χ is given by

$$\chi(t) = g(t)\sigma(T)$$

We assume that when the temperature is changing g

undergoes exponential relaxation with a time constant τ

$$\frac{dg}{dt} = -\frac{g(t) - g_e(T)}{\tau}$$

and hence, as for χ in the preceding section

$$g(t) = g_e(\overline{T}) + \sum_{n=1}^{\infty} \Delta_T^{\,n}(2^{1-n}/n!)g_e^{\,(n)}(\overline{T})\alpha_n \cos\,[n(\omega t + \phi_T) - \phi_n]$$

(17)

Assuming that σ is always in thermal equilibrium then

$$\sigma(t) = \sigma(\overline{T}) + \sum_{n=1}^{\infty} \Delta_T^{\,n}(2^{1-n}/n!)\sigma^{(n)}(\overline{T}) \cos\,n(\omega t + \phi_T)$$

(18)

For nth harmonic detection we consider only the terms in the

product $g(t)\sigma(t)$ which have a frequency $n\omega$. For first

harmonic detection this leads to

$$\chi_1(t) = \Delta_T\{g\sigma' \cos\,(\omega t + \phi_T) + \sigma g'\alpha_1 \cos\,(\omega t + \phi_T - \phi_1)\} \quad (19)$$

where the values of σ, g and their derivatives all correspond

to the equilibrium functions for the mean temperature $\overline{T}$. For

slow modulation $(\omega\tau \to 0)$, $\chi_1(t) \to \Delta_T \chi_e^1(\overline{T}) \cos\,(\omega t + \phi_T)$

which is expected is the same as (5) for the case of no

relaxation effects. For fast modulation $(\omega\tau \to \infty)$

$$\chi_1(t) \to \Delta_T g(\overline{T})\sigma'(\overline{T}) \cos\,(\omega t + \phi_T)$$

(20)

and here also there is no phase shift caused by the relaxation,

g remaining equal at all times to $g_e(\overline{T})$ with the signal

being produced solely by the oscillation in σ. Equation (19)

may also be written as

$$\chi_1(t) = \Delta_T \{ (g\sigma' + \sigma g' \alpha_1^2)^2 + (g'\sigma\omega\tau\alpha_1^2)^2 \}^{\frac{1}{2}} \cos(\omega t + \phi_T + \phi_r)$$

(21)

where the phase shift ϕ_r due to the relaxation is given by

$$\tan \phi_r = -\sigma g_e' \omega\tau / (\chi_e^1 + g\sigma' \omega^2 \tau^2)$$

(22)

It is instructive to examine the effects of this relaxation

at temperatures where $\chi_e^1 = 0$. Here, in the absence of any

relaxation effects ($\omega\tau = 0$), the first harmonic signal should

be zero. Zone values of χ_e^1 will occur when the contributions

from the temperature dependences of σ and g cancel, i.e.,

when $g\sigma' = \sigma g'$. Relaxation of $g(t)$ will introduce an imbalance

and equation (21, 22) shows that the signal amplitude will

then be non-zero with a phase shift given by

$$\tan \phi_r = 1/(\omega\tau)$$

For slow modulation ($\omega\tau \ll 1$) small signal amplitudes with

a large phase lead will result. For fast modulation ($\omega\tau \gg 1$)

there will be large, almost in-phase ($\phi_r \simeq 0$), signals. A

more detailed discussion of these effects is given in III

where the theoretical predictions are compared with experimental

data for gadolinium.

For second harmonic detection, collection of terms in

$g(t)\sigma(t)$ with a frequency 2ω leads to

$$\chi_2(t) = \frac{1}{4}\Delta_T^2 \{ \alpha_2 \sigma g'' \cos[2(\omega t + \phi_T) - \phi_2] + 2\alpha_1 g'\sigma' \cos$$

$$[2(\omega t + \phi_T) - \phi_1] + g\sigma'' \cos 2(\omega t + \phi_T) \}$$

(23)

For slow modulation ($\omega\tau \to 0$)

$$\chi_2(t) \to \frac{1}{4}\Delta_T^2 \chi_e^{(2)}(\overline{T}) \cos 2(\omega t + \phi_T)$$

in agreement with (12). For fast modulation ($\omega\tau \to \infty$)

$$\chi_2(t) \to \frac{1}{4}\Delta_T^2 g(\overline{T})\sigma''(\overline{T}) \cos 2(\omega t + \phi_T)$$

Note that, as the mean temperature is varied, in the limits
of both slow and fast modulation, a phase reversal of the
second harmonic signal is expected near the Curie point.

3.   Effects of the thermal skin depth

We consider here the effects of the thermal skin depth δ
upon the signal amplitude and phase for both DC and AC experiments.
The role of the electromagnetic skin depth can be eliminated in AC
experiments by choosing an AC frequency ω_c sufficiently low so that
this skin depth is large compared with the sample dimensions. The
effect of the thermal skin depth will be to produce a variation of
the temperature modulation amplitude and phase with position in the
sample. The signal for a DC experiment is then given by

$$v = - \xi H \chi'(\overline{T}) \frac{d}{dt} <T-\overline{T}> \tag{24}$$

and for an AC experiment

$$v = - \xi H_o \omega_c \chi'(\overline{T}) <T-\overline{T}> \tag{25}$$

where

$$<T-\overline{T}> = \int (T-\overline{T}) dV \tag{26}$$

The only effect of the time derivative in (24) is to introduce an
additional factor of ω and a phase shift of $\pi/2$ as in Sec. 1 so that
we now consider only the average modulation term $<T-\overline{T}>$. The treatment
in Sec. 1 applies to the case where δ is much greater than the sample
radius.

Before treating the more general case of cylindrical symmetry
we first consider the plane wave solution which should apply whenever
δ is much smaller than the sample radius. The equation for planar
geometry is

$$\frac{\partial T}{\partial t} = \frac{K}{\rho C} \frac{\partial^2 T}{\partial x^2} \tag{27}$$

where x is the distance from the surface, and K and ρ are the thermal conductivity and density respectively. Using phasor notation the steady state oscillatory term in T may be written as

$$\underset{\sim}{T}(x,t) = \underset{\sim}{\Theta} \, \ell^{i\omega t - (i + 1)kx} \tag{28}$$

where

$$k = (\rho \omega C/2K)^{\frac{1}{2}} = 1/\delta \tag{29}$$

The phasor $\underset{\sim}{\Theta}$ gives the amplitude and phase of the oscillation and is determined by the boundary condition

$$P' \cos \omega t = b'T(0,T) - K(\partial T/\partial x) \quad x = 0 \tag{30}$$

which relates the heater power to the heat loss to the surroundings and the heat entering unit surface area of the sample. Here P' and b' are normalized so that $P' = P/A$ and $b' = b/A$ where A is the surface area. By substituting the phasor (28) into (30) we obtain the steady state solution

$$T = \overline{T} + \Delta_T \ell^{-kx} \cos (\omega t - kx + \phi_T) \tag{31}$$

where the surface modulation amplitude and phase are given by

$$\Delta_T = P'(b'^2 + 2b'kK + 2k^2K^2)^{-\frac{1}{2}} \tag{32}$$

and

$$\phi_T = \arctan \{kK/(b' + kK)\} \tag{33}$$

The average modulation is given by

$$\langle T-\overline{T} \rangle = A \int_0^\infty (T-\overline{T}) \, dx$$

leading to

$$\langle T-\overline{T} \rangle = (A\delta/\sqrt{2}) \cos (\omega t + \phi_T - \pi/4) \tag{34}$$

The main difference between this and the results (2) for the case of a large skin depth is the effective volume factor $(A\delta/\sqrt{2})$, the difference between equations (4, 33) for ϕ_T and the additional phase lag of $\pi/4$ resulting from the integration over the thermal wave. The

dependence of phase upon the specific heat is now such that as

$\rho \omega CK/b'^2$ tends to 0 and ∞ the total phase $(\phi_T - \pi/4)$ will tend

to $- \pi/4$ and $- \pi/2$ respectively compared with the case of a large

skin depth where the phase ϕ_T tends to 0 and $- \pi/2$ as $\omega mC/b \to 0$

and ∞ respectively.

For the more general case of cylindrical symmetry, with a

cylindrical or toroidal sample, the differential equation is then

$$\frac{\partial T}{\partial t} = \frac{K}{\rho C} \left[\frac{\partial^2 T}{\partial r^2} + \frac{1}{r} \frac{\partial T}{\partial r} \right] \tag{35}$$

where T is the temperature at a radial distance r from the centre

of the cylinder of radius R. The steady state oscillatory term in

T may be written as (e.g., Arparci 1966)

$$\underset{\sim}{T}(r,t) = \underset{\sim}{\Theta} \ell^{i\omega t} I_O(\sqrt{2i}\, kr) \,/\, I_O(\sqrt{2i}\, kR) \tag{36}$$

where I_j are modified Bessel functions and $\underset{\sim}{\Theta}$ is determined from the

boundary condition

$$P' \ell^{i\omega t} = b' \underset{\sim}{T}(R,t) + K \left(\frac{\partial \underset{\sim}{T}}{\partial r} \right) r=R \tag{37}$$

leading to

$$\underset{\sim}{T}(r,t) = P' \ell^{i(\omega t + \phi)} I_O(\sqrt{2i}\, kr) \, (X^2 + Y^2)^{-\frac{1}{2}} \tag{38}$$

where, writing

$$I_j(\sqrt{iy}) = R_j(y) + i\, M_j(y),$$

$$X = b'R_O + Kk(R_1 - M_1)$$

$$Y = b'M_O + Kk(M_1 + R_1)$$

with all the R_j, M_j being calculated for $y = \sqrt{2}\, kR$. The phase is

given by

$$\phi = - \arctan(Y/X)$$

with a surface oscillation phase $\phi_T = \phi + \arctan(M_O/R_O)$.

The average modulation is then

$$<T-\overline{T}> \;=\; L \int_{O}^{R} (T-\overline{T}) \; 2\pi r \; dr$$

where L is the sample length. Hence

$$<T-\overline{T}> \;=\; \sqrt{2}\pi RL\delta P'[(R_1^2 + M_1^2) \,/\, (X^2 + Y^2)]^{\frac{1}{2}}$$

$$cos \; (\omega t + \phi_T + \phi') \tag{39}$$

where ϕ' is the additional phase shift associated with the integration and is given by

$$\phi' \;=\; arctan \left\{(M_1 - R_1)/(M_1 + R_1)\right\} - arctan \; (M_o/R_o)$$

In the limit $y \to 0$ (i.e., $\delta \gg R$) the expression (39) for $<T-\overline{T}>$ becomes identical to (2) in both amplitude and phase. For $y \to \infty$ (i.e., $\delta \ll R$) it becomes identical to the plane wave solution (31) as is also expected.

REFERENCES

Arparci V S "Conduction Heat Transfer" (Addison-Wesley, U S A, 1966)

Chaplin D H, Sydney K R and Wilson G V H 1973 Phys.Lett. <u>46A</u> 55-6

Russell A M and Torchia D A 1962 Rev.Sci.Instr. <u>33</u> 442-4

Sydney K R, Chaplin D H and Wilson 1975 J.Phys.F., accompanying
        papers to be referred to as II and III.

Sydney K R, Wilson G V H, Chaplin D H and McKenna T J 1974
        J.Phys.F. <u>4</u> L98-101

Wilson G V H 1963 J.Appl.Phys. <u>34</u> 3276-85

AC SUSCEPTIBILITY STUDIES OF GADOLINIUM
NEAR THE CURIE POINT

K R Sydney, D H Chaplin and G V H Wilson

Department of Physics, Royal Military College, Canberra
Australia

ABSTRACT: Measurements of the AC susceptibility of poly-
crystalline gadolinium at temperatures near the Curie point
T_c are reported. Frequencies from 0.2 Hz to 10 kHz and RMS
applied fields from 10^{-3} to 10^3 A/m were used. Field-
independent exchange-enhanced susceptibility was observed
above T_c. Below T_c the susceptibility at low fields ($\lesssim 8$ A/m)
is field-independent and also has a frequency dependence
which is characteristic of a magnetic after-effect. At
temperatures within about 3K below T_c, effects associated with
domain nucleation were observed; also when the temperature was
changed, non-equilibrium effects with a characteristic time of
about 2-6 secs resulted.

1.   Introduction

Recently we reported AC susceptibility studies of gadolinium in the region of the Curie temperature T_c; the onset of ferromagnetic domain nucleation at T_c was indicated by the temperature dependences of the low-field susceptibility and of the coercive field (Sydney et al 1974). This work was in association with that on the application of temperature modulation techniques to study gadolinium near T_c (Chaplin et al 1973, Sydney et al 1975 to be referred to as III). In a paper outlining the theory of temperature modulation experiments (Wilson et al 1975 to be referred to as I) we included a study of the effects of relaxation of the domain properties on the susceptibility. In this paper we elaborate on the previous susceptibility studies with measurements of both the real and imaginary components of the AC susceptibility χ over a wide range of frequencies and field amplitudes. The results also indicate the occurrence of non-equilibrium effects at temperatures within a few degrees below T_c.

Gadolinium has a Curie temperature which has been reported to lie between 289 and 298K (Griffel et al 1954, Nigh et al 1963, Darnell 1963, Rhyne 1972). It has an absolute saturation magnetic moment of $7.55\mu_B$ per atom (Banister et al 1954, Nigh et al 1963). The crystal structure is hcp and above about 240K the easy direction of magnetization is the c-axis (Corner et al 1962, Graham 1963, Cable and Wollan 1968, Milstein and Robinson 1969). Because of the unusual dependences of the susceptibility upon applied field and temperature, Belov and Ped'ko (1962) suggested that in low fields there may be weak helical antiferromagnetism, but this has not been supported by neutron diffraction studies (Will et al 1964, Cable and Wollan 1968, Kuchin et al 1969). Specific heat studies have revealed a sharp maximum in the specific heat at 291.8K (Griffel et al 1954). Measurements of the AC susceptibility have previously

been reported by Gerstein and Olander (1971) who used fields greater than 150 A/m; the present study indicates that this is well above the maximum field at which initial field-independent susceptibility can be obtained.

2.   Experimental

2.1 Apparatus: The samples were cut from polycrystalline gadolinium ingots supplied by Rare Earth Products Ltd. (99.9% pure); they were not annealed because of the uncertainties about the effects of any gas which might be absorbed during annealing. For the majority of experiments the sample was in the form of a toroid (OD 0.024m, ID 0.018m). Two copper-constantan thermocouples (48 SWG) were placed with the thermometer heads in small holes drilled on either side of the sample. An insulated heater coil of "Moleculoy" wire was wound non-inductively over the whole sample, followed by a primary coil of 500 turns of copper wire. Temperature variation throughout the sample was less than 0.05K provided the heater current was not excessive.   A 1500 turn secondary coil was wound over half the toroid so that one of the thermocouples was situated centrally in relation to it. The whole sample assembly was placed in a thermostatic bath (Lauda K24R Electronic); temperature control and measurement was better than ± 0.05K.

For larger applied fields cylindrical samples were used together with Helmholtz coils. Experiments were also carried out on gadolinium foil samples; here the sample was wrapped into a hollow cylinder around a non-magnetic

core and then studied in the same manner as for the cylindrical samples.

A phase-sensitive detector (PSD) system (Princeton 124AL, 127) formed the core of the detection system, and permitted simultaneous measurement of both the in-phase and in-quadrature voltages, thus leading to both the absorptive and dispersive components of the AC susceptibility. The signal generator was such that the primary coil current was almost constant; correction to constant current was made possible by monitoring the primary current with a series standard resistance and an additional PSD. The fields generated by the primary coil were calculated from the current and the known turns configuration. Most of the results presented here were for the toroid for which no correction for demagnetizing fields was necessary. Also no correction for the effect of the earth's magnetic field on the AC susceptibility was required as it had been previously observed (Sydney et al 1974) that the application of a large (2400 A/m) DC field did not significantly affect the AC susceptibility obtained with a small (<1 A/m) AC field.

2.2 AC Susceptibility Measurements: These were conventional studies. The secondary voltage is given

by $v = N H_o \omega[(\mu_0 + \xi\chi') \sin \omega t - \xi\chi'' \cos \omega t]$ \hfill (1)

where N is the number of secondary turns, ξ is a sample filling factor assumed here to be unity, χ' and χ'' are the real and imaginary components of the AC susceptibility χ, and the applied field is $H = H_o \cos \omega t$. In the

magnetic hysteresis measurements the secondary output

was integrated and recorded in a conventional manner

on an oscilloscope.

2.3 <u>Thermal relaxation experiments</u>: By applying square

wave voltage pulses to the heater coil the temperature of

the sample could be alternately raised and lowered with

a response time of about 0.2 sec. The PSD output and the

thermocouple voltage were monitored on a chart recorder

and the response of the susceptibility to sudden

temperature changes was observed. That the slow response

observed just below T_c was due to relaxation processes

was supported by the observation of a fast response of

the secondary voltage at temperatures above T_c.

3. <u>Experimental results</u>

3.1 <u>AC susceptibility results</u>: Figure 1 shows $\chi(\overline{T})$

curves obtained with a frequency of 100 Hz. The curves

are qualitatively similar to the 2 kHz data previously

published (Sydney et al 1974) except that in higher

fields at lower temperatures where the permeability is

highest, it was found that the 2 kHz curves were somewhat

distorted as the electromagnetic skin depth was no longer

far greater than the sample diameter. As shown below,

distortion of the curves by eddy current effects was

negligible at 100 Hz. For high ($\gtrsim$ 700 A/m) AC fields

there is little evidence of structure in an essentially

monatonically varying $\chi(T)$. In low fields $\chi(T)$ exhibits

a peak near T_c with a minimum at about 290.5K; also

there is a significant difference in $\chi(T)$ obtained over

a few degrees below T_c depending on whether the sample
was being cooled from above T_c or warmed from about 10K
below T_c. For intermediate fields there was still some
significant thermal hysteresis, and $\chi(T)$ exhibited an
inflection in the temperature range corresponding to the
structure in the low field $\chi(T)$ curves. Whilst the
cooling curves were always highly reproducible, the
warming curves showed some rate dependence for warming
rates greater than 0.2 K/min; however, no rate dependence
was observed for lower rates. In one low-field
experiment the sample was warmed to 291.4K where there
is the largest difference between the warming and
cooling curves, and no time dependence was observed while
the temperature was held constant for two hours.
Above T_c there was no temperature hysteresis, and a field
independent exchange enhanced paramagnetic susceptibility
was observed.

Figure 2 shows the temperature dependence of the phase
lag, $\phi = arctan$ (χ''/χ') caused by the presence of the
absorptive component of χ. In most respects, these
measurements reflect the qualitative details of the
coercive force measurements; however, they also permit
more accurate measurements of the absorption at low fields
than is possible from magnetic hysteresis measurements.
In the paramagnetic region the primary current and the
secondary voltage were observed to be exactly in
quadrature corresponding to $\phi = 0$ and hence $\chi'' = 0$ for
all values of applied field used. This indicates that
above T_c there are no relaxation effects on the time scale
of the 100 Hz frequency used. At temperatures $\leqslant$296 ± 0.3K

phase lags were observed at both low and high fields.

In Figure 3 the dependence of χ at 100 Hz upon the RMS applied field amplitude is shown. At temperatures above T_c the susceptibility is field-independent over the wide range of applied fields used. Below T_c the susceptibility is accurately field-independent for applied fields ranging over three decades below about 8 A/m. This appears to be the first observation of an initial field-independent susceptibility for a rare earth ferromagnet. For larger applied fields χ increases with increasing fields reaching a maximum at about 375 A/m which corresponds to the inflection in the virgin magnetization curve as the sample approaches saturation. The corresponding dependence of the phase lag ϕ upon field is shown in Figure 4. It is seen that at fields below $\sim$ 8 A/m the phase is effectively field - independent; the onset of irreversible processes in higher fields is well indicated by the abrupt increase in ϕ for fields above 8 A/m.

The dependences of χ and ϕ upon frequency both above T_c and also below T_c for several different values of the applied field are given in Figures 5 and 6. The data obtained above T_c shows a frequency-independent χ and an almost zero phase lag for frequencies up to $\sim$1 kHz; at higher frequencies the effects of the finite skin depth appear. Below T_c skin depth effects begin to occur at lower frequencies because of the higher susceptibility and this is most marked for larger applied fields where χ is largest. Otherwise, for large fields χ is almost frequency independent

whereas for lower fields the frequency dependences of both
χ and ϕ are characteristic of a small magnetic after-effect.
In Fig. 7 the temperature dependence of the low field
susceptibility is shown for a variety of frequencies from
0.2 to 100 Hz. A tendency to smooth out the trough in the
region of 290K as the frequency is lowered, is indicated.

The experiments on the gadolinium foil also showed
similar structure in $\chi(T)$ in low fields, thus confirming
that this structure is not due to electromagnetic skin
depths. This was further indicated by the retention of
this structure with field frequencies down to 0.2 Hz.

The experiments performed on the cylinder were mainly
supplementary in nature being carried out to complete the
experimental study via this technique. The low field AC $\chi(T)$
curves showed the same structure as for the toroid with some
distortion because of demagnetizing fields, and were relativ-
ely uneffected by the presence of a 2400 A/m DC field along
the cylindrical axis (Sydney et al 1974).

3.2 <u>Magnetic hysteresis measurements</u>: The magnetic
hysteresis studies performed below T_c indicated that for
applied fields less than $\sim$ 8 A/m the domain magnetization
processes are effectively reversible with a magnetization
which is proportional to the field, in agreement with the
susceptibility measurements. For larger applied fields,
magnetic hysteresis was observed. Figure 8 shows the
temperature dependence of the minor loop coercive field
for various applied fields. The form of these results bears
some resemblance to those of Bates and Pacey (1961) and

Belov et al (1961) but their results are not as sharply

defined in temperature as those of Fig. 8; they observed

a minimum in the coercive field at ~ 210K.

3.3   Thermal relaxation results: When carrying out the

thermal relaxation experiments, heating currents ~ 30 mA

were suddenly either switched on or off. This gave rise to

significant temperature inhomogeneities. The temperature

differential between the two thermocouples on either side

of the toroid grew at the rate of ~ 1.5K/min when the

heater was switched on, and fell at the rate of ~ 1K/min

when the heater was switched off, these rates being somewhat

dependent on the relative temperatures of the sample and the

environment. However, by measuring the broadened heating

and cooling $\chi(T)$ curves with these large heating currents on,

we were able to gain a qualitative approximation to the

"equilibrium" transition secondary voltage curve which would

result when the heater was switched on or off in the absence

of non-equilibrium effects in the sample. Figure 9(a) shows

the time dependence of the sample temperature (measured at the

centre of the secondary coil) after suddenly switching off the

heater. The initial temperature was 293.1K - at the peak of

the equilibrium low field $\chi(T)$ curve. Figure 9(b) shows the

response of the secondary voltage in a low field, together

with the approximate equilibrium curve described above. It

can be seen that a rise took place in the secondary output over

a period ~ 2 sec during which time the inhomogeneous temperature

differential across the sample would have fallen only about 0.03K,

insufficient to give any effect. The susceptibility then fell

slowly back to the equilibrium curve. Relaxation effects

during experiments in which the sample temperature was
suddenly raised from the region of the trough in $\chi(T)$ were
much weaker. No non-equilibrium effects were observed in
the paramagnetic region where χ always followed the equil-
ibrium curve regardless of the rate of temperature change.

4. Discussion

Above T_c the susceptibility is independent of applied field
for the range of fields used here, and is also frequency independent
apart from the effects of eddy currents at frequencies $\gtrsim$ 100 Hz.
Extremely careful measurements of χ by this technique and $d\chi/dT$ by
temperature modulation techniques are now in progress with the aim of
studying the critical behaviour in this exchanged-enhanced paramagnetic
region.

If the Curie point were to be defined to be the temperature at
which domain nucleation commences then, from the sharp onset of
hysteresis we obtain a value T_c = 294.1 ± 0.2K. Alternately, from the
temperature for which $d\chi/dT$ is a maximum we obtain T_c = 293.7 ± 0.2K in
reasonable agreement with the results of the temperature modulation
experiments reported in III. Below T_c there is a transition region of
several degrees in which the low initial field susceptibility actually
decreases with temperature and there is considerable temperature
hysteresis. We believe that this is associated with the domain nucleation
and this is supported by the observed relaxation effects and by the rapid
temperature variation of the coercive field. Below T_c an initial-field-
independent susceptibility is observed for applied fields up to ~ 8 A/m,
this value decreasing very slightly as the temperature is lowered. The
strain theory first sugtested by Becker (1932) as a possible mechanism

for the variation of domain wall energy with displacement in a non-uniform material predicts a critical field for the transition to irreversibility of

$$H_O \simeq \pi\lambda S_T/\sigma \qquad (2)$$

where λ is the magnetostriction constant, S_T is the internal stress of the material, and σ is its intrinsic magnetization. For a sample being cooled through the Curie point where the major strains contributing to irreversibility are due to magnetostriction, we would have

$$S_T = \lambda E_{YM} \qquad (3)$$

where E_{YM} is Young's modules for the material. Using

$$E_{YM} \simeq 4 \times 10^{10} \ N/m^2, \quad \sigma \simeq 0.5 \ W_b/m^2 \text{ and } \lambda \simeq 10^{-5},$$

we obtain

$$H_c \simeq 24 \ A/m. \qquad (4)$$

Alternately, one might use a pinning model similar to that proposed by Kernsten (1956) to explain the coercive force dependence on the composition of iron-nickel alloys. The wall is pinned at its ends and bulges under the pressure of the field. A discontinuous expansion will occur when the radius of curvative of the wall is ½ the separation between the constraining points. Here we have

$$H_c = W/\ell_1 \cos \theta \qquad (5)$$

where W is the domain wall energy per unit area, ℓ_1 is the separation distance between the constraining points, and θ is the angle between the applied field and the direction of easy magnetization. Using

$$W \simeq 1.2 \times 10^{-3} \ J/m^2, \quad \ell_1 \simeq 10^{-4}m \text{ and } \theta = 0,$$

we obtain

$$H_c \simeq 25 \ A/m \qquad (6)$$

ie, of the same order of magnitude as that predicted by the strain theory and reasonably close to the measured value of 8 A/m. The

inclusion theory (Kernsten 1943) on the other hand, predicts a

critical field some orders of magnitude too large, and similarly

the transition to irreversible rotation would seem to occur in

fields much larger than 8 A/m. In addition it is interesting to

note that the domain walls in Gd near T_c could be expected to be

thin due to its finite anisotropy in the critical region (Corner

et al 1962). Taylor (1971) has observed an intrinsic coercivity

in materials with thin domain walls but once again this would

seem to be much larger than 8 A/m in Gd near T_c. It would seem

therefore, that irreversibility in our Gd sample is due mainly to

strain or pinning mechanisms.

The large difference between the initial and the higher

field susceptibilities below T_c may in part be due to anisotropy in

the contribution of reversible domain wall displacement to the low-

field susceptibility. In the temperature range used here, the easy

axis of magnetization is the c axis and a uniaxial domain structure

is expected. The domain wall displacement contribution will then be

zero for applied fields in the basal plane and, for a polycrystalline

sample, the average contribution should be one third of that for

applied fields parallel with the c axis. Higher field processes such

as irreversible wall displacement and rotation should be more isotropic.

Whether the susceptibility should actually rise or fall as the temperat-

ure is lowered in the region of T_c as domains nucleate is not obvious.

As outlined in I there will be two competing effects - the intrinsic

magnetization will rise while the nucleation of domains will tend to

lower the susceptibility. Anisotropic effects will cause the low

field susceptibility to be considerably less than that in high fields,

so that it is not too surprising to observe a decrease in low fields

and an increase in higher fields as the temperature is lowered through the transition region. Several other ferromagnetic metals such as iron and nickel also show a decrease in the low field susceptibility with decreasing temperature in the region of T_c (Bates 1963, Chikazumi 1964). This is however, due to the expected proportionality of χ with $\sigma/\sqrt{K}$ (Kernsten 1956) and the fact that $K \rightarrow 0$ as $T \rightarrow T_c$ in these metals. For Gd K remains almost temperature independent in the vicinity of the Curie point (Corner et al 1962) so that this cannot be the origin of the behaviour in low fields in the transition region.

The thermal relaxation experiments show that when sudden changes of temperature are made in the transition region, the time dependence of the observed susceptibility is significantly different to that expected from the equilibrium curve and, in some cases, initially moves in the opposite direction to that for equilibrium. This fits well with the theory given in I in which the intrinsic magnetization is assumed to always remain in equilibrium while the contribution from the domain structure to the susceptibility exhibits relaxation. The present studies indicate that in the transition region the relaxation times are of order 2-6 secs.

The maximum in the phase lag which occurs for fields ~ 370 A/m as in Fig. 4 corresponds to the greatest percentage of irreversibility near the point in the $M(H)$ curves where χ reaches a maximum as in Fig. 3. It is known that reversible rotation mechanisms can dominate in a sample between the point of inflection in the $M(H)$ curve and saturation (see e.g., Chikazumi 1964). For low fields there is a residual phase lag which is field-independent; Fig. 2 shows that this is also temperature-independent and from Fig. 6 it is shown to be almost frequency independent, apart from a weak minimum at about

1 Hz. This behaviour is typical of a magnetic after-effect (Snoek 1949, Bozorth 1951, Chikazumi 1964) with a wide range of relaxation times. The minimum in phase at 1 Hz could indicate a weak peak in the distribution of relaxation times at about 1 sec. The steady decrease in the low field susceptibility as the frequency is increased from 0.5 to above 100 Hz is in agreement with this and, as expected, is not observed for high applied fields or for temperatures above T_c. The origin of this after-effect is probably associated with the presence of gaseous impurities in the samples (see e.g., Chikazumi 1964 p.310). The low frequency $\chi(T)$ curves in Fig. 7 also indicate the presence of an after-effect. The filling of the trough in $\chi(T)$ as the frequency is lowered is probably due to the expected increase in χ just below T_c with no corresponding change in χ above T_c. The absence of any low temperature satellite peak in the DC temperature modulation signal versus temperature curves given in III also suggests that the low field DC $\chi(T)$ curve does not exhibit any trough.

While the results presented here are in general qualitative agreement with those of Gerstein and Olander (1971) there are significant differences in detail. Firstly the 150 A/m fields they used are too large to observe initial-field behaviour in Gd. Also we consider that the theory of domain wall dynamics which they have used to interpret data in the very low frequency region to be inapplicable for that region in Gd. This view is supported by the fact that in our measurements $\chi'/|\chi|^2$ _rose_ by about 10% from 0.2 Hz to 50 Hz at 0.8 A/m, with a positive intercept at the zero frequency axis, whereas, if we were above the resonant frequency $\chi'/|\chi|^2$ should be falling with a decrease in frequency and a negative intercept would be required.

Finally, we have seen no significant temperature hysteresis in the magnetic losses (Figs. 2 and 6), whereas Gerstein and Olander reported temperature hysteresis in both χ' and χ'', the larger being in χ''.

Originally we suspected that the large difference in the $\chi(T)$ curves for low and high AC fields below T_c may have been due to field cooling effects in which the domain structure is influenced by the presence of the applied field while cooling through T_c. To test for this possibility some additional experiments were performed on the toroidal sample. In one the sample was cooled to 289.9K in an AC field of 75 A/m and thereafter in 0.5 A/m. The susceptibility changed abruptly to the low field curve when the field was decreased. In other such studies cooling experiments in high or low AC fields were followed by warming in low or high fields respectively; no changes were observed from the results of warming experiments presented elsewhere in this paper. These indications of the absence of field cooling effects are in agreement with our previous observation (Sydney et al 1975) that the low AC field $\chi(T)$ curve was not significantly affected by the presence of a large DC field.

5.   Conclusions

These studies show well-behaved exchange-enhanced paramagnetism above T_c. Below T_c the dependence of the AC susceptibility upon temperature, applied field and frequency has been determined. Over a wide range of applied fields up to $\sim$ 8 A/m a field-independent initial susceptibility is observed. The frequency and temperature dependences of the absorptive and dispersive components of the low field susceptibility are qualitatively explained by an impurity magnetic after-effect. The temperature dependences of the susceptibility and the coercive field within a few degrees below T_c are assoc-iated with domain nucleation. The observation of relaxation effects

in the low-field AC susceptibility when sudden temperature changes are made is in qualitative agreement with the theory of domain relaxation as given in I. A more detailed discussion of these relaxation effects is given in III in terms of the results of the temperature modulation experiments. Further studies of the critical behaviour in both polycrystalline and single crystal samples are now in progress.

Acknowledgements

FIGURE CAPTIONS

Figure 1 :   Temperature dependence of the AC susceptibility of

gadolinium at 100 Hz for various RMS fields in the

region of the Curie temperature:

X   cooling in 750 A/m;

□   cooling in 75 A/m;

0   cooling in 7.5 x 10^{-2} A/m;

Δ   corresponding warming curves.

Figure 2 :   Temperature dependence of the phase ϕ of the complex

susceptibility at 100 Hz in a range of applied RMS

AC fields:

X   cooling in 750 A/m;

□   cooling at 75 A/m;

0   cooling in 7.5 x 10^{-2} A/m;

Δ   corresponding warming curves.

Figure 3 :   Dependence of the AC susceptibility on applied AC field

amplitude at 100 Hz for various temperatures:

X   296.8K;

□   289.7K;

Δ   280.3K.

Figure 4 :   Dependence on applied AC field amplitude of the phase

ϕ of the complex susceptibility for various temperatures:

X   296.8K;

□   289.7K;

Δ   280.3K.

Figure 5 : Dependence of the AC susceptibility on the applied

AC field frequency for various conditions of temperature

and RMS AC field:

X   100 A/m at 277.9K;

☐   0.75 A/m at 278.2K;

0   100 A/m at 319.3K.

Figure 6 : Dependence on the applied AC field frequency of the

phase ϕ of the complex susceptibility for various

conditions of temperature and RMS AC field:

X   100 A/m at 277.9K;

☐   0.75 A/m at 278.2K;

0   100 A/m at 319.3K.

Figure 7 : Temperature dependence of the AC susceptibility of

gadolinium near the Curie temperature for cooling

experiments in AC fields of 0.38 A/m RMS with

various frequencies:

X   0.2 Hz;

☐   0.5 Hz;

0   1.0 Hz;

Δ   100 Hz.

Figure 8 : Temperature dependence of the minor loop coercive

force for AC fields of frequency 40 Hz and various

RMS amplitudes:

X   840 A/m;

☐   375 A/m;

0   126 A/m.

Figure 9 :   Relaxation resulting from sudden cooling from the

peak in the equilibrium AC $\chi(T)$ curve in a field

of 0.7 A/m RMS at 1000 Hz.

Figure 9(a) shows the time dependence of the

sample temperature.

Figure 9(b) shows the time dependence of the

secondary coil output (X) superimposed on the

equilibrium $\chi(T)$ curve (0).

REFERENCES

Banister J, Legvold S and Spedding F H   1954   Phys.Rev., $\underline{94}$ 1140

Bates L F and Pacey A J   1961   Proc.Phys.Soc. $\underline{78}$ 878–882

Bates L F   1963   Modern Magnetism 4th ed (London:Cambridge)

Becker R   1932   Phys.Zeits. $\underline{33}$ 905

Belov K P, Levitin R Z, Nikitin S A and Ped'ko A V   1961
        Zh.Eksp.Teor.Fiz (USSR) $\underline{40}$ 1562–1569 – Engl Trans
        Sov.Phys.JETP $\underline{13}$ 1096–1101

Belov K P and Ped'ko A V   1962   Zh.Eksp.Teor.Fiz.(USSR) $\underline{42}$ 87–90
        Engl Trans   Sov.Phys.JETP $\underline{15}$ 62–64

Bozorth R M   1951 Ferromagnetism (Princeton:Van Nostrand)

Cable J W and Wollan E O   1968   Phys.Rev. $\underline{165}$ 733–734

Chaplin D H, Sydney K R and Wilson G V H   1973   Phys.Lett. $\underline{46A}$ 55–56

Chikazumi S   1964 Physics of Magnetism (New York:Wiley)

Corner W D, Roe W C and Taylor K N R   1962   Proc.Phys.Soc.(London)
        $\underline{80}$ 927–933

Darnell F J   1963   Phys.Rev. $\underline{130}$ 1825–1828

Gerstein B C and Olander F   1971   J.Appl.Phys. $\underline{42}$ 3438–3445

Graham C D   1963   J.Appl.Phys. $\underline{34}$ 1341–1342

Griffel M, Skochdopole R E and Spedding F H   1954   Phys.Rev. $\underline{93}$
        657–661

Kernsten M   1943   Grundlagen einer Theorie der Ferromagnetischen
        Hysterese und der Koerzitivkraft (Leipzig:Herzel)

Kernsten M   1956   Z.Agnew.Phys. $\underline{7}$ 313 and $\underline{8}$ 382

Kuchin V M, Semenkov V A, Shil'shtein S Sh and Patrikeev Yu B
        1968   Zh.Eksp.Teor.Fiz. $\underline{55}$ 1241–1247   Engl Trans
        Sov.Phys.JETP. $\underline{28}$ 649–652 (1969)

Milstein F and Robinson L R   1969   Phys.Rev. $\underline{177}$ 904–909

Nigh H E, Legvold S and Spedding F H   1963   Phys.Rev. $\underline{132}$ 1092–1097

Rhyne J J   1972 in Magnetic Properties of Rare Earth Materials
        (R J Elliot ed) (London:Plenum)

Snoek J L   1949   New Developments in Ferromagnetic Materials
        (Amsterdam:Elsevier)

Sydney K R, Wilson G V H, Chaplin D H and McKenna T J   1974
        J.Phys.F. $\underline{4}$ L98–L101

Sydney K R, Chaplin D H and Wilson G V H   1975   J.Phys.F.
          accompanying paper to be referred to as III

Will G, Nathans R and Alperin H A   1964   J.Appl.Phys. 35 1045-1046

Wilson G V H, Chaplin D H and Sydney K R   1975   J.Phys.F., accompanying
          paper to be referred to as I

FIGURES

For the purposes of including this paper in the back of my thesis, the following correspondence is applicable between the figures of the paper and those of the thesis.

PAPER FIGURE	THESIS FIGURE
1	11
2	12
3	13
4	14
5	15
6	16
7	17
8	19
9	20

TEMPERATURE MODULATION STUDIES OF GADOLINIUM NEAR THE CURIE POINT

K R Sydney, D H Chaplin and G V H Wilson

Department of Physics, Royal Military College
Canberra, Australia

ABSTRACT: The application of temperature modulation techniques to the study of the magnetic properties of polycrystalline gadolinium in the vicinity of the Curie point T_c is reported. Below T_c differences in the temperature dependences of the low-field DC and AC susceptibilities are observed. In the transition region near T_c there are large phase leads in the modulation signals because of relaxation effects associated with domain nucleation.

1.   Introduction

        Recently we reported conventional AC susceptibility studies

of gadolinium in the region of the Curie temperature (Sydney et al

1974, 1975 to be referred to as II). These studies showed that

above the Curie temperature T_c there is a field-independent exchange

enhanced susceptibility while just below T_c domain nucleation takes

place. We report here further studies of both the AC and DC

susceptibilities χ near T_c using temperature modulation techniques.

A preliminary account of this (Chaplin et al 1973) and an outline

of the theory of temperature modulation experiments (Wilson et al

1975 to be referred to as I) have been given elsewhere. In these

experiments the temperature of the sample, or of just its surface

depending on the magnitude of the thermal skin depth, is modulated

at a frequency $\omega/2\pi$ ~ 1 Hz with a modulation amplitude of ~ 1-30 mK

by means of an electrical heater. In the DC technique a DC magnetic

field is applied to produce a net sample magnetization M and the

small oscillation in M due to the temperature modulation produces

an emf in a pick-up coil. This signal, which is measured using a

phase-sensitive detector (PSD), is proportional (in the absence of

relaxation effects) to the derivative dM/dT. In the AC technique the

sample is used as the core of a transformer operating at a

frequency ω_c which is typically ~ 1 kHz. The signal is then the

amplitude modulation of the secondary voltage and is proportional to

the derivative $\chi^1 = d\chi/dT$.

        In I we showed that if the thermal skin depth is much

greater than the sample diameter, the temperature modulation

amplitude will be

$$\Delta_T = P(b^2 + \omega^2 m^2 C^2)^{-\frac{1}{2}} \tag{1}$$

where the oscillatory heat input is $P \cos \omega t$, b is the Newton's law of cooling constant, m is the sample mass and C is the specific heat. The temperature modulation will also exhibit a phase lag given by

$$\phi_T = arctan \ \omega mC/b \tag{2}$$

Assuming, as usual, that $b \ll \omega mC$, the signal for a DC experiment becomes

$$v = \xi VPH\chi^1(\overline{T})/(mC) \ \cos \ (\omega t + \phi_T - \frac{\pi}{2}) \tag{3}$$

where ξ is a constant which depends on the coil and sample geometries, V is the sample volume, H the applied field and $\chi^1(\overline{T})$ is the first derivative with respect to temperature of the susceptibility $\chi = M/H$, at the mean temperature of the sample. The corresponding expression for an AC experiment is

$$v = \xi PVH_O\omega_c\chi^1(\overline{T})/(\omega mC) \ \cos \ (\omega t + \phi_T) \tag{4}$$

where H_O and ω_c respectively are the amplitude and frequency of the applied AC field. Comparison of equations (3, 4) shows that one main advantage of the AC technique is a signal enhancement of order ω_c/ω.

In applying temperature modulation techniques to the study of ferromagnetic materials near the Curie point, it was found that the direct measurement of a signal which is proportional to the derivative $\chi^1(\overline{T})$ and which is therefore peaked near T_c, leads to a better characterization of the critical behaviour than does the actual susceptibility. We had also expected to be able to simultaneously determine the specific heat from observations of the signal phase, but in practice, especially with the AC technique, the phase is dominated by relaxation effects. Temperature modulation

techniques were first used by Chynoweth (1958) for determining

Curie points, while Walser et al (1971) have used the pyromagnetic

effect in gadolinium for radiation detection. Chynoweth's and

Walser's experiments correspond to the DC technique. In the

results reported here the use of the AC technique resulted in a

signal enhancement by a factor ~ 1000.

2.   Experimental

2.1 Apparatus: The sample assembly (consisting of a

toroid with a heater coil; a primary coil and a secondary

coil), and methods of temperature control were described

in II. Indeed, in many cases simultaneous measurements

of both the AC susceptibility and the temperature

modulation signals were performed using a separate phase-

sensitive detection system. A sinusoidal current with

frequency $\omega/2$ was passed through the heater coil

producing temperature modulation of frequency ω. The

modulation amplitude Δ_T was typically a few mK. Modulation

frequencies from 0.3 Hz to 20 Hz were used.

2.2 DC temperature modulation experiments: A DC magnetic

field was applied to the sample by passing a DC current

through the primary coil; fields in the range 75 to 850 A/m

were used. The induced signal in the secondary coil was

measured using a Princeton 124AL PSD operating in second

harmonic mode. The technique of using a heater current with

frequency $\omega/2$ and detecting the modulation signal at ω has

the advantage of rejecting any spurious signals resulting

from pick-up from the heater coil.

2.3 <u>AC temperature modulation experiments</u>. Here no DC applied field is necessary. The sample formed the core of an AC transformer as in the conventional AC susceptibility studies reported in II. Temperature modulation resulted in an amplitude modulated secondary output voltage. A Princeton 124 PSD operating at ω_c was used to give an output proportional to the permeability as in II. The output time constant τ_0 used here was such that $\omega_c^{-1} \ll \tau_0 \ll \omega^{-1}$ so that signals at the carrier frequency were smoothed without removal of the temperature modulation signal. This output was then fed into a Princeton 124AL PSD with a two phase unit (Model 127) operating in second harmonic mode at frequency ω. The current in the primary coil was monitored as in II.

As shown in I, phase-sensitive detection at the nth harmonic of the temperature modulation yields a signal which is proportional to the nth derivative of the susceptibility $\chi^{(n)}(T)$ so that the above DC and AC arrangements yield the first derivative $\chi^1(T)$. By doubling the frequency of the input reference signal and also operating with the 124AL in the second harmonic reference mode, it was possible to detect the second harmonic (2ω) signal. The rapid decrease in signal-to-noise ratio as the order of the detected harmonic is increased made it impracticable to detect signals at higher harmonics.

2.4 <u>Relaxation of the first harmonic signal</u>: Here a sinusoidal current with frequency ω plus a DC offset was passed through the heater coil to produce temperature

modulation at frequency ω. The 124AL was then operated in the external reference (first harmonic) mode. By suddenly changing the DC offset current, with a compensating change in the amplitude of the sinusoidal heater current, it was possible to make rapid changes in the mean temperature of the sample without any change in the actual modulation amplitude. The time dependence of the in-phase and quadrature modulation signals and of the sample temperature were then monitored on a 3-pen chart recorder.

2.5 Measurement of modulation amplitudes: As reported in Sec. 1, the modulation signals for both the DC and AC techniques are proportional to the modulation amplitude Δ_T. In order to obtain curves of $\chi^1(\overline{T})$ from the signals, the temperature dependence of Δ_T caused by the variation in the specific heat must be allowed for. The temperature dependences of the modulation amplitude and phase were determined by measuring the output of the thermocouple on a 124AL PSD. To perform these measurements low modulation frequencies and a modulation amplitude of $\sim$ 35 mK were used.

3. Experimental results

3.1 Measurement of b: A linear relationship was found between the mean equilibrium temperature and the applied heater power, proving the applicability of the Newton's law of cooling term used in the modulation theory contained in I. The value of b was found to be $\sim 10^{-2}$ W/K, much smaller than ωmC. For a modulation frequency of 1 Hz, $\omega mC \sim 10$ W/K at room temperature.

3.2 <u>DC experiments</u>: Figure 1 shows the temperature
dependence of the signal amplitude for DC experiments over
a wide range of applied fields. The curves exhibit a single
peak centred at about 292.9K. For all fields used there is
no other structure apparent in the $S(T)$ curves. Supplementary
experiments performed on cylindrical samples in DC fields
showed that the peaks begin to broaden for fields $\gtrsim$ 1000 A/m
in agreement with previous observations of the temperature
dependence of the DC magnetization (Nigh et al 1963). The
dependence of the maximum signal amplitude upon applied fields
is shown in Fig. 2; this indicates the low sensitivity of this
technique in small applied fields. Figure 3 shows the
temperature dependence of the signal phase with respect to the
second harmonic of the heater current waveform; no strong
structure is apparent. Also, unlike the AC experiments, no
temperature hysteresis effects were observed in the DC signal
amplitude or phase.

3.3 <u>AC experiments</u>: The AC technique is most sensitive in
zero DC field although it can be used in the presence of DC
fields. Figure 4 shows a typical set of curves for the
temperature dependence of the signal amplitude for a
modulation frequency of 2 Hz and various AC magnetic field
strengths. A well-defined peak at 293.2 ± 0.2K for low
fields with a small shift to lower temperatures in larger
fields is seen. On the low temperature side of the main peak
a satellite peak is observed. The shape of the curves depicted
was not greatly altered for modulation frequencies down to

0.3 Hz, while for frequencies above about 6 Hz the
curves tended towards a single broad peak at about 291.5K.
The form of the curves was found to be independent of
field frequency provided skin depth effects were not present.
As in II, when modulation amplitudes $\geq$ 30 mK were used, the
$S(T)$ curves broadened because of inhomogeneities in the sample
temperature. For smaller amplitudes however this distortion
was not significant. As shown in Fig. 4, except for AC
fields as large as about 700 A/m, the signal amplitude
exhibited considerable temperature hysteresis, with the
signals for the warming curves being less than those for the
cooling curves.

The variation with temperature of the signal phase for
a modulation frequency of 2 Hz is shown in Fig. 5. Of
particular significance is the marked peak corresponding to a
relative phase lead at 290.7 ± 0.2K. This phase peak exhibits
an extremely large degree of temperature hysteresis being far
smaller in the cooling experiments. Experiments were also
carried out with a modulation frequency of 0.3 Hz; the
temperature dependence of the signal phase was almost unchanged
from that at 2 Hz.

Some AC temperature modulation experiments were carried
out for a cylindrical sample. The temperature dependences
of both the signal and the phase were very similar to those
for the toroidal sample except that the satellite structure,
though certainly present, was less pronounced. For this
assembly, AC field experiments were also carried out with an
additional DC field applied parallel to the cylindrical axis.

The presence of a DC field produced little change in the shape of the $S(T)$ curves. However large DC fields, as expected, greatly reduced the actual signal amplitudes.

AC temperature modulation experiments with detection at the second harmonic of the modulation were found to be very dependent on the rates of cooling and warming. Above about 0.2K/min, very complex behaviour was found, the most significant feature being a very sudden appearance of the signal at 294.6K when cooling. For rates ~ 0.1K/min a single broad maximum at 292.9K was observed in the second harmonic signal without any other significant structure. Because there was still some rate dependence even for rates ~ 0.1K/min, it was not possible to determine if any temperature hysteresis was present. A typical warming curve is given in Fig. 6; a modulation amplitude of $\Delta_T \simeq 35$ mK was used, with the modulation and carrier frequencies being 0.3 and 1000 Hz respectively, with an applied field of 8 A/m RMS. A fairly sharp peak in the phase of the second harmonic signal occurred at about 292.9K with a total phase variation of about 20°.

3.4 Relaxation results: Figure 7 shows the approximate initial directions of the first harmonic signal change during the relaxation experiments, superimposed on an equilibrium $S(T)$ curve. A close analysis of these changes revealed qualitative conformity with the second harmonic results outlined above: below the peak in $S(T)$ the first harmonic signal initially moves upwards in response to sudden cooling. Therefore we do not find the 180° phase change in the second harmonic signal which is otherwise

expected near the peak in the first harmonic signal in the absence of relaxation effects.

3.5   Measurement of the modulation amplitude: The variation with temperature of the modulation amplitude as determined from phase-sensitive detection of the thermocouple output is shown in Fig. 8 for a modulation frequency of 0.6 Hz. Although there will be some modulation broadening produced because of the large modulation amplitude ($\Delta_T \sim 35$ mK) used, this should not appreciably distort the curve because of the lack of any sharp temperature dependence of Δ_T. The minimum in Δ_T occurs at 291.3 ± 0.2K, below the peak in the first harmonic $S(T)$ curve.   Figure 9 shows the corresponding temperature dependence of the phase of the modulation.   It peaks where the modulation amplitude is a minimum.   The presence of a DC magnetic field of 750 A/m appears to have no significant effect on the amplitude or phase of the temperature modulation.

4.   Discussion

The temperature dependence of the modulation amplitude as given in Fig. 8 indicates a maximum in specific heat at 291.3 ± 0.2K, in reasonable agreement with the maximum observed at 291.8K by Griffel et al (1954); however this agreement may be somewhat fortuitous in view of the dependence of T_c upon sample purity.   This temperature is significantly lower than the value of 293.7 ± 0.2K corresponding to the largest value of $\chi^1(T)$ as in II and the largest signal amplitudes in both the AC and DC modulation experiments.   This is not surprising as the specific heat maximum should occur when $\sigma \, d\sigma/dT$ is a maximum whereas the results given both in this paper and in II indicate that domain properties strongly influence the temperature dependence of

the susceptibility. The observed temperature dependence of the
phase of the temperature modulation as given in Fig. 9 is very
different to the expected behaviour with a minimum at 291.3K;
the temperature modulation monitored by the thermocouple is at
one point in the sample and the observed temperature dependence
may be due to the dependence of the thermal skin depth δ upon
temperature. Here $\delta \sim$ 1mm which is comparable with the sample
radius. In this paper the only phase variation to be considered
will be the dominant sharp peak in the phase observed for low field
AC experiments. Further careful studies of the temperature
dependences of the modulation amplitude and phase are in progress
with the particular aim of making corrections to the results of
temperature modulation experiments to permit extremely accurate
measurements of critical behaviour to be made. A conventional
calorimetric study of the specific heat of the samples is also in
progress.

     To facilitate discussion of the effects of relaxation on the
low field AC experiments, curves showing the temperature variations
of the AC susceptibility and the signal amplitude and phase of the
temperature modulation signals for a low field warming experiment
are given together in Fig. 10. These results exhibit some of the
main characteristics of domain relaxation effects as treated
theoretically in I. As in I, points where the derivative $\chi^1(T)$ is
zero are the easiest to consider; here this occurs at 291.9 ± 0.2
and 290.0K ± 0.4K. At 291.9K there is a large modulation signal and
small phase lead which is as expected for slow relaxation ($\omega\tau \gg 1$).
At 290K there is a small signal amplitude and large phase lead
corresponding to relatively fast relaxation ($\omega\tau \lesssim 1$). One concludes

that the domain properties responsible for these effects relax
very slowly at the Curie point where nucleation is commencing and
faster at lower temperatures.

Writing $\chi = g\sigma$ and ascribing the relaxation effects to the
domain g term as in I requires that the same effects be observed in
both AC and DC experiments - in low fields the same process of
reversible domain displacement will be dominant in both the AC and
DC susceptibilities. Hence we now consider the implications of our
observation that there are no significant relaxation or temperature
hysteresis effects in the DC experiments. This means that there are
no such effects in the temperature dependence of the DC susceptibility;
this is quite feasible in view of the variation of the $\chi(T)$ curves
with the frequency of the AC field as given in Fig. 7 of II. The
trough in the AC $\chi(T)$ curves together with the temperature hysteresis
must then be due to the magnetic after-effect. The lack of anomalous
behaviour in the DC experiments indicates that there is no significant
temperature hysteresis or slow relaxation in the actual domain
nucleation; rather, the temperature hysteresis and relaxation effects in
the low field AC susceptibility must be caused by hysteresis and
relaxation in the after-effect at temperatures where domains nucleate
and denucleate. An impurity after-effect is not expected to affect
the DC susceptibility but, because of a damping of domain wall motion,
produces a reduction of the AC susceptibility as observed in the
frequency dependence of the susceptibility in II. The relaxation
theory of I is easily extended to cover this case by again writing
$\chi = g\sigma$ for the low field susceptibility and putting

$$g = g_O - \Delta g \tag{5}$$

where Δg is the decrease in g due to the after-effect. The term

$\sigma \Delta g$ is the difference between the AC and DC susceptibilities so

that Δg will be frequency dependent, tending to zero at very low

frequencies. As the frequency is increased Δg will increase

tending to an almost frequency independent value at high frequencies.

It is assumed that g_O does not exhibit relaxation or temperature

hysteresis effects and that Δg satisfies a relaxation equation

$$\frac{d\Delta g}{dt} = - \frac{\Delta g - \Delta g_e}{\tau} \qquad (6)$$

where the equilibrium value Δg_e is a function of temperature.

Above T_c there are no domains and, as expected, no relaxation

effects so that $\Delta g_e = 0$. As the temperature is lowered below T_c,

Δg_e will increase and, as indicated by Fig. 7 of II, will then

become approximately temperature independent. In the region of T_c,

Δg_e exhibits temperature hysteresis with a polarity such that,

from Fig. 1 of II, it is greater on warming than on cooling;

this polarity is in agreement with an impurity after-effect in

which the pinning of walls by impurities is stronger on warming than

on cooling at temperatures in the nucleation region. This model

leads to results which are of the same form as the corresponding

equations in I. Equations (19, 22) of I for the first harmonic

oscillation $\chi_1(t)$ and for the resultant phase become

$$\chi_1(t) = \Delta_T \{ (\sigma g'_O + \sigma'g) \cos(\omega t + \phi_T)$$

$$- \sigma \Delta g' \alpha_1 \cos(\omega t + \phi_T - \phi_1) \} \qquad (7)$$

and $\qquad tan \ \phi_r = \dfrac{\sigma \Delta g' \omega \tau}{\chi^1 + \omega^2 \tau^2 (\sigma'g + \sigma g'_O)} \qquad (8)$

where $tan \ \phi_1 = \omega \tau$, $\alpha_1 = (1 + \omega^2 \tau^2)^{-\frac{1}{2}}$; also g, Δg and their

derivatives are assumed to be the equilibrium functions for the mean

temperature $\overline{T}$. These equations are the same as in I except that the

relaxing term $\sigma g'$ has become $-\sigma \Delta g'$ and the 'fast' term $\sigma'g$ has become $(\sigma'g + \sigma g'_o)$. Equation (8) can be simplified to

$$tan \; \phi_{\gamma} \; = \; \beta \omega \tau \; / \; (1 - \beta + \omega^2 \tau^2) \qquad\qquad (9)$$

where $\beta = \sigma \Delta g' / (\sigma'g + \sigma g'_o) = (1 + \chi' / \sigma \Delta'g)^{-1} \qquad (10)$

is the ratio of the relaxing and fast components of $\chi'(T)$. At temperatures where $\chi^1(T) = 0$, $\beta = 1$ and $tan \; \phi_{\gamma} = 1/(\omega\tau)$ as in I. As above a consideration of such points shows that, in the nucleation region, τ decreases as the temperature is lowered. Curves of ϕ_{γ} versus $\omega\tau$ are given in Fig. 11 for several values of β. For $\beta < 1$ the relaxing term is always less than the fast term in (7) and the phase lead is less than it would have been for $\beta = 1$. For $\beta > 1$ the signal amplitude passes through zero at points where $\omega\tau = \sqrt{\beta - 1}$ and the phase then changes discontinuously between $\pm \frac{\pi}{2}$. This corresponds to exact cancellation of the relaxing and fast terms in (7). Such effects were not observed in our experiments but certainly would be if extremely low modulation frequencies were used.

We now discuss the features of the three curves in Fig.10 in terms of the above relaxation theory. Because the temperature dependence of the initial-field DC susceptibility is not known this discussion must remain qualitative. Above T_c no domain effects are expected and, apart from the variation of Δ_{γ}, the signal amplitude should vary as the derivative $\chi^1(T)$. The maximum signal amplitude occurs at 293.2K, where ϕ_{γ} is still small and this is just a little below the temperature at which $\chi^1(T)$ is a maximum. Here the domains are just beginning to nucleate, the relaxation of Δg will be extremely slow ($\omega\tau \gg 1$) and the large signal will be given by $\chi_1(t) \simeq \Delta_{\gamma} (\sigma g'_o + \sigma'g) \; cos \; (\omega t + \phi_{\gamma})$, the relaxing term

in (7) being effectively zero because of the small value of α_1.
At 291.9K where $\chi^1(T) = 0$ the large signal amplitude requires
that still $\omega\tau \gg 1$ and this is in agreement with the observation
in II that here $\tau \sim 2\text{-}6$ sec. Between the two temperatures
where $\chi^1(T) = 0$, $\beta > 1$ since $\Delta g'$ is always negative in the
nucleation region and the phase lead will increase as $\omega\tau$ decreases.
The maximum phase lead occurs at 290.7 ± 0.2K, just above the trough
in $\chi(T)$, since below this β will decrease below 1. Figure 11 shows
that when $\beta < 1$ and $\omega\tau \to 0$ the phase lead tends to zero. The large
phase maximum must also occur at a point where the first harmonic
amplitude is a minimum and this agrees well with the results.

The temperature dependences of both the signal amplitude
and phase for modulation frequencies of 0.3 Hz and 2 Hz were almost
identical and this requires that at any one temperature there is a
broad range of relaxation times. The difference between the cooling
and warming curves will be partly due to a difference in $\Delta g(T)$. As
above, at any temperature in the nucleation region Δg will be greater
on warming than on cooling; in the region of the phase peak $|\Delta g'|$
will be greater on cooling than on warming. However to explain the
temperature hysteresis it is necessary to postulate that the
average relaxation time during warming is considerably shorter than
during cooling. This is in agreement with the observation in II that
the effects of relaxation on the susceptibility following sudden
temperature changes were much weaker during warming experiments.
Possibly the slow relaxation caused during cooling is associated with
the diffusion of impurities to the newly-nucleated walls whereas, in
warming from lower temperatures, more stable impurity-wall configur-
ations have been set up. The assumption of a shorter relaxation time
for warming experiments is consistent with both the larger phase leads
and smaller signal amplitudes than for cooling experiments.

Figures 4 and 5 show that the relaxation effects, temperature hysteresis and the lower temperature satellite peak in the AC modulation signals all vanish for sufficiently large AC field amplitudes. This is as expected since for large fields the susceptibility will not be greatly affected by the impurity-diffusion after-effect ($|\Delta g| \ll g_o$).

One result of relaxation effects in any experiment in which modulation and phase-sensitive detection is used is that the signal amplitude, for small modulation amplitudes, is not proportional to the appropriate derivative. In Fig. 12 $\chi(T)$ curves for cooling experiments with a low (12.8 A/m RMS) and high (850 A/m RMS) applied AC field are given together with suitably normalized curves obtained by integrating the corresponding temperature modulation signal amplitude with respect to temperature starting from a high temperature. Above T_c there is good agreement between $\chi(T)$ and the integrated curves, as expected for slow modulation ($\omega\tau \ll 1$). Below T_c the two curves are also very similar for the large AC field as expected in the absence of the after-effect. However in lower fields the integrated curve is considerably greater than $\chi(T)$. This requires that the relaxing component is one which reduces the equilibrium AC suscept-ibility, in agreement with the assumptions of our relaxation theory.

The results of relaxation experiments in which the effects of sudden temperature changes on the first harmonic signal amplitude are studied for low AC fields, are in agreement with the observation of a single peak in the temperature dependence of the second harmonic signal amplitude. One result of a comparison between theory and these results is that the temperature at which $\sigma'(T)$ is a maximum must be somewhat lower than the temperature 293.7K at which

$\chi^1(T)$ is a maximum – in agreement with the observation of the minimum in Δ_T, and hence in specific heat, at a temperature ~291.3K.

5.   Conclusions

These studies indicate that the anomalous behaviour (relaxation and temperature hysteresis) in the low field AC susceptibility in the region of the Curie temperature are well described by a theoretical treatment of a domain property which influences the susceptibility and is assumed to exhibit simple relaxation. By noting the lack of anomalous behaviour in the DC modulation experiments it is suggested that the relaxation is associated with the onset of a magnetic after-effect in the domain nucleation region and that the relaxation times exhibit temperature hysteresis. The slowest relaxation occurs when the sample is cooled from higher temperatures to T_c. After correction for the temperature dependence of the modulation amplitude, the first harmonic modulation experiments yield a signal amplitude which is proportional to the derivative $\chi^1(T)$ at temperatures above T_c; below T_c this proportionality breaks down because of the relaxation.

REFERENCES

Chaplin D H, Sydney K R and Wilson G V H   1973   Phys.Lett. $\underline{46A}$ 55-6

Chynoweth A G   1958   J.Appl.Phys. $\underline{29}$ 563-565

Griffel M, Skochdopole R E and Spedding F H   1954   Phys.Rev. $\underline{93}$ 657-661

Nigh H E, Legvold S and Spedding F H   1963   Phys.Rev. $\underline{132}$ 1092-1097

Sydney K R, Wilson G V H, Chaplin D H and McKenna T J   1974
        J.Phys.F. $\underline{4}$ L98-101

Sydney K R, Chaplin D H and Wilson G V H   1975   J.Phys.F.
        accompanying paper to be referred to as II.

Walser R M, Benê R W and Caruthers R E   1971   IEEE Trans. on Electron
        Devices $\underline{ED-18}$ 309-315

Wilson G V H, Chaplin D H and Sydney K R   1975   J.Phys.F., accompanying
        peper to be referred to as I

FIGURE CAPTIONS

Figure 1 :   Temperature dependence of the signal amplitude

for cooling experiments using the DC technique with

a modulation frequency of 0.3 Hz, a modulation

amplitude $\simeq$ 6 mK, and various applied DC fields:

X 750 A/m; 0 600 A/m; Δ 375 A/m; $\square$ 75 A/m.

Figure 2 :   Dependence of the maximum signal amplitude on

applied DC field.

Figure 3 :   Temperature dependence of the phase of the DC field,

temperature modulation signal with respect to the

heater power waveform for cooling experiments with a

modulation frequency of 0.3 Hz, modulation amplitude

$\simeq$ 6 mK, and various applied DC fields: X 750 A/m;

0 600 A/m; Δ 375 A/m; $\square$ 75 A/m.

Figure 4 :   Temperature dependence of the AC field, temperature

modulation signal amplitude normalized with respect

to the AC field amplitude. Modulation frequency 2 Hz;

AC field frequency 100 Hz; modulation amplitude $\simeq$ 6 mK;

RMS AC magnetic fields: X 750 A/m cooling; Δ 750 A/m

warming; $\square$ 75 A/m cooling; $\blacksquare$ 75 A/m warming;

0 10 A/m cooling; $\bullet$ 10 A/m warming.

Figure 5 :   Temperature dependence of the phase of the AC field,

temperature modulation signal with respect to the

heater power waveform with a modulation frequency 1 Hz.

AC field frequency 100 Hz, modulation amplitude $\simeq$ 6 mK,

RMS AC magnetic fields: X 750 A/m cooling; Δ 750 A/m

warming; $\square$ 75 A/m cooling;   ∎   75 A/m warming;

0   10 A/m cooling;   ● 10 A/m warming.

Figure 6 :   Temperature dependence of the AC field, temperature

modulation second harmonic signal amplitude for a

warming experiment with modulation frequency 0.3 Hz,

AC field frequency 1000 Hz, modulation amplitude $\simeq$ 6 mK,

and RMS AC field 8 A/m.

Figure 7 :   Approximate directions for the changes in the AC field,

temperature modulation signal in response to sudden

changes in temperature, superimposed on an equilibrium

AC modulation curve.   Modulation frequency 0.3 Hz,

AC field frequency 1000 Hz, modulation amplitude $\simeq$ 35 mK,

RMS AC field 75 A/m, ↖ cooling,   ↘ warming.

Figure 8 :   Temperature dependence of the temperature modulation

amplitude with a modulation frequency of 0.6 Hz for

various conditions: X   cooling in zero magnetic field;

0   warming in zero magnetic field; Δ cooling in 750 A/m

DC field.

FIGURES

For the purposes of including this paper in the back of my thesis, the following correspondence is applicable between the figures of the paper and those of the thesis.

PAPER FIGURE	THESIS FIGURE
1	24
2	25
3	26
4	27
5	30
6	32
7	34
8	35
9	36
10	37
11	38
12	39